

Stochastic effects and uncertainties in assessing electromagnetic interactions with control systems

Dissertation

zur Erlangung des akademischen Grades

Doktoringenieur (Dr.-Ing.)

von Dipl.-Ing. Velislav Varbanov
geb. am 07.01.1972 in Burgas

genehmigt durch die Fakultät für Verfahrens- und Systemtechnik
der Otto-von-Guericke-Universität Magdeburg

Gutachter: Prof. Dr.-Ing. habil. Ulrich Hauptmanns
Prof. Dr.-Ing. Günter Wollenberg
Dr.-Ing. Ralf-Michael Zander

Promotionskolloquium am 09.06.2005

Abstract

Nowadays the control system units operate at very low threshold energy levels. It is very important that such devices are not susceptible to emissions (either conducted or radiated) produced by other systems, or by the electromagnetic fields of natural sources, such as, lightning. The most frequent mechanism of electromagnetic interference caused by lightning on electronic components is the interaction of the discharge with the transmission line to whose end the device is connected. In order to protect the system against such events, an investigation of the voltage surges at the end of the line caused by this external field is necessary. The present work evaluates the voltage surges at the end of an underground-located low-voltage transmission line in the case of nearby lightning. The knowledge of the extent of the surges will allow appropriate decisions for the protection of the devices at the end of the line to be taken. Very important in this investigation is to take into account the stochastic nature of the input parameters. It manifests itself by differences in distance between the wires in the conductors, variation of the conductor and insulation diameters and different properties of the insulation and surrounding medium, along the length of the line. In many cases this stochastic nature is neglected, but it can be responsible for variations of the results up to several orders of magnitude.

Kurzreferat

Kontrollsysteme von heute arbeiten mit sehr niedriger Energie. Es ist wichtig, dass solche Systeme nicht beeinflusst werden durch die elektromagnetischen Emissionen anderer Geräte oder durch die von einer natürlichen Quelle hervorgerufenen elektromagnetischen Felder wie z.B. Blitzeinschläge. Die häufigste Ursache einer elektromagnetischen Störung verursacht durch einen Blitzeinschlag auf elektronischen Komponenten ist der Einfluß der Blitzentladung auf das Endgerät durch Übertragung in der elektrischen Leitung. Um die Systeme vor solchen Einwirkungen zu schützen, müssen Untersuchungen bezüglich des Spannungsverhaltens am Ende der elektrischen Leitung gemacht werden. Diese Arbeit beschäftigt sich mit dem Spannungsverhalten am Ende der Leitung von unter der Erde befindlichen elektrischen Leitungen mit einer niedrigen Spannung bei einem unmittelbaren Blitzeinschlag. Das Wissen über die Größe des Störungssignals würde uns die Einrichtung passender Schutzmassnahmen für solche Ereignisse ermöglichen. Sehr wichtig für die Untersuchung ist es, die stochastische Natur von Eingangsparametern zu berücksichtigen. Die stochastische Natur berücksichtigt die realen Bedingungen von Leitungen unter der Erde ebenso wie die Beschaffenheit der Umgebung. In den meisten Berechnungen wird dies vernachlässigt, obwohl der Einfluss auf das Ergebnis mehrten Größenordnungen ausmachen kann.

Contents

- 1. Introduction 1
 - 1.1 Motivation 2
 - 1.2 Approach and outline 3
- 2. Electromagnetic interference 5
 - 2.1 Sources of natural disturbance 6
 - 2.1.1 The magnetic field of the earth and geomagnetic storms 6
 - 2.1.2 Atmospheric noise 9
 - 2.2 Disturbances due to human activities 11
 - 2.2.1 Disturbances caused by radio-frequency transmitters 12
 - 2.2.1.1 Radio and television broadcasting transmitters 13
 - 2.2.1.2 Radars 14
 - 2.2.2 Unintentional sources of radiation 14
 - 2.2.2.1 Industrial, scientific and medical (ISM) equipment 15
 - 2.2.2.2 Electronic data-processing (EDP) equipment 15
 - 2.2.2.3 Ignition systems for internal combustion engines of vehicles 16
 - 2.3 Electromagnetic compatibility - standards 16
- 3. Lightning discharge as a major source of interference 25
 - 3.1 The discharge process of negative cloud-to-ground lightning 25
 - 3.2 The return strokes 30
 - 3.2.1 Lightning current at the base of the channel 31
 - 3.2.2 Mathematical modeling of the subsequent return stroke current waveform 33
 - 3.2.3 Electromagnetic field produced by the lightning discharge 37
 - 3.2.4 Mathematical model of the electromagnetic field radiated by the subsequent return stroke 39
 - 3.2.5 Simulation models for the return stroke 45
 - 3.2.6 “Engineering” models for the simulation of the return stroke process 46
 - 3.2.7 “LEMFieldE” – a program for simulation of the consequences of a lightning stroke 50
 - 3.2.8 Comparison of the results calculated by “LEMFieldE” with those stated in the literature 58
 - 3.3 The stochastic nature of lightning 68
- 4. Case study – investigation of lightning flash interaction with a transmission line as part of the control system 73
 - 4.1 Description of the line 73
 - 4.2 Electrical dimensions of a transmission line 77
 - 4.3 Deterministic study of the interaction of lightning with the line 80

4.3.1	Distant strike and electromagnetic field coupling.....	81
4.3.2	Direct lightning strike and crosstalk between the conductors.....	85
4.3.3	Results of the deterministic approach	92
4.4	Stochastic simulation of a direct strike over the line	94
4.4.1	Pdf distribution of the input stochastic parameters	95
4.4.2	Development and comparison between the 22-point model and the 204-point model	97
4.4.2.1	Partial stochastic simulation showing the influence of individual parameters.....	103
4.4.2.2	Stochastic simulation with all parameters	107
4.4.2.3	Evaluation of the stochastic results	112
4.5	Determination of the expected lightning frequency as an initiating event.....	120
5.	Summary and outlook	128
	Bibliography	130
	Appendix I	139
	Appendix II	158
	Appendix III	167

Table of utilized symbols and abbreviations

Latin Symbols

Symbol	Unit	Unit Symbol	Description
\mathbf{I}_n	-	-	Identity matrix
$\hat{\mathbf{A}}$	-	-	Vector potential function in frequency domain
\vec{a}_n	-	-	Normal unit vector
$\hat{A}_r, \hat{A}_\theta, \hat{A}_\phi$	-	-	Components of vector potential function in spherical coordinate system in frequency domain
$\hat{A}_x, \hat{A}_y, \hat{A}_z$	-	-	Components of vector potential function in cartesian coordinate system in frequency domain
\mathbf{B}	tesla	T	Magnetic flux density
\mathbf{b}	hertz	Hz	Receiver bandwidth
$\vec{\mathcal{B}}$	tesla	T	Magnetic flux density vector
$\vec{\mathcal{B}}_t$	tesla	T	Magnetic flux density in transverse plane
c	meter/second	m/s	Wave velocity (speed of light - free space)
\mathbf{c}	meter	m	Closed contour
\mathbf{C}	farad	F	Capacitance
c	farad/meter	F/m	Per-unit-length capacitance
\mathbf{C}	farad/meter	F/m	Per-unit-length capacitance matrix
\mathbf{D}	coulomb/meter ²	C/m ²	Electric field density
D	meter	m	The distance from the lightning flash
$\vec{\mathcal{D}}$	coulomb/meter ²	C/m ²	Electric flux density vector
d_{ij}	meter	m	Distance
ΔZ	meter	m	Distance
\mathbf{E}	volt/meter	V/m	Electric field strength
$\hat{\mathbf{E}}$	volt/meter	V/m	Phasor form of electric intensity vector in frequency domain
E_p	volt/meter	V/m	Lightning electric field peak current normalized to 100 km
\hat{E}_r	volt/meter	V/m	Lightning produced horizontal electric field in frequency domain
E_r	volt/meter	V/m	Lighting produced horizontal electric field in time domain
$\hat{E}_r, \hat{E}_\theta, \hat{E}_\phi$	volt/meter	V/m	Components of the electric intensity vector in spherical coordinate system in frequency domain
$\vec{\mathcal{E}}_t$	volt/meter	V/m	Electric intensity vector in the transverse mode of propagation of electromagnetic wave
$\mathcal{E}_x, \mathcal{E}_y, \mathcal{E}_z$	volt/meter	V/m	Components of the electric intensity vector in cartesian coordinate system
\hat{E}_z	volt/meter	V/m	Lightning produced vertical electric field in frequency domain
E_z	volt/meter	V/m	Lighting produced vertical electric field in time domain
\mathcal{F}	-	-	Fourier transform
f	hertz	Hz	Frequency

TABLE OF UTILIZED SYMBOLS AND ABBREVIATIONS

F_a	decibel	dB	External noise power level
f_a	-	-	Power ratio of the external noise
G	siemen	S	Conductance
g	siemen/meter	S/m	Per-unit-length conductance
\mathbf{G}	siemen/meter	S/m	Per-unit-length conductance matrix
H	ampere/meter	A/m	Magnetic field strength
h	meter	m	Height
$\hat{\mathbf{H}}$	ampere/meter	A/m	Phasor form of magnetic intensity vector in frequency domain
H	kilometer	km	Height of the lightning channel
\hat{H}_ϕ	ampere/meter	A/m	Lightning produced azimuthal magnetic in frequency domain
H_ϕ	ampere/meter	A/m	Lighting produced azimuthal magnetic field in time domain
$\hat{H}_r, \hat{H}_\theta, \hat{H}_\phi$	ampere/meter	A/m	Components of the magnetic intensity vector in spherical coordinate system in frequency domain
$\vec{\mathcal{H}}_t$	ampere/meter	A/m	Magnetic intensity vector in the transverse mode of propagation of electromagnetic wave
$\mathcal{H}_x, \mathcal{H}_y$	ampere/meter	A/m	Components of the magnetic intensity vector in cartesian coordinate system
\hat{I}	ampere	A	Phasor current
$i(h,t)$	ampere	A	Lightning current wave, measured at the top of the tower
$\hat{I}(j\omega)$	ampere	A	Current at the base of the lightning in frequency domain
$I(t)$	ampere	A	Lightning current waveform at the base of the lightning channel
$\hat{\mathbf{I}}(z)$	ampere	A	Line currents vector in phasor form
$\hat{I}(z), \hat{I}_i(z)$	ampere	A	Line current in phasor form
$\hat{I}(z', j\omega)$	ampere	A	Current distribution along the lightning channel in frequency domain
$I(z,t)$	ampere	A	Current in the conductors of the transmission line
$\mathbf{I}(z,t)$	ampere	A	Vector of currents in multiconductor transmission line
$i(z',t), I(z',t)$	ampere	A	Current distribution in the lightning channel in time domain
I, I_i, I_j	ampere	A	Electrical current
I_0	ampere	A	Amplitude parameter for the lightning base current
$i_0(t)$	ampere	A	Lightning return-stroke current pulse
I_{0i}	kiloampere	kA	Amplitude parameter of the lightning channel base current
$\hat{\mathbf{I}}_m$	ampere	A	Vector of modal currents in frequency domain
I_{\max}	ampere	A	Maximum current of the lightning current waveform at the base of the channel
\hat{I}_m	ampere	A	Mode current in frequency domain
I_{PC}	ampere	A	Peak current induced in bare copper conductors
$\hat{\mathbf{J}}$	ampere/meter ²	A/m ²	Phasor form of current density vector in frequency domain
j	-	-	Imaginary unit
$\vec{\mathcal{J}}$	ampere/meter ²	A/m ²	Electric current density vector
$\hat{J}_x, \hat{J}_y, \hat{J}_z$	ampere/meter ²	A/m ²	Components of current density in cartesian coordinate system in frequency domain
\mathcal{J}_z	ampere/meter ²	A/m ²	The z-component of the electric current density vector in cartesian coordinate system

TABLE OF UTILIZED SYMBOLS AND ABBREVIATIONS

k	joule/kelvin	J/K	Boltzmann's constant
k	-	-	Electrical dimensions of a transmission line
l	meter	m	length
L	meter	m	Length of a transmission line
L	henry	H	Inductance
l	henry	H/m	Per-unit-length inductance
\mathbf{L}	henry	H/m	Per-unit-length inductance matrix
v	meter/second	m/s	Lightning return-stroke velocity
v	meter/second	m/s	Current wave propagation speed
v	meter/second	m/s	Effective channel velocity
N_d	-	-	Density of the lightning strikes to the ground
N_k	-	-	Keraunic level
P_n	watt	W	Mean power received by an omni-directional lossless antenna
\mathbf{Q}	coulomb/meter	C/m	Per-unit-length total charge matrix
q	coulomb/meter	C/m	Per-unit-length charge distribution
$\hat{q}(0, j\omega)$	coulomb	C	Charge at the base of the lightning in frequency domain
$q(0, t)$	coulomb	C	Charge at the base of the lightning in time domain
$Q(z', t)$	coulomb/meter	C/m	Charge distribution along the lightning channel
r	meter	m	Distance
R	meter	m	Distance
r	ohm/meter	Ω/m	Per-unit-length resistance
\mathbf{R}	ohm/meter	Ω/m	Per-unit-length resistance matrix
r, θ, ϕ	-	-	Space coordinates in spherical coordinate system
r, r_1, r_2	meter	m	Radius
R, R_1, R_2	meter	m	Radius
R_{H1}, R_{H2}	ohm	Ω	Resistance of the housing
R_L	ohm	Ω	Load resistance
R_{leak}	ohm	Ω	Leak resistance
R_S	ohm	Ω	Source resistance
s	meter	m	Depth under the ground
s	meter ²	m ²	Surface
s	meter	m	Distance
S_C	meter ²	m ²	Critical ground surface
S_{xy}	meter ²	m ²	Area
t	second	s	Time
T_0	kelvin	K	Temperature
T_{rise}	microsecond	μs	Rise time of the lightning current waveform at the base of the channel
$\hat{\mathbf{T}}_V, \hat{\mathbf{T}}_I$	-	-	Similarity transformation matrices in frequency domain
v	meter/second	m/s	Velocity of propagation of electromagnetic wave

TABLE OF UTILIZED SYMBOLS AND ABBREVIATIONS

v'	meter ³	m^3	Volume
$\hat{\mathbf{V}}(z)$	volt	V	Line voltages vector in phasor form
$\hat{V}(z), \hat{V}_i(z)$	volt	V	Line voltages in phasor form
$V(z,t)$	volt	V	Electric voltage between the conductors of the transmission line
$\mathbf{V}(z,t)$	volt	V	The vector of voltages in multiconductor transmission line
V_{ab}	volt	V	Voltage between point a and b
v_f	meter/second	m/s	Upward propagating front speed (return stroke speed)
\hat{V}_m	volt	V	Mode voltage in frequency domain
$\hat{\mathbf{V}}_m$	volt	V	Vector of modal voltages in frequency domain
\hat{V}_s	volt	V	Source voltage in phasor form
$V_s(t)$	volt	V	Voltage source in time domain
x, y, z	-	-	Space coordinates in cartesian coordinate system
$\hat{\mathbf{Y}}$	siemen	S	Admittance matrix in phasor form
z	meter	m	Height
$\hat{\mathbf{Z}}$	ohm	Ω	Impedance matrix in phasor form
z'	meter	m	Height
\hat{Z}_c	ohm	Ω	Characteristic impedance of the line in phasor form
$\hat{\mathbf{Z}}_c$	ohm	Ω	Characteristic impedance matrix in frequency domain
$\hat{Z}_{in}(z)$	ohm	Ω	The input impedance of the line in phasor form
\hat{Z}_L	ohm	Ω	Load impedance in phasor form
\hat{Z}_s	ohm	Ω	Source impedance in phasor form
\hat{Z}_t	ohm	Ω	Transverse impedance

Greek Symbols

Symbol	Unit	Unit Symbol	Description
∇	-	-	Vector differential operator (del)
α	1/second	1/s	Parameter in lightning current waveform equation
α	1/kilometer	1/km	Attenuation constant
α	neper/meter	Np/m	Attenuation constant
$\alpha_{corrected}, \alpha_1, \alpha_2$	degree	°	Angle
β	1/second	1/s	Parameter in lightning current waveform equation
β	radian/meter	1/m	Phase constant
β_0	radian/meter	1/m	Phase constant (wavenumber)
ϵ	farad/meter	F/m	Electric permittivity

TABLE OF UTILIZED SYMBOLS AND ABBREVIATIONS

ϵ_r	-	-	Relative permittivity
ϵ_{rg}	-	-	Relative ground permittivity
ϵ_0	farad/meter	F/m	Permittivity of free space
ϕ	degree	°	Angle
$\hat{\phi}_{ij}$	-	-	Components of the chain parameter matrix in phasor form
$\hat{\Phi}$	-	-	Scalar potential function in frequency domain
$\hat{\Phi}$	-	-	Chain parameter matrix in phasor form
$\hat{\Gamma}_L$	-	-	Reflection coefficient at the load in phasor form
$\hat{\Gamma}_S$	-	-	Reflection coefficient at the source in phasor form
$\hat{\gamma}$	-	-	Propagation constant in phasor form
$\hat{\gamma}$	-	-	Propagation matrix in frequency domain
η	-	-	Amplitude correction factor
η_0	ohm	Ω	Impedance of free space
λ	meter	m	Current decay constant
λ	meter	m	Wavelength of the electromagnetic wave
μ	henry/meter	H/m	Magnetic permeability
μ	-	-	Expected value (mean) of a random variable
μ_r	-	-	Relative permeability
μ_0	henry/meter	H/m	Permeability of free space
θ	degree	°	Angle
ρ	coulomb	C	Electric charge
ρ	ohm-meter	Ω -m	Earth resistivity
$\rho(z',t)$	coulomb/meter	C/m	Charge density in the lightning channel
ρ_b	-	-	Reflection coefficient at the bottom of the tower
ρ_t	-	-	Reflection coefficient at the top of the tower
$\hat{\rho}$	coulomb	C	Phasor form of electric charge used in frequency domain
σ	siemen	S	Conductivity
σ	-	-	Standard deviation of a random variable
σ_g	siemen/meter	S/m	Ground conductivity
τ_D	microsecond	μ s	Time constant
τ_{i1}, τ_1	microsecond	μ s	Front time constant
τ_{i2}, τ_2	microsecond	μ s	Decay time constant
ω	radian/second	1/s	Angular frequency
ψ	webwer	Wb	Magnetic flux
ψ_m	weber	Wb	Magnetic flux
Ψ	webwer/meter	Wb/m	Per-unit-length magnetic flux matrix

Acronyms

AV	Average detector
BG	Bruce-Golde model
CISPR	International Special Committee on Radio Interference
dc	Direct current
EDP	Electronic data-processing
EMC	Electromagnetic compatibility
EMI	Electromagnetic interference
EN	European Norms or EURONORMs
FCC	Federal Communication Commission
FFT	Fast Fourier transform
ISM	Industrial, scientific and medical (equipment)
ITE	Information technology equipment
ITU	International Telecommunication Union
LISN	Line impedance stabilization network
LLP	Lightning location and protection (system)
MTL	Multiconductor transmission line
MTLE	Modified transmission line model with exponential current decay with height
MTLL	Modified transmission line model with linear current decay with height
PCB	Printed circuit board
pdf	Probability density function
PE	Polyethylene
QP	Quasi-peak detector
RF	Radio frequency
RFI	Radio-frequency interference
SD	Standard deviation
TCS	Traveling current source model
TEM	Transverse electro-Magnetic
TL	Transmission line model
TL	Transmission line
TTL	Transistor-transistor logic
UHF	Ultrahigh frequency (300 MHz – 3 GHz)
VHF	Very high frequency (30 MHz – 300 MHz)

Chapter 1

1. Introduction

The study of electromagnetic compatibility (EMC) can be considered as a young old problem. It is relatively old, because the problem of radio-frequency interference (RFI) arose nearly 100 years ago with the first use of radio waves as a communication medium. However, the progress in the numerical computation in the last few decades has allowed scientists and engineers to use the existing models for better understanding and visualization of these phenomena.

EMC means avoiding disturbance to other devices caused by electromagnetic interference (EMI), whether through conduction, radiation or induction of the electromagnetic energy. EMI began to gain recognition as a subject of practical importance in the 1920s. With the beginning of radio broadcast transmissions, the interference from electromagnetic noise was viewed with worry by the manufacturers of electric power equipment and electric utility companies. Later in the 1940s and 1950s it was a concern mostly as an electromagnetic noise caused by motors that was conducted over the power lines into the sensitive equipment. During this period and through the 1960s, EMI/EMC was primarily of interest to the US military to ensure electromagnetic compatibility of their devices or weapon systems. With the computer proliferation during the 1970s and 1980s interference from computing devices became a significant problem for television and radio reception, as well as emergency services radio reception. During the 1990's the concern with EMI/EMC has been broadened dramatically. At that time we witnessed the construction of, among other things, an aircraft having no mechanical controls (such as A320 Airbus), whose vital functions and overall stability are controlled by on-board computers, and cars in which not only basic operations

(ignition, fuel supply) but also safety, acceleration and braking are controlled by a few microprocessors. What would have happened in such aircraft in the event of nearby lightning discharge, which creates electric field pulses of the order of 1000 V/m at a distance of a few hundreds meters if no provision is made for the correct operation of its electronic systems? The problem is made more acute by the fact that in order to make the plane lighter many parts of the cabin and wing structures are made of composite materials, substantially reducing the screening effect provided by a metal fuselage. What would have been the disappointment of a driver if the ignition of his car was interrupted or the brakes refused to work when he drives in the vicinity of a high-tension line or a radar installation? Such events may become reality if the compatibility of equipment with its electrical or electronic environment is not sufficiently ensured.

Nowadays, processor-based control systems take over many functions which were formerly controlled by electromechanical or analogue equipment such as relay logic or proportional controllers. Such a structure is more susceptible to an interference firstly because of the low level of energy needed to induce a change of state and in the second place because the effects of the interference are impossible to predict. A pulse lasting for only $1\mu\text{s}$ and amounting to a total energy of less than 0.1 mJ can completely or partially destroy such a system. One-hundredth of this amount causes temporary malfunction [30].

The objective of electromagnetic compatibility is to achieve compatibility between the operation of a sensitive system and its electromagnetic environment, where disturbances may be generated either by another part of the system or by external sources as, for example, a nearby lightning strike.

1.1 Motivation

Interaction between different parts of the same system or between different devices and, electromagnetic disturbance, respectively caused by one device to other pieces of equipment is not so difficult to evaluate compared with disturbances caused by external natural sources as nearby lightning. There is a lot of literature devoted to the problem of electromagnetic compatibility between different pieces of equipment. The standards which postulate the maximum electromagnetic energy radiated by one product are already accepted worldwide and are related to man-made products. But we can't compel the natural sources of electromagnetic interference to obey the same standards as those made by man. Therefore, natural sources, as for example, lightning are much more dangerous for the equipment than

artificial ones. Another feature of lightning is that we don't know when and where it is about to strike i.e. it is unpredictable and very mobile. There exist, of course, man-made highly mobile devices whose purpose is to radiate and receive electromagnetic energy, i.e. mobile phones. However, its radiated energy cannot be compared with the energy produced by nearby lightning. Especially endangered by the lightning are devices at the end of the long transmission lines. The electromagnetic energy produced by the discharge can be transferred to the line either by a direct strike over the line or by the electromagnetic coupling in the case of a distant strike. Without proper lightning protection this energy can destroy the devices at the end of the line.

It is well known that a transmission line located under the ground is less prone to the induction effects caused by nearby lightning. Therefore cables which, for example, connect devices that are part of the control systems and other low-voltage installations are laid under the ground. There is a lot of literature, which give detailed explanation, together with good examples [31], [43], [93] on the interaction of lightning electromagnetic fields with overhead power lines and low-voltage installations. However, there is not so much literature which investigates the problem of the interaction of lightning with underground-located cables. Therefore a more detailed investigation of induction effects in this case is necessary.

The goal of the present work is to evaluate the voltage surges at the end of the underground-located low-voltage transmission line in the case of nearby lightning. The knowledge of the extent of these surges will allow appropriate decisions for the protection of the devices at the end of the line to be taken. It is very important in this investigation to take into account the stochastic nature of the input parameters. This manifests itself by differences in distance between the wires in the conductors, variations of the conductor and insulation diameters as well as different properties of the insulation and surrounding medium along the length of the line. In many cases this stochastic nature is neglected, but it can be responsible for the variation of the results up to several orders of magnitude. Therefore, it is an objective of this thesis to show the importance of accounting for stochastic effects.

1.2 Approach and outline

The thesis is organised as follows:

In Chapter 2 briefly various sources of electromagnetic interference are discussed. Both natural and man-made sources are considered. Man-made sources are divided into sources causing intentional disturbance and sources of unintentional disturbance. Further in the

chapter electromagnetic compatibility standards are considered. The history of the standards is traced from their origin as military standards for the US army to the adoption of European electromagnetic compatibility standards as worldwide-accepted standards. Then the most popular standard, namely the standard which is responsible for imposing limitations for digital devices is briefly reviewed.

Chapter 3 is devoted to the lightning phenomenon. It starts with a detailed description of the discharge process. Furthermore, the most important part of the lightning flash, namely the subsequent return stroke is discussed. Various portions from this process, starting with the current which flows at the base of the lightning and ending with a model of the process are described. Then the code “LEMFieldE” is presented. The program is written in FORTRAN and is used for the simulation of the consequences of a subsequent return stroke above and under the ground. Finally, the results obtained by the program are compared with similar results stated in the literature.

In Chapter 4 the interaction of lightning strike with the transmission line, located underground as part of the control system, is presented. Two possible cases are studied, namely a lightning strike close to the line and a strike directly over the line. In the first case, interference voltages are caused by the lightning-radiated electromagnetic field. For this case the Agrawal approach is used to find the voltage surges at the far-end of the line. In the second case, interference voltages are caused mainly by crosstalk between the conductors of the line. Further in this chapter, stochastic simulation is performed. This simulation accounts for the fact that, for example, the diameters of the conductors are not constant, but vary along the length of the line. Variation of the distance between the conductors and of the properties of the insulation and of the surrounding soil are also considered. The simulation is accomplished using the Monte Carlo method [130]. As a result of this simulation, the response at the far-end of the line is not a single curve for the voltage, but a family of curves whose number depends on the number N of the Monte Carlo trials. These curves give a better notion of the extent of the surge at the far-end of the line, taking into account the stochastic nature of the input parameters. At the end of this chapter an evaluation of the stochastic results is performed.

Chapter 2

2. Electromagnetic interference

Since the invention of radio and telegraph communication it is known that a spark gap generates electromagnetic waves rich in spectral content. These waves can cause interference or noise in various electronic and electrical devices such as radio receivers and telephone communication equipment. Other examples of events that generate electromagnetic waves rich in spectral content and, hence, are considered as sources of interference are lightning, the switching of relays, dc electric motors and fluorescent lights.

Nowadays, electromagnetic interference (EMI) is a serious and increasing form of environmental pollution. Although it is not so obvious as, for example, the pollution caused by big industrial facilities, it may cause electrical and electronic malfunctions, can prevent the proper use of the radio frequency spectrum or can even ignite flammable atmospheres. The ability to control EMI or with other words electromagnetic compatibility (EMC) is gaining importance on one hand because of the increasing pollution of the electromagnetic environment and on the other hand because of the increased penetration of digital electronic devices into all spheres of human activity. Tasks that were previously controlled by electromechanical or analogue devices are now run by microprocessors. This leads to a reduction of operation energy and an increase of potentially disturbing factors. In this case fault-free operation of electronic devices is especially important if safety control systems are involved. Here, the sources of electromagnetic interference are briefly reviewed. They are divided into natural and man-made sources. Also, standards that are intended to reduce the man-made noise will be presented.

2.1 Sources of natural disturbance

The earth has an approximately constant electromagnetic field which can be compared with a big dipole magnet with its north pole orientated to the south and its south pole orientated to the north (Fig. 2.1). Although it cannot be directly discerned, the earth's magnetic field interacts with the flow of solar particles (known as the solar wind) and from this interaction a change in the Earth's electromagnetic field can be observed. This can be considered as a natural electromagnetic disturbance. In the lower layers of the atmosphere, another source of electromagnetic disturbance are thunderstorms. They create a constant electromagnetic noise known as atmospheric noise. The disturbance created by thunderstorms prevails over the disturbance from the solar wind. The nature of both natural sources of electromagnetic disturbances of the earth is briefly reviewed in what follows.

2.1.1 The magnetic field of the earth and geomagnetic storms

The origin of the magnetic field of the earth is not completely understood, but it is thought to be associated with electrical currents produced by the coupling of convective effects and rotation in the spinning liquid metallic outer core of iron and nickel. This mechanism is termed "dynamo effect". The Earth's magnetic field, also called the geomagnetic field, is directed downwards in the northern hemisphere and upwards in the southern hemisphere. (Fig.2.1).

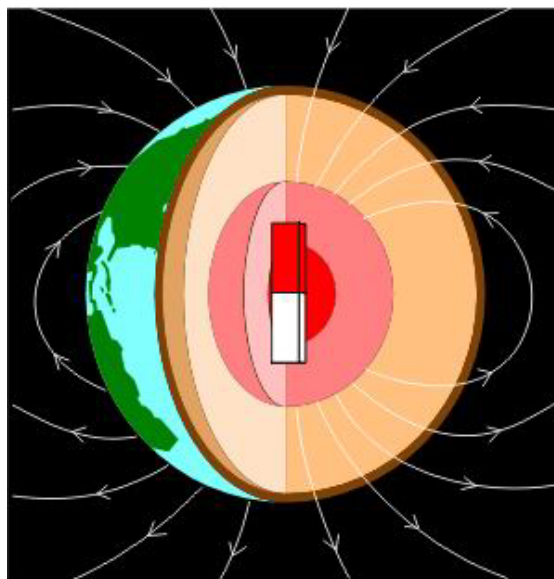


Fig. 2.1 The Earth's electromagnetic field

It can be quantified and characterized by the following parameters: total intensity, vertical intensity, horizontal intensity, inclination and declination.

The geomagnetic field is at its maximum near both magnetic poles and at its minimum near the equator. For example, the total intensity or magnetic strength of the Earth's magnetic field ranges from approximately 19 A/m, which is equivalent to 23 μT (in air) around Sao Paolo, Brazil to 54 A/m or 67 μT near the magnetic south pole in Antarctica.

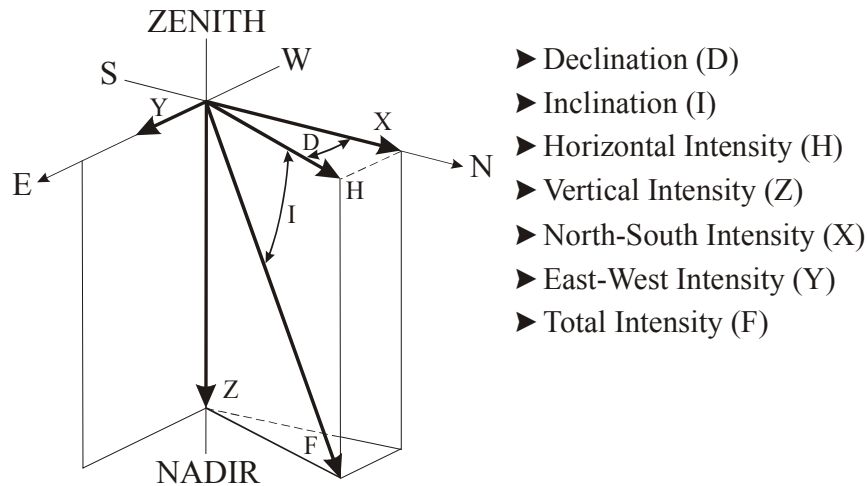


Fig. 2.2 Components of the Earth's electromagnetic field

Vertical and horizontal intensity are components of the total intensity. The angle of the field relative to the ground level is the inclination or dip, which is 90° at the northern magnetic pole. Finally, the angle of the horizontal intensity with respect to the geographic north pole is the declination (Fig.2.2). In common terms, declination is the angle between the direction in which a compass needle points and the true north pole.

The geomagnetic field is not always constant. Small variations in its amplitude can be observed and recorded. These variations are weak and normally do not exceed 1% of its constant value. Their amplitudes are expressed in γ (gammas, $1 \gamma = 1 \text{ nT}$), which in air is equivalent to a field of $7.96 \times 10^{-4} \text{ A/m}$. The main variation among them, which may reach thousands of nanotesla, is caused by interactions between the magnetosphere and the solar wind.

The solar wind is a stream of ionized gases which blow outward from the sun at about 400 km/s and which varies in intensity with the amount of surface activity on the sun. The magnetic field of the earth protects it from most of the solar wind. When the solar wind encounters the magnetic field of the earth at a distance of approximately ten times the Earth's radius, it is deflected like water around the bow of a ship (Fig. 2.3).

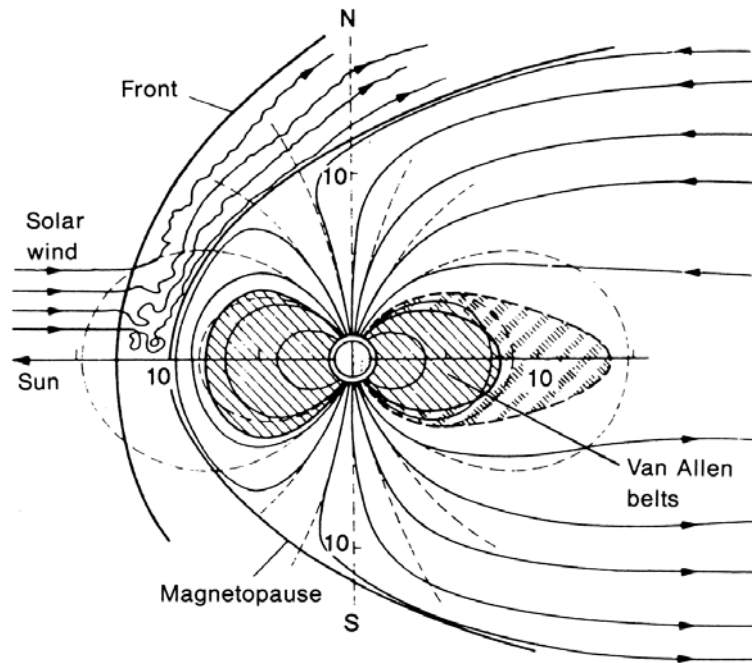


Fig. 2.3 Interaction of the solar wind with the Earth's magnetic field [30]

The imaginary surface at which the solar wind is first deflected is called “bow shock”. The corresponding region of space sitting behind the bow shock and surrounding the earth is termed “the magnetosphere”. It represents a region of space dominated by the Earth’s magnetic field in the sense that it largely prevents the solar wind from entering. However, abrupt gusts of solar plasma increase the intensity of the solar wind and cause high – amplitude disturbances in the geomagnetic field. These disturbances are called “geomagnetic storms”. According to [30] the storm begins normally with a sudden increase in the horizontal component of the field (Fig. 2.4).

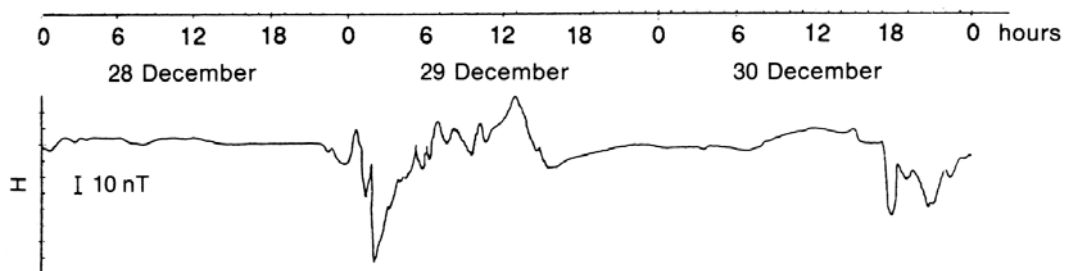


Fig. 2.4 Magnetic storm recorded at the Lannion station during December 1976 [30]

In medium or low geomagnetic latitudes this increase amounts to some tens of nanotesla in a few minutes. Similar variations are observed all over the earth. The increase of the field continues for some hours. This is the initial phase of the storm. Then the field decreases and

in a few hours it can fall to only one hundredth or one thousandth of the normal mean for a given point of observation. This is the main phase of the storm. After falling to a minimum, the horizontal component of the field will return to its mean value. This may take several hours or several days. During this period the field varies irregularly and is subject to micro pulsations lasting from several minutes to several hours. They may reach approximately one hundred gammas.

An electric field is associated with this variation; it is calculated by the relationship: $E/B=c$, assuming plane wave ($c=3 \times 10^8$ m/s – the speed of light), i.e. $E=3$ V/m if $B=10$ nT.

2.1.2 Atmospheric noise

The volume contained between the surface of the earth and the layer in the atmosphere at a height of approximately 50 km, known as the electrosphere, can be considered as a very big spherical capacitor. It is negatively charged on the ground surface and positively charged in the upper layers of the atmosphere. The voltage between the Earth and the electrosphere in regions of fine weather is about 300 kV. To maintain this voltage the Earth has about 10^6 C of negative charge on its surface, an equal positive charge being distributed throughout the atmosphere [151].

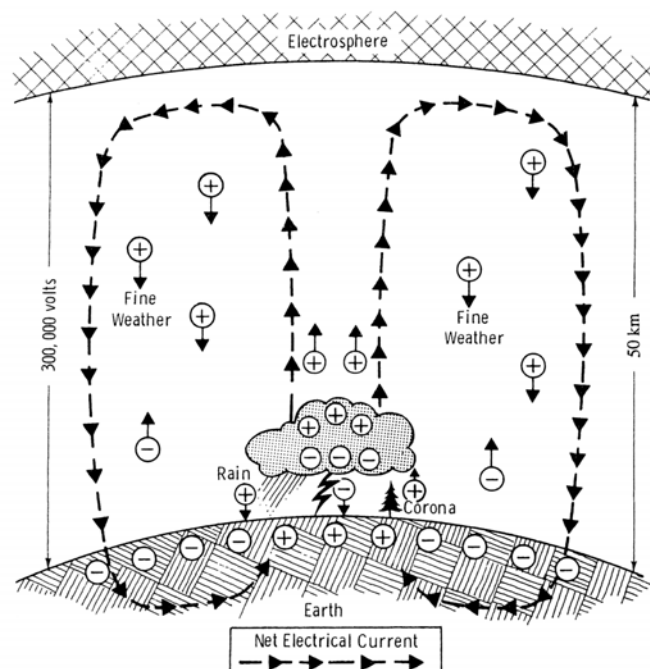


Fig. 2.5 Thunderstorm acting as a battery to keep the Earth charged negatively and the atmosphere charged positively [151]

The conductivity of the air between the Earth’s surface and the electrosphere can vary from 1.33×10^{-14} to 100×10^{-14} S/m, due to positive and negative ions formed in the atmosphere. Their density, which depends on numerous of factors, such as latitude, time, season, intensity of solar activity, defines the air conductivity. Because of this conductivity in regions of fine weather, atmospheric currents of the order of 1000 A are continuously depleting the charge between the surface of the earth and the electrosphere. The charge is apparently replaced by the action of thunderstorms including lightning. The thunderstorm system acts as a type of a battery to keep the fine weather system charged [151] (Fig. 2.5).

Approximately 2000 thunderstorms are simultaneously active around the Earth [30]. Taking into consideration the large number of lightning strokes occurring simultaneously around the globe and the fact that over much of their frequency spectrum the electromagnetic fields produced by the lightning are trapped within the earth - ionosphere waveguide, there is a resultant continuous noise or “atmospheric noise”. This noise dominates sometimes the other sources of electromagnetic disturbances such as those due to human activities, galactic noise and solar noise (Fig. 2.6).

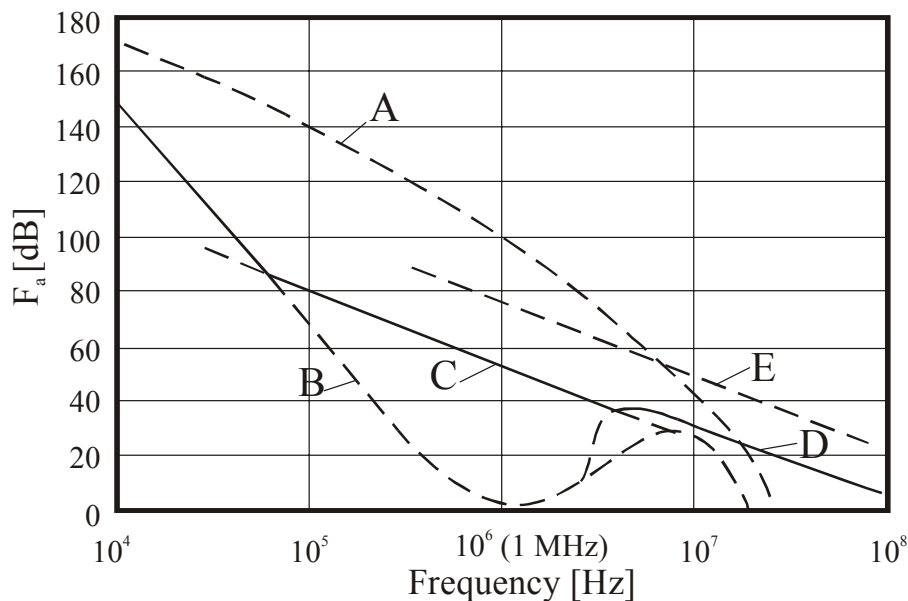


Fig. 2.6 External noise F_a as a function of frequency: A, atmospheric noise, the value is exceeded 0.5% of the time; B, atmospheric noise, the value is exceeded 99.5 % of the time; C, noise due to human activities, quiet receiving site; D, galactic noise; E, median value of the noise due to human activities in an industrial area. [30]

The amplitude scale on Fig. 2.6 is described by the equivalent noise factor expressed in decibels with [30]:

$$F_a = 10 \cdot \log(f_a) \quad (2.1)$$

with

$$f_a = \frac{P_n}{kT_0b} \quad (2.2)$$

where P_n is the mean power (W) received by an omnidirectional lossless antenna, k is Boltzmann's constant, T_0 is the reference temperature (288 K) and b is the receiver bandwidth (Hz).

From the noise factor F_a it is possible to determine the effective vertical electric field component. Although this presentation is acceptable for distant (galactic or solar) or continuous (thermal) noise sources, it is incomplete for atmospheric noise, which has a pulse character [30].

The curves of Fig 2.6 undergo diurnal and seasonal variations firstly because the quality of the ionospheric reflector differs widely between day and night and secondly because the daily development of the centers of thunderstorm activity depends on the season.

2.2 Disturbances due to human activities

Since the beginning of the industrial revolution and especially since the invention of the radio-transmission at the beginning of the last century, human activity has given rise to many forms of electromagnetic pollution. This electromagnetic pollution is called man-made electromagnetic noise. This noise interferes with radio-communication or data transmission and can cause degradation in the operation of the electronic systems. This noise predominates the noise of natural origin at frequencies above a few kHz in heavily industrialized urban surroundings [30].

The first cases of radio interference appeared at the beginning of the 20th century, at the time of the initiation of radio links and the arrival of cars with internal combustion engines, whose ignition systems were very quickly found to create difficulties with radio reception. These phenomena of interference or disturbance are now an everyday occurrence: receivers are interfered by illuminated signs, microcomputers are disturbed by electrical household appliances, electronic telephones pick up radio signals, and so on [30].

Therefore electromagnetic compatibility is becoming increasingly important in our contemporary world. In this section some of the main sources of man-made electromagnetic

disturbance are briefly reviewed (Fig. 2.8). Potential influence of such sources on electronic equipment is discussed.

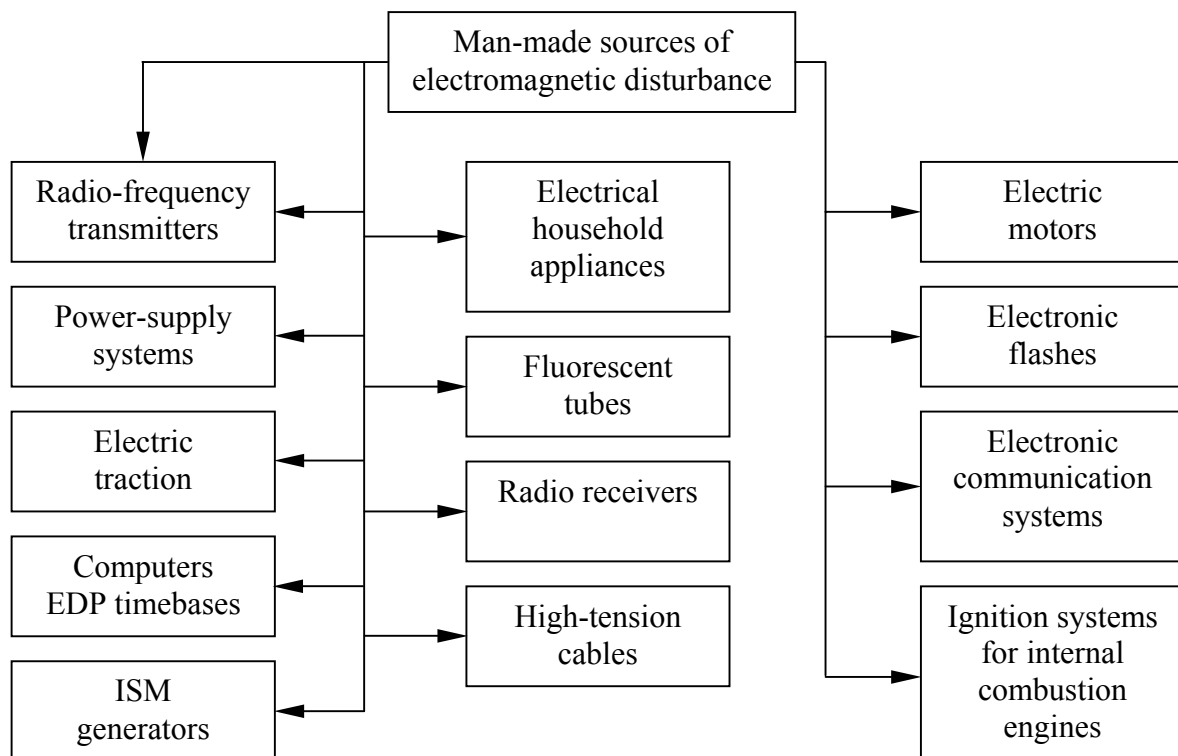


Fig. 2.8 The main sources of man-made electromagnetic noise [30]

The disturbance caused by electric and electronic equipment can be classified in the following way [30]:

- Intentional disturbance caused by radio transmitters;
- Unintentional disturbance caused by radiated or conducted signals from electrical and electronic equipment.

2.2.1 Disturbances caused by radio-frequency transmitters

A very large number of radio transmitters exist around the world, from remote-control systems for toys, radiating a power of some tens of microwatts, to airport radars having peak power levels of several megawatts. These emitters can sometimes interfere with the receivers of other radio services or even disturb the operation of electronic equipment that is either sensitive to, or inadequately protected from strong electromagnetic fields.

The transmitters with the biggest disturbance capacity are radio and television broadcasting transmitters and radars.

2.2.1.1 Radio and television broadcasting transmitters

Radio broadcasting transmitters create disturbances due to their high power (up to several MW). Sometimes they are installed in the vicinity of urban areas and can give rise to electromagnetic interference in electronic devices such as audio-frequency amplifiers, telephones, and tape recorders.

Table 2.1 gives the frequencies, powers, and distances resulting in a field of 1 V/m for some long-wave transmitters. 1 V/m is considered to be a relatively strong field that can cause disturbances or even lead to impaired operation of electronic or data-processing systems.

Station	Frequency (kHz)	Power (MW)	Distance (km) at which E=1 V/m
France Inter	162	2	7.8
Europe 1	183	1.8	7.3
RMS	216	1.7	7.1
RTL	234	1.7	7.1

Table 2.1 Examples of powerful long-wave transmitters in Western Europe [30]

These transmitters can disturb the operation of systems connected to very long power lines or telephone lines which act as receiving antennas. The high common-mode voltages thus picked up will disturb equipment connected to these lines.

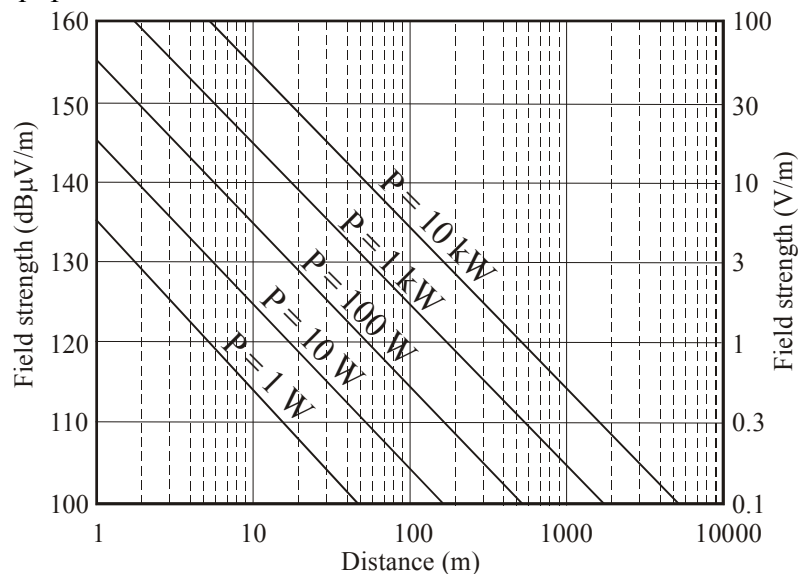


Fig. 2.9 Relationship between field and distance for given equivalent radiated power levels [30]

An important problem is associated with setting up local radio stations in the VHF band and locating their transmitting antennas in an urban area. If their transmitted power is excessive (it is sometimes higher than 10 kW), fields of over 1 V/m can be detected in buildings located on a line of sight from antennas and within one hundred meters of them (Fig. 2.9). Many electronic devices can be disturbed by direct radiation and considering the frequency involved, no effective external filtering is possible [30].

2.2.1.2 Radars

Radars are significant sources of radio disturbances in their near vicinity (i.e. in a range of less than 1 km) due to their high power and the nature of the signal they emit. The most seriously disturbing radars are those of air traffic control. They operate at frequencies between 1220 MHz and 1370 MHz and at peak powers of the order of 1.5 MW. Their antennas generally have a gain of approximately 30 dB in the main lobe. They emit RF pulses having durations of a few microseconds and a repetition rate of some 100 Hz. The antennas normally rotate at a speed of a few revolutions per minute.

Field measurements at a radius of 1 - 2 km around airport radars have shown peak electric field values between 3 and 120 V/m [30]. Under such conditions, certain analogue or digital equipment operating at low signal levels and insufficiently protected can be disturbed or even disabled.

Examples of disturbances caused by these radars to electrical household appliances using microprocessors, magnetic-tape playback equipment, or computer disks, have often been encountered. Precautions have also to be taken in order to protect direct satellite television receivers, whose intermediate frequencies lie between 900 and 1700 MHz.

In some cases, radars for air-movement control that use a magnetron as their radiation source emit non-essential unwanted signals at frequencies that are quite close to their fundamental frequency but outside the band allocated to them. They may thus interfere with other radio services, including radio transmissions in their vicinity [30].

2.2.2 Unintentional sources of radiation

Any electrical or electronic equipment can be a source of unintentional electromagnetic radiation or can be responsible for distributing undesired signals through the cables of the commercial power distribution network. Details are given in what follows

2.2.2.1 Industrial, scientific and medical (ISM) equipment

This equipment produces and uses radio-frequency energy for purposes other than telecommunications, for example, the welding of plastics, the drying of wood, the steaming and blanching of vegetables, the cooking of meals, and the defrosting of foodstuffs.

For the use of ISM equipment, the International Telecommunications Union (ITU) authorizes certain frequency bands.

Many ISM devices, particularly ovens or heating apparatus using induction, operate outside the frequency bands defined by the ITU. These devices use frequencies below 1 MHz. It should be noted that no frequency band below 6 MHz has been allocated by the ITU. The unwanted signals produced by ISM equipment are usually narrow-band sinusoids, accompanied by modulation that may or may not be intentional. Microwave ovens on the market use a frequency between 2400 and 2500 MHz with a power output of 300 to 1000 W. Until now, they have not created any particular interference problem, but the fifth harmonic of the frequencies they use lies within the band used by direct satellite television receivers. Therefore checks for EMC have to be made at 12 GHz [30].

2.2.2.2 Electronic data-processing (EDP) equipment

Computers and their peripheral equipment are the major part of data-processing equipment. They are intended for installation in offices and in industry, but are also used to an increasing extent by the general public in residential areas. The introduction of personal computers, video games, and so forth has multiplied the sources of radio-frequency disturbances. These devices are in fact potential sources of disturbance, not only because of their use of switched-mode power supplies but also because of their fast logic units, particularly quartz timebases serving to synchronize microprocessor systems, EHT (extra-high tension) power systems used in displays, and relays in printers or other electro-mechanical systems.

They can create a variety of conducted and radiated disturbances, of wide or narrow bands, but mainly the latter. The various sources of disturbance contained within the equipment are such that their combination causes disturbances spanning several decades of frequency, often ranging from a few kilohertz to several hundred megahertz.

At frequencies above a few megahertz the radiation from oscillators or quartz timebases is such that it can sometimes interfere with the reception in radiotelephones, private radio

networks, or television. Quartz oscillators in fact commonly emit rectangular-waveform signals at frequencies between 1 and 20 MHz. The harmonics of these signals are not negligible and extend to several hundred megahertz. Because of the rates of power they currently use, digital data-transmission systems are large disturbing sources in the range of VHF and UHF frequencies [30].

2.2.2.3 Ignition systems for internal combustion engines of vehicles

The radio environment in urban areas is very heavily affected by radio noise created by ignition systems in the internal combustion engines of vehicles.

In spite of the primary shielding provided by motor manufacturers, this remains the most widespread source of radio interference of artificial origin.

Measurements have shown that certain vehicles can radiate unwanted signals up to 10 GHz and can sometimes disturb digital wide-band radio systems installed in the vicinity of roads. Unwanted signals due to ignition are therefore a parameter to be taken into account in the design of digital radiotelephone systems having a high throughput. They limit the thresholds of reception of these types of radiotelephone.

The use of sparking plugs that are shielded by means of a resistor incorporated into the body of the plug or by resistive sparking-plug caps permits a noticeable (10-20 dB) reduction in these unwanted signals [30].

The list with the sources of man-made disturbance stated above is far from exhaustive, but the goal here was to draw attention to those most frequently encountered ones and to the effects of such disturbance signals. The analysis of disturbance sources is a very complex task. Sometimes, such sources are detected in places where they are at least expected with an electromagnetic field not exceeding a few $\mu\text{V}/\text{m}$. Each case should be treated individually and depends on the interaction between disturbing and disturbed equipment.

2.3 Electromagnetic compatibility - standards

In the previous section it was shown what a vast number of sources (natural and man-made), can cause electromagnetic pollution and unwanted electromagnetic interference with electric and electronic devices. Against natural sources no measures can be taken in order to reduce the magnitude of their intensity. But against man-made noise measures are taken and

implemented with electromagnetic compatibility standards that will be briefly described in this section.

Historical development of radio frequency disturbance control has always been limited to the range of the radio frequency spectrum in use at the time of the problem and the development of electromagnetic compatibility (EMC) specifications have followed the evolution of the electrical engineering technology. Since the invention of radio-frequency transmission and with the increased use of electric power, the emissions associated with electric arcs from switching, commutation and discharge processes required control. Because the frequency band associated with these sources was generally limited to 30 MHz, most efforts were spent on the lower frequency ranges. Later, some fast transients from ignition systems and commutator motors had a significant spectrum up to 300 MHz; therefore, emission control procedures and limits were developed up to 300 MHz [115].

From the 1970's, the increasing use of digital devices such as switching power supplies, monitors, microprocessors and central processors, due to the specific clock frequency they used, has broadened the international emission control requirements to 1000 MHz. For specific devices interference control is also required up to 40 GHz.

The origin of the first detailed and unified electromagnetic compatibility standards can be traced to the late 60's of the last century. These were MIL-STD-461, 462 and 463, published and used by the U.S. army [115]. The 461 document pertained to limits and requirements, 462 pertained to test techniques and configurations and 463 contained terms and definitions. For about a decade these standards were the only ones that were used not only by the military, but also by commercial organizations in America and Europe. For commercial organizations these standards were in the form of recommendations on how a product or a device should be produced, according to EMC requirements. They never had the force of a law.

Later, first in United States in 1979 and then in Europe in 1985, commercial EMC standards were developed and published. These standards already had the force of a law and were impossible to be waived. Any product which was sold on the market, should comply with the requirements imposed by these standards.

In the United States, the organization responsible for issuing the EMC standards is U.S. Federal Communication Commission (FCC). The FCC Rules and Regulations have several parts and are contained in Title 47 of the Code of Federal regulations [115]. Part 15 (also known as FCC Part 15) applies to radio frequency devices and has had a considerable impact on the electrical and electronic industry. The FCC Part 15 consists of three subparts:

- Subpart A: General requirements
- Subpart B: Unintentional radiators
- Subpart C: Intentional radiators

In Europe, the organization responsible for the control of radio interference is the International Special Committee on Radio Interference – generally identified as CISPR from its French name. It has the status of an international organization. The specification, published as CISPR 22 [115], concerns limits and methods of measurement of radio interference characteristics of information technology equipment (ITE). It is the European equivalent of the FCC Part 15B publication. This was Europe’s basic standard for EMC before adopting the unified European Community standards.

The initially published EMC standards were far from perfect. Therefore, they followed the progress of electrical and electronic industry and underwent further development. For example the originally published military standards MIL-STD-461, 462 and 463 have had several revisions and the current actual version is MIL-STD-461D and MIL-STD-462D, published in January 1993 [115].

In Europe, the actual EMC standards are contained in European Norms or EURONORMs (EN). They are based on the existing work of various organizations (including CISPR). In European Standards the CISPR numbering has been retained. For example, EN 55022 is the same as CISPR 22 [115]. EN 55022 is also adopted as a world standard not only in the European Community, but also in Japan as a voluntary standard and in the United States as an alternative to FCC Part 15B.

The difference between military and commercial standards is that the limits and applicability of the military standards are much more complicated than FCC or CISPR 22 requirements.

FCC Part 15B and EN 55022 (originated from CISPR 22) are not the only commercial standards (Table 2.2). There are a number of similar standards related to the different type of electric and electronic equipment such as industrial scientific and medical equipment, radio receivers and household appliances. Because of the importance and the extensive use of information technology equipment, and because their fundamental idea underlies in all other standards, FCC Part 15B and CISPR 22 standards will be briefly considered.

Denomination of the standard		Description
Europe	USA	
EN 55011	FCC Part 18	Emission standard for industrial, scientific and medical (ISM) equipment
EN 55013	FCC Part 15	Emission standard for Radio Receivers
EN 55014		Emission standard for appliances (household electrical equipment, portable tools and other electrical equipment)
EN 55015		Emission standard for fluorescent equipment
EN 55022 (CISPR 22)	FCC Part15	Emission standard for information technology equipment (ITE)
EN 60555		Emission standard for power line harmonics, generated by semiconductor-controlled power supplies
EN 50081-1		Standard for electrical and electronic apparatus for which no dedicated product or product-family emission standard exists, installed in residential, commercial and light-industrial locations and intended to be connected to a low voltage public power network
EN 50081-2		Standard for electrical and electronic apparatus for which no dedicated product or product-family emission standard exists, installed in industrial location and connected to an industrial power distribution network

Table 2.2 EMC standards in the European Community and the U.S.A.

In both standards the equipment is divided into two classes - Class A and Class B digital devices. Class A digital devices are intended for use in an industrial environment and Class B digital devices are intended for use in residential areas. The limits and requirements for Class B devices are more rigorous than the limits for Class A electronic devices. There are two reasons for that. In the first place it is assumed that there is more space in industrial buildings than in residential houses and devices are situated not so close to one another. Thus, the interference between them is not so strong as if they were situated in a residential area. The second reason is the assumption that the personnel, who operates this device in an industrial area is more experienced and will be able to handle or to correct the consequences of potential electromagnetic disturbances better than the home user. The limits that are covered by both standards concern *conducted* and *radiated* emissions of a digital product.

The conducted emissions are those currents that are passed out through the device's power supply cable and spread in the common power net, where they can cause interference with other devices either directly via the power cord cables or from the radiation of

electromagnetic energy from the power net cables due to the much larger length of these cables and their transformation in “radiating antennae” in this case. The limits for the conducted emissions extend from 150 kHz to 30 MHz for CISPR 22 standard and from 450 kHz to 30 MHz for FCC Part 15 requirements. CISPR requirements are extended and begin from 150 kHz in order to cover the emissions of switching power supplies, which successfully substitute linear power supplies due to their efficiency and light weight. The upper limit for both standards is 30 MHz. This is assumed to be the frequency where conduction along power wires converts to radiation. The measurements of conducted emissions are made using the line impedance stabilization network (LISN), which is inserted into the unit’s power cord. The limits are given in volts and more exactly in dB μ V because this is what is measured in the output of LISN. This voltage can be directly related to the current using equation (2.3) [104].

$$I_{measured} = \frac{I}{50\Omega} \cdot V_{measured} \quad (2.3)$$

The role of LISN is in the first place to block the external noise from the common power net and in the second place to ensure that constant impedance is connected to the equipment at the corresponding frequencies.

Radiated emissions concern the electric and magnetic fields radiated by the device that may be received by other electronic devices, causing interference in those devices. Both standards require measurements of the radiated electric field only. The limits are given in terms of that field. The radiated electric field is measured in dB μ V/m. The frequency range for radiated emissions begins for both standards at 30 MHz and extends to 1 GHz for CISPR 22 standard and up to 960 MHz for FCC Part 15 requirements. The measurements are made with measurement antennae in both vertical and horizontal polarization with respect to the ground plane. The distances between the test object and the measurement antennas are different for Class A and Class B devices as well as for the CISPR 22 and FCC Part15 limits. CISPR requires measurement distance of 10 m for Class B devices and 30 m for Class A devices. FCC Part 15 requires 3 m measurement distance for Class B devices and 10 m measurement distance for Class A devices. The CISPR 22 limits are summarized in Table 2.3 and FCC Part 15 requirements are summarized in Table 2.4

Frequency Range (MHz)									
0.15 ←———— 0.5 ←———— 5 —————→ 30 —————→ 230 —————→ 1000									
Measurement port	dB μ V		dB μ V		dB μ V		dB μ V/m	dB μ V/m	Notes
	QP	Avg	QP	Avg	QP	Avg	QP	QP	
AC Mains, A	79	66	73	60	73	60	-	-	Class A
AC Mains, B	66-56	56-46	56	46	60	50	-	-	Class B
Enclosure, A	-	-	-	-	-	-	30	37	At 30 m
Enclosure, B	-	-	-	-	-	-	30	37	At 10 m

Table 2.3 CISPR 22 conducted and radiated emission limits [115]

Frequency (MHz)	B limit		A limit	
Conducted emissions				
	μ V	dB μ V	μ V	dB μ V
0.45 – 1.705	250	48	1000	60
1.705 – 30	250	48	3000	69.5
Radiated emissions				
	μ V/m at 3 m	dB μ V/m at 3 m	μ V/m at 10 m	dB μ V/m at 10 m
30 – 88	100	40	90	39
88 – 216	150	43.5	150	43.5
216 – 960	200	46	210	46
> 960	500	54	300	49.5

Table 2.4 FCC Part 15 emission limits for Class A and Class B digital devices [115]

It is of interest to compare both standards – CISPR 22 and FCC Part 15. As far as radiated emissions are concerned, a method for scaling the measurements from one measurement distance to another should be used. In the comparison presented here, the inverse distance method is applied [104]. Using this method it is assumed that the emissions decrease proportionally with increasing distance to the measurement antenna. Thus, it is assumed that the emissions at 3 m would to be reduced by 3/10 of the source strength, if the measurement antenna is moved to a further distance of 10 m. To translate the Class B CISPR limits for a distance of 10 m to 3 m (Class B FCC limits), we add $20 \cdot \log_{10} (10/3) = 10.46 \text{ dB} \approx 10 \text{ dB}$ to the Class B CISPR limits, since moving the measurement point closer to the source is expected to increase the electric field levels that are measured [104].

The comparison between radiated emissions of CISPR 22 and FCC Part15 requirements is shown in Fig. 2.10 (a) and (b)

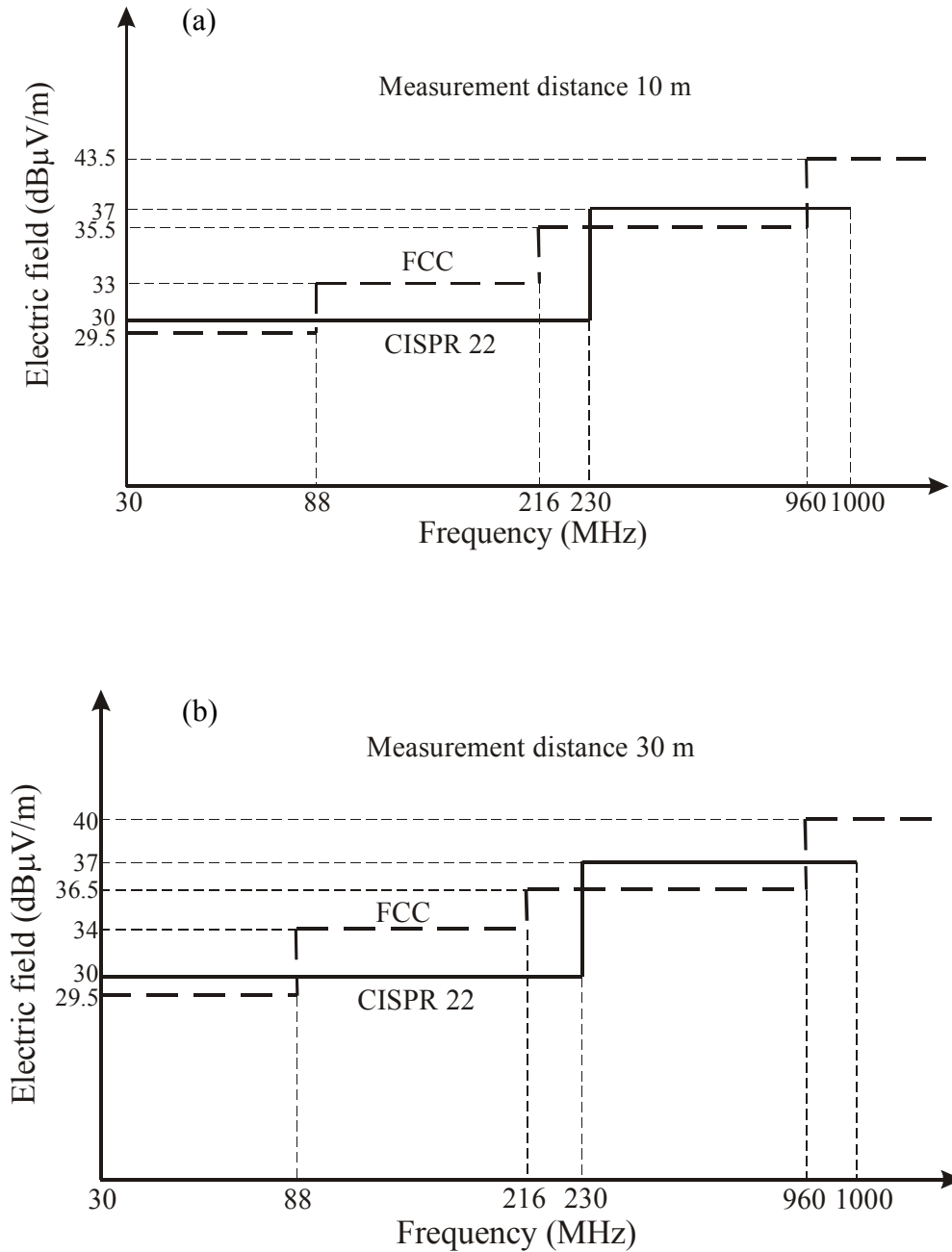


Fig. 2.10 Comparison between CISPR 22 and FCC Part 15 radiated emissions: (a) Class B; (b) Class A. [104]

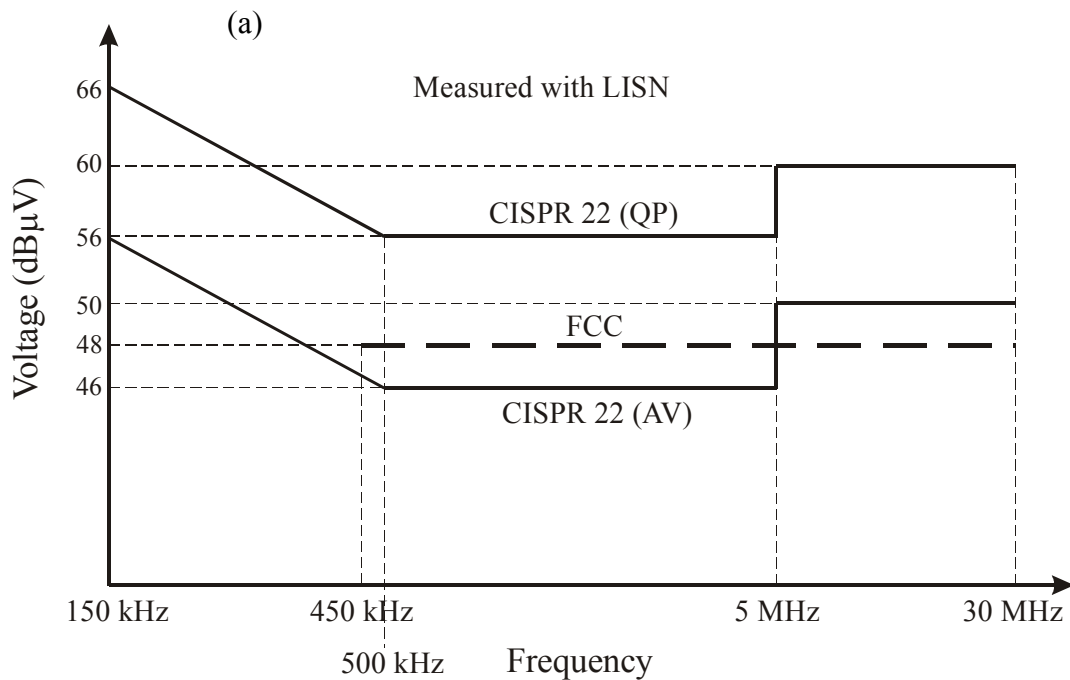
CISPR 22 Class B limits are compared with the FCC Class B limits extrapolated to a measurement distance of 10 m. This is done by subtracting 10.46 dB or approximately 10 dB

from the FCC Class B limits at 3 m to translate them to 10 m. From this comparison we see that in the frequency range from 30 MHz to 88 MHz FCC Class B limits are more restrictive than CISPR 22 Class B limits by about 0.5 dB. The CISPR 22 Class B limits are more restrictive than the FCC Class B limits in the frequency range of 88 - 230 MHz. From 88 to 216 MHz the CISPR 22 limits are 3 dB more restrictive, and from 216 to 230 MHz they are 5.5 dB more restrictive. From 230 to 960 MHz the FCC limits are more restrictive by about 1.5 dB [104].

The radiated emission limits for CISPR 22 Class A devices are measured at 30 m. The FCC Class A limits are translated to a 30 m measurement distance from their specified measurement distance of 10 m by subtracting 9.54 dB ($20 \cdot \log_{10} (10/30) = -9.54 \text{ dB}$) or approximately 10 dB. Again we see that in the frequency range from 30 MHz to 88 MHz FCC Class A limits are more restrictive than CISPR 22 Class A limits by about 0.5 dB. CISPR 22 limits for Class A digital devices are more restrictive than the FCC limits in the frequency range of 88 - 216 MHz by some 4 dB and 6.5 dB in the range of 216 - 230 MHz. From 230 to 960 MHz the CISPR 22 limits are less restrictive than the FCC limits by 0.5 dB [104].

From this comparison it can be concluded that there is almost no difference in the radiated limits proposed by these both standards.

The CISPR 22 and FCC limits on conducted emissions are compared in Fig. 2.11 (a) and (b)



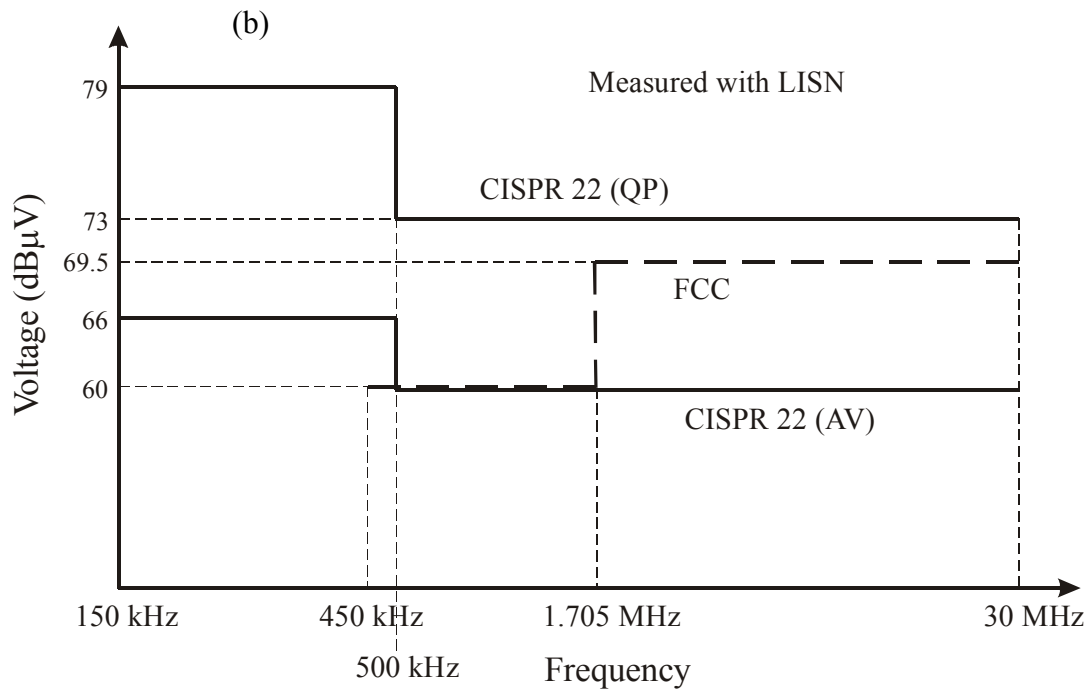


Fig. 2.11 Comparison between CISPR 22 and FCC Part 15 conducted emissions: (a) Class B; (b) Class A. [104]

A significant difference between the CISPR 22 and FCC conducted emission limits is in the frequency range of applicability. The CISPR 22 conducted emission limits extend down to 150 kHz instead of 450 kHz as for the FCC limits. Both extend to an upper limit of 30 MHz. The extension of the CISPR 22 lower limit is made in order to cover the emissions from switching power supplies that generate conducted noise in this frequency range [104].

The FCC Class B limits are 2 dB less restrictive than the CISPR 22 limits from 500 kHz to 5 MHz but, 2 dB more restrictive from 5 to 30 MHz. The CISPR 22 Class A limits are 9.5 dB more restrictive than the FCC Class A limits from 1.705 to 30 MHz.

The CISPR 22 limits for the conducted emissions are presented when the receiver uses a quasi-peak detector (QP) and when the receiver uses an average detector (AV). Both the FCC and CISPR 22 radiated emission limits and the FCC conducted emission limits apply to the use of a quasi-peak detector [104].

Chapter 3

3. Lightning discharge as a major source of interference

In the previous chapter it was described how the electromagnetic noise caused by the lightning activity around the earth sometimes dominates the other sources of natural electromagnetic noise. But not only this makes the lightning flash the source of disturbance with the most destructive potential. Its pulse character and the capability of releasing a large amount of energy within less than a second makes it the most dangerous threat compared to all other sources of electromagnetic disturbance. Therefore its hazardous range is much larger than that of any other source.

Another dangerous feature of the lightning is its stochastic nature. It is not known where exactly the lightning is about to strike, or what amount of the energy is to be released. The released energy can vary within wide ranges [30] thus making this event unpredictable. No satisfactory measures can be recommended if we want full protection of electronic devices.

In this chapter, it is briefly described what is known about this phenomenon and the available approaches for collecting information about it. A model for simulating the lightning strike is presented. This model will be used to evaluate the potential impact of a lightning strike over the low voltage transmission line laid under the ground.

3.1 The discharge process of negative cloud-to-ground lightning

According to [151], lightning is a transient high-current electric discharge with a path length of a few kilometres and a typical duration of about half a second. The most common source of lightning is the electric charge separated in ordinary thunderstorm clouds.

There are two types of lightning flashes: cloud-to-ground and cloud discharges. Cloud discharges, respectively, are divided into intracloud, cloud-to-cloud and cloud-to-air discharges. Approximately half the lightning discharges during a thunderstorm are intracloud discharges. In the second place are cloud-to-ground discharges. Cloud-to-cloud and cloud-to-air discharges are less common than the first two types of lightning discharges.

Cloud-to-ground lightning is more extensively studied than the other types of lightning discharge because of its destructive potential for people and man-made structures like power transmission lines or electronic equipment and because it is more easily photographed and studied with optical instruments.

Berger [13] made the first more detailed study of the cloud-to-ground lightning flashes. He categorized lightning in terms of the direction of motion, upward or downward and the sign of the charge, positive or negative, of the leader that initiated the discharge. The most common lightning that accounts for approximately 90 % of all statistical data is the one which is initiated by a downward-moving negatively charged leader and thereby lowers the negative charge to the earth. Less than 10 % of the lightning flashes are caused by downward-moving positively charged leaders. The other two types of lightning are characterized by leaders moving upwards from the ground to the cloud and hence a lightning flash branching upward. These two types of lightning are not so common and mainly occur on mountain tops or tall man-made structures.

Negative cloud-to-ground lightning discharges represent approximately 90 % of all cloud-to-ground lightning. Therefore, this discharge process with its specific components is briefly reviewed.

In chapter 2 it was mentioned that in the regions of fine weather the ground is negatively charged and the upper layer of the atmosphere, known as the electrosphere carries an equal positive charge. Contrary to this, in the areas of thunderstorm activity the ground is positively charged and the lower part of thunderstorm clouds is negatively charged. The discharge between the thunderstorm clouds and the earth that lowers the negative charge to the earth can be considered as a part of the global current circuit between electrosphere and the earth. (Fig. 2.5)

The whole process of the negative cloud-to-ground lightning is depicted in Fig. 3.1. The total discharge process is termed a *flash*. The flash consists of various discharge components among which there are several typical high-current pulses called *strokes* [151].

The flash begins with a downward moving *stepped leader*. The stepped leader is initiated by a *preliminary breakdown* in the lower part of the cloud between the negative (N) and small positively charged (P) regions (Fig. 3.1).

The stepped leader propagates from the cloud to the ground in a series of discrete steps, lowering the negative charge.

The steps are typically 1 μ sec in duration and tens of meters of length, with a pause time between steps of about 50 μ sec.

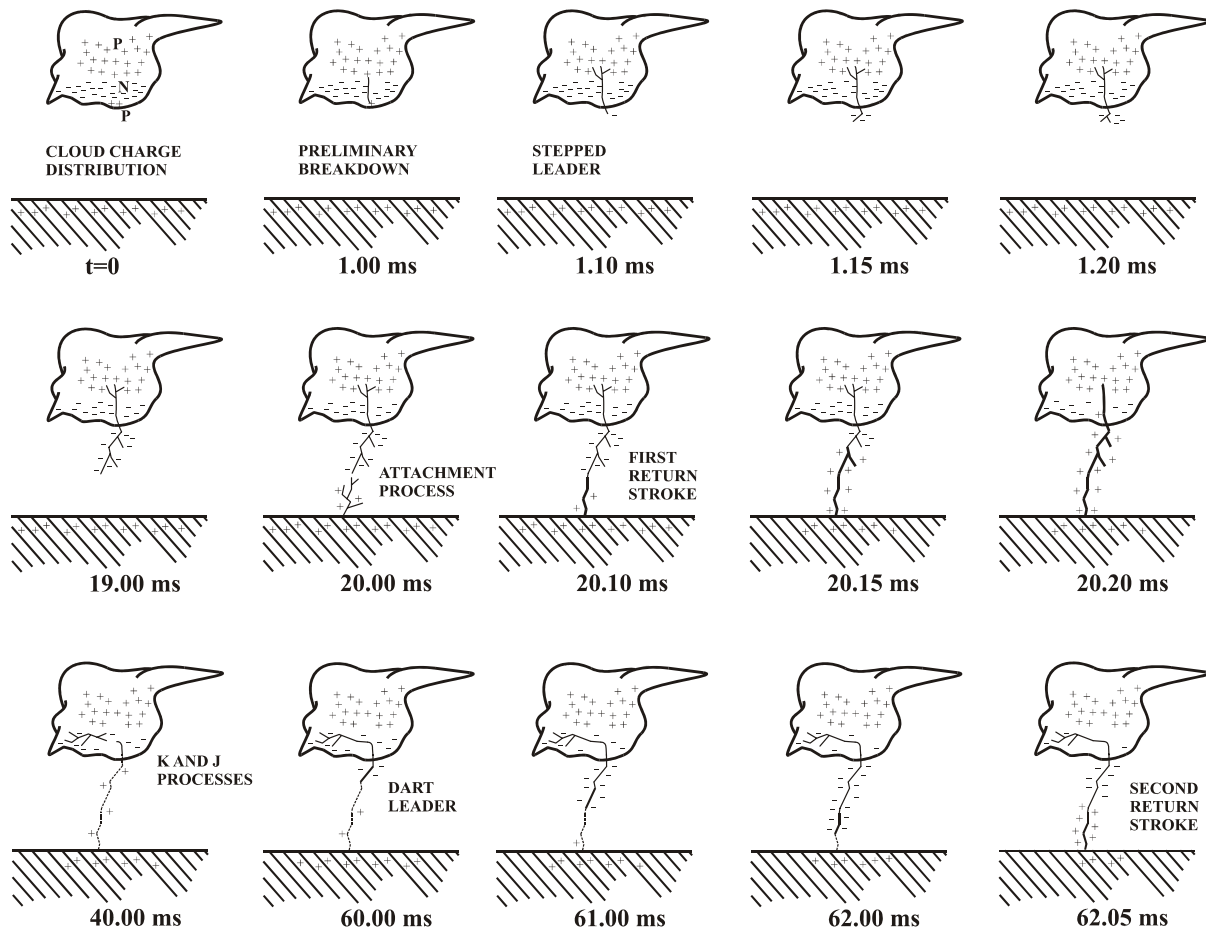


Fig. 3.1 A drawing illustrating negative cloud-to-ground lightning flash process (adapted from [151])

A fully developed stepped leader lowers up to 10 or more coulombs of negative cloud charge towards the ground in tens of milliseconds with an average download speed of about 2×10^5 m/sec. The average leader current is between 100 and 1000 A. The steps have peak pulse current of at least 1 kA [151].

During its progression towards the ground the stepped leader branches in a downward direction producing the downward-branched geometrical structure (Fig. 3.1).

The potential difference between the lower portion of the negatively charged downward propagating stepped leader and the earth has a magnitude that exceeds 10^7 V. As the tip of the leader approaches the ground, the electric field at sharp objects on the ground or at irregularities of the surface increases until it exceeds the breakdown value in air. At that time, one or more upward-moving discharges are initiated from those points, thus beginning the *attachment process*. When one of the upward-moving discharges from the ground contacts the downward-moving stepped leader some tens of meters above the ground, the leader is effectively connected to the ground potential. From this moment a continuous ionized channel from the ground to the cloud is established. Thus, the main discharge takes place. The leader channel is then discharged by an ionizing wave of ground potential that propagates up the previously ionized leader channel. This process is termed the *first return stroke*. It is characterized by an intense impulse current and an increase of luminosity in the lightning channel. The upward speed of a return stroke near the ground is typically one-third the speed of light. Its speed decreases with height. The total transit time between the ground and the cloud is of the order of 100 μ sec. The first return stroke produces a peak current near the ground of typically 30 kA, with a time from zero to a peak of a few microseconds. Currents measured at the ground fall to half the peak value in about 50 μ sec, and currents of the order of hundreds of amperes may flow for times of a few milliseconds up to several hundred milliseconds [152].

Some tens of milliseconds later (10 to 90 ms), after the first return-stroke current has ceased to flow, a *dart leader* may propagate down the residual first-stroke channel. The dart contrary to the stepped leader propagates continuously and more rapidly, while depositing less charge along the channel. The dart leader grounds a charge of the order of 1 C by virtue of a current of about 1 kA. The dart leader then initiates the *second* (or any *subsequent*) *return stroke*. Dart leaders and return strokes subsequent to the first are usually not branched. The time between return strokes in a flash is usually several tens of milliseconds, but can be tenths of a second if a continuing current flows in the channel after a return stroke. Continuing current magnitudes are of the order of 100 A and represent a direct transfer of charge from cloud to ground. Between 25% and 50% of all cloud-to-ground flashes contain a continuing current component [151].

In conclusion it can be stated that a lightning flash consists of a series of leaders and return strokes. Based on statistical data published in the literature, Thomson [144] calculated a mean number of 3,5 strokes per lightning flash.

As an example depicting the process of lightning discharge, Fig. 3.2 represents a hypothetical streak photograph and a corresponding still photograph of a three-stroke lightning flash.

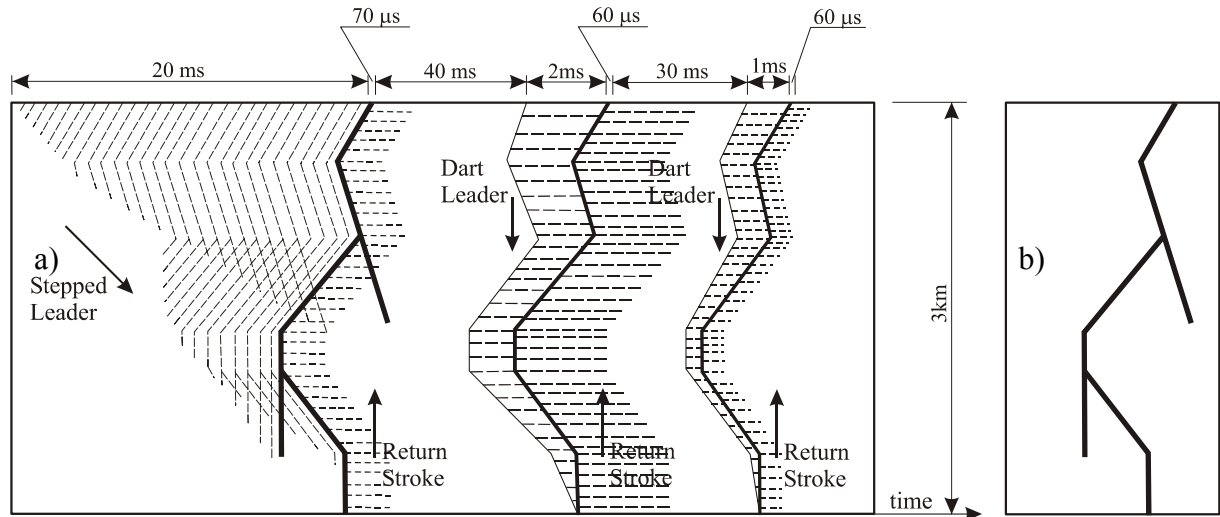


Fig. 3.2 Investigation of a lightning flash using photographic techniques: (a) hypothetical streak photograph; (b) the same lightning flash as would be recorded with a normal camera. (adapted from [30])

The next figure shows a record of the lightning current which flows at the base of the lightning discharge. The peaks in the current curve, whose magnitude is several tenths of kA correspond to the dart leader – return stroke sequences.

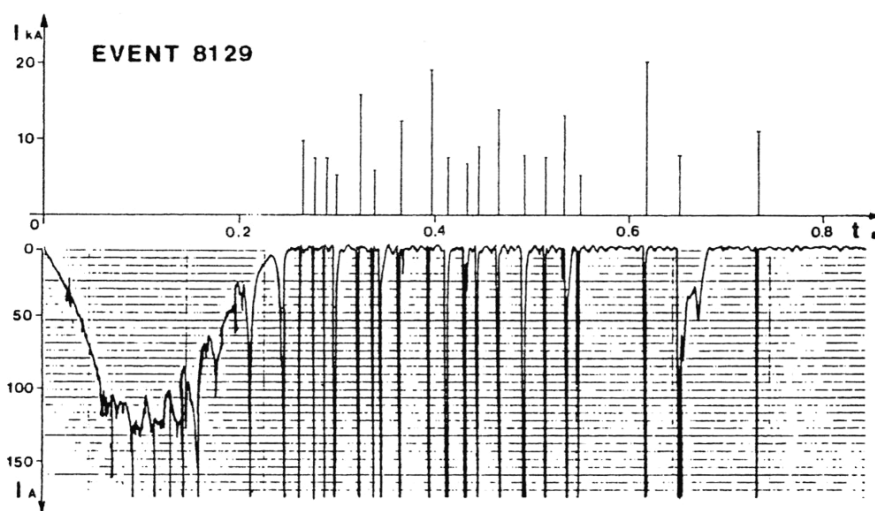


Fig. 3.3 Current at the channel base in rocket-initiated lightning discharge. [63]

3.2 The return strokes

The most profoundly investigated process is the return stroke process of negative cloud-to-ground lightning. A large number of the models simulating the lightning strike refer to it. The big interest in studying this process is quite normal. Both its components, namely the pulse current that propagates the lightning channel and the electromagnetic field generated by this current are the phases with the most destructive power of the entire lightning discharge process. From the point of view of electromagnetic compatibility the pulse radiation from the return stroke is the event that can cause the greatest disturbance in electrical devices and electronic equipment. As illustrated in Fig. 3.4, the pulse radiation of the electric field is more than 1 V/m at a distance of more than 200 km and exceeds 1kV/m at a distance of less than 1 km.

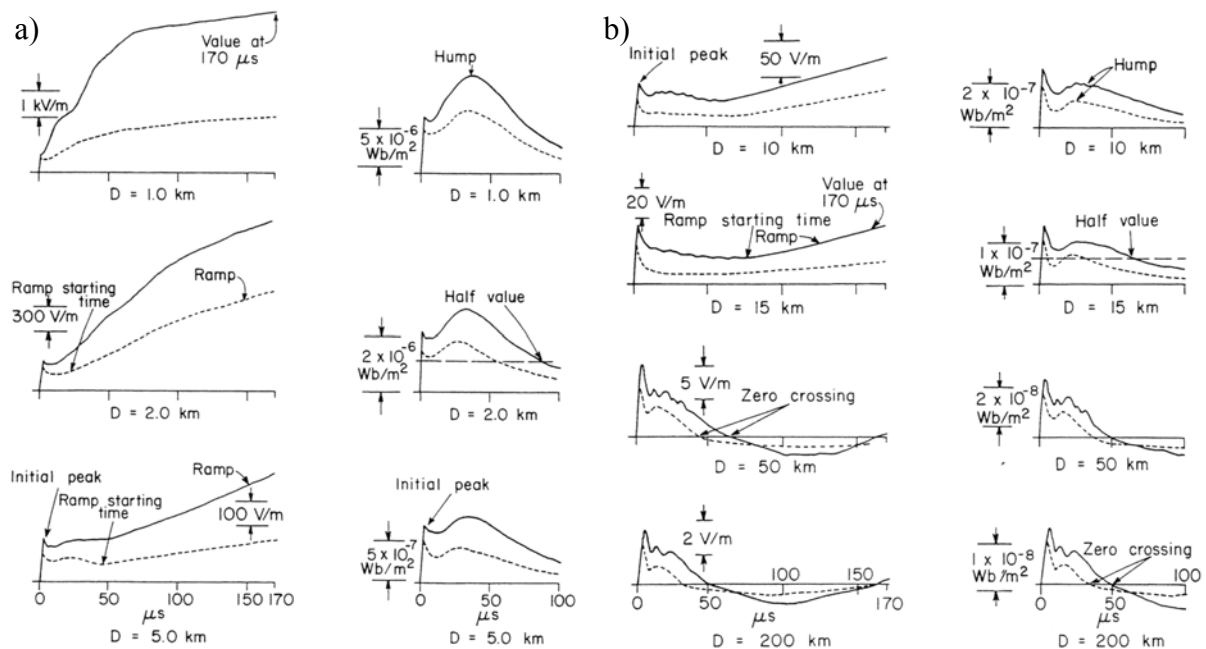


Fig. 3.4 Typical electric (left column) and magnetic field (right column) pulses for first strokes (full line) and subsequent strokes (broken line): (a) for distances of 1, 2 and 5 km; (b) for distances of 10, 15, 50 and 200 km; [78]

The figure presents the waveforms and amplitudes of typical first and subsequent return strokes electromagnetic pulses as functions of distance.

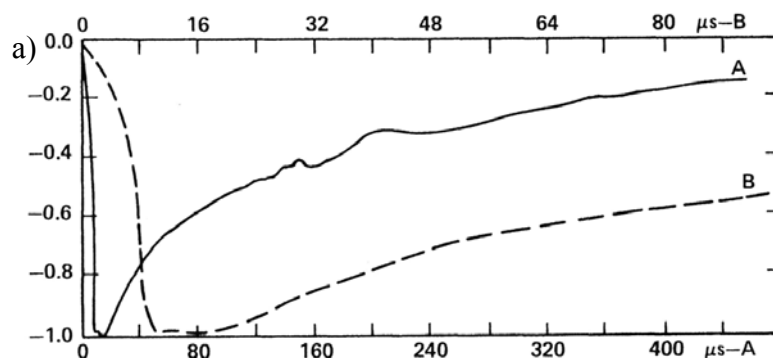
As becomes clear from the mathematical model presented below, the electric field consists of three components. An electrostatic component that decreases with the cube of the distance, an induced component that decreases with the square of distance and a radiated component that

decreases proportionally to the distance. The magnetic field is comprised only of induced and radiated components.

The influence of these components on the overall behaviour of the field can be clearly distinguished in the figure. In the case of the electric field at close range and after some tens of microseconds the electrostatic component becomes the dominant one. This is the only component which is non-zero after the stroke current has ceased to flow. It represents the new stage of the electric charge in the thundercloud. The behaviour of the magnetic field is somewhat different, but again at close range and after few microseconds a “hump” appears corresponding to the induced component of the field. At a range of 50 km and more, only the radiated component defines the curves for both the electric and magnetic fields. As can be seen from the figure at these distances both the electric and magnetic field waveshapes are identical and bipolar. The first peak in the waveshape, which can be identified for both the electric and magnetic fields at any distance, is mainly caused by the radiated component of the field.

3.2.1 Lightning current at the base of the channel

The most comprehensive description of the lightning return stroke current at the base of the lightning channel is made by Berger [13]. The currents were derived from measurements of the voltages induced in resistive shunts located at the tops of two towers, each of them with a height of 55 m situated at the top of Mt. San Salvatore in Lugano. Although only 10% of all lightning strikes to these towers were caused by downward moving negative stepped leaders, their number was enough for a representative statistical analysis, which is accepted and cited by many other authors. Fig. 3.5 shows the normalized average current waveshape for the negative first and subsequent return strokes observed in strikes to Mt. San Salvatore.



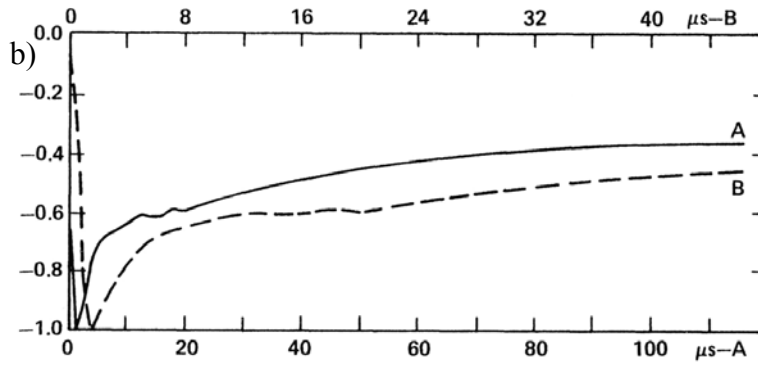


Fig. 3.5 Mean negative return-stroke current waveshapes normalized to unity peak amplitude and represented on two timescales: (a) first return stroke; (b) subsequent return strokes; [13]

As can be seen from the diagram, the amplitude and slope of the first stroke differ from those of subsequent strokes. The slope of the first stroke is weaker. From the statistical data in Table 3.9 it is also evident that the average amplitude of the first stroke is greater than that of the subsequent ones. The first stroke is also characterized by longer rise times than subsequent return strokes. Therefore, one has to distinguish the first from the subsequent return strokes. Rise time and maximum amplitude of the return stroke current are shown in Fig. 3.6.

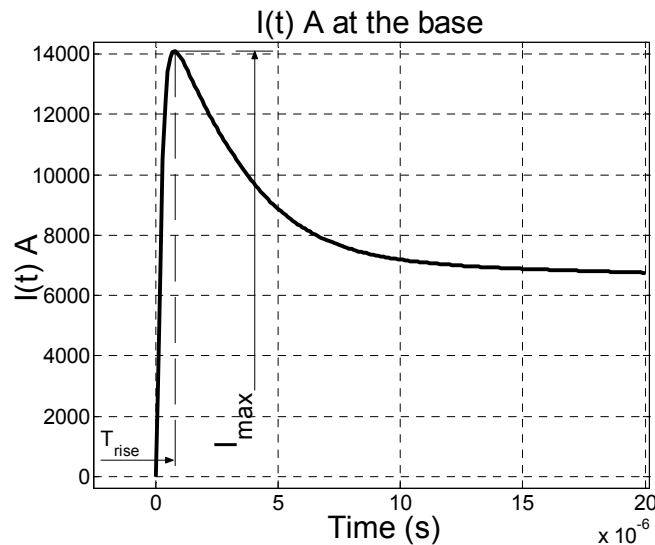


Fig. 3.6 Rise time and maximum amplitude of the return stroke current waveform

From the statistical data collected, Berger [13] concluded that lightning strike parameters follow a lognormal probability distribution. This conclusion was confirmed by subsequent statistical observation of the lightning phenomenon. It is now widely accepted among the lightning researchers that lightning parameters are log-normally distributed. The peak current for the first stroke is generally thought to have a median value in the range of 20 - 40 kA.

Subsequent stroke peak currents have a median value of approximately 12 kA, as can be seen in Table 3.9. The median of the subsequent stroke current amplitude is about half that of the first stroke. From Table 3.9 it is evident also that the rise time of the first stroke is considerably longer than those of subsequent strokes. The median of the first stroke rise time is about 5.5 μs , compared to 1.1 μs in subsequent ones.

Another very important parameter is the maximum derivative dl/dt of the pulse. This parameter is important because very often the amplitudes of the voltages and currents induced in electrical installations by coupling with the lightning electromagnetic field are proportional to it. According to Berger [13], the median value of the peak current derivative is 40 kA/ μs for the subsequent strokes, compared to 12 kA/ μs for the first return stroke. In more recent publications [77], some authors state the value of this parameter to be about 110 kA/ μs for the subsequent strokes. Anyway, this parameter is subject to controversy and according to Thottappillil [146] measurements conducted by Berger for the peak current derivative have suffered from limited bandwidth and limited time resolution of the original oscilloscopic traces and therefore, his values are so small compared to the data stated in recent publications.

Another interesting parameter is the charge deposited to the ground by the return stroke. It can be determined by integrating the current waveform over time. As indicated in Table 3.9 the value of this parameter for subsequent return stroke is about 1.4 C.

3.2.2 Mathematical modeling of the subsequent return stroke current waveform

The simulations performed in the present work concern primarily the consequences of subsequent return strokes on electric cables. Therefore, from now on emphasis will be placed on the description of the subsequent return stroke. The main feature of the process which has to be modeled, is the current waveform at the base of a lightning channel. In early publications concerning the modeling of lightning, the following analytical expression for the simulation of the current waveform was proposed [30]:

$$I(t) = I_0(e^{-\alpha t} - e^{-\beta t}) \quad (3.1)$$

with parameters I_0 , α and β given in Table 3.1. These correspond to a current amplitude of approximately 12 kA, and a rise time of about 1 μs . The current waveform is shown in Fig. 3.7a.

I_0 (kA)	α (s ⁻¹)	β (s ⁻¹)
12.3	3x10 ⁴	1x10 ⁷

Table 3.1 Common parameters for equation (3.1)

In more recent publications concerning the simulation of the subsequent return stroke, a more appropriate analytical expression was proposed. The expression consists of the sum of two so-called Heidler's functions [57]:

$$I(t) = \frac{I_{01}}{\eta_1} \frac{(t/\tau_{11})^n}{1+(t/\tau_{11})^n} \cdot e^{-t/\tau_{12}} + \frac{I_{02}}{\eta_2} \frac{(t/\tau_{21})^n}{1+(t/\tau_{21})^n} \cdot e^{-t/\tau_{22}} \quad (3.2)$$

In eq. (3.2):

$$\eta_i = e^{-(\tau_{i1}/\tau_{i2}) \cdot (n \cdot \tau_{i2}/\tau_{i1})^{1/n}} \quad i=1,2 \quad (3.3)$$

and:

I_{0i} - amplitude parameter of the channel base current;

τ_{i1} - front time constant;

τ_{i2} - decay time constant;

η - amplitude correction factor;

n - exponent (2 ... 10);

Parameters of equation (3.2) for the typical current waveform at the base of a lightning are given in Table 3.2.

Func. № (i)	I_{0i} (kA)	τ_{i1} (μs)	τ_{i2} (μs)	n	$\eta_i = \exp[-(\tau_{i1}/\tau_{i2})(n\tau_{i2}/\tau_{i1})^{1/n}]$
1	10.7	0.25	2.5	2	0.639407319
2	6.5	2.1	230	2	0.873599903

Table 3.2 Parameters for equation (3.2), representing a common lightning strike

The current waveform calculated with these parameters is represented in Fig. 3.7b. On the figure are also plotted the two Heidler functions, which compose the equation.

It should be noted that the analytical expressions for the current waveforms computed with the parameters of Tables 3.1 and Table 3.2, respectively, agree with the median subsequent return stroke current waveform obtained from the statistical data in Table 3.9. These give an average peak current of 12 kA and an average rise time of 1.1 μs.

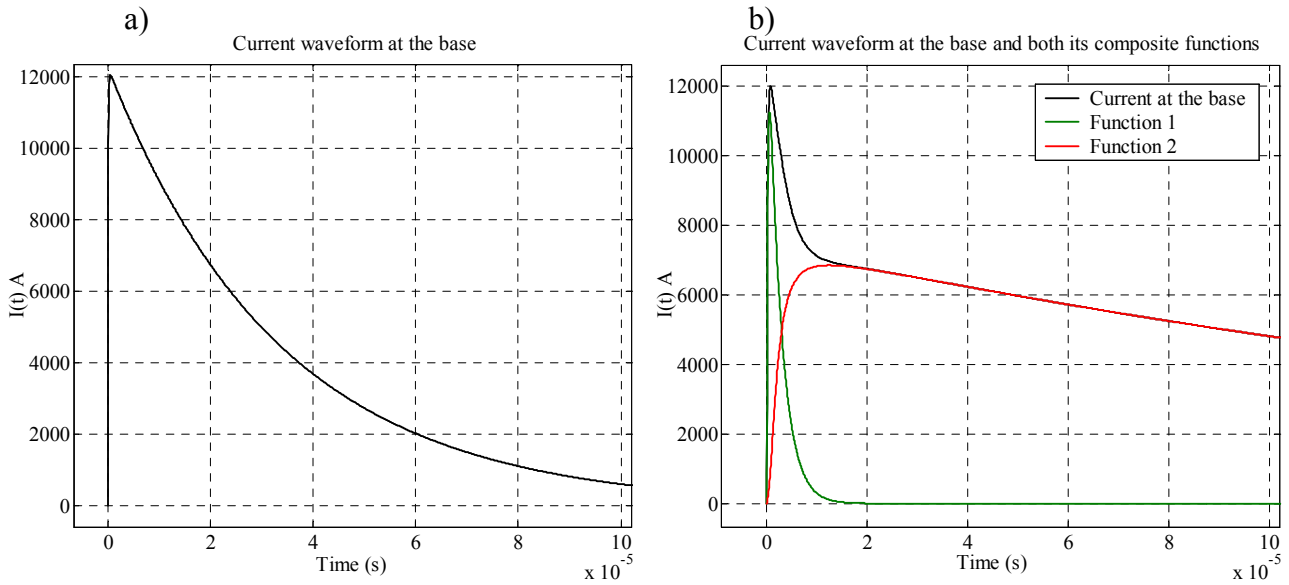


Fig. 3.7 Lightning current waveform used for simulations: (a) Waveform used in early simulations and computed with equation (3.1); (b) Waveform used at present and computed with equation (3.2);

Equation (3.2) is preferred to the double exponential function (equation (3.1)) because it allows one to easily change return stroke current amplitude, maximum current derivative and the electrical charge transferred to the ground by simply exchanging I_{0i} , τ_{i1} and τ_{i2} respectively. Equation (3.2) also has a time derivative equal to zero at $t=0$, which is in agreement with the measured waveshapes of return stroke currents. Furthermore, as is evident from Fig. 3.8, the charge deposited to the ground by the return stroke using these two expressions is approximately 0.4 C for equation (3.1) and 1.7 C for equation (3.2).

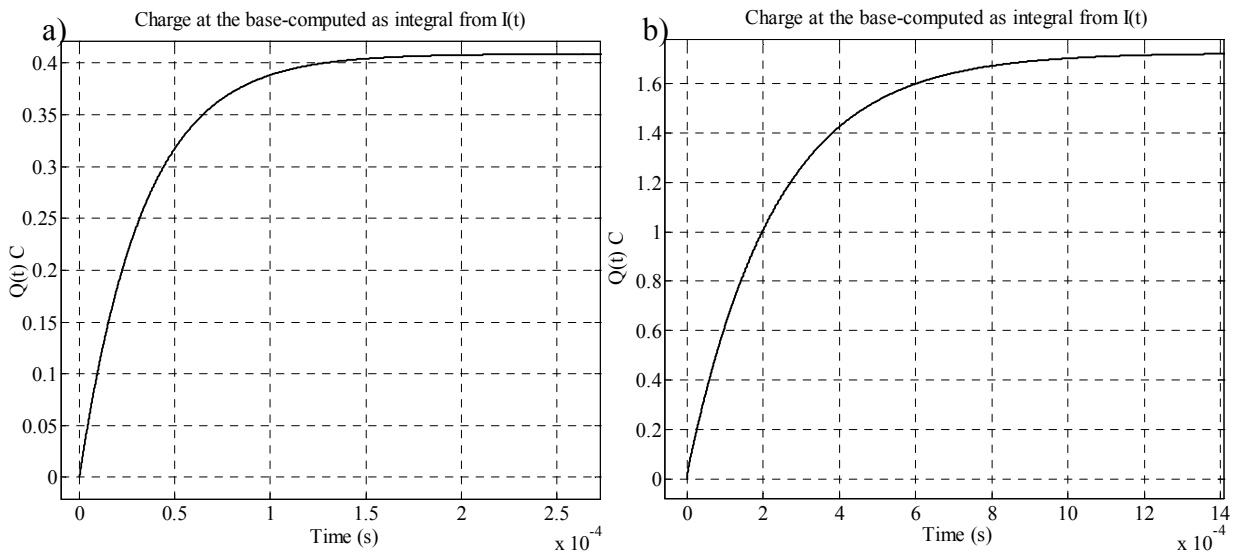


Fig. 3.8 Electrical charge deposited to the ground computed as an integral from (3.1) or (3.2): (a) Integration of equation (3.1); (b) Charge obtained using equation (3.2);

Table 3.9 indicates that the median value for the charge deposited to the ground by the subsequent return stroke is about 1.4 C. Equation (3.2) is closer to this value than equation (3.1). Therefore, equation (3.2) is more appropriate for simulation models.

Another important aspect of the lightning current waveform is its stochastic nature. The specific parameters which define the waveform, are maximum current I_{\max} and rise time T_{rise} . These two parameters are considered to be well described by a log-normal distribution. The parameter values for their distributions are given in Table 3.3.

Parameters of a lightning	Distribution Parameters according to eq. (3.38)	
	μ	σ
I_{\max} (kA)	2.485	0.557
T_{rise} (μs)	0.095	0.856

Table 3.3 Values for the lognormal distribution of the lightning current parameters derived from experimental data

The probability density functions for I_{\max} and T_{rise} based on data from Table 3.3 are shown in

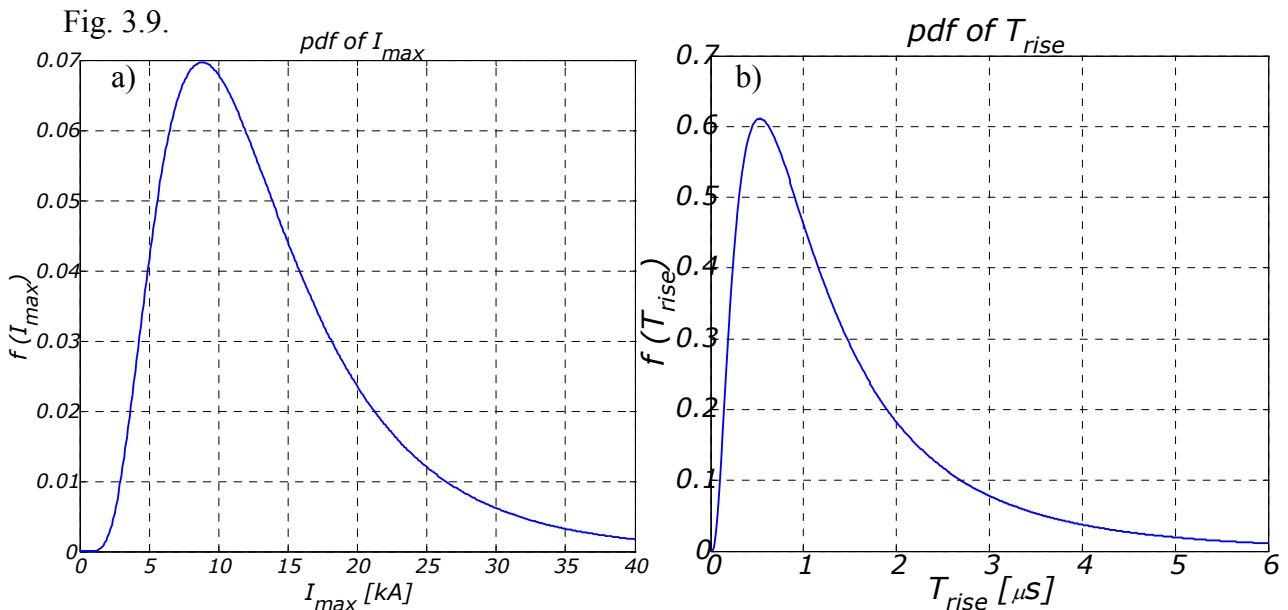


Fig. 3.9 Lognormal probability distributions: (a) Maximum current I_{\max} ; (b) Rise time T_{rise} .

The 5th, 50th and 95th percentile values of I_{\max} and T_{rise} are important for the simulations. According to probability density functions shown in Fig. 3.9 these values are:

- I_{\max} : 4.6 kA (5%), 13 kA (50%), 30 kA (95%);
- T_{rise} : 0.22 μs (5%), 1.1 μs (50%), 4.5 μs (95%);

In order to simulate the current waveform with equation (3.2) making all the possible combinations for I_{\max} and T_{rise} , parameters I_{0i} , τ_{i1} and τ_{i2} should be specified. Table 3.4 gives such sets of example combinations.

Lightning current waveshape properties	Parameters for equation (3.2)					
	I_{01}	τ_{11}	τ_{12}	I_{02}	τ_{21}	τ_{22}
$I_{\max}=4.6$ kA; $T_{\text{rise}}=0.22$ μs	4300	0.5×10^{-7}	2.2×10^{-6}	1800	2.1×10^{-6}	1.8×10^{-4}
$I_{\max}=4.6$ kA; $T_{\text{rise}}=1.1$ μs	4300	4.8×10^{-7}	2.5×10^{-6}	1800	2.8×10^{-6}	1.8×10^{-4}
$I_{\max}=4.6$ kA; $T_{\text{rise}}=4.5$ μs	4700	33.0×10^{-7}	4.0×10^{-6}	1900	5.0×10^{-6}	1.6×10^{-4}
$I_{\max}=13$ kA; $T_{\text{rise}}=0.22$ μs	12200	0.5×10^{-7}	2.2×10^{-6}	6300	2.1×10^{-6}	2.1×10^{-4}
$I_{\max}=13$ kA; $T_{\text{rise}}=0.7$ μs	11700	2.5×10^{-7}	2.5×10^{-6}	6500	2.1×10^{-6}	2.3×10^{-4}
$I_{\max}=13$ kA; $T_{\text{rise}}=1.1$ μs	12000	4.8×10^{-7}	2.5×10^{-6}	6200	2.8×10^{-6}	2.1×10^{-4}
$I_{\max}=13$ kA; $T_{\text{rise}}=4.5$ μs	12700	33.0×10^{-7}	4.0×10^{-6}	6200	5.0×10^{-6}	1.8×10^{-4}
$I_{\max}=30$ kA; $T_{\text{rise}}=0.22$ μs	28000	0.5×10^{-7}	2.5×10^{-6}	15000	2.1×10^{-6}	2.3×10^{-4}
$I_{\max}=30$ kA; $T_{\text{rise}}=1.1$ μs	28000	4.8×10^{-7}	2.4×10^{-6}	15000	2.8×10^{-6}	2.1×10^{-4}
$I_{\max}=30$ kA; $T_{\text{rise}}=4.5$ μs	29000	33.0×10^{-7}	4.0×10^{-6}	14000	5.0×10^{-6}	1.8×10^{-4}

Table 3.4 Example combination sets for the parameters of equation (3.2) enabling calculation of the current waveform with different values for I_{\max} and T_{rise}

After substitution of one set of parameters given by Table 3.4 into equation (3.2), a current waveform with desired I_{\max} and T_{rise} can be calculated.

3.2.3 Electromagnetic field produced by the lightning discharge

Due to the current that flows in the lightning channel, an electromagnetic field is radiated from the lightning. The visible part of the spectrum of this field represents only a small part of the whole electromagnetic energy, dissipated by the lightning stroke. The instantaneous energy released from the stroke is so big that, even at the distance of 100 km, the amplitude of the electric field pulse wave amounts to several V/m. As explained above the initial peak in the electric field caused by the return stroke current that propagates the lightning channel is caused mainly by the radiation component of the field. This component, as stated in [151], decreases inversely with distance if there are no significant propagation effects. Thus, the initial peak fields produced by return strokes at known different distances can be normalized for comparison, e.g. to 100 km. This is achieved by simply multiplying the measured field by $D/100$ where D is the stroke distance in kilometers.

Figure 3.10 shows an example of the electric field change of a four-stroke flash, which contains also and long continuing current after the third return stroke. The flash in the figure was recorded during a thunderstorm in Tampa, Florida on July 27, 1979 at a distance of 6.5 km from its origin. Initial electric field peaks due to return strokes normalized to 100 km are also shown on the diagram and are labeled E_p .

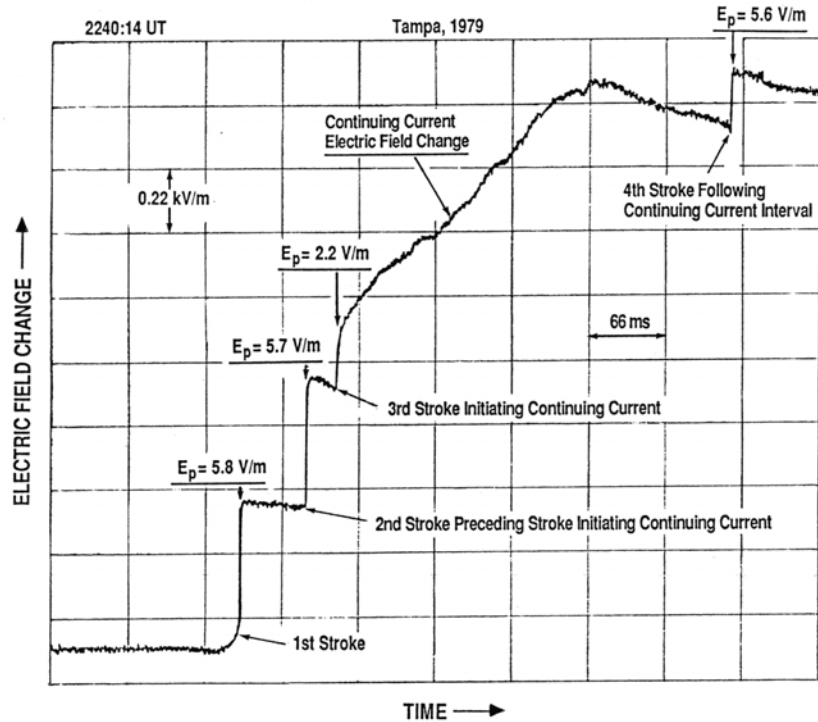


Fig. 3.10 Overall electric field change for a four-stroke flash with long continuing current following the third stroke [123]

It is evident from the figure that the fast transitions of the electric field are caused by the return strokes within the flash. These fast transitions are the main source of disturbance to the electric and electronic equipment.

Statistics on the normalized initial peak electric field derived from various studies, are presented in Table 3.5.

	First strokes			Subsequent strokes		
	№ of strokes	Mean	SD	№ of strokes	Mean	SD
Initial peak, normalized to 100 km (V/m)						
Master <i>et al.</i> (1984)	112	6.2	3.4	237	3.8	2.2
Krider and Guo (1983)	69	11.2	5.6	84	4.6	2.6
	31	8.8	4.0	31	6.0	1.9
Cooray and Lundquist (1982)	553	5.3	2.7			
McDonald <i>et al.</i> (1979)	54	5.4	2.1	119	3.6	1.3
McDonald <i>et al.</i> (1979)	52	10.2	3.5	153	5.4	2.6
Tiller <i>et al.</i> (1976)	75	9.9	6.8	163	5.7	4.5
Lin <i>et al.</i> (1979)						
[KSC]	51	6.7	3.8	83	5.0	2.2
[Ocala]	29	5.8	2.5	59	4.3	1.5
Taylor (1963)	47	4.8				
Zero-to-peak risetime (µsec)						
Master <i>et al.</i> (1984)	105	4.4	1.8	220	2.8	1.5
Cooray and Lundquist (1982)	140	7.0	2.0			
Lin <i>et al.</i> (1979)						
[KSC]	51	2.4	1.2	83	1.5	0.8
[Ocala]	29	2.7	1.3	59	1.9	0.7
Tiller <i>et al.</i> (1976)	120	3.3	1.0	163	2.3	0.9
Lin and Uman (1973)	12	4.0	2.2	83	1.2	1.1
Fisher and Uman (1972)	26	3.6	1.8	26	3.1	1.9
10-90% risetime (µsec)						
Master <i>et al.</i> (1984)	105	2.6	1.2	220	1.5	0.9

Slow front duration (μsec)						
Master <i>et al.</i> (1984)	105	2.9	1.3			
Cooray and Lundquist (1982)	82	5.0	2.0			
Cooray and Lundquist (1985)	104	4.6	1.5			
Weidman and Krider (1978)	62	4.0	1.7	44	0.6	0.2
	90	4.1	1.6	120	0.9	0.5
Slow front, amplitude as percentage of peak						
Master <i>et al.</i> (1984)	105	28	15			
Cooray and Lundquist (1982)	83	40	11			
Cooray and Lundquist (1985)	108	44	10			
Weidman and Krider (1978)	62	52	20	44	20	10
	90	40	20	120	20	10
Fast transition 10-90% risetime (nsec)						
Master <i>et al.</i> (1984)	1020	970	680	217	610	270
Weidman and Krider (1978)	38	200	100	80	200	40
	15	200	100	34	150	100
Weidman and Krider (1980, 1984)	125	90	40			

Table 3.5 Statistics on return-stroke vertical electric field from strokes lowering negative charge to the ground [151]

It is evident from the table that the mean of the electric field initial peak value normalized to 100 km is generally found to be in the range of 5 - 10 V/m for the first stroke and of 4 - 6 V/m for the subsequent strokes. Additionally, some other parameters of the initial electric field as for example the rise time of the pulse are given also in the table.

3.2.4 Mathematical model of the electromagnetic field radiated by the subsequent return stroke

The model presented here is mainly applicable to the subsequent return stroke because it considers the lightning channel as a straight unidimensional antenna above a perfectly conducting ground plane. This assumption can be applied to the subsequent return stroke because it is not branched, contrary to the first return stroke which is broadly branched. The equations describing the model are introduced in the frequency domain. This holds also for the calculated results. The transformation of the results into the time domain is achieved using the inverse fast Fourier transform. The first goal in deriving the model for calculating the lightning stroke fields is to find the field radiated by a current element of infinitesimal length dl , the so called Hertzian dipole, located at the origin of the spherical coordinate system (Fig. 3.12). Starting point are Maxwell's equations [112] which give the relations between the electric and magnetic fields at any point of free space:

$$\nabla \times \hat{\mathbf{E}} = -j\omega\mu_0\hat{\mathbf{H}} \quad (3.4a)$$

$$\nabla \times \hat{\mathbf{H}} = j\omega\varepsilon_0\hat{\mathbf{E}} + \hat{\mathbf{J}} \quad (3.4b)$$

$$\nabla \cdot \epsilon_0 \hat{\mathbf{E}} = \hat{\rho} \quad (3.4c)$$

$$\nabla \cdot \hat{\mathbf{H}} = 0 \quad (3.4d)$$

Equations (3.4a) to (3.4d) describe the relationship between the electric field $\hat{\mathbf{E}}$ and the magnetic field $\hat{\mathbf{H}}$ in the presence of a material characterized by three parameters: the permittivity ϵ , the permeability μ and the conductivity σ (in the case of empty space these are permittivity ϵ_0 and permeability μ_0). According to eqs. (3.4a) and (3.4b), a time-varying electric field produces a time-varying magnetic field and vice-versa. Equation (3.4c) relates the electric flux $\epsilon_0 \hat{\mathbf{E}}$ to the electric charge ρ and (3.4d) is an confirmation of the absence of the magnetic charge (the magnetic lines are closed lines without beginning or end).

Although it is possible to derive general vector wave equations for the $\hat{\mathbf{E}}$ and $\hat{\mathbf{H}}$ fields, a simpler solution is to introduce the vector and scalar potential functions $\hat{\mathbf{A}}$ and $\hat{\Phi}$ from which the fields may be evaluated as:

$$\hat{\mathbf{H}} = \frac{1}{\mu_0} \nabla \times \hat{\mathbf{A}} \quad (3.5)$$

$$\hat{\mathbf{E}} = -\nabla \hat{\Phi} - j\omega \hat{\mathbf{A}} \quad (3.6)$$

The potentials $\hat{\mathbf{A}}$ and $\hat{\Phi}$ are related by the Lorentz condition:

$$\nabla \cdot \hat{\mathbf{A}} = -j\omega \mu_0 \epsilon_0 \hat{\Phi} \quad (3.7)$$

After a few transformations using the above stipulations, it is possible to show that the vector potential function $\hat{\mathbf{A}}$ satisfies the following form of the wave equation:

$$\nabla^2 \hat{\mathbf{A}} + \beta_0^2 \hat{\mathbf{A}} = -\mu_0 \hat{\mathbf{J}} \quad (3.8)$$

where $\beta_0 = \omega \sqrt{\mu_0 \epsilon_0} = \frac{\omega}{c}$ and $c=3.0 \times 10^8$ m/s is the speed of light in vacuum.

In a rectangular coordinate system, equation (3.8) becomes the following set of equations:

$$\nabla^2 \hat{A}_x + \beta_0^2 \hat{A}_x = -\mu_0 \hat{J}_x \quad (3.9a)$$

$$\nabla^2 \hat{A}_y + \beta_0^2 \hat{A}_y = -\mu_0 \hat{J}_y \quad (3.9b)$$

$$\nabla^2 \hat{A}_z + \beta_0^2 \hat{A}_z = -\mu_0 \hat{J}_z \quad (3.9c)$$

The integral form of the solution to each of these equations is [112]:

$$\hat{A}_x = \frac{\mu_0}{4\pi} \int_{v'} \frac{\hat{J}_x e^{-j\beta_0 R}}{R} dv' \quad (3.10a)$$

$$\hat{A}_y = \frac{\mu_0}{4\pi} \int_{v'} \frac{\hat{J}_y e^{-j\beta_0 R}}{R} dv' \quad (3.10b)$$

$$\hat{A}_z = \frac{\mu_0}{4\pi} \int_{v'} \frac{\hat{J}_z e^{-j\beta_0 R}}{R} dv' \quad (3.10c)$$

or in vector form:

$$\hat{\mathbf{A}} = \frac{\mu_0}{4\pi} \int_{v'} \frac{\hat{\mathbf{J}} e^{-j\beta_0 R}}{R} dv' \quad (3.10d)$$

In these equations, v' encloses $\hat{\mathbf{J}}$ and R is the distance between a differential volume element (the source point) and the point at which $\hat{\mathbf{A}}$ is computed as illustrated in Fig. 3.11.

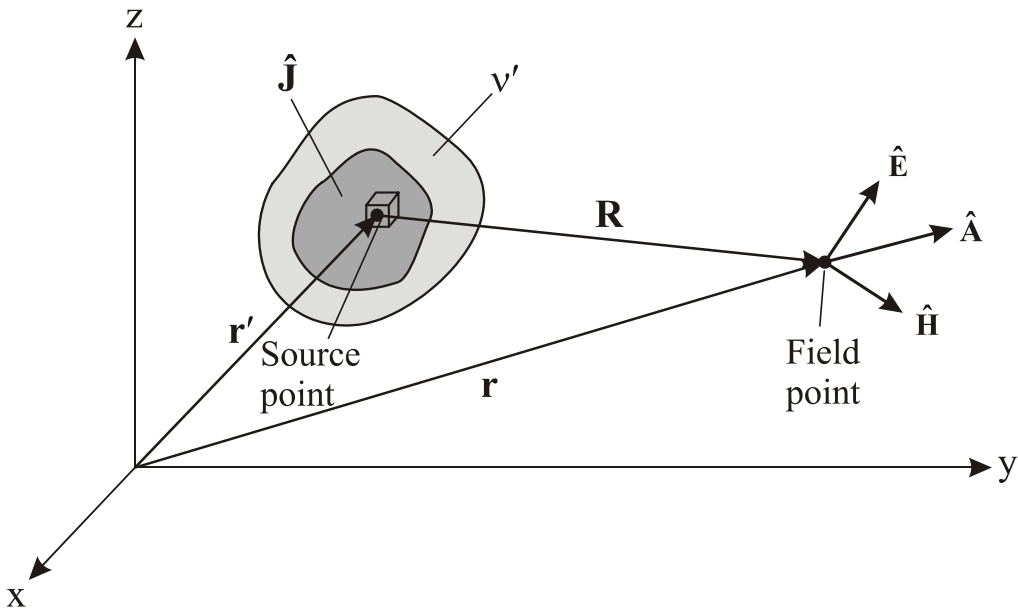


Fig. 3.11 Computation of the fields due to a given current distribution

Therefore, if we know the current distribution along the structure, we can compute the vector potential function $\hat{\mathbf{A}}$ and find from this function the $\hat{\mathbf{E}}$ and $\hat{\mathbf{H}}$ fields produced by the structure at every point in the space.

After this short introduction to electromagnetic field theory, it is now possible to compute the fields produced by a Hertzian dipole, as illustrated in Fig. 3.12.

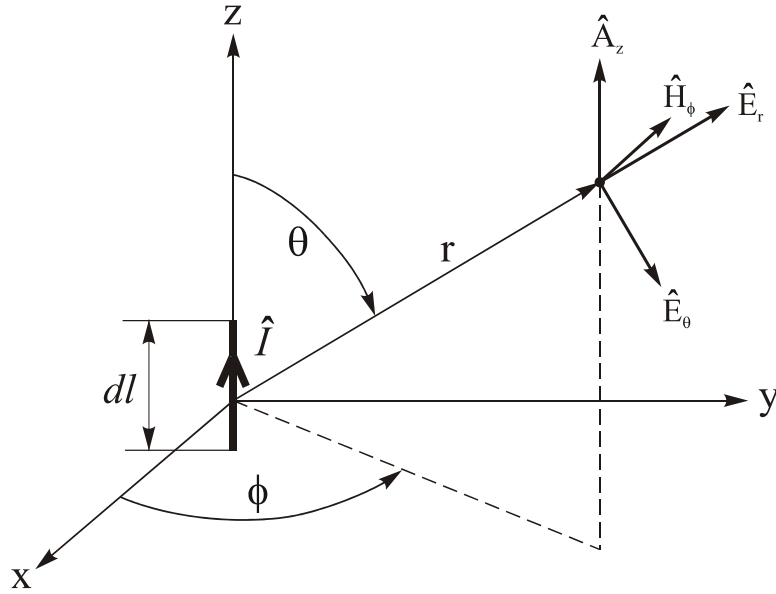


Fig. 3.12 Elemental hertzian dipole antenna in spherical coordinate system

The antenna consists of an infinitesimal current element of length dl carrying a phasor current \hat{I} that is assumed to be the same (in magnitude and phase) at all points along the element length. The element is placed for convenience at the origin of a spherical coordinate system. From Fig.3.12 we see that the vector potential function $\hat{\mathbf{A}}$ in eq. (3.10) has only a z component, which can be determined from (3.10c). Assuming the element length to be infinitesimal, equation (3.10c) reduces to:

$$\hat{A}_z = \frac{\mu_0}{4\pi} \hat{I} \cdot dl \frac{e^{-j\beta_0 r}}{r} \quad (3.11)$$

In spherical coordinates:

$$\hat{A}_r = \hat{A}_z \cos \theta \quad (3.12a)$$

$$\hat{A}_\theta = -\hat{A}_z \sin \theta \quad (3.12b)$$

$$\hat{A}_\phi = 0 \quad (3.12c)$$

Now, by using equation (3.5) it is possible to determine the components of the magnetic field as:

$$\hat{H}_r = 0 \quad (3.13a)$$

$$\hat{H}_\theta = 0 \quad (3.13b)$$

$$\hat{H}_\phi = \frac{\hat{I} \cdot dl}{4\pi} \beta_0^2 \sin \theta \left(j \frac{1}{\beta_0 r} + \frac{1}{\beta_0^2 r^2} \right) e^{-j\beta_0 r} \quad (3.13c)$$

The electric field components can be obtained from the magnetic field via Ampere's law at points away from the current distribution ($\hat{\mathbf{J}}=0$)

$$\hat{\mathbf{E}} = \frac{1}{j\omega\epsilon_0} \nabla \times \hat{\mathbf{H}} \quad (3.14)$$

After substitution of (3.13) in (3.14) the following components of the electric field are obtained:

$$\hat{E}_r = 2 \frac{\hat{I} \cdot dl}{4\pi} \eta_0 \beta_0^2 \cos\theta \left(\frac{1}{\beta_0^2 r^2} - j \frac{1}{\beta_0^3 r^3} \right) e^{-j\beta_0 r} \quad (3.15a)$$

$$\hat{E}_\theta = \frac{\hat{I} \cdot dl}{4\pi} \eta_0 \beta_0^2 \sin\theta \left(j \frac{1}{\beta_0 r} + \frac{1}{\beta_0^2 r^2} - j \frac{1}{\beta_0^3 r^3} \right) e^{-j\beta_0 r} \quad (3.15b)$$

$$\hat{E}_\phi = 0 \quad (3.15c)$$

where

$$\eta_0 = \sqrt{\frac{\mu_0}{\epsilon_0}} \quad (3.16)$$

is the intrinsic impedance of empty space.

Now it is possible to apply the equations derived above in order to find the fields radiated by the lightning. As indicated in Fig. 3.13, the lightning channel is presented as a straight wire antenna with height H situated above a perfectly conducting ground.

The field radiated by the element dz' at a height z' above the ground is the same as the field radiated by the Hertzian dipole.

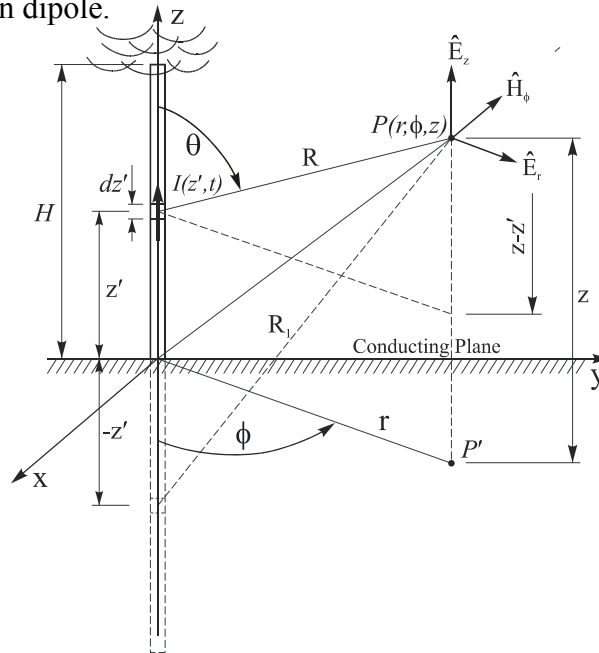


Fig. 3.13 Representation of the lightning channel geometry used for the derivation of the lightning field components

In order to obtain the field components in cylindrical coordinates as illustrated in Fig. 3.13, it is necessary to transform spherical coordinate into cylindrical ones. The transformation of the spherical components of the field into the cylindrical coordinate system is:

$$\hat{E}_\rho = \hat{E}_r \sin \theta + \hat{E}_\theta \cos \theta \quad (3.17a)$$

$$\hat{E}_z = \hat{E}_r \cos \theta - \hat{E}_\theta \sin \theta \quad (3.17b)$$

$$\hat{H}_\phi = \hat{H}_\phi \quad (3.17c)$$

Now, shifting the dipole location to a point z' in the cylindrical coordinate system shown in Fig. 3.13 and performing the operations from (3.17) in (3.13) and (3.15), in order to transform the components to cylindrical coordinates, the following equations for the field components at a point P can be developed (using the notations from Fig. 3.13).

$$d\hat{E}_r(r, \phi, z, j\omega) = \frac{\hat{I}(z', j\omega) \cdot dz'}{4\pi\epsilon_0} \left[\frac{3r(z-z')}{R^5} \frac{1}{j\omega} + \frac{3r(z-z')}{cR^4} + \frac{r(z-z')}{c^2R^3} j\omega \right] e^{-j\omega R/c} \quad (3.18a)$$

$$d\hat{E}_z(r, \phi, z, j\omega) = \frac{\hat{I}(z', j\omega) \cdot dz'}{4\pi\epsilon_0} \left[\frac{2r(z-z')^2 - r^2}{R^5} \frac{1}{j\omega} + \frac{2r(z-z')^2 - r^2}{cR^4} - \frac{r^2}{c^2R^3} j\omega \right] e^{-j\omega R/c} \quad (3.18b)$$

$$d\hat{H}_\phi(r, \phi, z, j\omega) = \frac{\hat{I}(z', j\omega) \cdot dz'}{4\pi} \left[\frac{r}{R^3} + \frac{r}{cR^2} j\omega \right] e^{-j\omega R/c} \quad (3.18c)$$

The complete electromagnetic field radiated by the lightning assuming perfectly conducting ground can be obtained by integrating (3.18) with respect to the z' coordinate in the lightning channel from 0 to H and over the image of the channel under the ground from 0 to $-H$. Using (3.18) the fields can be expressed as: (the subscript p designates that these are equations obtained assuming perfectly conducting ground)

$$\hat{E}_{rp}(r, z, j\omega) = \frac{1}{4\pi\epsilon_0} \int_{-H}^H \hat{I}(z', j\omega) e^{-j\omega R/c} \left[\frac{3r(z-z')}{R^5} \frac{1}{j\omega} + \frac{3r(z-z')}{cR^4} + \frac{r(z-z')}{c^2R^3} j\omega \right] dz' \quad (3.19a)$$

$$\hat{E}_{zp}(r, z, j\omega) = \frac{1}{4\pi\epsilon_0} \int_{-H}^H \hat{I}(z', j\omega) e^{-j\omega R/c} \left[\frac{2(z-z')^2 - r^2}{R^5} \frac{1}{j\omega} + \frac{2(z-z')^2 - r^2}{cR^4} - \frac{r^2}{c^2R^3} j\omega \right] dz' \quad (3.19b)$$

$$\hat{H}_{\phi p}(r, z, j\omega) = \frac{1}{4\pi} \int_{-H}^H \hat{I}(z', j\omega) e^{-j\omega R/c} \left[\frac{r}{R^3} + \frac{r}{cR^2} j\omega \right] dz' \quad (3.19c)$$

As is evident from eq. (3.19) and depicted in Fig. 3.13, in the cylindrical coordinate system the electromagnetic field radiated by the lightning strike has three components: one magnetic component, namely the azimuthal magnetic field - $\hat{H}_{\phi p}$, and two electric components - horizontal and vertical electric field \hat{E}_{rp} and \hat{E}_{zp} . The analysis of the expressions for the

electric field components reveals that there are three terms in the bracketed part of the integrand. The first term, which is inversely proportional to the cube of the distance is called electrostatic or near field. The second component is inversely proportional to the square of the distance and is called electric induction or intermediate field. The third term is reciprocally proportional to the distance and is called electric radiation field. The magnetic component of the field has only the latter two terms, namely induction and radiation terms.

Assuming the ground is a perfect conductor, calculations based on equations (3.19b) and (3.19c) for the vertical electric and azimuthal magnetic field at distances which do not exceed a few kilometers, are correct. As stated by several authors [93], [45, pp.377-400], at greater distances attenuation and distortions of the field when propagating along an imperfectly conducting ground are no longer negligible. The intensity of the horizontal component of the electric field is more affected by the finite conductivity of the ground. There are several approaches proposed in the literature [120] for obtaining correct results. The best, however, are the results calculated with the so-called Cooray-Rubinstein formula

$$\hat{E}_r(r, z, j\omega) = \hat{E}_{rp}(r, z, j\omega) - \hat{H}_{\phi}(r, 0, j\omega) \frac{c\mu_0}{\sqrt{\epsilon_{rg} + \sigma_g / j\omega\epsilon_0}} \quad (3.20)$$

Using this formula the field is computed from the horizontal field assuming perfectly conducting ground and subtracting a correction factor which is based on the azimuthal magnetic field on the ground multiplied by an expression which represents the surface impedance of the finitely conducting ground.

3.2.5 Simulation models for the return stroke

In order to calculate the electromagnetic field radiated by the lightning using the equations introduced in the previous sub-section, a model for the current distribution along the lightning channel $\hat{I}(z', j\omega)$ has to be applied. Therefore, here we concentrate on models which relate the remote electromagnetic field to the lightning channel currents.

There are basically three levels of sophistication in the mathematical modeling of return strokes. The most sophisticated models describe the detailed physics of the lightning channel in terms of the equations of the conservation of mass, momentum and energy, equations of state and Maxwell's equations. These types of models require a detailed knowledge of physical parameters such as the ionization and recombination coefficients and thermodynamic properties such as the thermal and electrical conductivities [30]. Using this approach, it is

possible to predict the channel current as a function of vertical distance from the surface of the earth and time. Once the expression for the current has been derived, the remote electric and magnetic fields can be calculated from the equations presented above.

A less sophisticated level of modeling involves mathematically describing the return stroke channel as a transmission line characterized by resistance (R), inductance (L) and capacitance (C), with circuit elements which vary with height and time. The intention again is to predict a channel current as a function of height and time and then to use this current to calculate the fields.

The so-called “engineering” models are inscribed in the least sophisticated approach of modeling. In these models a spatial and temporal distribution of the channel current is specified based on such observed lightning return stroke characteristics as current at the channel base, the speed of the upward propagating front and the channel luminosity profile. In these models the physics of the lightning return stroke is deliberately ignored and emphasis is placed on achieving agreement between the model-predicted electromagnetic fields and those observed at distances from tens of meters to hundreds of kilometers. While in the first two types of models there are a large number of adjustable parameters, the number of the latter in “engineering” models is small, usually one or two besides the measured or assumed channel base current.

Although the first type of models gives realistic results, they are very complex and are not appropriate for use when the influence of the lightning on the conductor lines is considered. They are more appropriate if a better understanding of the lightning discharge process is sought. The second type of models, so-called R-L-C transmission line models also lead to a more complex formulation without yielding any substantial improvement in the results obtained from the “engineering” models. Therefore, emphasis will be put on the “engineering” modeling of the current distribution along the lightning channel.

3.2.6 “Engineering” models for the simulation of the return stroke process

An “engineering” return stroke model is defined as an equation which relates the longitudinal channel current $I(z',t)$ at any height z' and any time t to the current at the base of the lightning channel ($z'=0$). An equivalent expression in terms of the charge density $\rho(z',t)$ on the channel can be obtained using the continuity equation:

$$\nabla \cdot \mathbf{J} = -\frac{\partial \rho}{\partial t} \quad (3.21)$$

Equation (3.22) gives the expression which describes in general form the most used “engineering” models [125].

$$I(z', t) = u(t - z'/v_f)P(z')I(0, t - z'/v) \quad (3.22)$$

where u is the Heaviside function equal to unity for $t \geq z'/v_f$ and zero elsewhere, $P(z')$ is the height-dependent current attenuation factor, v_f is the upward propagating front speed (also called return stroke speed) and v is the current-wave propagation speed.

In Table 3.6 $P(z')$ and v are summarized for five of the most frequently used “engineering” models, namely the transmission line model TL [153]; the modified transmission line model with linear current decay with height MTLL [122]; the modified transmission line model with exponential current decay with height MTLE [91]; the Bruce-Golde model BG [17] and the traveling current source model TCS [57].

	Model	P(z')	v
TL	<i>(Uman and McLain)</i>	1	v_f
MTLL	<i>(Rakov and Dulzon)</i>	$1 - z'/H$	v_f
MTLE	<i>(Nucci et al.)</i>	$\exp(-z'/\lambda)$	v_f
BG	<i>(Bruce and Golde)</i>	1	∞
TCS	<i>(Heidler)</i>	1	$-c$

Table 3.6 P(z') and v for five “Engineering” models (adapted from [125])

In Table 3.6 H is the total channel height, λ is the current decay constant (assumed to be 2000 m) and c is the speed of light.

The three simplest models, namely TCS, BG and TL are illustrated in Fig 3.14a and TCS and TL models additionally are shown in Fig. 3.14b.

It is assumed that all three models have the same current waveform at the channel base ($z'=0$) and the same front speed v_f represented in the $z' - t$ coordinates by the slanted line labeled v_f . The current wave speed is represented by the line labeled v which coincides with the vertical axis for the BG model and with the v_f for the TL model. For each model current versus time waveforms at the channel base ($z'=0$) and at height z'_1 and z'_2 are shown. Because of the finite front propagation speed v_f , the current at heights z'_1 and z'_2 begins with a delay z'_1/v_f and z'_2/v_f , respectively, compared to the current at the channel base. The shaded portion of the waveform indicates the current which actually flows through a given channel section. The blank portion is shown only for illustrative purpose. The relation between the TL and TCS models is further illustrated in Fig. 3.14b. It is shown that the spatial

current wave moves into the positive z' direction for the TL model and in the negative z' direction for the TCS. It should be noted that the current at the ground ($z'=0$) and the upward moving front speed v_f are the same for both TL and TCS models. Here again the shaded portion of the waveform indicates the current which actually flows in the channel.

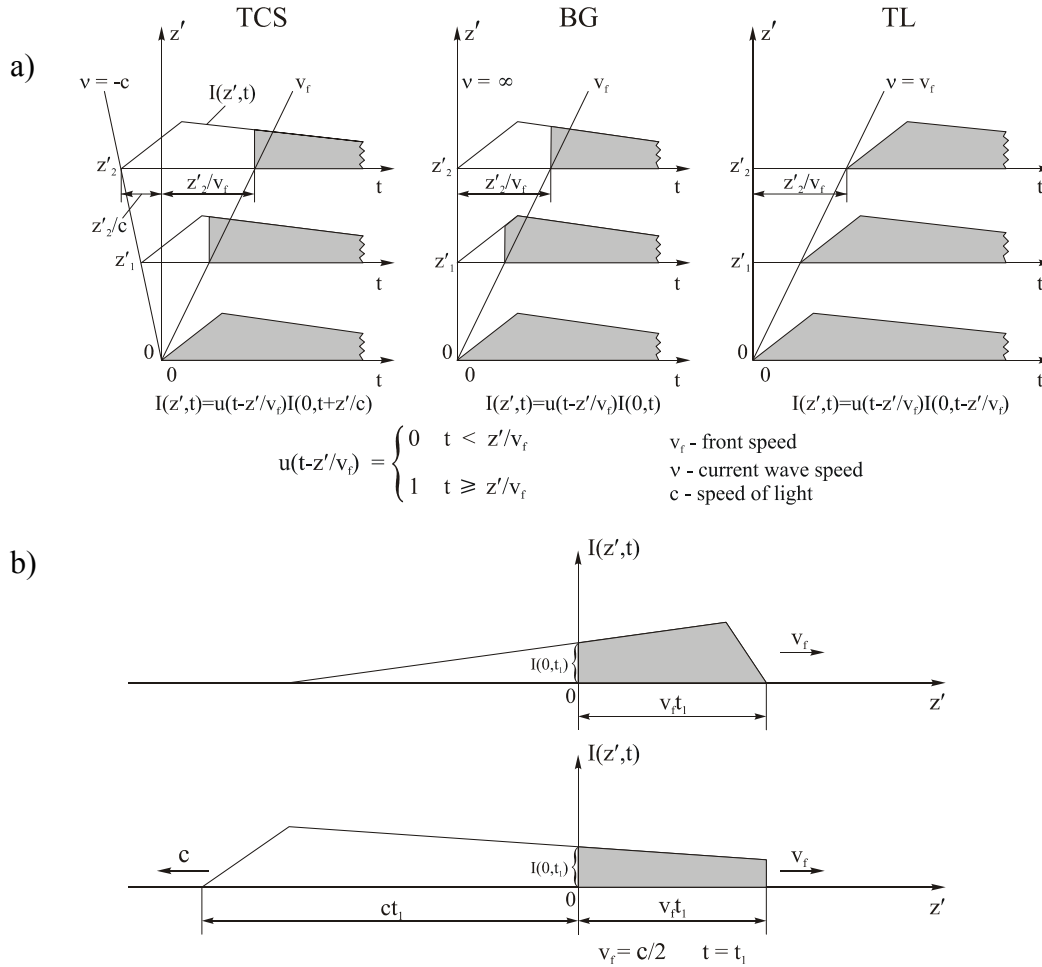


Fig. 3.14 Current distribution along the lightning channel according to three different models: (a) Current versus time waveforms for TCS, BG and TL return stroke models; (b) Current versus height z' at an arbitrary fixed instant of time $t=t_1$ for the TL and TCS models; Adapted from [125]

The “engineering” models can be grouped into two categories: the transmission-line-type models and the traveling-current-source models. Their properties are summarized in Table 3.7. Each model in the table is represented by both current and charge density equations.

Transmission-line-type models, $t \geq z' / v_f$			
TL	(Uman and McLain)	$I(z', t) = I(0, t - z' / v)$ $\rho_L(z', t) = \frac{I(0, t - z' / v)}{v}$	
MTLL	(Rakov and Dulzon)	$I(z', t) = \left(1 - \frac{z'}{H}\right) I(0, t - z' / v)$ $\rho_L(z', t) = \left(1 - \frac{z'}{H}\right) \frac{I(0, t - z' / v)}{v} + \frac{Q(z', t)}{H}$	
MTLE	(Nucci et al.)	$I(z', t) = e^{-z' / \lambda} I(0, t - z' / v)$ $\rho_L(z', t) = e^{-z' / \lambda} \frac{I(0, t - z' / v)}{v} + \frac{e^{-z' / \lambda}}{\lambda} Q(z', t)$	
		$Q(z', t) = \int_{z'/v}^t I(0, \tau - z' / v) d\tau$	$v = v_f = \text{const.} \quad H = \text{const.} \quad \lambda = \text{const.}$
Traveling-current-source models, $t \geq z' / v_f$			
BG	(Bruce and Golde)	$I(z', t) = I(0, t)$ $\rho_L(z', t) = \frac{I(0, z' / v_f)}{v_f}$	
TCS	(Heidler)	$I(z', t) = I(0, t + z' / c)$ $\rho_L(z', t) = -\frac{I(0, t + z' / c)}{c} + \frac{I(0, z' / v^*)}{v^*}$	
DU	(Diendorfer and Uman)	$I(z', t) = I(0, t + z' / c) - I(0, z' / v^*) e^{-(t - z' / v_f) / \tau_D}$ $\rho_L(z', t) = -\frac{I(0, t + z' / c)}{c} - \left[\frac{I(0, z' / v^*)}{v_f} + \frac{\tau_D}{v^*} \frac{dI(0, z' / v^*)}{dt} \right] e^{-(t - z' / v_f) / \tau_D} + \frac{I(0, z' / v^*)}{v^*} + \frac{\tau_D}{v^*} \frac{dI(0, z' / v^*)}{dt}$	
		$v^* = v_f / (1 + v_f / c)$	$v_f = \text{const.} \quad \tau_D = \text{const.}$

Table 3.7 Mathematical description of the models [125]

The transmission-line-type models can be viewed as incorporating a current-source at the channel base which injects a specified current wave into the channel. This current wave propagates either without attenuation (TL model) or with a specified attenuation (MTLL and MTLE models), as can be seen from the corresponding current equations given in the table.

In traveling-current-source-type models, the return stroke current may be viewed as generated at the upward-moving return stroke front and propagating downward. In the TCS model, the current at a given channel section turns on instantaneously as this section is passed by the front, while in the DU model, the current turns on gradually (exponentially with a time constant τ_D). The channel current in the TCS model may be viewed as a downward – propagating wave originating at the upward-moving front, as illustrated in Fig. 3.14b.

The principal distinction between the two types of the “engineering” models formulated in terms of current is the direction of the propagation of the current wave. In the transmission-

line-type models the current wave propagates in upward direction ($v = v_f$) while in traveling-current-source-type models it propagates in downward direction ($v = -c$), as can be seen for TL and TCS models respectively in Fig.3.14.

Even though the direction of propagation of the current wave in a model can be either up or downward, the direction of the current is the same i.e. the charge of the same sign is effectively transported to the ground in both types of “engineering” models.

3.2.7 “LEMFieldE” – a program for simulation of the consequences of a lightning stroke

In order to simulate fields and currents produced by the lightning stroke, a computer code was developed. The code was written in FORTRAN. It computes the fields in the frequency domain. The time domain results are then obtained using fast Fourier transforms (FFT). The general model which is implemented in the program, is based on the following assumptions.

Firstly, equation (3.2) for the current at the base of the lightning channel is used.

Then the MTLE return stroke current model (modified transmission line model with exponential current attenuation in the channel) for the current distribution in the lightning channel is adopted. According to this model, the current distribution in the lightning channel is described with the following equation:

$$i(z', t) = i(0, t - z' / v) \cdot e^{-\alpha \cdot z'} \quad (3.23)$$

where for $(t - z' / v) < 0$, $i(z', t) = 0$ and:

z' – current height;

v - effective channel velocity $\approx 0.6 \div 2 \times 10^8$ m/s;

α - attenuation constant $\approx 0.5 \div 1$ km⁻¹;

In order to be employed in the code equation (3.23) has to be transformed into the frequency domain.

Utilizing the property of the Fourier transform that states that:

$$\mathcal{F}\{f(t - t_0)\} = e^{-j\omega t_0} \mathcal{F}\{f(t)\} \quad (3.24)$$

equation (3.23) turns into:

$$\mathcal{F}\{i(z', t)\} = e^{-(\alpha + j\omega/v)z'} \hat{I}(j\omega) = e^{-\hat{\gamma} z'} \hat{I}(j\omega) \quad (3.25)$$

where:

$$\mathcal{F}\{i(0, t)\} = \hat{I}(j\omega) \quad (3.26)$$

With the parameters from the Table 3.2 the current distribution along the lightning channel according to this model is illustrated in Fig. 3.15

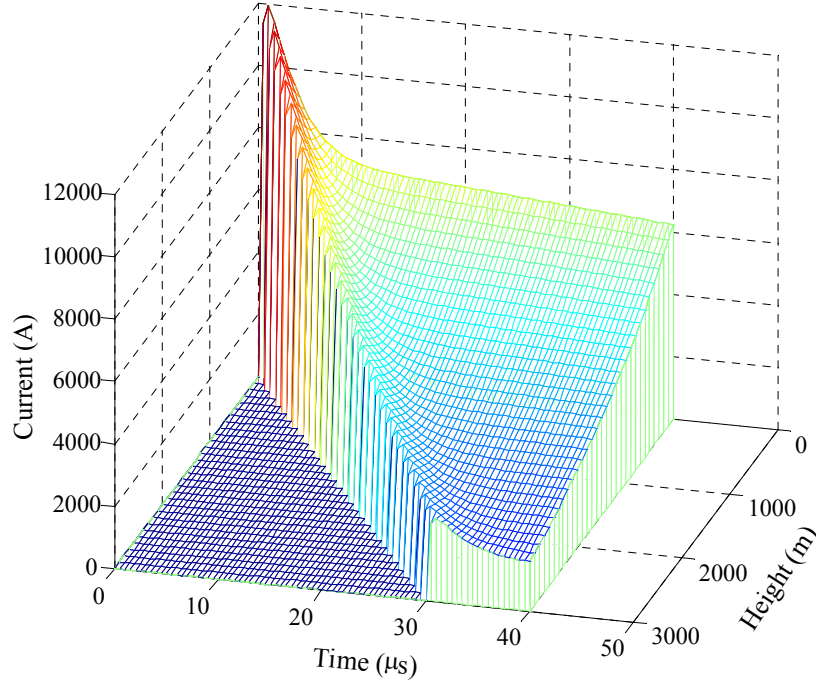


Fig. 3.15 Current distribution along the lightning channel according to the MTLE model

The current which flows in the base of a lightning corresponds to the zero point in the axis for the height.

Additionally, if a modified transmission line model with linear current attenuation with height (MTLL) had been used

$$i(z', t) = \left(1 - \frac{z'}{H}\right) i(0, t - z' / v) \quad (3.27)$$

then the transformation in frequency domain would have been given by:

$$\mathcal{F}\left\{\left(1 - \frac{z'}{H}\right) i(0, t - z' / v)\right\} = \left(1 - \frac{z'}{H}\right) e^{-j\omega z' / v} \hat{I}(j\omega) \quad (3.28)$$

Now substituting equation (3.25) for the current distribution in the lightning channel in (3.19) the following final expressions for the field components are obtained:

$$\hat{E}_{rp}(r, z, j\omega) = \frac{\hat{I}(j\omega)}{4\pi\epsilon_0} \int_{-H}^H e^{-\hat{\gamma}_c |z|} e^{-j\omega R/c} \left[\frac{3r(z-z')}{R^5} \frac{1}{j\omega} + \frac{3r(z-z')}{cR^4} + \frac{r(z-z')}{c^2 R^3} j\omega \right] dz' \quad (3.29a)$$

$$\hat{E}_{zp}(r, z, j\omega) = \frac{\hat{I}(j\omega)}{4\pi\epsilon_0} \int_{-H}^H e^{-\hat{\gamma}_c |z|} e^{-j\omega R/c} \left[\frac{2(z-z')^2 - r^2}{R^5} \frac{1}{j\omega} + \frac{2(z-z')^2 - r^2}{cR^4} - \frac{r^2}{c^2 R^3} j\omega \right] dz' \quad (3.29b)$$

$$\hat{H}_{\phi}(r, z, j\omega) = \frac{\hat{I}(j\omega)}{4\pi} \int_{-H}^H e^{-\hat{\gamma}_c |z|} e^{-j\omega R/c} \left[\frac{r}{R^3} + \frac{r}{cR^2} j\omega \right] dz' \quad (3.29c)$$

$$\hat{E}_r(r, z, j\omega) = \hat{E}_{rp}(r, z, j\omega) - \hat{H}_{\phi p}(r, 0, j\omega) \frac{c\mu_0}{\sqrt{\epsilon_{rg} + \sigma_g / j\omega\epsilon_0}} \quad (3.29d)$$

Eq. (3.29) are implemented in the “LEMFieldE” code for computing the electromagnetic field components at a distance r and height z from the point of the strike. The Cooray-Rubinstein formula (eq.3.29d) is used for computing the horizontal part of the electric field.

One of the objectives of the present work is to analyse the influence of a lightning stroke over a transmission line which is buried under the ground. Therefore the equations for the field components at a distance D and depth s under the surface of the earth are required. Such equations were recently introduced by Cooray [25]. He gives the following equations for the field components in the frequency domain assuming a finitely conducting ground with conductivity σ , on the surface and s meter under the ground, with respect to Fig. 3.16:

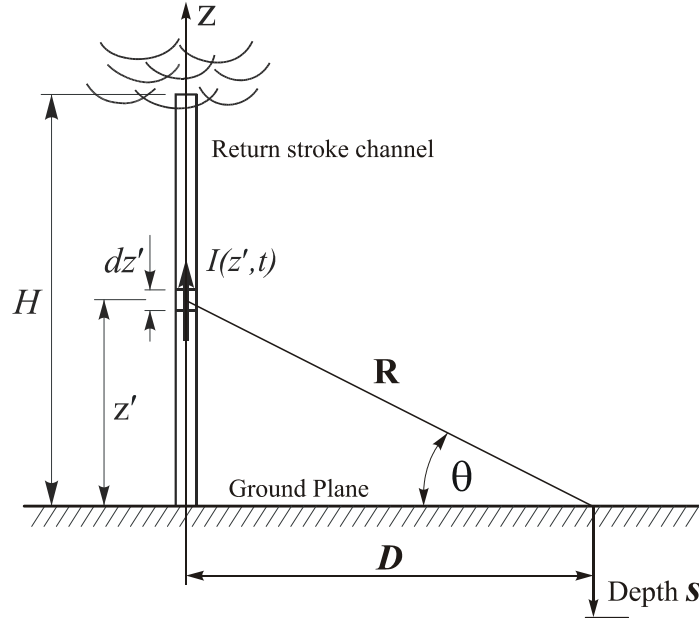


Fig. 3.16 Geometry for deriving the electromagnetic fields on and under the ground

$$\hat{E}_{z,\sigma}(D, 0, j\omega) = \frac{1}{4\pi\epsilon_0} \int_0^H \hat{I}(z', j\omega) \cdot e^{-j\omega R/c} \frac{\cos^2 \theta}{c^2 R} j\omega \cdot [(1 + \Gamma) + (1 - \Gamma)F(w, z')] dz' \quad (3.30a)$$

$$\hat{H}_{\phi,\sigma}(D, 0, j\omega) = \frac{1}{4\pi} \int_0^H \hat{I}(z', j\omega) \cdot e^{-j\omega R/c} \frac{\cos \theta}{cR} j\omega \cdot [(1 + \Gamma) + (1 - \Gamma)F(w, z')] dz' \quad (3.30b)$$

$$\hat{E}_{r,\sigma}(D, 0, j\omega) = c\mu_0 \hat{H}_{\phi,\sigma}(D, 0, j\omega) \frac{\gamma_0}{\gamma} \quad (3.30c)$$

$$\hat{E}_{z,\sigma}(D, s, j\omega) = \hat{E}_{z,\sigma}(D, 0, j\omega) \frac{\epsilon_0 e^{-\gamma \cdot s}}{\sigma_g + j\omega\epsilon_0\epsilon_{rg}} \quad (3.30d)$$

$$\hat{H}_{\phi,\sigma}(D, s, j\omega) = \hat{H}_{\phi,\sigma}(D, 0, j\omega)e^{-\gamma \cdot s} \quad (3.30e)$$

$$\hat{E}_{r,\sigma}(D, s, j) = \hat{E}_{r,\sigma}(D, 0, j\omega)e^{-\gamma \cdot s} \quad (3.30f)$$

where:

$$\gamma_0 = \sqrt{-\omega^2 \mu_0 \epsilon_0} = \frac{j\omega}{c} \quad (3.31a)$$

$$\gamma = \sqrt{j\omega\mu_0\sigma_g - \omega^2\mu_0\epsilon_{rg}\epsilon_0} \quad (3.31b)$$

$$\Delta = \left(\frac{\gamma_0}{\gamma}\right) \sqrt{1 - \left(\frac{\gamma_0}{\gamma}\right)^2 \cos^2 \theta} \quad (3.31c)$$

$$\Gamma = \frac{\sin \theta - \Delta}{\sin \theta + \Delta} \quad (3.31d)$$

$$w = -\frac{\gamma_0 R}{2} (\sin \theta + \Delta)^2 \quad (3.31e)$$

$$F(w, z') = 1 - j(\pi w)^{1/2} e^{-w} \operatorname{erfc}(j\sqrt{w}) \quad (3.31f)$$

Using the MTLE model for the current distribution along the lightning channel and substituting $\hat{I}(z', j\omega)$ in (3.30a) and (3.30b) with (3.25), the following final expressions are obtained

$$\hat{E}_{z,\sigma}(D, 0, j\omega) = \frac{\hat{I}(j\omega)}{4\pi\epsilon_0} \int_0^H e^{-\hat{\gamma}_c |z'|} \cdot e^{-j\omega R/c} \frac{\cos^2 \theta}{c^2 R} j\omega \cdot [(1 + \Gamma) + (1 - \Gamma)F(w, z')] dz' \quad (3.32a)$$

$$\hat{H}_{\phi,\sigma}(D, 0, j\omega) = \frac{\hat{I}(j\omega)}{4\pi} \int_0^H e^{-\hat{\gamma}_c |z'|} \cdot e^{-j\omega R/c} \frac{\cos \theta}{cR} j\omega \cdot [(1 + \Gamma) + (1 - \Gamma)F(w, z')] dz' \quad (3.32b)$$

Equations (3.32a), (3.32b) and (3.30c) to (3.30f), together with (3.31a) to (3.31f) are employed in the code in order to compute the components of the electromagnetic field on the surface of the earth and s meters under the ground at a specified distance D from the lightning stroke.

The program reads the input data from a text file named LEMFIELD.DAT where the initial conditions and parameters are specified. These parameters are:

- Distance from the lightning r (with respect to Fig. 3.13), height above the ground z , and depth below the earth surface s for which the field components have to be computed;
- Parameters specifying properties of a finite conducting ground plane - σ_g (ground conductivity) and ϵ_{rg} (relative ground permittivity);

- Data needed for specifying the number of points used for FFT and the total computational time in μsec for time-domain transformation;
- Parameters specifying the function of the current at the base of the lightning and the distribution of the current along the channel – I_{01} , I_{02} , τ_{11} , τ_{12} , τ_{21} , τ_{22} , v , α and H (height of the lightning channel);

As an output, ASCII files for each component of the field both in the frequency and time domains are produced. The calculated data are written in these files. Separate files are created for the field radiated from each of the components above, on and under the ground as well as for the computations performed in the time and frequency domains.

Computations were initially made using 8192 points in FFT, but it was noticed that the same results are obtained when the number of points is 4096. In the latter case, however, the computational time was halved.

Two approaches were applied, represented by two versions of the code. Firstly, the field was calculated assuming for the current at the base the function presented in Fig. 3.17a.

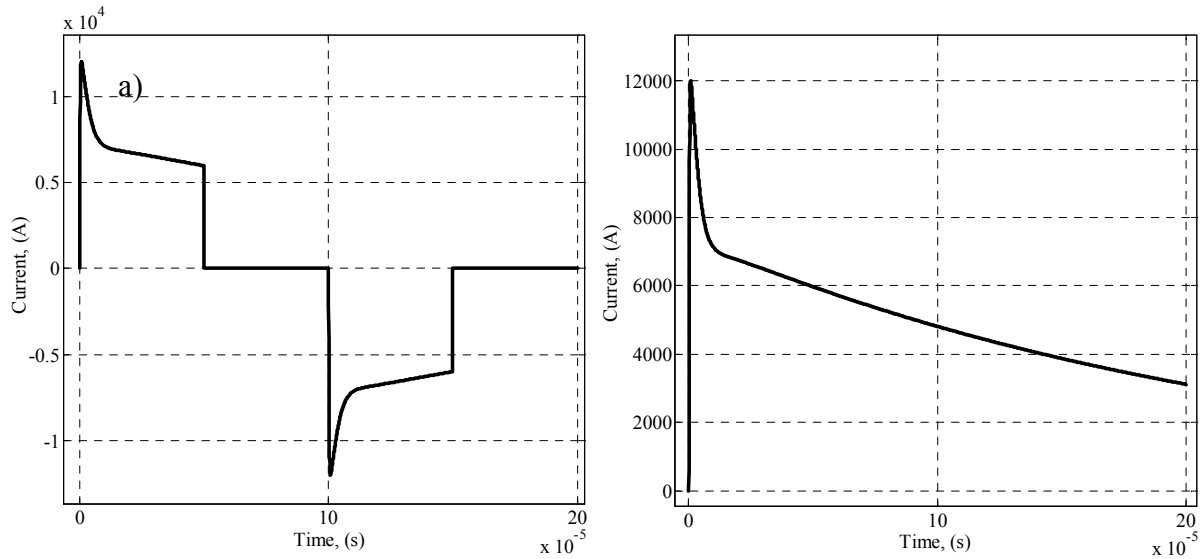


Fig. 3.17 Functions, used for the base current; (a) first approach; (b) second approach;

When performing the frequency domain calculations for the zero frequency ($\omega=0$), it is known that $\hat{I}(j\omega)=0$. Hence, there is no problem for making calculations according to the formulae stated above. In the second case, it is assumed that the current at the channel base is represented by the function shown in Fig. 3.17b. Then for $\omega=0$, $\hat{I}(j\omega)\neq 0$ and there is a problem to use equations for \hat{E}_z and \hat{E}_r , since the $j\omega$ term appears as a denominator and results in a division by zero. This problem is avoided in the following way.

We know that:

$$\mathcal{F}\left\{\int_0^t i_0(\tau)d\tau\right\} = \frac{I}{j\omega} \hat{I}(0, j\omega) = \hat{q}(0, j\omega) \quad (3.33)$$

If the charge at the base of the channel is found as an integral from the base current:

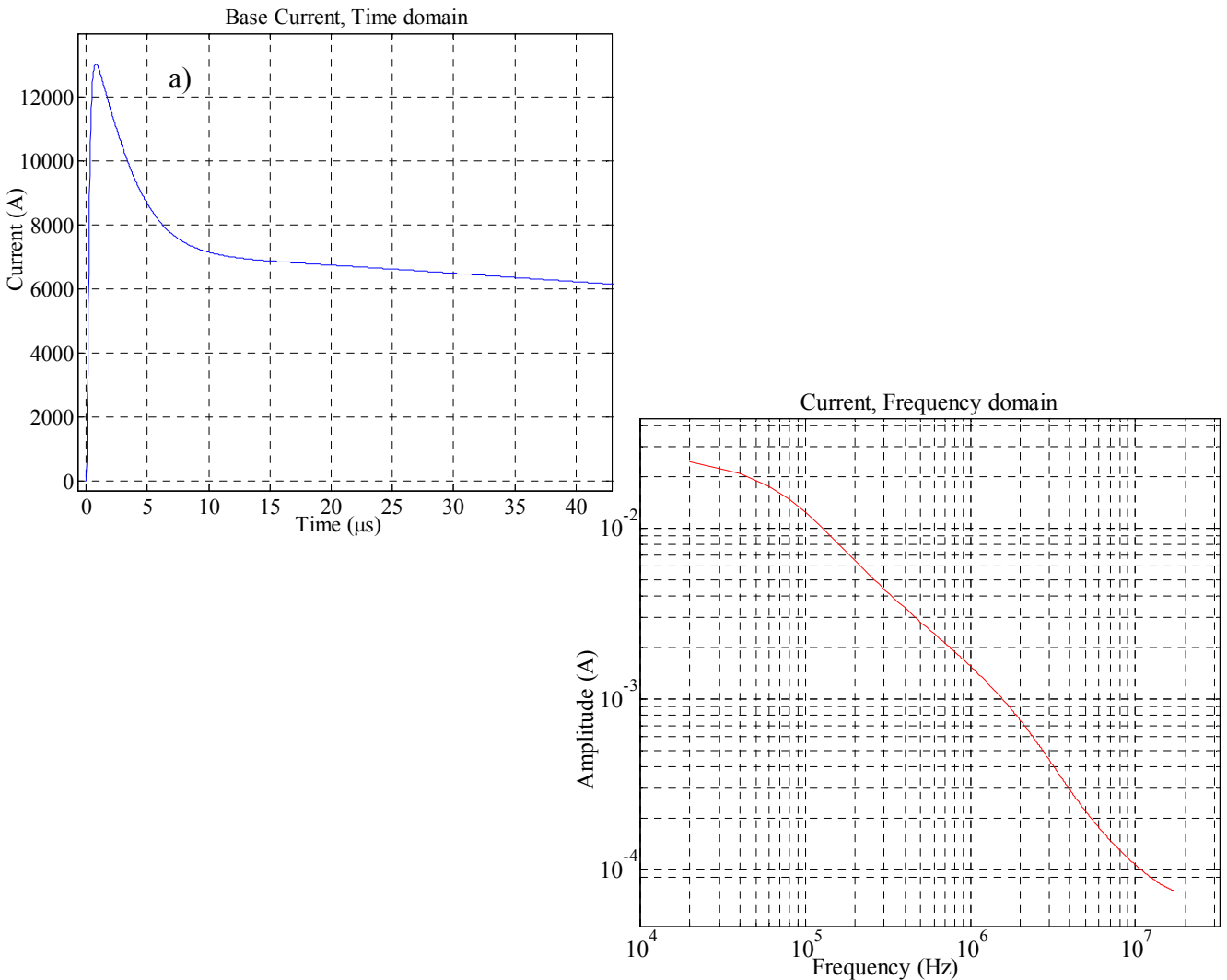
$$q(0, t) = \int_0^t i_0(\tau)d\tau \quad (3.34)$$

then transforming the charge into the frequency domain gives

$$\mathcal{F}\{q(0, t)\} = \hat{q}(0, j\omega) \quad (3.35)$$

If for the calculations performed in the frequency domain, the value of the charge corresponding to the zero frequency is used, the division by zero is avoided and the problem is solved.

As an example in Fig. 3.18 calculations made by the “LEMFieldE” code for the base current and vertical aboveground component of the electric field - E_z are shown. Here the distance to the point of the stroke is chosen to be 2 km and the height above the ground is 10 m. Both time domain waveforms and frequency domain spectrum magnitude are presented. The ground parameters are $\epsilon_{rg}=10$ and $\sigma_g=0.001$ S/m respectively.



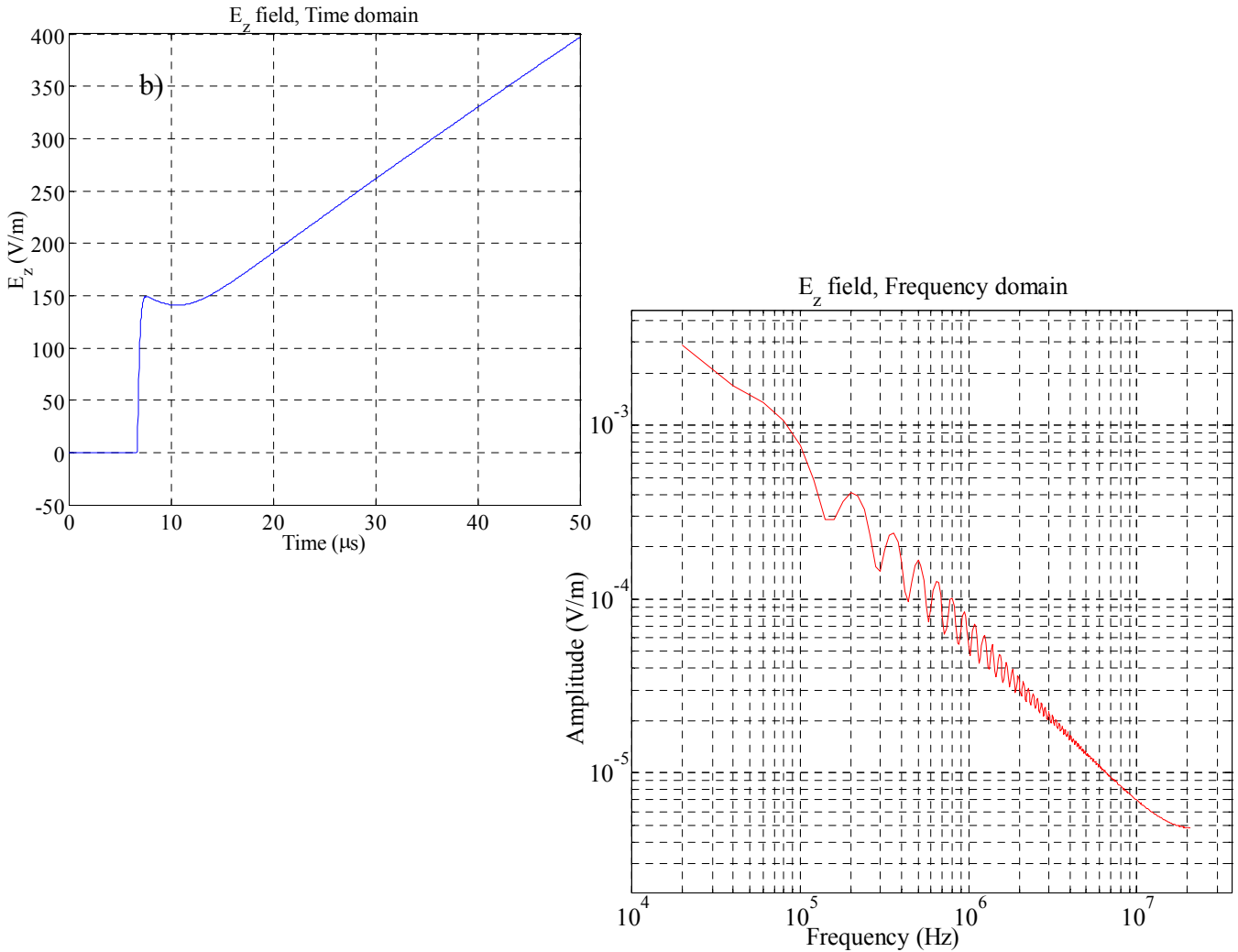


Fig. 3.18 Example calculations performed by “LEMFieldE” code; (a) current at the base of the lightning; (b) vertical electric field component E_z ;

Considering the frequency domain spectrum of the lightning, it is of interest to compare the spectrum of the vertical electric field with the data presented in Chapter 2. In Fig. 2.6 values of the external noise F_a in the frequency domain are given. For the purpose of this comparison only the curves A and B of the diagram are important, which represent the 95th and 5th percentile of the atmospheric noise value. As described in [30], the external noise F_a can be related to the effective vertical component of the electric field strength E by the following equation

$$E = F_a + 20 \log f + 10 \log b - 95.5 \quad (3.36)$$

Here F_a is the external noise in dB, f is the frequency in MHz, b is the receiver bandwidth in Hz and E is the vertical electric field component expressed in dB μ V/m.

Considering the frequency of 10^5 Hz, the values of the external noise F_a , according to Fig. 2.6 are 140 dB and 69 dB. Assuming that the receiver bandwidth is 9 kHz – the value rigorously defined in CISPR16 standard [162], the values of the vertical electric field for the curves A and B at a frequency of 0.1 MHz are as follows

$$E_A = 140 + 20 \log 10^{-1} + 10 \log 9 \cdot 10^3 - 95.5 = 64,04 \text{ dB}\mu\text{V}/\text{m}$$

$$64,04 \text{ dB}\mu\text{V} / \text{m} = 10^{\frac{64,04}{20}} \cdot 10^{-6} = 1,59 \cdot 10^{-3} \text{ V} / \text{m} = 1,59 \text{ mV} / \text{m}$$

$$E_B = 69 + 20 \log 10^{-1} + 10 \log 9 \cdot 10^3 - 95.5 = -6,96 \text{ dB}\mu\text{V}/\text{m}$$

$$-6,96 \text{ dB}\mu\text{V} / \text{m} = 10^{\frac{-6,96}{20}} \cdot 10^{-6} = 0,413 \cdot 10^{-6} \text{ V} / \text{m} = 0,413 \mu\text{V} / \text{m}$$

As we can obtain from Fig. 3.18b, the amplitude of the vertical electric field at a frequency of 0.1 MHz is approximately 0.8 mV/m. This value is close to the upper bound of the atmospheric noise defined by curve A in Fig. 2.6.

From the results presented in Fig. 3.18 it can be concluded also that most of the spectrum content of the lightning stroke ranges from 0 to approximately 10 MHz. This enables one to approximately define parameters which determine the number of the points of the FFT and the period of the signal in the time domain calculations in order to optimize the calculations. These parameters are given as an input for the program in the third line of the LEMFIELD.DAT file. (Appendix I). For the diagrams presented in Fig. 3.18 the following values were used in the input file: $n=11$ and $T_{input}=50 \mu\text{s}$. The number n defines the number of the points written by the code in the output files as 2^n . Thus all the output files generated by the code contain $2^{11}=2048$ rows with output values. The code, however, performs the calculations for $N=2^{n+2}=2^{13}=8192$ points. Similarly T_{input} gives the length of the time signal in the output files. In the code the period of the time signal is $T=4 \cdot T_{input}$. Now with input values $n=11$ and $T_{input}=50.0$, the following value is obtained for the sampled interval T_S used in the inverse FFT

$$T_s = \frac{4T_{input}}{2^{n+2} - 1} = \frac{200\mu s}{8191} = 2,4417.10^{-8} s$$

The sample spacing T_s determines the highest frequency used in frequency domain calculations as

$$F_{max} = \frac{1}{2T_s} = \frac{1}{2.2,4417.10^{-8}} = 20,4775MHz$$

And the period of the time signal $T=4.T_{input}$ determines the frequency spacing as

$$f_s = \frac{1}{T} = \frac{1}{200\mu s} = 5kHz$$

As mentioned above, performing the computation with 4096 points instead of calculating with 8192 points halves the computation time. Therefore calculations presented below were made with 4096 points. The third row of the LEMFIELD.DAT file presented in the Appendix I contains exactly the values used in these calculations. Using the latter, the following values are obtained for the T_s, f_s , and F_{max}

$$T_s = \frac{4.60\mu s}{2^{10+2} - 1} = \frac{240\mu s}{4095} = 5,86.10^{-8} s$$

$$f_s = \frac{1}{240\mu s} = 4,16kHz$$

$$F_{max} = \frac{1}{2.5,86.10^{-8}} = 8,532MHz$$

Making the frequency domain calculations where the maximum frequency spans to 8,532 MHz is enough in order to obtain correct results, as shown bellow.

3.2.8 Comparison of the results calculated by “LEMFieldE” with those stated in the literature

In this section, some results calculated with the “LEMFieldE” code are presented. They are compared with similar results from the literature. In Fig. 3.19a the vertical electric field at a distance of 2 km and height of 10 m from the lightning as calculated by Tesche [142] is shown. Fig. 3.19b represents the result computed by “LEMFieldE”. As can be seen, there is a very good match, of both in the maximum amplitude and the curve pattern.

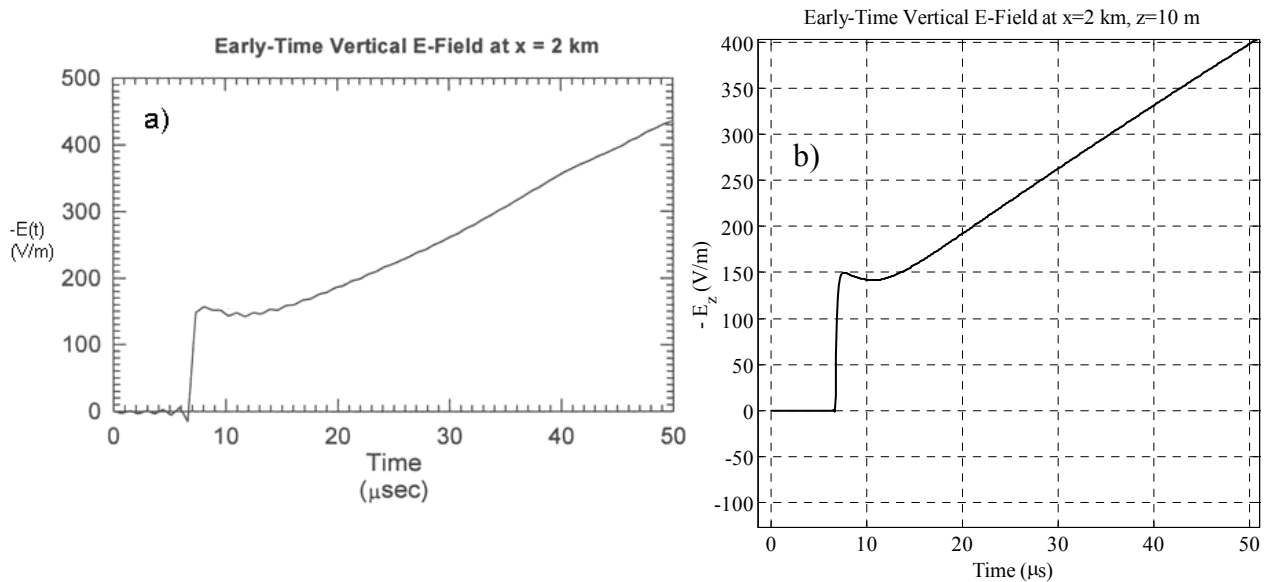


Fig. 3.19 Vertical electric field: (a) as stated by Tesche [142]; (b) as computed by the “LEMFieldE” code;

In his model, Tesche uses also the MTLE model in combination with frequency domain calculations. The MTLE model parameters used by Tesche are as follows: effective channel velocity $v=1,1 \cdot 10^8$ m/s, current decay constant $\lambda=1,7$ km. The same parameters were used in the “LEMFieldE” code

Fig. 3.20a gives the vertical electric component of the field as stated by Nucci et al. [93]. The distance to the point of the stroke is 2 km. Fig. 3.20b shows the results obtained by “LEMFieldE”. Again a very good match is observed.

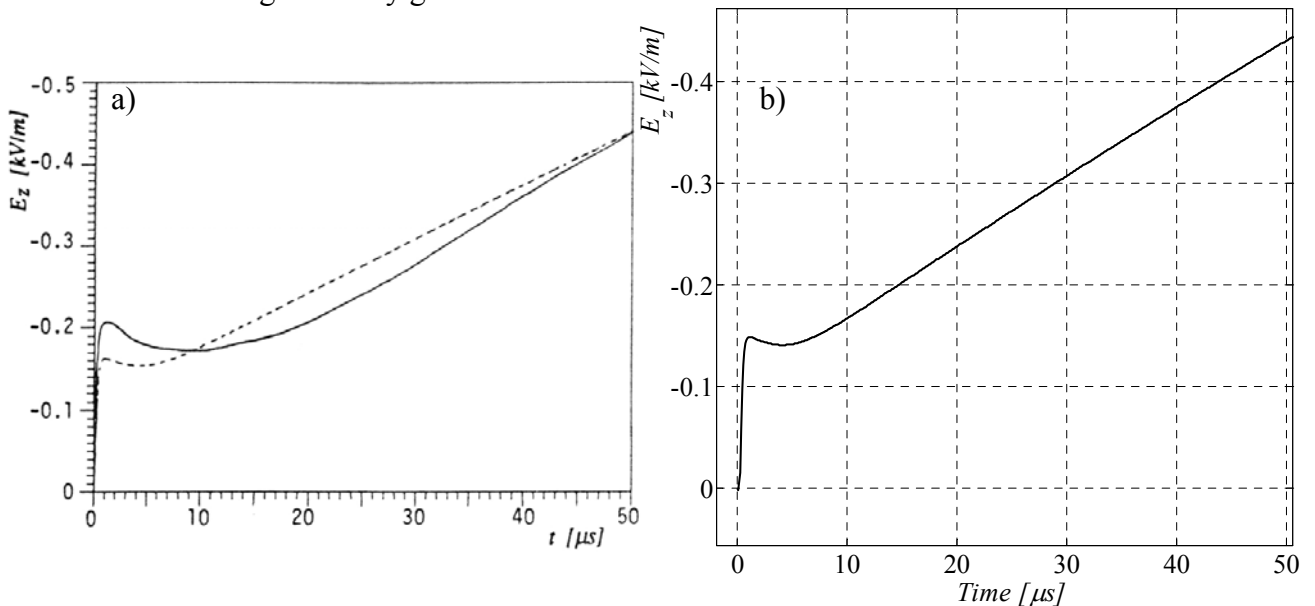


Fig. 3.20 Vertical electric component of the field: (a) as stated by Nucci [93]: solid line-experimental data, dotted line-calculated results; (b) as computed by “LEMFieldE” code;

In Fig. 3.21a, the vertical electric and azimuthal magnetic fields at a distance 2 km from the lightning channel as computed by Rachidi et al. [119] are presented. Additionally, the contributions of the different parts of the electric and magnetic fields, namely static, induction and radiation component of the field are shown in the figure with dotted lines. Comparison with the results from “LEMFieldE” is made in Fig. 3.21b. The small difference in the initial peak of the vertical electric field E_z illustrated in Fig. 3.21b compared to that in Fig. 3.20b is due to the different input parameters used by Rachidi, respectively used in “LEMFieldE”.

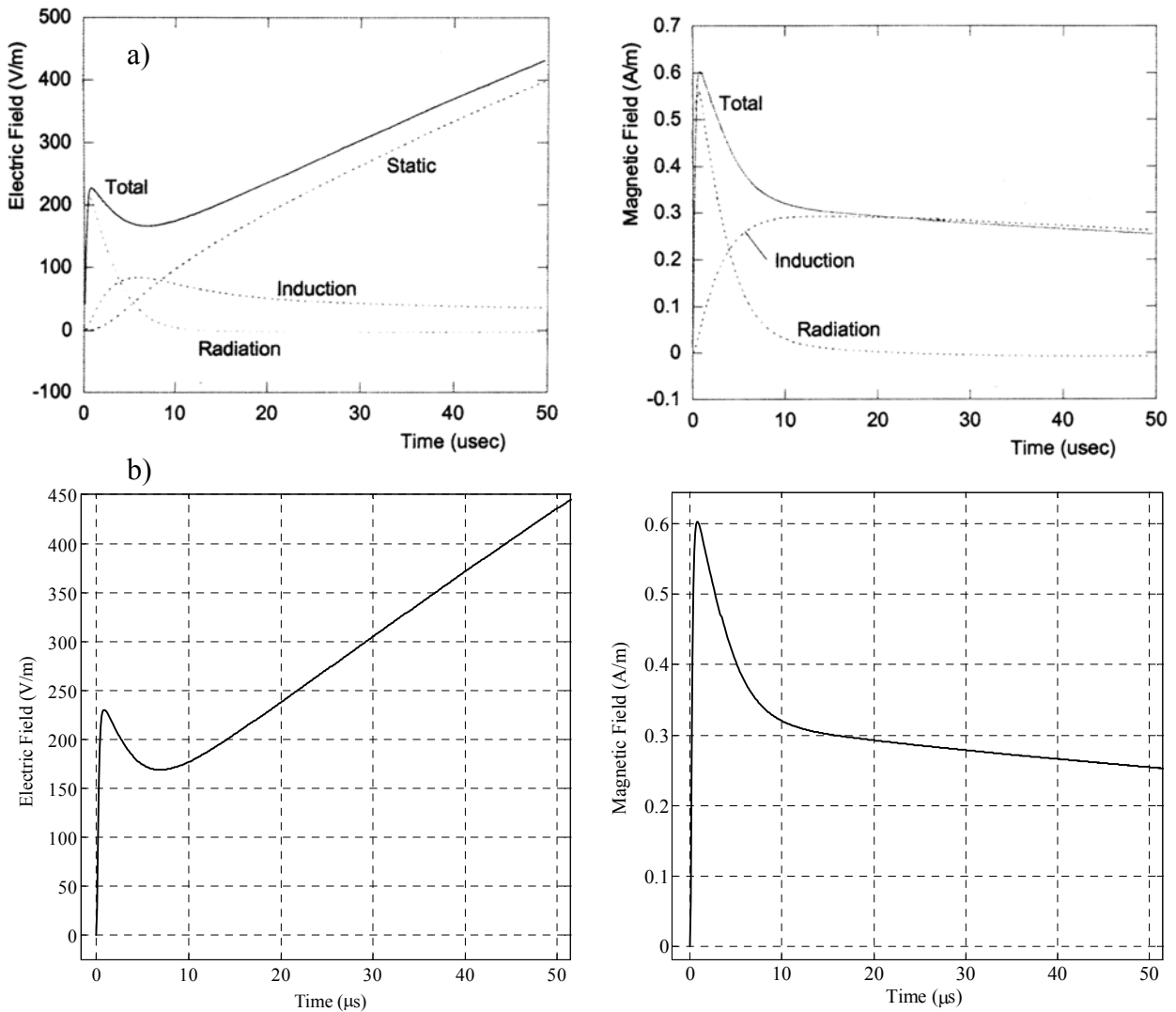


Fig. 3.21 Vertical electric and azimuthal magnetic fields: (a) as computed by Rachidi [119]; (b) calculations performed by “LEMFieldE” code;

Rachidi [119] assumes that the current wave speed in the lightning channel is 1.9×10^8 m/s and the decay constant λ used in the MTLE model is 2 km. These values are adopted for calculating the results shown above.

Fig. 3.22a shows calculations made by Diendorfer [31] of the vertical electric field at ground level and the horizontal electric field multiplied by 20 at a height of 10 m above the ground. The distance from the striking point is 500 meters. Fig. 3.22b illustrates, respectively, calculations with “LEMFieldE”.

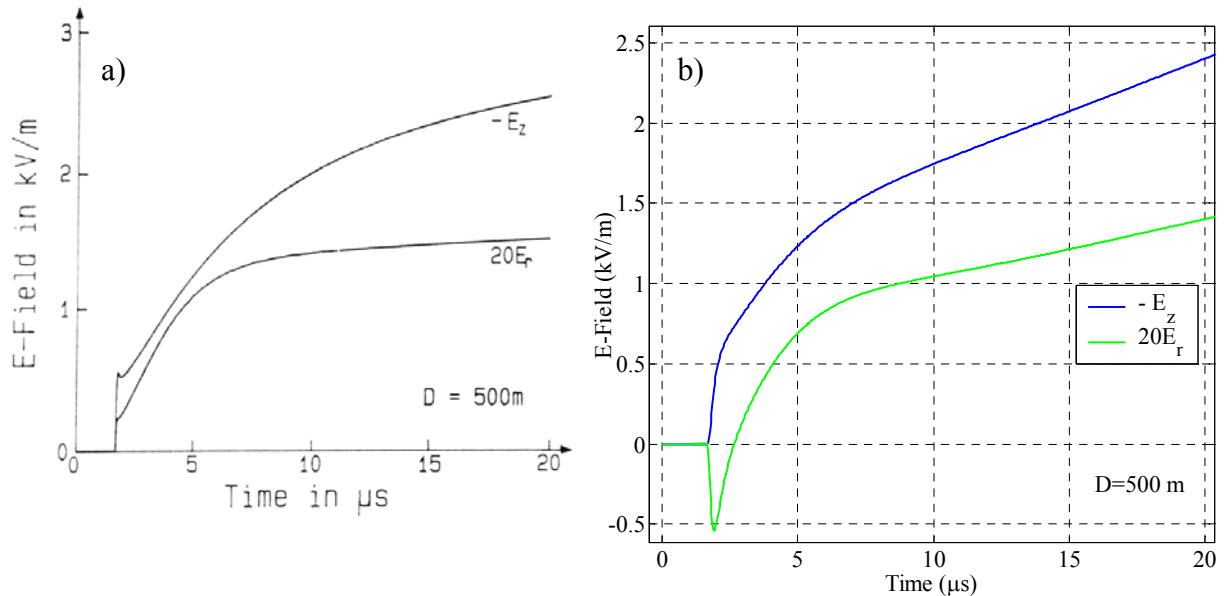


Fig. 3.22 Vertical electric and horizontal electric field multiplied by 20: (a) calculations from Diendorfer [31]; (b) calculations made by “LEMFieldE” code;

The differences between Fig. 3.22a and Fig. 3.22b are due to a different current distribution model used by Diendorfer, namely the TCS model. Furthermore, Diendorfer uses “wavetilt function” instead of the “Cooray-Rubinstein” formula for the calculation of the horizontal component of the field. But the important point here is the magnitude of the field which in both computations is approximately the same.

It should be noted that an extract from the literature is presented for these field components, for which information about the base current and current distribution along the lightning channel is available. If the base current and the other parameters which describe the lightning current distribution model are unknown, then these parameters cannot be specified correctly in the calculations conducted by “LEMFieldE”. A reasonable comparison is then impossible.

Very important is the comparison of the field components under the ground. As a source for the latter the article written by Cooray [25] is used. This comparison is essential because firstly Cooray calculates the field using time domain expressions. In the second place he utilizes his own model for the current distribution along the lightning channel. Therefore, proving his results using the MTLE current distribution model and frequency domain equations for the field components will justify the model implemented in the “LEMFieldE” code.

Fig. 3.23a shows the horizontal electric field 5 km away from the return stroke at different depths below the ground as calculated by Cooray [25]. Fig. 3.23b represents respectively results from “LEMFieldE”.

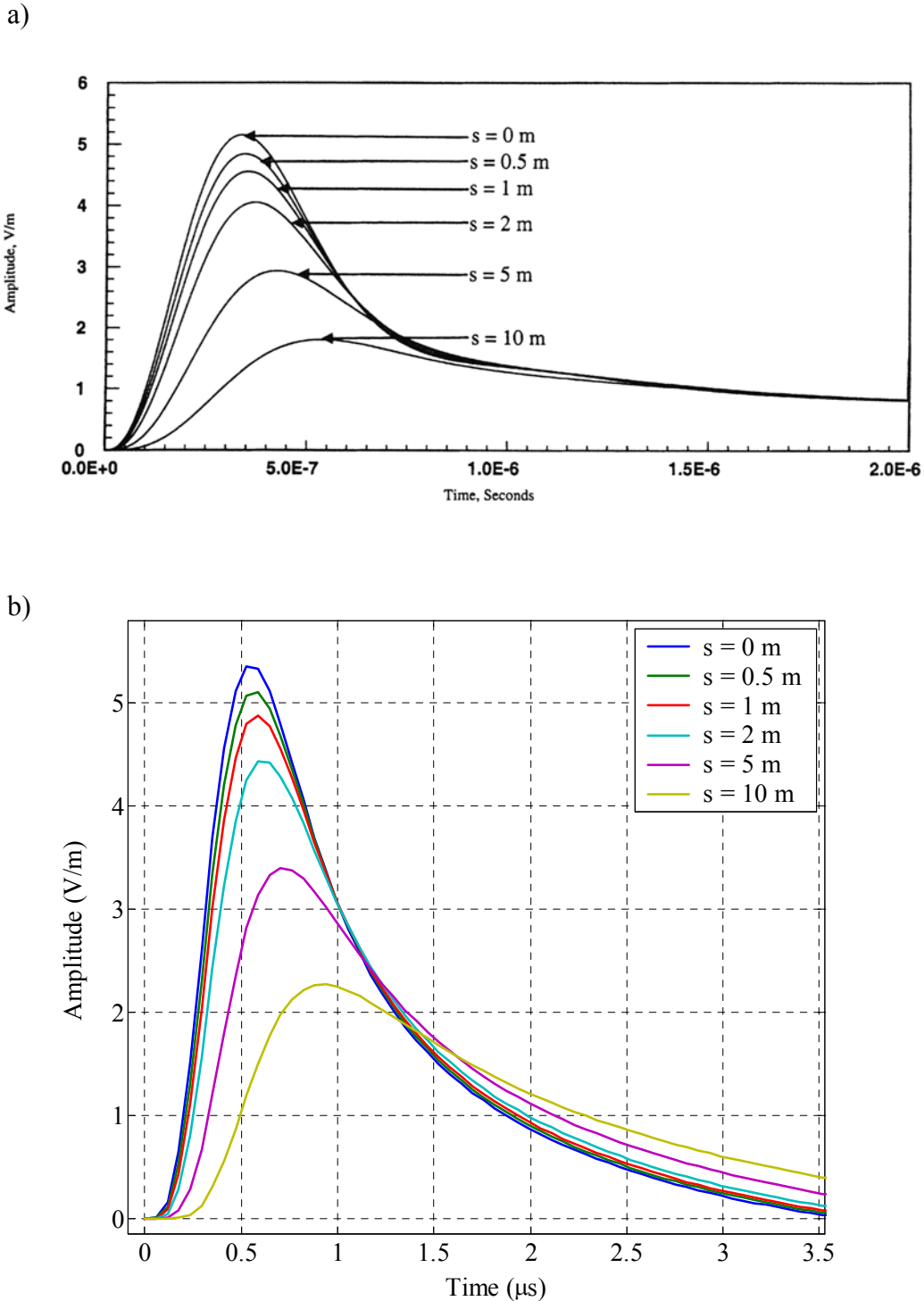
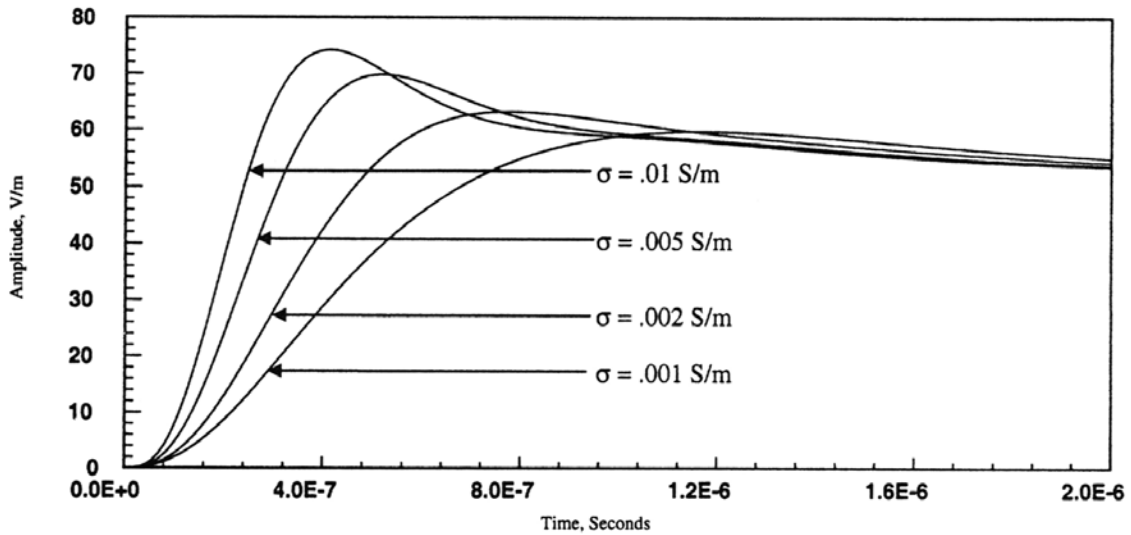


Fig. 3.23 Horizontal electric field calculated for different depths below the ground: (a) calculations from Cooray [25]; (b) calculations from “LEMFieldE” code; Peak current 13 kA

The vertical electric field on the surface of the earth vs. different ground conductivities is illustrated in Fig. 3.24. The distance from the lightning is 5 km. The peak current is 13 kA.

a)



b)

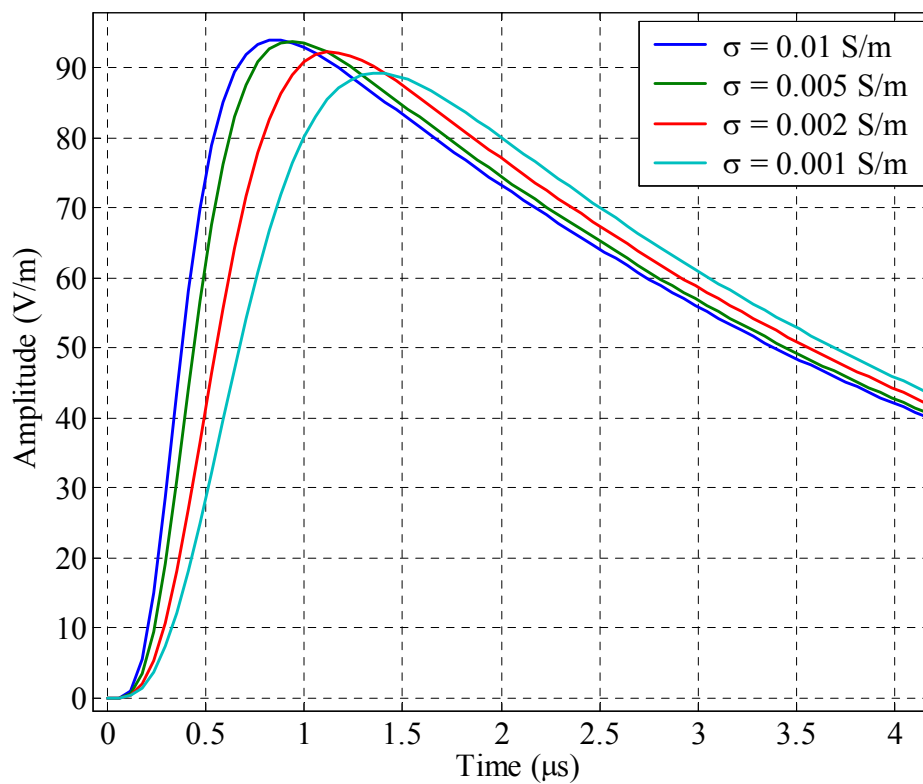


Fig. 3.24 Vertical electric field at the surface of the earth vs. different ground conductivities: (a) calculations from Cooray [25]; (b) as computed by “LEMFieldE” code;

The horizontal electric field for different ground conductivities 1 m under the ground according to Cooray is presented in Fig. 3.25a. The corresponding calculations made by “LEMFieldE” are shown in Fig. 3.25b. Here the distance to the point of observation from the return stroke is again 5 km and the peak current is 13 kA.

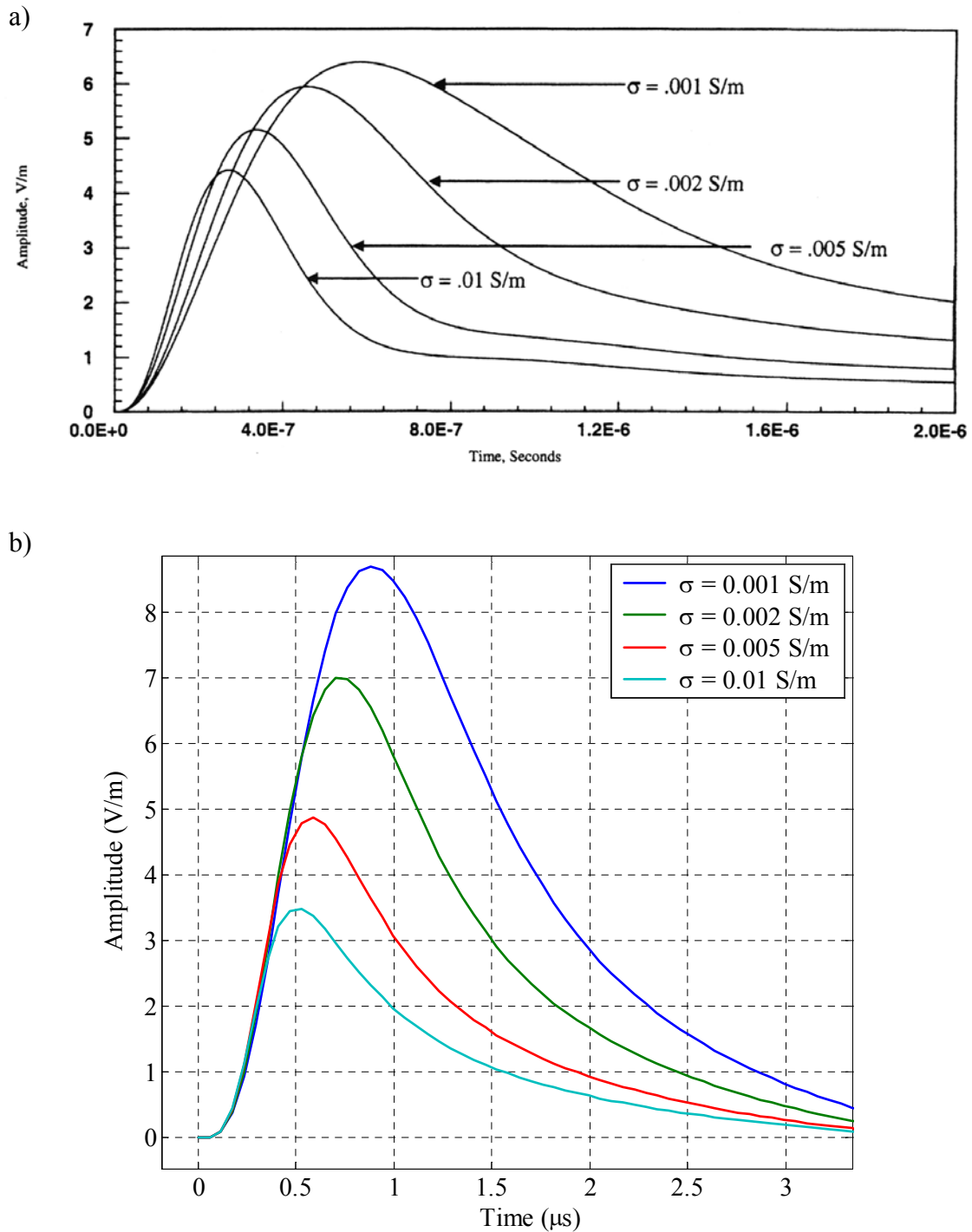


Fig. 3.25 Horizontal electric field for different ground conductivities: (a) calculations from Cooray [25]; (b) calculations made by “LEMFieldE” code;

The vertical electric field on the surface of the earth for different distances from the point of the stroke is shown in Fig. 3.26. Conductivity of the ground is $\sigma=0.005$ S/m and the peak current is 13 kA

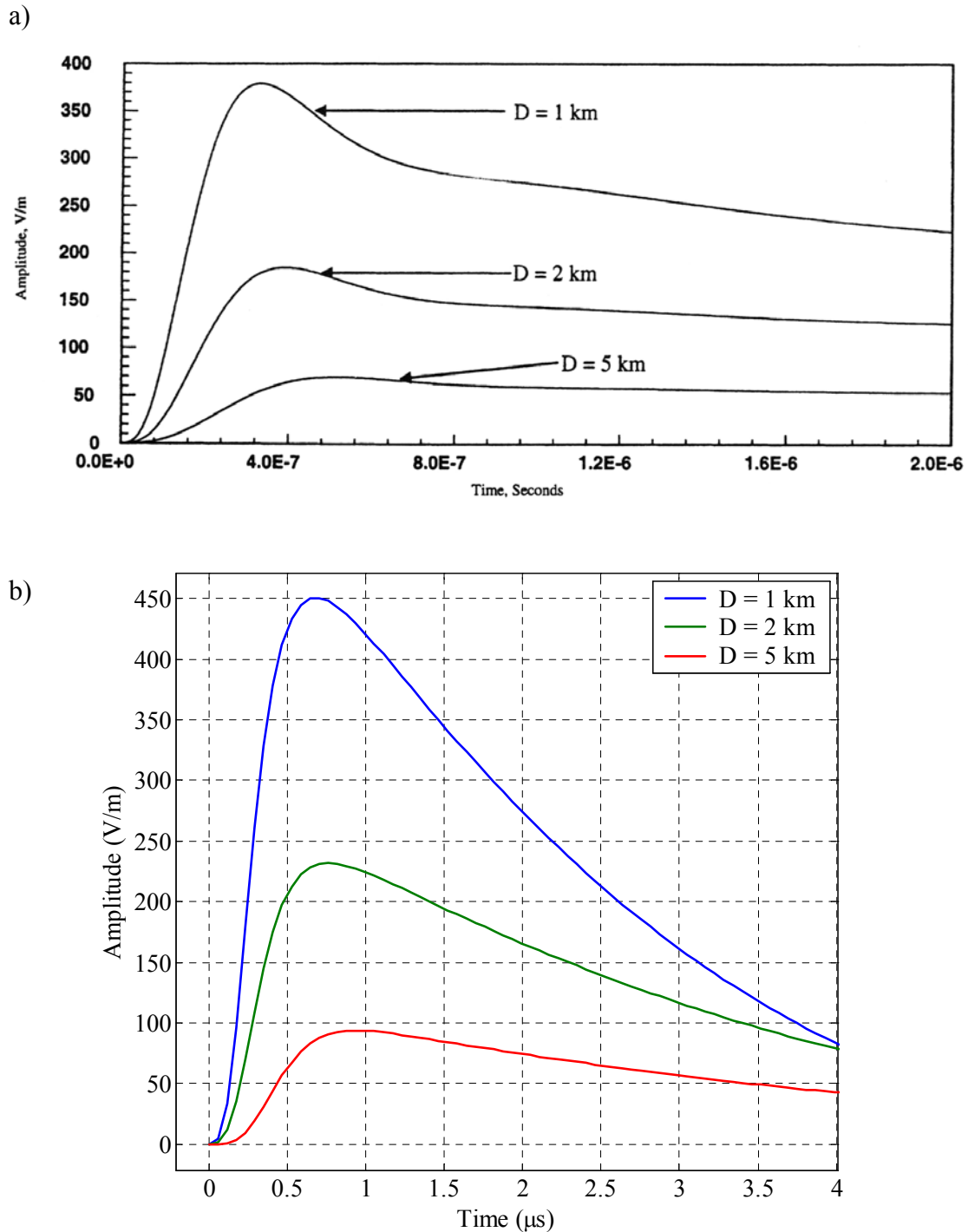


Fig. 3.26 Vertical electric field at the surface of the earth for different distances from the point of the stroke: (a) calculations from Cooray [25]; (b) calculations from “LEMFieldE” code;

Finally, the horizontal electric field for different distances from the lightning stroke on the ground and 1 m under the ground is presented in Fig. 3.27 and Fig. 3.28.

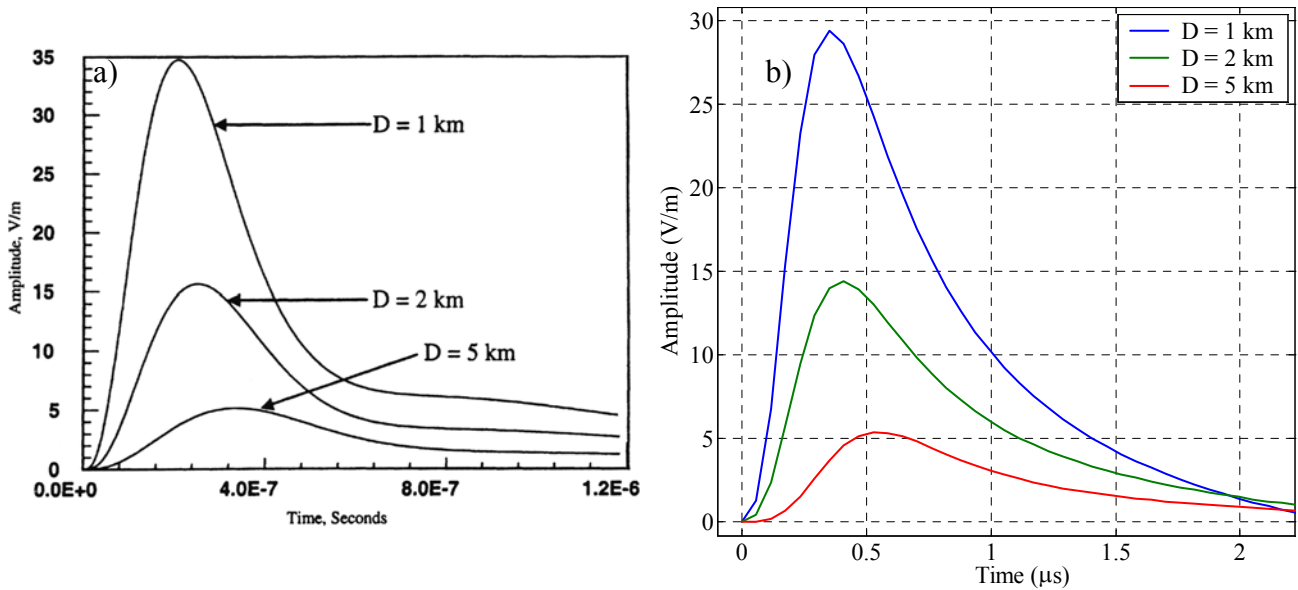


Fig. 3.27 Horizontal electric field on the ground for different distances from the lightning stroke: (a) calculations from Cooray [25]; (b) calculations made by “LEMFieldE” code;

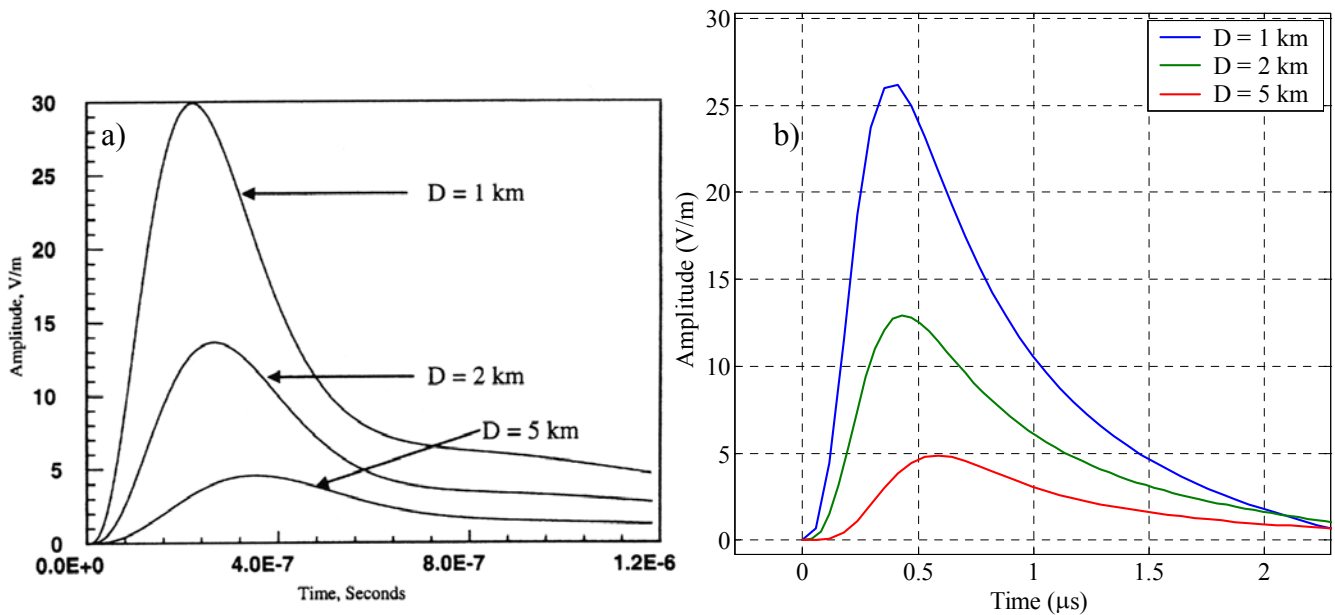


Fig. 3.28 Horizontal electric field 1 m under the ground for different distances from the lightning stroke: (a) calculations from Cooray [25]; (b) calculations from “LEMFieldE”;

Despite the fact that the current distribution model used by Cooray is completely different from those implemented in “LEMFieldE” code, and the methods for calculation of the field

components differs, a good match both in peak values and curve patterns in all results is observed.

Another proof that results computed with “LEMFieldE” code for the fields on and under the ground are correct is given in Fig. 3.29.

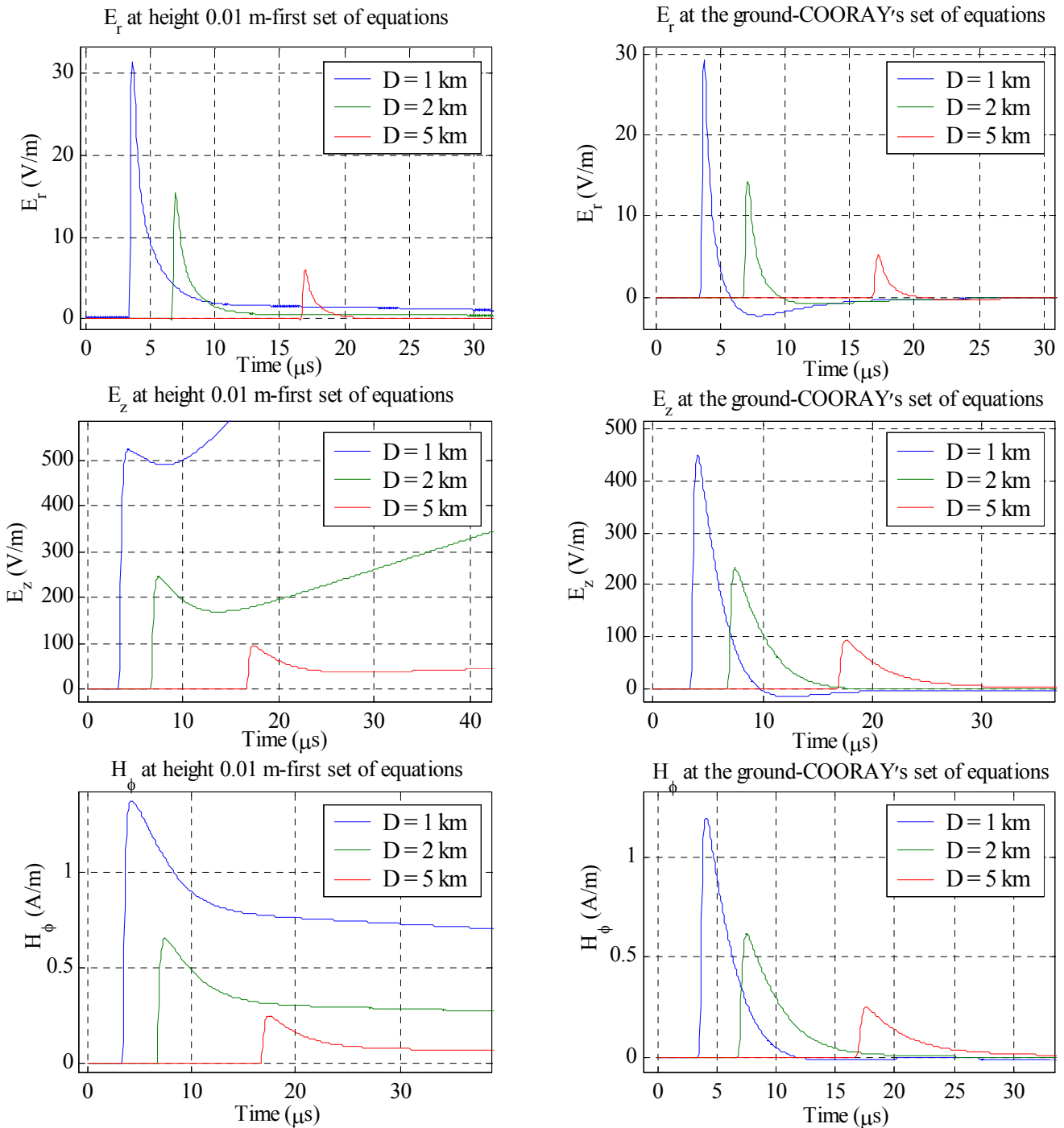


Fig. 3.29 Fields radiated by a lightning stroke at a distance 1, 2 and 5 km, computed with LEMFieldE, using two different sets of equations;

It shows a parallel between the field components as computed with the two different set of equations implemented in the code, namely for computing the field components above the ground and for computing the field components on and under the ground with the equations given by Cooray. The height above the ground used in the first set of equations is chosen to be 0.01 m. A good match of the initial maximum amplitude is observed in this comparison for all distances. The form of the curve in the results is different because only the radiation component of the field is calculated with equations given by Cooray. This component, however, plays the most important role when coupling of the electromagnetic field with the transmission line is investigated, since it is responsible for the initial peak of the field as can be clearly seen in the figure.

From the data presented above, it can be concluded that the results calculated with the “LEMFieldE” code for the return stroke lightning field components are in agreement with the data published in the literature and can be further used for the investigation of the impact of lightning over the underground transmission line.

3.3 The stochastic nature of lightning

The lightning discharge is a stochastic event. Neither the point where the lightning is about to strike nor the amount of energy released during the discharge process can be predicted.

The stochastic nature of the strike point is described by the so-called keraunic level. It defines the number of days in the year on which thunder is heard. This parameter is not very precise because it does not distinguish between a long thunderstorm with a lot of strokes or one with just a single lightning stroke. A more representative parameter for the thunderstorm activity at a given site is the density of lightning strokes to the ground. It is expressed as the number of strokes per km² per year. More or less complex empirical expressions have been established between the density of lightning strokes to the ground (N_d) and the keraunic level (N_k). This relationship, however, depends on many factors and on the local meteorological characteristics of the region. For Europe the following expression is generally accepted.

$$N_d = 0.04N_k^{1.25} \quad (3.37)$$

A rough map, indicating the keraunic level of the earth is given in Fig. 3.30.

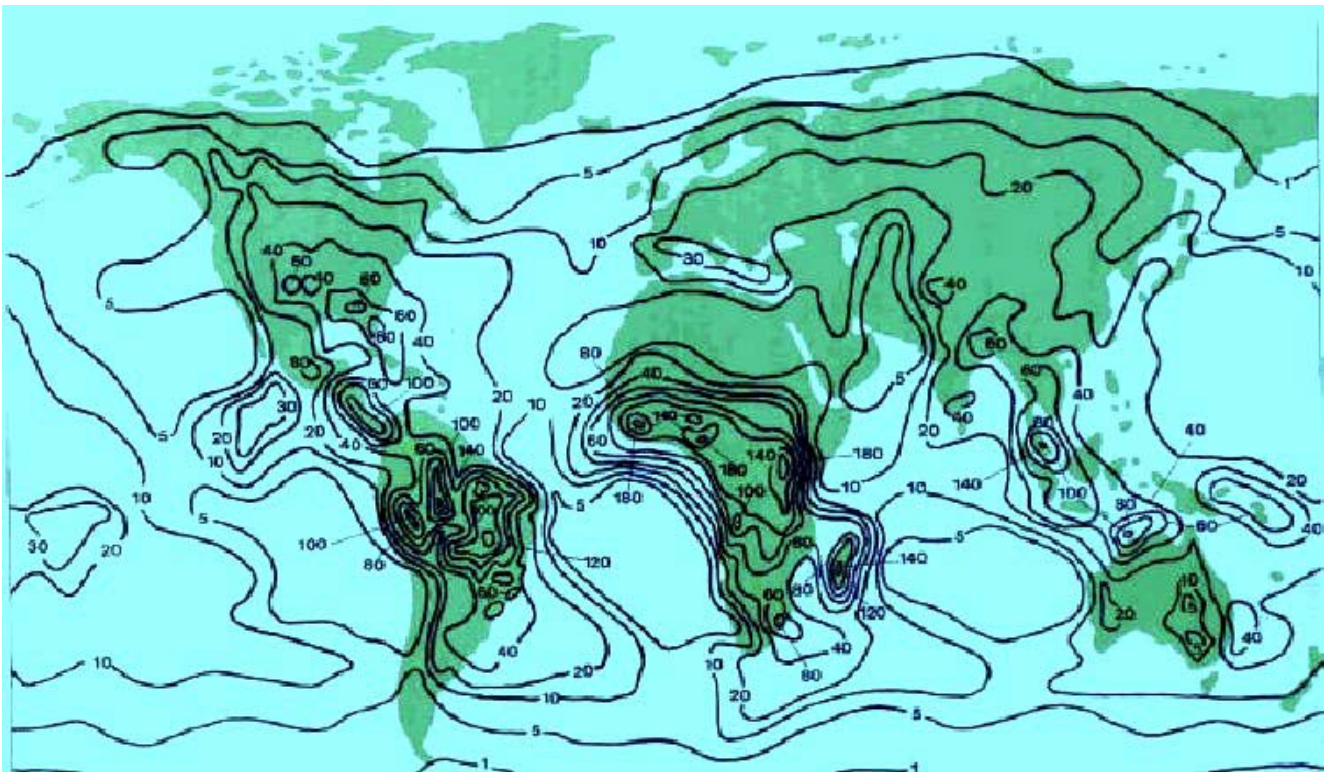


Fig. 3.30 A map representing the number of thunderstorm days per year (the keraunic level) of the planet

The most precise way to find the density of the lightning stroke in a given area is to use the lightning location and protection (LLP) systems. Such systems have been installed in many countries during the last decade of the 20th century. Based on the electromagnetic field radiated by the lightning, special devices equipped with sensors, called direction finders are installed in certain places in the area of the country. The sites where these sensors are installed should fulfil certain requirements [32]. For example, the number of the direction finders in Austria is 8 and in Denmark is 4 [32].

As an example, Table 3.8 presents the comparison between the keraunic levels as computed with equation (3.37), and the density of lightning strokes as detected by the LLP system in Austria. The keraunic level was detected from data measured by the location system, considering that there had been a stormy day when at least one lightning flash struck the ground. A mountainous region was compared with a plain region.

Region	Keraunic level	Density according to (3.36)	Density given by the LLP system	Difference as %
Mountainous	45	4.66	1.0	+366%
Plain	30	2.8	3.8	-36%

Table 3.8 Comparison of the keraunic level and density of lightning strikes

The above example shows that care should be taken when using the keraunic level to characterize the severity of thunderstorms in a given region. The better approach is to use the data from the lightning location and tracking systems. Fig 3.31 shows the lightning density in southern Germany measured by the LLP system and keraunic level in the German State of Bavaria.

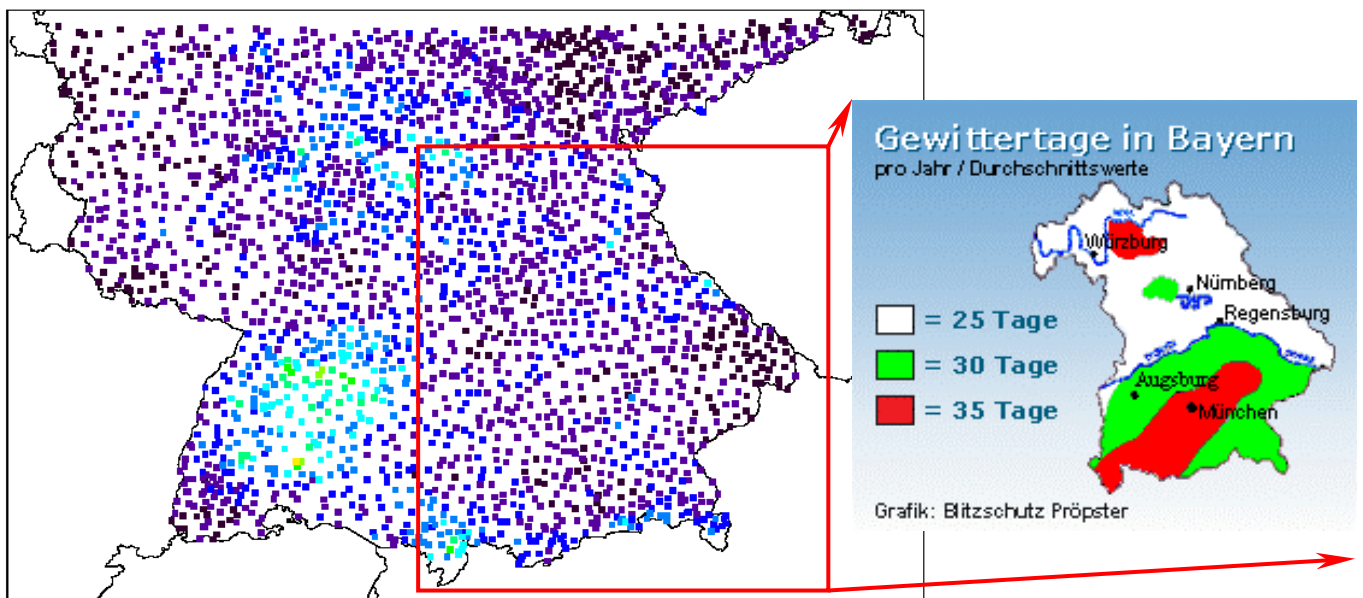


Fig. 3.31 Lightning density in southern Germany measured by the LLP system and keraunic



The second aspect concerning the stochastic nature of the lightning is the intensity of the stroke. The exact amount of the energy which is released during the lightning discharge cannot be predicted. Conclusions on that energy are made by measuring several lightning parameters. These lightning parameters are either directly measured as for example the lightning current at the base of a channel or are remotely obtained. Good examples of the latter are the records of the lightning electromagnetic field.

Statistical data for the distribution of the lightning parameters have been collected for years. They are published periodically in the literature. It was found and accepted among the lightning community researchers that lightning parameters can best be described by a log-

normal probability distribution whose probability density function (pdf) is given by the following equation:

$$f(y) = \frac{1}{y\sigma\sqrt{2\pi}} e^{-\frac{(\ln y - \mu)^2}{2\sigma^2}} \quad (3.38)$$

The most comprehensive research on this subject was made by Berger [13]. Part of the results from this study are reproduced in Table 3.9.

№ of events	Parameters	Unit	Percentage of cases exceeding tabulated value		
			95%	50%	5%
<i>Peak current (minimum 2 kA)</i>					
101	Negative first strokes	kA	14	30	80
135	Negative subsequent strokes	kA	4.6	12	30
26	Positive first strokes (no positive subsequent strokes recorded)	kA	4.6	35	250
<i>Charge</i>					
93	Negative first strokes	C	1.1	5.2	24
122	Negative subsequent strokes	C	0.2	1.4	11
94	Negative flashes	C	1.3	7.5	40
26	Positive flashes	C	20	80	350
<i>Impulse charge</i>					
90	Negative first strokes	C	1.1	4.5	20
117	Negative subsequent strokes	C	0.22	0.95	4.0
25	Positive first strokes	C	2.0	16	150
<i>Rise time</i>					
89	Negative first strokes	µsec	1.8	5.5	18
118	Negative subsequent strokes	µsec	0.22	1.1	4.5
19	Positive first strokes	µsec	3.5	22	200
<i>Maximum di/dt</i>					
92	Negative first strokes	kA/µsec	5.5	12	32
122	Negative subsequent strokes	kA/µsec	12	40	120
21	Positive first strokes	kA/µsec	0.20	2.4	32
<i>Stroke duration</i>					
90	Negative first strokes	µsec	30	75	200
115	Negative subsequent strokes	µsec	6.5	32	140
16	Positive first strokes	µsec	25	230	2000
<i>Integral (i²dt)</i>					
91	Negative first strokes	A ² sec	6.0x10 ³	5.5x10 ⁴	5.5x10 ⁵
88	Negative subsequent strokes	A ² sec	5.5x10 ²	6.0x10 ³	5.2x10 ⁴
26	Positive first strokes	A ² sec	2.5x10 ⁴	6.5x10 ⁵	1.5x10 ⁷
<i>Time interval</i>					
133	Between negative strokes	msec	7	33	150
<i>Flash duration</i>					
94	Negative (including single stroke flashes)	msec	0.15	13	1100
39	Negative (excluding single stroke flashes)	msec	31	180	900
24	Positive (only single flashes)	msec	14	85	500

Table 3.9 Lightning current parameters [13]

The parameter in this table which can be object of controversy is the maximum derivative dI/dt of the lightning current. More precise results concerning this parameter were recently presented [77]. These results are given in Table 3.10. The complementary probability distributions of the data indicated in the table are illustrated additionally in Fig. 3.32.

Source	No of events	Percentage of cases exceeding tabulated values, kA/ μ s		
		95%	50%	5%
<i>Leteinturier et al.</i> [1990]	31	53	103	199
<i>Berger et al.</i> [1975]	122	12	40	120
<i>Garbagnati and Lo Piparo</i> [1982]	33	7.5	33	145
<i>Anderson and Eriksson</i> [1980]	113	9.9	39.9	162
<i>Weidman and Krider</i> [1984]*	121	78	154	309
<i>Leteinturier et al.</i> [1985]*	62		227	

* Estimates derived from remote electric radiation field measurements.

Table 3.10 Comparison of subsequent return stroke dI/dt measurements [77]

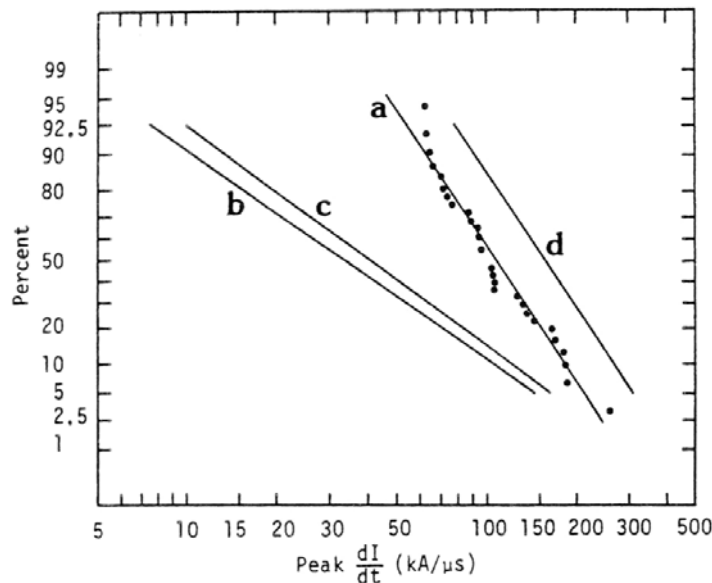


Fig. 3.32 Complementary probability distribution of return stroke peak dI/dt measurements:

Line **a** - *Leteinturier et al.* [1990]; Line **b** - *Anderson and Eriksson* [1980]; Line **c** - *Garbagnati and Lo Piparo* [1982]; Line **d** - *Weidman and Krider* [1984]; [77]

Stochastic data for the statistical distributions concerning electromagnetic fields radiated by the lightning were presented above in Table 3.5.

Chapter 4

4. Case study – investigation of lightning flash interaction with a transmission line as part of the control system

There is a general consensus [25] that a transmission line under the ground is less prone to the induction effects caused by a nearby lightning flash. However, the low thresholds of the operation energy levels of modern electronic equipment can be attained in the transmission line due to coupling of electromagnetic fields radiated by the lightning, even if the line is underground. There are numerous references, e.g. [31], [43], [93], in which the influence of a lightning discharge on above-ground power lines and low-voltage installations is investigated. Yet, there is not so much information about the behaviour of lines under the ground. Therefore, a more detailed investigation of induction effects is required for this case.

The present chapter investigates the potential influence of a lightning strike above a buried control system line of conductors. The effects arising from the fact that many of the input parameters for the simulation are stochastic, are also considered

4.1 Description of the line

A drawing illustrating the investigated transmission line is shown in Fig. 4.1. The line is used to connect two buildings in an industrial complex. The line is buried under the ground and the depth at which it is located varies from 1.6 to 6 m below the ground surface. There are concrete housings at both ends of the line which connect the latter with the buildings. The housings are also used to access the cables at the beginning and at the end of the line. Along

the route of the line the cables are placed inside polyethylene (PE) tubes. A cross-section showing how these tubes are situated along the way of the line is also presented in Fig. 4.1. It is evident that there are two types of PE tubes. The high voltage power cables are laid in the tubes with the bigger diameter (\varnothing 125 mm). The cables intended for low-voltage signals are placed in the tubes with a diameter of \varnothing 75 mm. The cross-section also shows that the two types of tubes (the two types of cables, respectively) are separated. The purpose of this separation is to avoid the interference in the low-voltage cables caused by the signals carried in the high-voltage cables. Additionally, the low-voltage cables are protected against a lightning flash by bare copper conductors situated above and on both sides of the tubes, as illustrated in the cross-section.

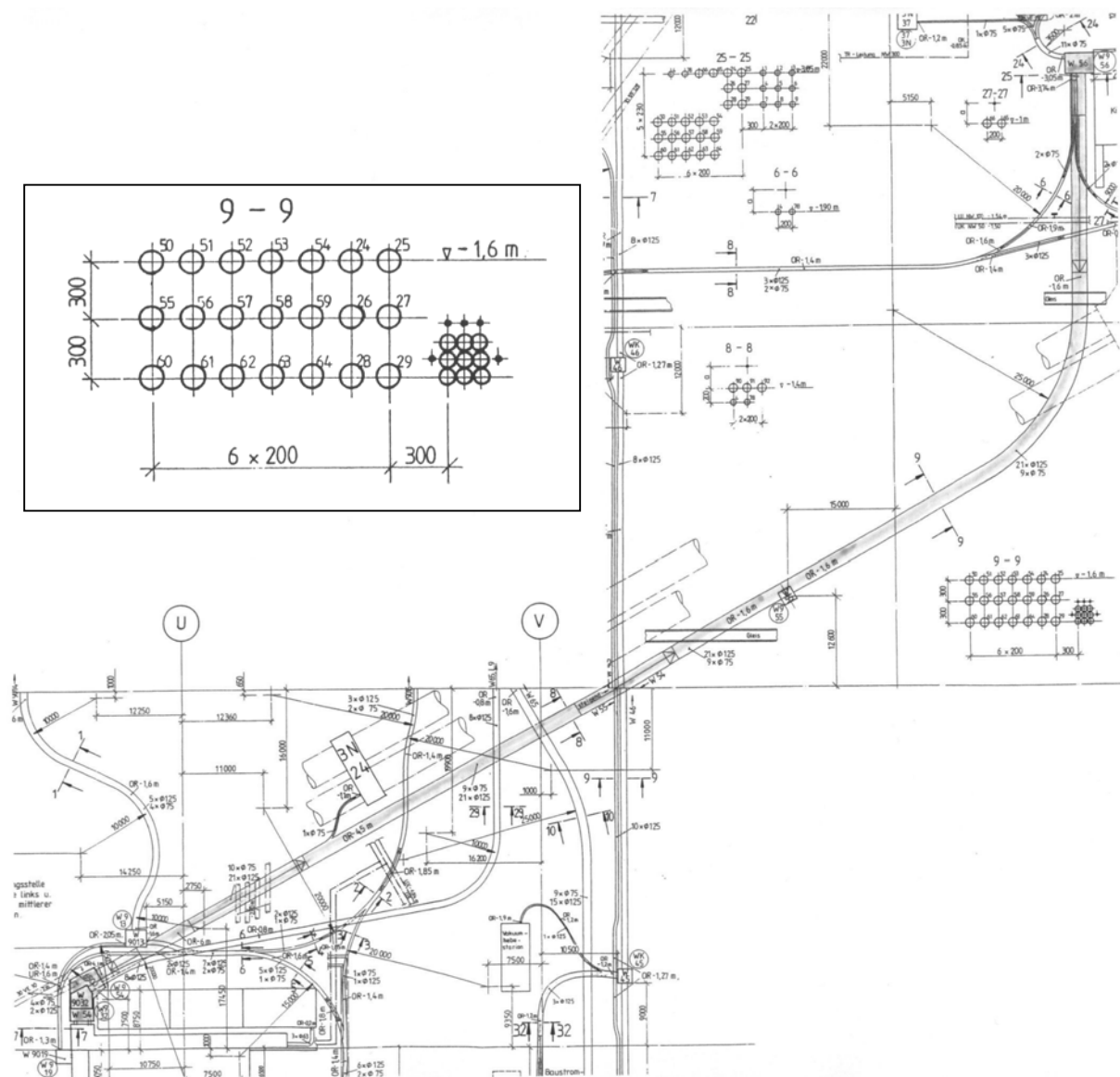


Fig. 4.1 A draft of the transmission line with cross-section showing the PE tubes along the line and the protective bare copper conductors

Given the system geometry, the goal here is to estimate the induced voltage surges caused by a nearby or direct lightning strike on the line in the low-voltage cables at the point of entering the second enclosure. The knowledge of the levels of the typical responses will permit the specification and design of appropriate surge protection devices needed for protecting the equipment connected to the end of the line.

A 3D illustration of the route of the line showing also the line dimensions is presented in Fig. 4.2.

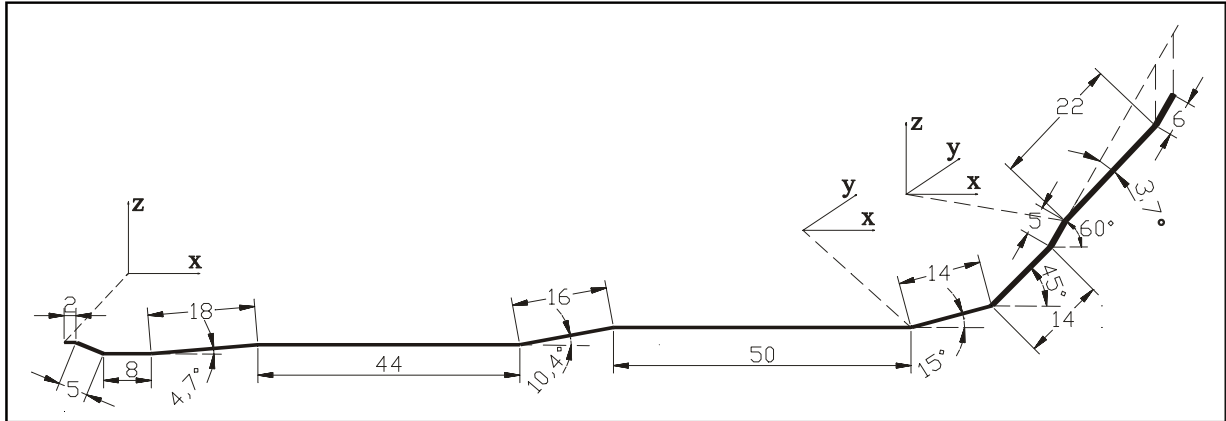
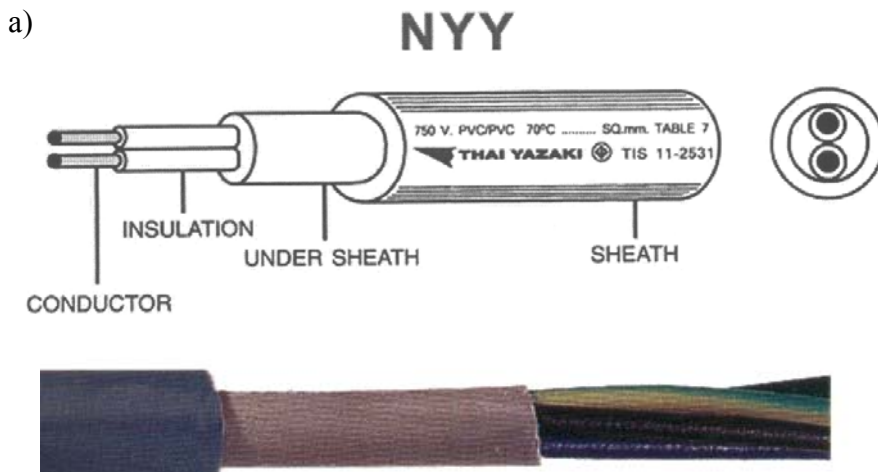


Fig. 4.2 3D illustration of the transmission line. Overall dimensions (in meters) are also given

A reference to the documentation [140] reveals that the following cables are placed in the tubes with diameter 75 mm (the low-voltage cable tubes):

- AJ-LIICYDY;
- AJ-Y(ST)YDY;
- A-2YF(L)2Y;
- NYY-O;
- NYY-J;

Sections of these cables are shown in Fig. 4.3



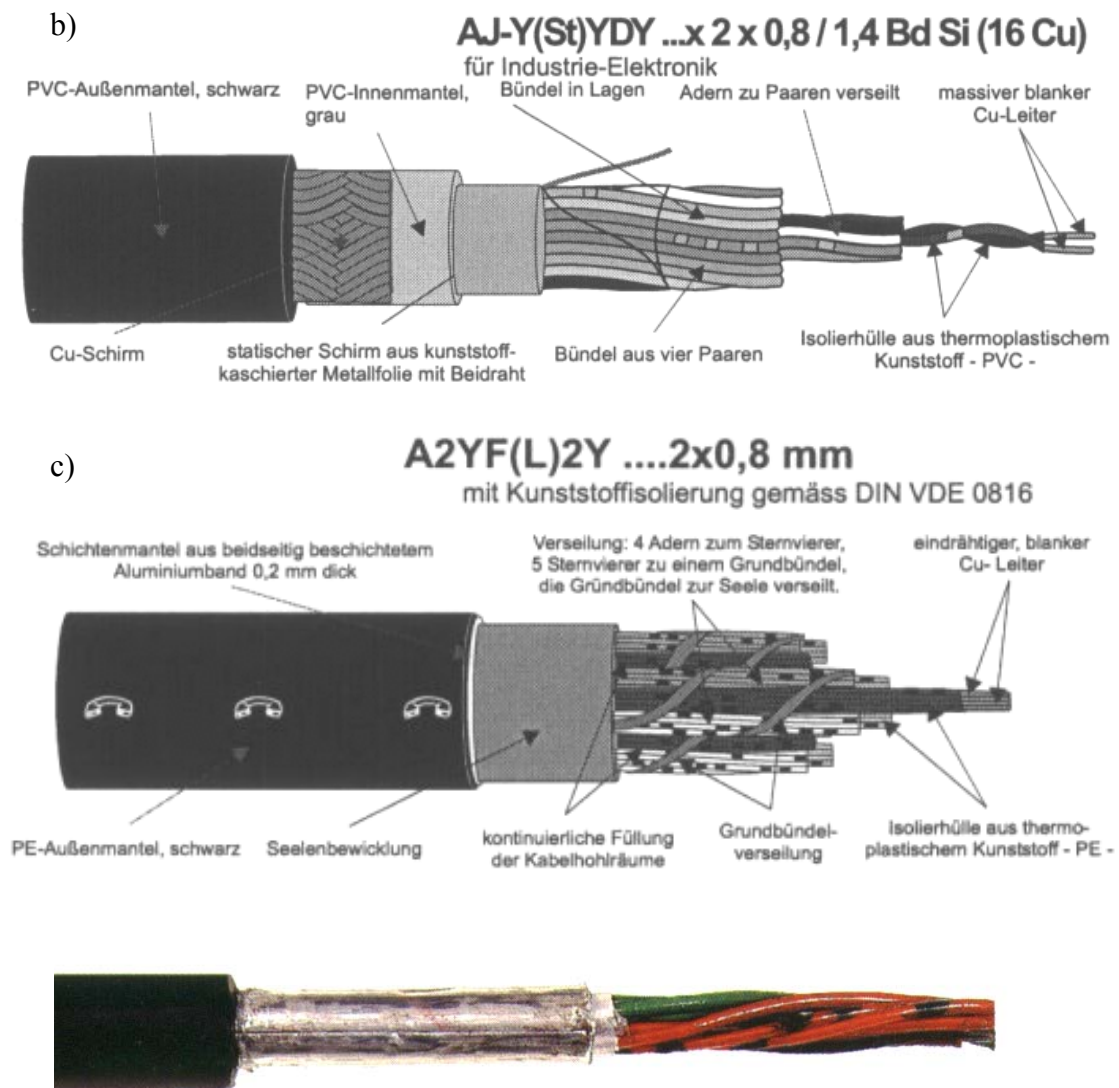


Fig. 4.3 Illustration of the cables used for the low-voltage part of the line:
(a) Cable types *NYY-O* and *NYY-J*; (b) *AJ-Y(ST)YDY*; (c) *A-2YF(L)2Y*;

As is evident from Fig. 4.3, the cables *NYY-O* and *NYY-J* consist of conductors and PVC insulation. There is no solid or braided shield layer in these cables, which serves to protect the signal-carrying conductor from external electromagnetic (EM) influence. This fact makes these cables exposed to the EM effects caused by external electromagnetic fields. Secondly, the presence of a metallic shield makes the analysis of the voltages and currents in the internal conductors much more complicated, involving the so-called transfer impedance \hat{Z}_t . The simulation of the latter is not possible with the means available here. The above two reasons justify their choice for carrying out the simulations.

The geometry of the cable *NYY-O 4x4 re* which is used in the model, is shown in Fig. 4.4.

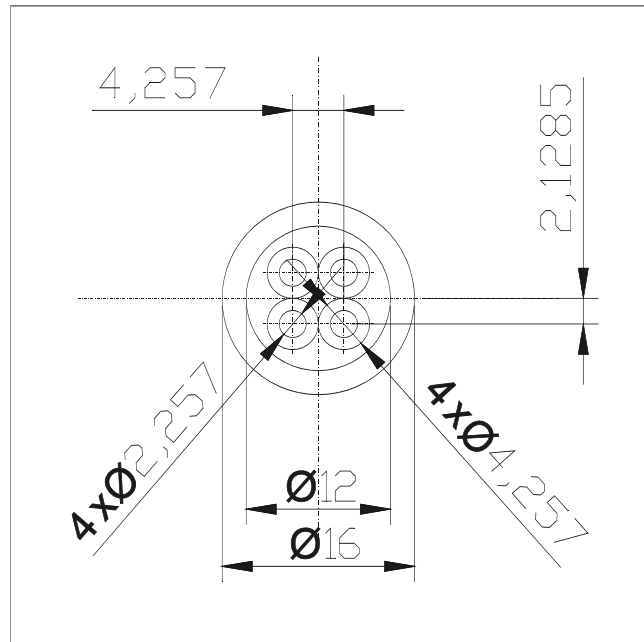


Fig. 4.4 Illustration of the geometry of the cable *NYY-O 4x4 re* (dimensions in millimeters)

4.2 Electrical dimensions of a transmission line

Before describing the simulations performed on the above transmission line in detail, one very important concept concerning transmission lines, namely their electrical dimensions is discussed. The physical dimensions of a given transmission line are of secondary importance when its electromagnetic properties are investigated. Electrical dimensions of a given line are measured in wavelengths, considering the electromagnetic wave which propagates in it. The wavelength of the electromagnetic wave (in the case of a uniform plane wave) is the distance between corresponding adjacent points in the wave which have the same amplitude. The wavelength is denoted by λ (Fig. 4.5). For lossless (nonconductive) media, the wavelength can be calculated using the following expression:

$$\lambda = \frac{v}{f} \quad (4.1)$$

where v is the velocity of propagation of the wave in the corresponding medium and f is the frequency of the wave. In case an electromagnetic wave is propagated in vacuum, its velocity is that of light $c = 3 \times 10^8$ m/s. Equation (4.1) then takes the form: $\lambda = c / f$

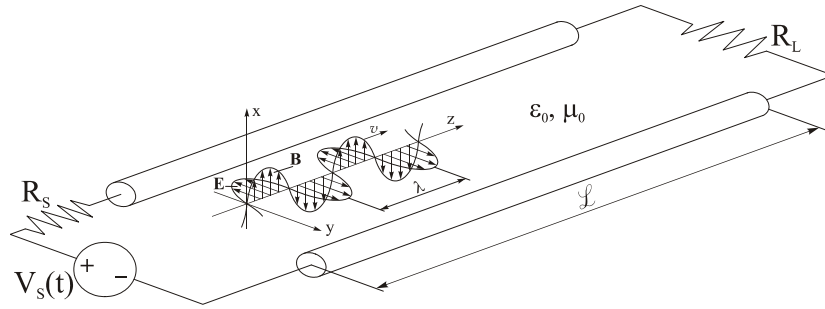


Fig. 4.5 Illustration a transmission line and the electromagnetic wave propagating in it

Generally, the velocity of propagation of a wave in a non-conductive medium other than vacuum is determined by the permittivity ϵ and the permeability μ of the medium. It is given by the equation

$$v = \frac{1}{\sqrt{\epsilon\mu}} \quad (4.2)$$

For vacuum equation (4.2) reads

$$c = \frac{1}{\sqrt{\epsilon_0\mu_0}} \quad (4.3)$$

where ϵ_0 and μ_0 are the permittivity and permeability, in vacuum. Any other medium is characterized by its permittivity and permeability relative to that of empty space, ϵ_r and μ_r , so that $\epsilon = \epsilon_r\epsilon_0$ and $\mu = \mu_r\mu_0$.

Then equation (4.2) can be rewritten as

$$v = \frac{1}{\sqrt{\epsilon\mu}} = \frac{c}{\sqrt{\epsilon_r\mu_r}} \quad (4.4)$$

For typical nonconductive materials $\mu_r \approx 1$ and ϵ_r is usually between 2 and 6, so that the velocity of propagation ranges from $0.4c$ to $0.7c$. Thus, the wavelength of the electromagnetic wave propagated in these materials is shorter as compared with its propagation in vacuum. The same is true if the frequency of an electromagnetic wave is increased. Its wavelength then decreases.

If we have a transmission line, whose largest dimension is \mathcal{L} , then this line has electrical dimensions in terms of wavelength k , given by [104]

$$k = \frac{\mathcal{L}}{\lambda} \quad (4.5)$$

From eqs. (4.1) and (4.5) it is evident that the electrical dimensions of the line depend on its physical dimensions, the frequency of operation and the velocity of propagation of the wave in the medium in which the line is immersed.

The transmission line is said to be electrically small if its largest dimension \mathcal{L} is much smaller than the wavelength of the electromagnetic wave propagated in it, i.e. $\mathcal{L} \ll \lambda$. Although only an approximate criterion, it is accepted that a line is electrically small if

$$\mathcal{L} < \frac{\lambda}{10} \quad (4.6)$$

If the line length \mathcal{L} is commensurable or larger in comparison with wavelength of the electromagnetic wave, then the line is said to be electrically large.

The notion of electrically small lines and circuits is very important. If the line is electrically small then simpler concepts, as for example Kirchhoff's voltage and current laws along with the lumped-circuit modelling of the line enable one to find voltages and currents along it. If the line is electrically large, then the wave propagation effects must be taken into account and the only choice is to use Maxwell's equations or one of their approximations as, for example, the transmission line equations in order to find these voltages and currents.

The importance of the correct calculation of the electrical dimensions of a transmission line will be illustrated by the following simple example. Assuming that a transmission line with a length of $\mathcal{L}=9$ m operates in air at a frequency of 3 MHz. Then, because for air $\epsilon_r=1$ and $\mu_r=1$, the propagation of the electromagnetic wave is that in vacuum, namely $c=3 \times 10^8$ m/s. The wavelength of the electromagnetic wave then is

$$\lambda = \frac{v}{f} = \frac{c}{f} = \frac{3 \times 10^8 \text{ m/s}}{3 \times 10^6 \text{ Hz}} = 100 \text{ m}$$

and

$$\mathcal{L} = 9 \text{ m} < \frac{1}{10} 100 = 10 \text{ m}$$

Thus, at a frequency of 3 MHz this line is electrically small. If the same line now operates at a frequency of 30 MHz, then

$$\lambda = \frac{c}{f} = \frac{3 \times 10^8 \text{ m/s}}{30 \times 10^6 \text{ Hz}} = 10 \text{ m}$$

and the line is electrically large since

$$\mathcal{L} = 9 \text{ m} > \frac{1}{10} 10 = 1 \text{ m}$$

In this case the transmission line equations should be used if we want to find voltages and currents along the line. The other possibility is to divide the line into sections, each of them with a length of l m and to apply the lumped-circuit approach to each section of the line.

4.3 Deterministic study of the interaction of lightning with the line

In this section, the development of models of lightning strike interaction with the transmission line is discussed. It is assumed that all input parameters are fixed, i.e. neither the lightning strike nor the line parameters are considered to be random variables. After obtaining the results from the deterministic models presented here, the stochastic effects and uncertainties are taken into account in the following section. In this section, two general cases are studied, as illustrated in Fig. 4.6

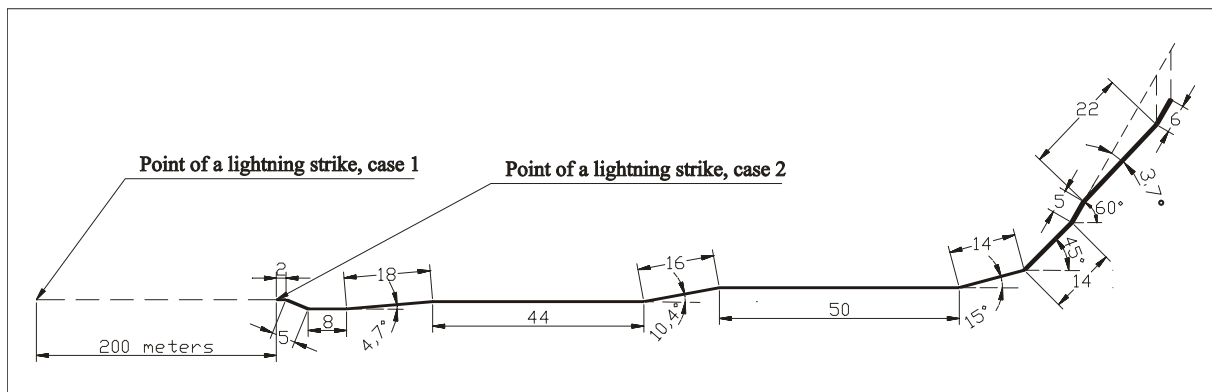


Fig. 4.6 Illustration of the assumed points of the lightning strike for the two cases investigated here

- 1) A lightning strike at a distance of 200 m from one of the ends of the line. In this case the interference in the conductors of the line is caused by the electromagnetic induction from the external field generated by the lightning
- 2) A direct lightning strike on one of the enclosures of the line. Here, interference voltages are generated by “crosstalk” between the conductors in the investigated cross-section as explained below

4.3.1 Distant strike and electromagnetic field coupling

In the first case considered, the lightning flash is assumed to occur at a distance of 200 m from the end of the line (Fig. 5.5). The distance is chosen to be 200 m because, as stated by Cooray [21], this is the smallest distance for which the horizontal part of the electric field radiated by the lightning is calculated correctly with the formulae provided. Also 200 m is assumed to be a distance sufficient for the voltages induced in the line to be generated only by the electromagnetic field radiated by the lightning. This case is simulated with the most widely used approach, that by Agrawal which is briefly described in Appendix III. According to this formulation, the horizontal part of the electric field gives rise to voltage sources along the line, because conductors there are laid in horizontal direction, if two conductors and an arbitrary incident electromagnetic field are present. The tangential part of the electric field gives rise to voltage sources at both ends of the line – where conductors are oriented vertically. An important aspect: If the conductors are laid under the ground, only the horizontal part of the electric field is of importance [30]. Firstly, because the vertical part of the electric field is strongly attenuated when being propagated through the ground in contrast to the horizontal field which is almost unchanged [25]. Secondly, the distance between the conductors is very small so that the coupling of the field at the ends of the transmission line can be neglected. Hence, in the coupling of the field with the conductors only the voltage sources along the line caused by the horizontal part of the electric field are presented. In simulating this case, only two conductors from the cable *NYO 4x4 re* are considered, as illustrated in Fig. 4.7.

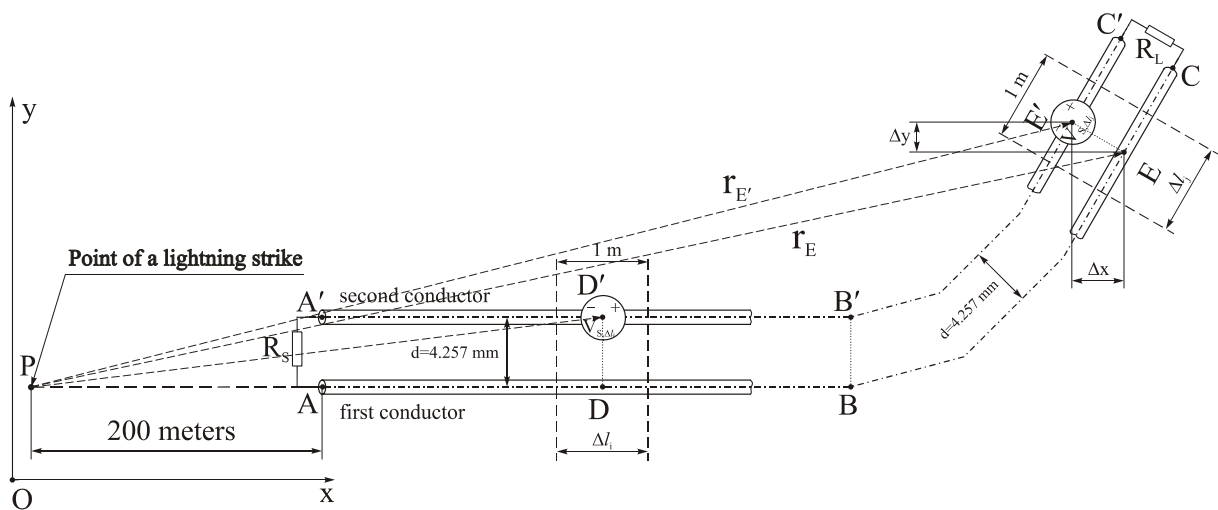


Fig. 4.7 Geometry of the conductors used in the simulation and the point of the lightning strike

The first conductor is assumed to be the reference conductor for the signal which flows in the second conductor. The conductors terminate at both ends with resistances R_S and R_L , with the value of 50Ω being taken for both of them in the simulation. In Fig. 4.7, the assumed point of the lightning strike is also shown. Considering a section Δl_i with a length of 1 m, the voltages generated by the lightning in this section can be approximated as a lumped circuit voltage source as illustrated in Fig. 4.7. It is obtained as the difference of the horizontal electric field between points D and D' , situated at the middle of the section of the first and the second conductor respectively

$$V_{S,\Delta l_i}(t) = \mathcal{E}_{rD'}(t) - \mathcal{E}_{rD}(t) \quad (4.7)$$

This approach is possible because the major part of the frequency spectrum of the lightning as it was shown in Chapter 3 extends to a maximum of 10 MHz. At this frequency, the length of the electromagnetic wave is

$$\lambda = \frac{c}{f} = \frac{3 \times 10^8}{10 \times 10^6} = 30m \quad (4.8)$$

Therefore, 1 m is electrically small compared to the highest frequency of interest and the lumped circuit approximation is justified. Because of the choice of the point of the lightning strike (cf. Fig. 4.7), the distance PD is almost equal to the distance PD' . The difference in the latter two is smaller than one hundredth of a millimetre and the difference of the horizontal electric field between the two conductors from point A to point B can be considered to be zero. Therefore, there are distributed voltage sources only from point B to point C . These voltage sources are situated in the second conductor and the distance between any two of them is 1 m. Taking into account the total length of the line, there should exist a total of 204 voltage sources. But, due to the choice of the lightning strike point, the number of the voltage sources is reduced from 204 to 61.

In order to calculate the voltage sources $V_{S,\Delta l_j}(t)$, a modification of the “LEMFieldE” program was developed. The modified code calculates only the horizontal component of the underground electric field at a depth s and distance r from the point of the stroke.

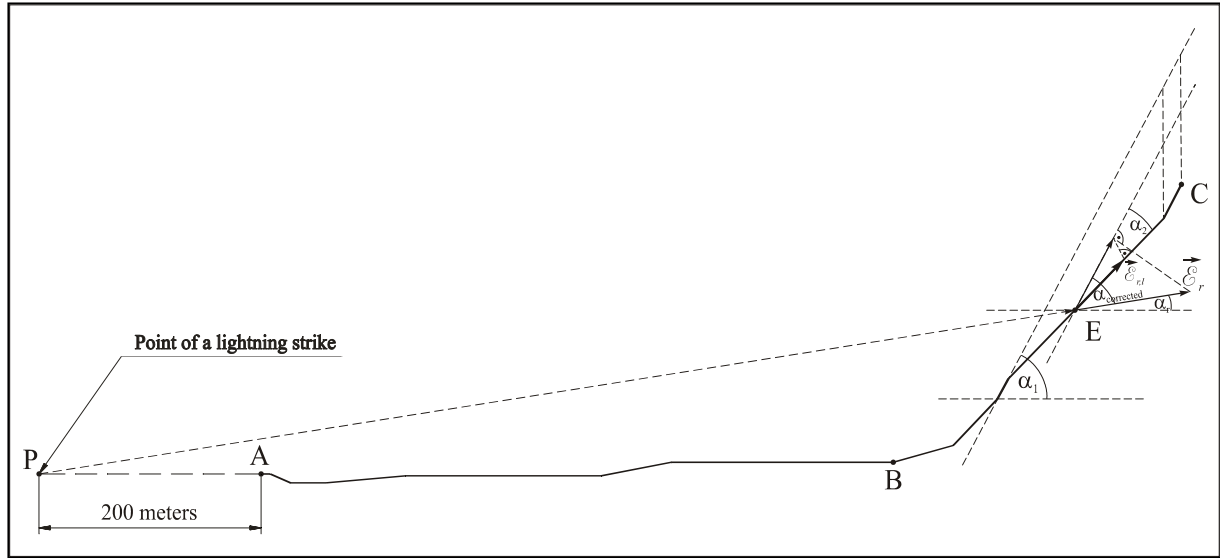


Fig. 4.8 Illustration of the geometry for computation of the longitudinal component of the horizontal electric field implemented in the modified “LEMFieldE” code

Additionally, as shown in Fig. 4.8, only the longitudinal component of the horizontal electric field vector is needed for the points from point B to point C. At point E, for example, this component can be calculated as

$$E_{r,l}(t) = E_r(t) \cos \alpha_{corrected} \cos \alpha_2 \quad (4.9)$$

where $\alpha_{corrected}$ is obtained as

$$\alpha_{corrected} = \alpha_1 - \alpha_r \quad (4.10)$$

The modified code uses two ASCII input files: LEMFIELD.DAT and DIM.DAT. In LEMFIELD.DAT the lightning strike parameters and the parameters of the ground are specified. DIM.DAT contains the distance r and the depth s for each point along the axis of the first and the second conductor, where the computation of the horizontal electric field is necessary, as described above. In this file the angles α_1 , α_2 and α_r for the calculation of the longitudinal component of the field at each point are also given.

As an output ASCII files are produced which contain the values for the lumped voltage sources in the time domain. The names of these files are of the form $E_{r_RSxXXT}.TIM$, where XX is the number corresponding to the respective voltage source starting from number 144.

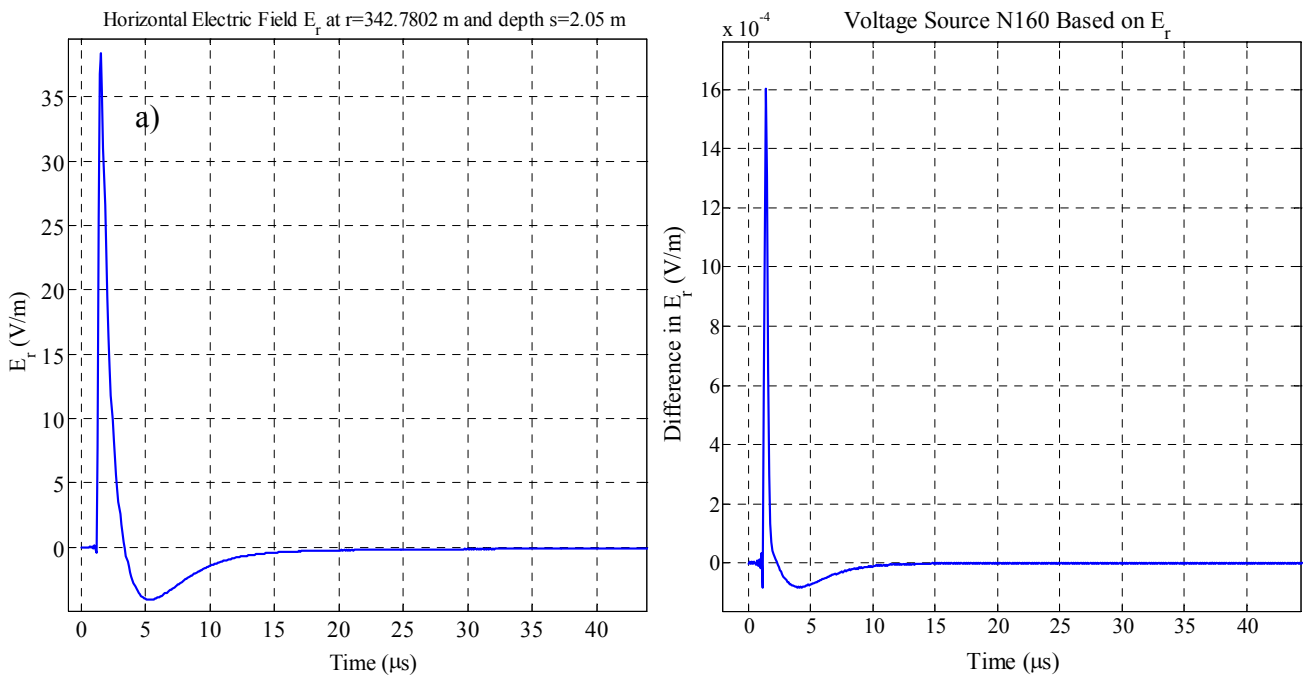


Fig. 4.9 Example calculation of: (a) the horizontal electric field at distance $r=342.78$ m and depth $s=2.05$ m; (b) the voltage source $Er_Sx160T.TIM$

As an example, the horizontal electric field at a distance $r=342.7802$ m and depth $s=2.05$ m from the point of the strike and the voltage source number 160 which is the voltage source in the section with number 160 from the beginning of the line, are shown in Fig. 4.9. This voltage source is calculated as the difference of the horizontal field between the points $r_1=357.62569$ m and $r_2=357.62866$ m respectively. The depth s is 2.05 m. The full DIM.DAT file is given in Appendix I.

The simulation is made with the program “CableMod” [18]. This is a program whose purpose is to analyze complex cable structures. It has a powerful two-dimensional field solver for the calculation of the per-unit-length parameters of the given geometry and a SPICE equivalent network simulator for the calculation of the voltages and currents in the simulated conductor system. The voltage sources calculated with “LEMFieldE_M” are used as an external input in the program “CableMod” for finding the response at the far end of the conductors in the cable *NYO 4x4 re*. The result of the simulation is presented in section 4.3.3.

4.3.2 Direct lightning strike and crosstalk between the conductors

In the second case investigated, it is assumed that the lightning strikes directly the shielded enclosure at the beginning of the line, as illustrated in Fig. 4.10.

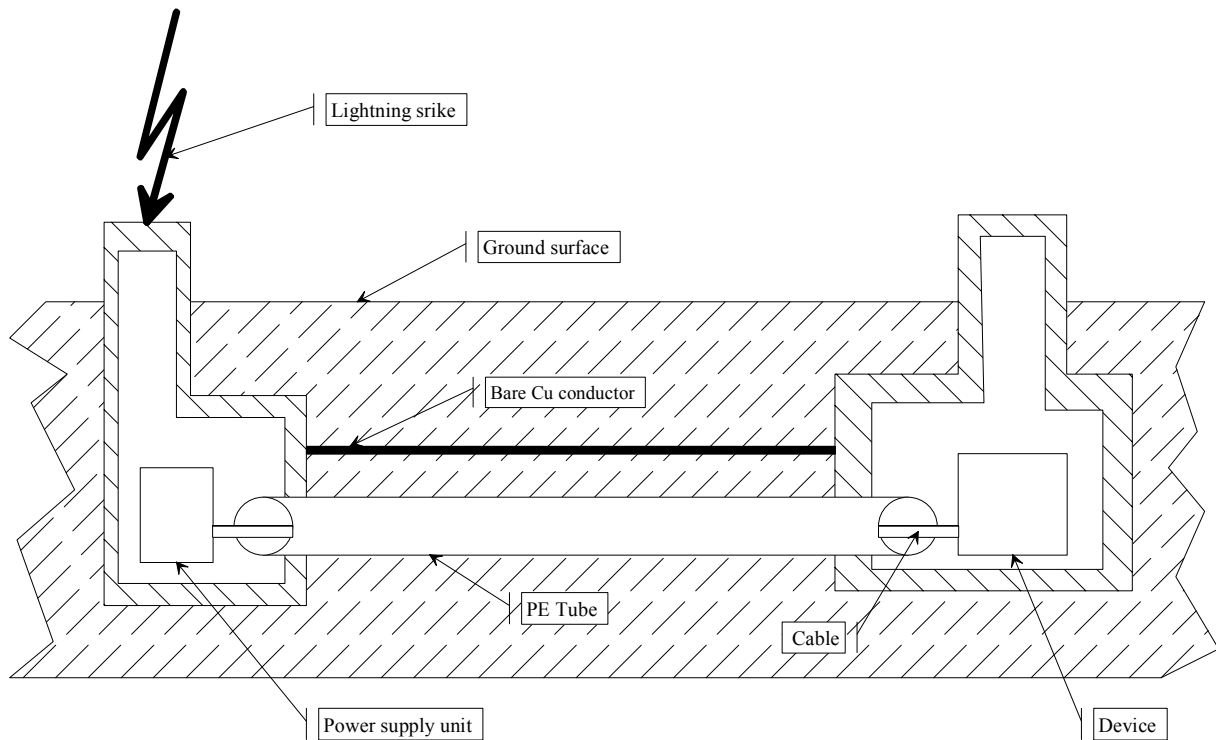


Fig. 4.10 Basic configuration of the second case – direct lightning strike

The voltages in the control conductors in this case are induced by the crosstalk between the latter and the lightning current which flows in the protective bare copper conductors. A detailed cross-section of the line topology is shown in Fig. 4.11.

Here, again the potential surge voltages which can be induced at the far end of the cable *NYY-O 4x4 re* are considered. It is assumed that the cable is situated in the middle of the polyethylene (PE) tube, as shown in the figure. There are 5 bare copper conductors with a diameter of $d=9.5$ mm each of which is situated above and on both sides of the PE tubes bundle. Their purpose is to protect the system from different effects caused by a nearby lightning strike (e.g. the current that flows from the lightning to the ground).

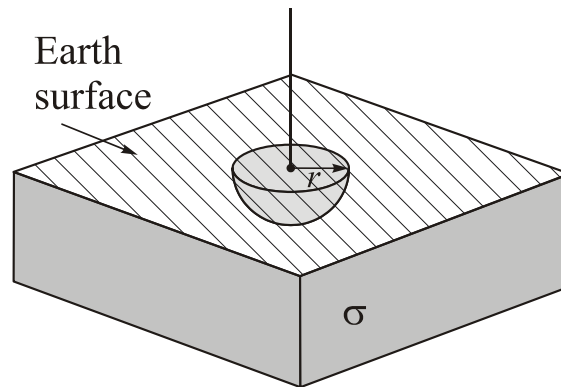


Fig. 4.12 Illustration of resistance calculation of the enclosure

Hence, its resistance is calculated with the formula [142]

$$R = \frac{l}{2\pi\sigma r} \quad (4.11)$$

Assuming that the radius of the hemisphere is $r=1.5$ m and that the conductivity of the ground is $\sigma=0.005$ S/m for the resistance of the two housings at the beginning and the end of the line, we obtain

$$R_{H_1} = R_{H_2} = \frac{l}{2 \cdot 3.14 \cdot 0.005 \cdot 1.5} = 21.22\Omega$$

Thus, the current from the lightning flows through the resistance of the enclosure R_{H_1} into the bare copper conductors. Additionally, because the bare copper conductors are in direct contact with the ground, part of the current leaks away from the conductors into the earth. This effect is electrically simulated by the resistances R_{leak} which connect the protective conductors with the ground.

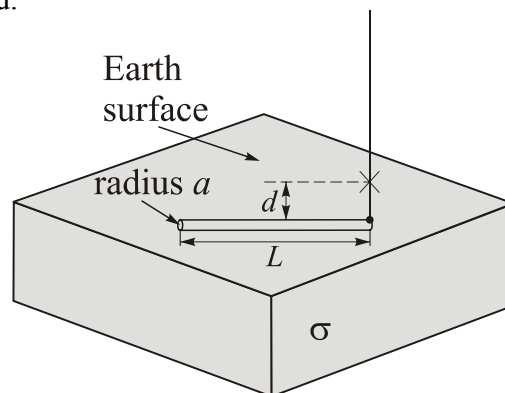


Fig. 4.13 Illustration of resistance calculation of the bare copper conductors

For a buried horizontal rod this resistance with respect to Fig. 4.13 is calculated according to [142] as

$$R = \frac{l}{\pi\sigma L} \left[\ln\left(\frac{2L}{\sqrt{2ad}}\right) - 1 \right] \quad (d \ll L) \quad (4.12a)$$

$$R = \frac{l}{2\pi\sigma L} \left[\ln\left(\frac{2L}{a}\right) - 1 + \frac{L}{4d} \right] \quad (d \gg L) \quad (4.12b)$$

A description of the line in this case from the electrical point of view, taking into account the above considerations, is shown in Fig. 4.14.

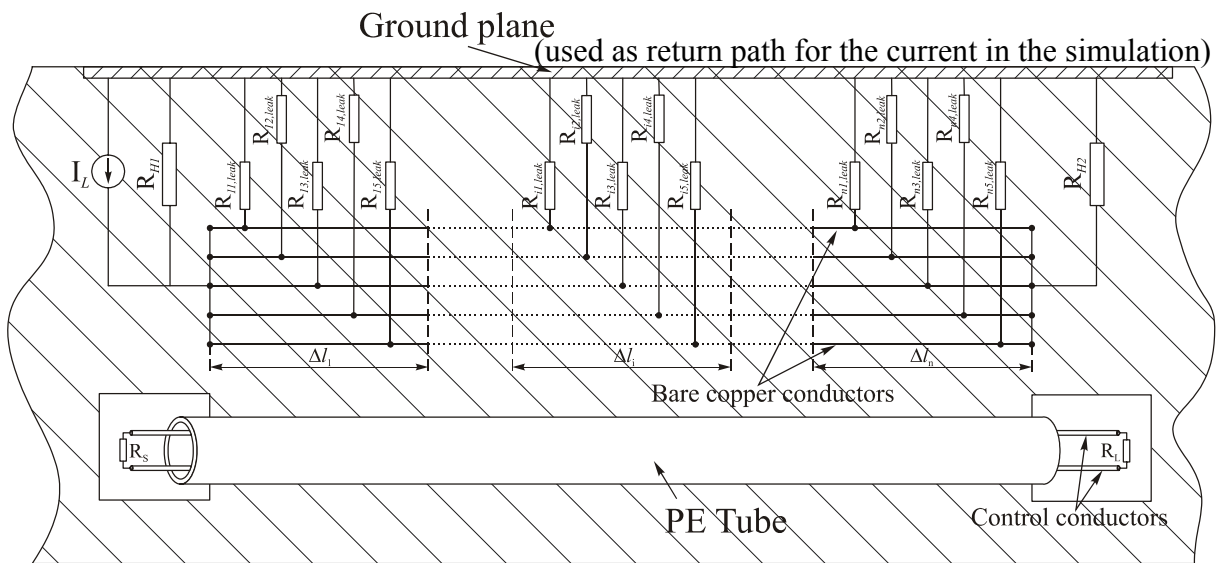


Fig. 4.14 Illustration of lumped circuit electrical approximation of the line

For the simulation, the line is divided into sections, each of a length of 1 m. Taking into account the total length of the line, there are a total of 204 such sections. Assuming that $L=1$ m (cf. Fig. 4.13) and substituting into the eq. (4.12b), the following result is obtained for one of the resistances $R_{ij,leak}$

$$R = \frac{1}{2 \cdot 3.14 \cdot 0.005 \cdot 1} \left[\ln\left(\frac{2 \cdot 1}{9.5 \cdot 10^3}\right) - 1 + \frac{1}{4 \cdot 4.9} \right] = 162.15 \Omega$$

In this calculation the depth under the ground is taken to be $d=4.9$ m.

Crosstalk voltages induced in the far end of the control conductors, caused by the current which flows in the protective conductors are obtained by directly solving the transmission line equations for the specific cross-section of the line. For this purpose, again the program

“CableMod” is utilized. The program has a well developed graphical user interface (GUI), where it is possible for each section of the line to define the cross-section shown in Fig. 4.11. One of these cross-sections used in the program for computation of the per-unit-length parameters of the section is illustrated in Fig. 4.15 and per-unit-length matrices calculated for one section are given in the end of Appendix I.

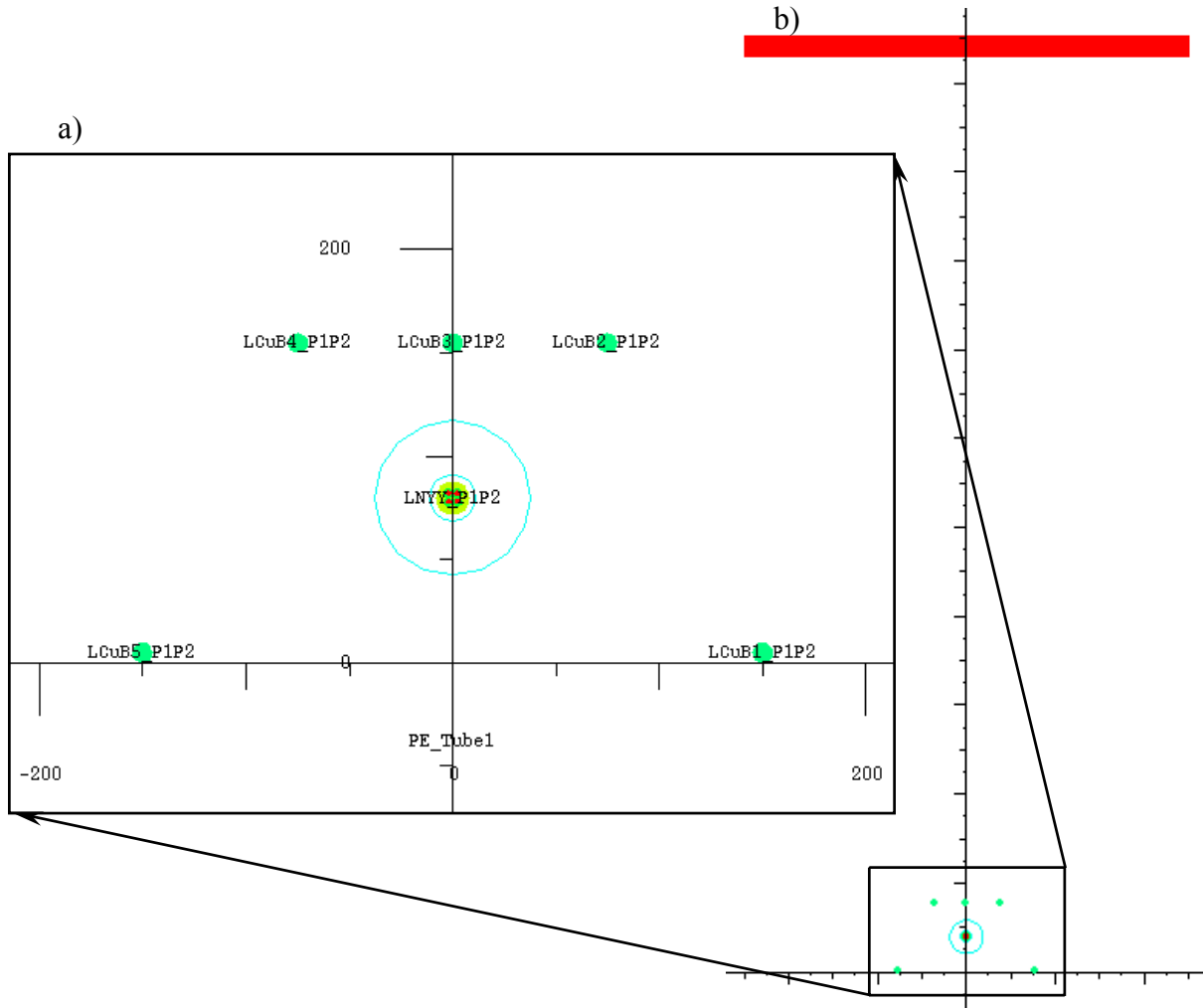


Fig. 4.15 Cross-section of the line defined in the program “CableMod”: (a) cross-section without ground plane; (b) cross-section with ground plane;

The multiconductor transmission line equations resulting for each section are solved using a SPICE network simulator. In SPICE, the MTL equations are solved in a way similar to that described in Appendix III. Once the per-unit-length matrices for a given cross-section are obtained, it is possible to find similarity transformations \mathbf{T}_V and \mathbf{T}_I which diagonalize them and which are used for the calculation of the voltages and currents of the line through the mode voltages and currents.

$$\mathbf{V}(z, t) = \mathbf{T}_V \mathbf{V}_m(z, t) \quad (4.13a)$$

$$\mathbf{I}(z, t) = \mathbf{T}_I \mathbf{I}_m(z, t) \quad (4.13b)$$

Via the mode transformations, it is possible to uncouple the MTL equations for a given section of a line, to n uncoupled two-conductor transmission line equations whose solution can be obtained in terms of the mode voltages and currents[106]. The solution for the line voltages and currents for two conductor transmission lines in the time domain is implemented in one of the commands of the SPICE program. So we can easily obtain the solution for the mode voltages and currents at the both ends of each section for this set of n uncoupled two-conductor transmission line equations. It is more important to find the real voltages and currents of the line which are related to the mode voltages and currents through the mode transformations. Writing the latter in expanded form gives [106]

$$\begin{bmatrix} V_1(z, t) \\ V_2(z, t) \\ \vdots \\ V_n(z, t) \end{bmatrix} = \begin{bmatrix} T_{V11} & T_{V12} & \cdots & T_{V1n} \\ T_{V21} & T_{V22} & \ddots & \vdots \\ \vdots & \vdots & \ddots & \vdots \\ T_{Vn1} & \cdots & \cdots & T_{Vnn} \end{bmatrix} \begin{bmatrix} V_{m1}(z, t) \\ V_{m2}(z, t) \\ \vdots \\ V_{mn}(z, t) \end{bmatrix} \quad (4.14a)$$

$$\begin{bmatrix} I_1(z, t) \\ I_2(z, t) \\ \vdots \\ I_n(z, t) \end{bmatrix} = \begin{bmatrix} T_{I11} & T_{I12} & \cdots & T_{I1n} \\ T_{I21} & T_{I22} & \ddots & \vdots \\ \vdots & \vdots & \ddots & \vdots \\ T_{In1} & \cdots & \cdots & T_{Inn} \end{bmatrix} \begin{bmatrix} I_{m1}(z, t) \\ I_{m2}(z, t) \\ \vdots \\ I_{mn}(z, t) \end{bmatrix} \quad (4.14b)$$

where the entries in \mathbf{T}_V and \mathbf{T}_I are denoted as T_{Vij} and T_{Iij} respectively.

Inverting (4.14b) gives

$$\begin{bmatrix} I_{m1}(z, t) \\ I_{m2}(z, t) \\ \vdots \\ I_{mn}(z, t) \end{bmatrix} = \begin{bmatrix} T_{I11}^{-1} & T_{I12}^{-1} & \cdots & T_{I1n}^{-1} \\ T_{I21}^{-1} & T_{I22}^{-1} & \ddots & \vdots \\ \vdots & \vdots & \ddots & \vdots \\ T_{In1}^{-1} & \cdots & \cdots & T_{Inn}^{-1} \end{bmatrix} \begin{bmatrix} I_1(z, t) \\ I_2(z, t) \\ \vdots \\ I_n(z, t) \end{bmatrix} \quad (4.14c)$$

where the entries in \mathbf{T}_I^{-1} are denoted as T_{Iij}^{-1} .

The transformations in (4.14a) and (4.14c) can be implemented in SPICE using the controlled source representation illustrated in Fig. 4.16.

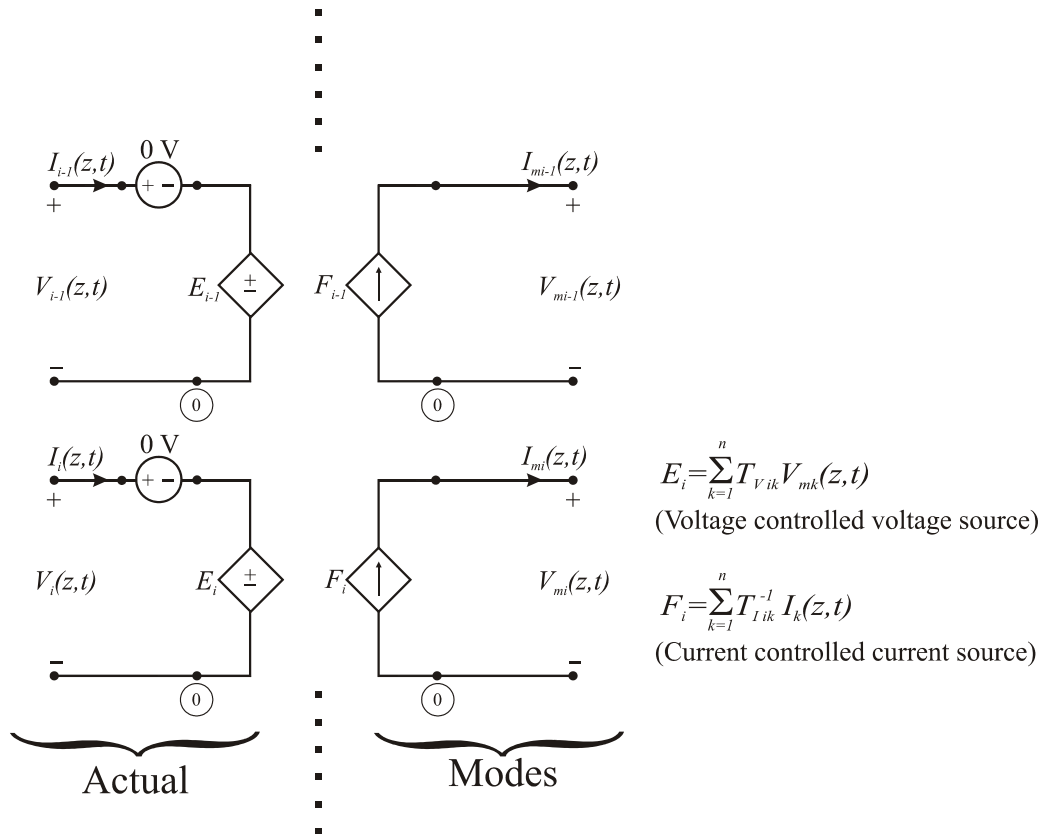


Fig. 4.16 Illustration of the implementation of the mode transformations using controlled sources.

Zero voltage sources are placed in each input to sample the current. $I_i(z, t)$ for use in the controlled sources representing the transformation in (4.14c).

Through the transformation illustrated in Fig. 4.16 the decoupling of the MTL equations is achieved and the solution for the modal voltages for both ends of the section is obtained. The real voltages and currents at the far end of the section are obtained through the same transformation illustrated in Fig. 4.16, where as mode voltages and currents those calculated at the far end of the line are used. Thus through the solution for the voltages and currents for each section of the line, the solution for the voltages and currents at the end of the line can be found.

In the simulations the conductivity of the conductor used for the simulation of the ground plane as a return path for the current illustrated in Fig. 4.15b is taken to be 100 S/m. This value is a little bigger compared with the real ground conductivity values, but this was the smallest conductivity value for a given conductor allowed by the “CableMod” program.

As an external input parameter in this case, the current which flows at the base of the lightning, is used. The lightning strike provides the injection of this current into the building

and the current spreads over the enclosure in a search for a path to ground. Part of the current flows directly from the building into the ground through the resistance R_{H_I} of the building. The remaining part of the current is split up between the five protective conductors (cf. Fig. 4.14). Assuming that the current waveform is similar to that depicted in Fig. 3.18a with a maximum current of $I_{max}=13$ kA, the current which flows at the beginning of each one of the five bare copper conductors is illustrated in Fig. 4.17.

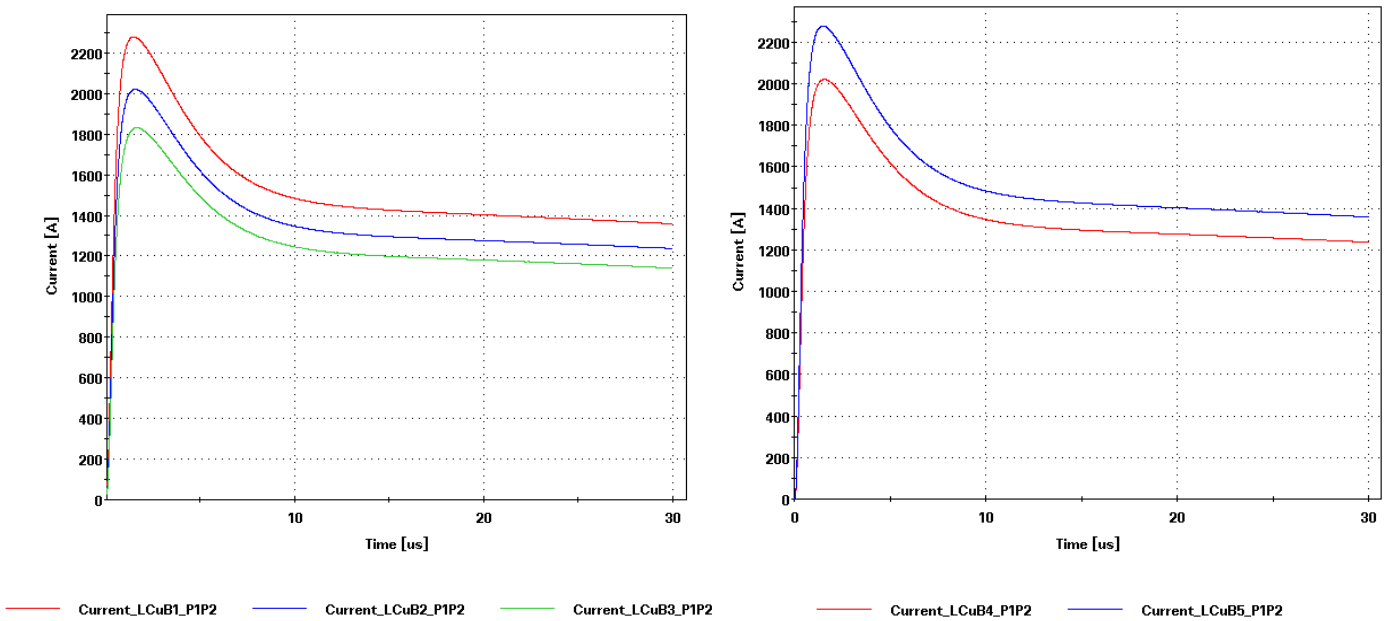


Fig. 4.17 Current which flows in each of the five bare copper conductors as calculated by the program “CableMod” (for notation of the conductor currents see Fig. 4.15a)

The voltage induced by this current in the far end of the cable *NYY-O 4x4 re* is presented in the next section. Here again only two conductors from this cable are examined. One of them serves as the signal carrying conductor and the second as a reference conductor. In the simulation it is assumed that there is no voltage source at the near end of the line. Also the line is terminated with resistances $R_S=R_L=50 \Omega$ at its ends. (cf. Fig. 4.14)

4.3.3 Results of the deterministic approach

In this section, the results of the simulations described above are presented. But before that, regardless of what the results show, it is important to note that the intention of these two simulations was to investigate the two principally different mechanisms of interaction of the

lightning with the transmission line. In the first case, the coupling of the electromagnetic field produced by the lightning or the so-called far-field coupling is considered. The second case concerns the near-field coupling phenomenon represented by crosstalk between the conductors of the line.

The results of these two simulations are shown in Fig. 4.18 and Fig. 4.19

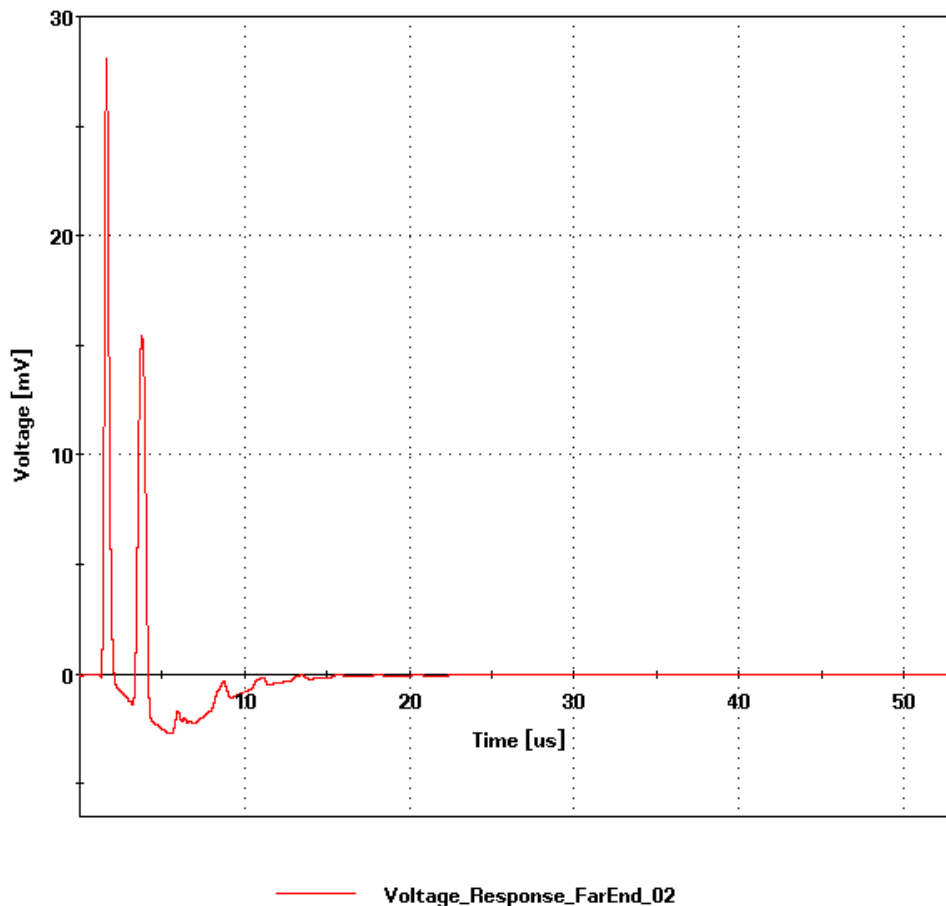


Fig. 4.18 Response at the far end of the line – electromagnetic field coupling

Fig. 4.18 illustrates the result in the case of electromagnetic field coupling, when the lightning strikes away from the line, and Fig. 4.19 shows the induced voltage at the far-end of the line in the case of a direct lightning strike and crosstalk between the conductors of the line.

The results show that, in the case of a direct lightning strike, the response at the far-end of the line is bigger than in the case when lightning strikes away from the line, as is to be expected. In the latter case the response at the far-end of the line is so small because the distance between the wires of the conductor *NYY-O 4x4 re* is very small. Hence, there is a small difference in the horizontal electric field at the points where it is calculated. The further the distance between the wires, the larger is the response at the far-end of the line.

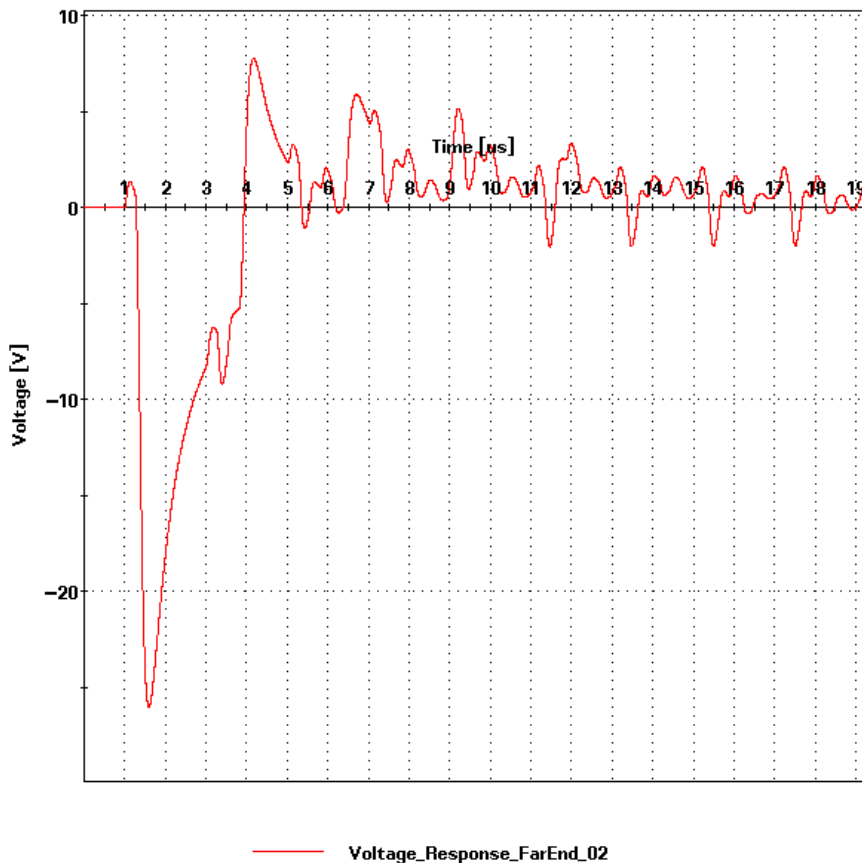


Fig. 4.19 Crosstalk response in the control conductors due to the lightning current injected in the protective conductors

4.4 Stochastic simulation of a direct strike over the line

In the previous section, two basic cases of interaction of lightning with underground conductor transmission line were presented. In the presentation it is assumed that all dimensions and other parameters of the simulations are fixed (i.e. they have specific values which do not vary). But rarely, the processes can be described in this way. It is more likely that the parameters we are interested in are not constants but random variables. In other words, these parameters are characterized by probability distributions. Therefore, the stochastic analysis of a given problem is gaining at present importance. In engineering calculations dimensioning is usually made using the postulate of a maximum strength of the interference. The latter as well as the desired parameters use single (point) values for the calculation. Possible design errors caused by ignoring the stochastic nature of many of these quantities are counteracted by safety factors. Such a procedure does, however, not permit safety margins to be quantified. By treating stochastic quantities as random variables and

propagating their variation through the simulating model, the desired output parameter is obtained as a probability distribution. This enables one to judge whether the degree of protection expressed in terms of a probability is sufficient or not.

In our case, the response at the far-end of the line can vary due to the geometry of the conductors which is not constant along the line, different properties of the surrounding medium and above all because of the stochastic nature of a lightning and weather impact on the soil. Therefore, a stochastic simulation is important in order to evaluate the magnitude of the interference signal.

The above results show that the disturbance at the end of the line is bigger in the case of a direct strike over the line, as is to be expected. In the case of the remote stroke, the response is small compared to the operating level signal. Therefore, it can be neglected. This is the main reason for choosing the direct strike for the simulation which takes into account stochastic variations of the input parameters.

4.4.1 Pdf distribution of the input stochastic parameters

The following parameters in the simulation are considered to be stochastic. Their quantities are treated as random variables, which are described by statistical distributions.

- the lightning stroke parameters;
- material properties of the conductors and insulation;
- geometric dimensions of the conductors and insulation;
- relative permittivity (ϵ_r) of the soil surrounding the cables;

The lightning current waveform was shown in Fig. 3.6. The two most important parameters, which determine this waveform, namely the peak current I_{max} and the maximum rate of rise T_{rise} were also presented there. The probability density functions (pdf) of these two parameters were shown in Fig. 3.9. Since the current is an external input to “CableMod”, and since the current waveform is the most decisive parameter for the form of the curve of the interference voltage at the far-end of the line, nine current waveforms resulting from nine datasets obtained from combining the above two parameters are used as an input for the “CableMod”. These datasets are obtained by joining the 5th, 50th and 95th percentiles of I_{max} and T_{rise} with one another as shown in Table 4.1. According to the data stated in the literature [41], which show that there is no evidence that these two parameters are dependent, permit this combination.

I_{max} [kA]			T_{rise} [μ s]		
5%	50%	95%	5%	50%	95%
4.6	13	30	0.22	1.1	4.5
No	Dataset combinations of I_{max} and T_{rise}				
1	$I_{max}=4.6$ kA; $T_{rise}=0.22$ μ s				
2	$I_{max}=4.6$ kA; $T_{rise}=1.1$ μ s				
3	$I_{max}=4.6$ kA; $T_{rise}=4.5$ μ s				
4	$I_{max}=13$ kA; $T_{rise}=0.22$ μ s				
5	$I_{max}=13$ kA; $T_{rise}=1.1$ μ s				
6	$I_{max}=13$ kA; $T_{rise}=4.5$ μ s				
7	$I_{max}=30$ kA; $T_{rise}=0.22$ μ s				
8	$I_{max}=30$ kA; $T_{rise}=1.1$ μ s				
9	$I_{max}=30$ kA; $T_{rise}=4.5$ μ s				

Table 4.1 Combinations of I_{max} and T_{rise} serving as the basis of calculating the current waveform used as an input for the simulations

Table 4.2 shows the remaining of the input stochastic parameters along with their probability distributions (cf. Fig. 4.11).

Quantity	Unit	Type of distribution	μ	σ
Conductor diameter	mm	normal	2.275	0.0416
Conductor diameter of protective conductor	mm	normal	9.5	0.073
Insulation diameter of conductors	mm	normal	16.6	0.5333
PE Tube thickness	mm	normal	4.5	0.1333
Uniform distribution			min	max
Copper conductivity	S/m	rectangular	1.2×10^7	5.7×10^7
Relative permittivity of the PVC insulation	-	rectangular	2.5	3.5
Relative permittivity of the PE Tube	-	rectangular	2.25	2.38
Relative ground permittivity:	-	rectangular		
dry			4	6
wet			15	30

Table 4.2 Input stochastic parameters and their probability distributions

Two types of distributions are used for the input parameters. The normal distribution is appropriate for parameters such as the deviation of the diameter of the conductors and insulation from their means and the diameter of the PE tubes. The rectangular distribution (uniform pdf) is used for the parameters for which only ranges are known and which cannot be associated with an other probability distribution. In our case, these are electrical properties of the conductors and insulation and the relative ground permittivity. Additionally, with respect to the relative ground permittivity, the simulations are divided into two parts. Firstly, the weather is considered to be fine and the soil to be dry. The relative soil permittivity then lies between 4 and 6. Secondly, stormy weather and wet soil are assumed with a relative soil permittivity ranging from 15 to 30 [81].

4.4.2 Development and comparison between the 22-point model and the 204-point model

Above in this chapter, the model which is used for the simulation of a direct lightning strike on the conductor transmission line, was presented. The line is divided into sections, each of them of 1 m length. The current from the lightning is injected at the beginning of the line and flows through the bare copper conductors. In each section these conductors are connected by the resistances R_{leak} with the ground. These connections represent the leakage of the current into the ground due to the absence of insulation of the conductors. Because there are 204 sections in this model, it is called the 204-point model. This model has one serious difficulty. The program “CableMod” takes approximately 21 hours for a single calculation of an interference voltage at the far end of the line. Therefore, this model is not very appropriate for stochastic simulations where the repetition of the calculations is needed.

In order to perform stochastic simulations a new model was developed. In this model, the transmission line is divided into 21 sections only, which are formed by 22 node points. Therefore, this model is called the 22-point model. There are three reasons justifying the division of the line in the new model. In the first place, the number of sections has to be reduced in order to achieve reasonable calculation times for making the stochastic simulation. Reducing the number of node points should be taken into account that the length of each section has still to be electrically small compared with the wavelength of the electromagnetic wave of the highest frequency of interest. Thirdly, the division has to conform to the

geometry of the line. The division of the line, taking into consideration the above stated reasons, is shown in Fig. 4.20.

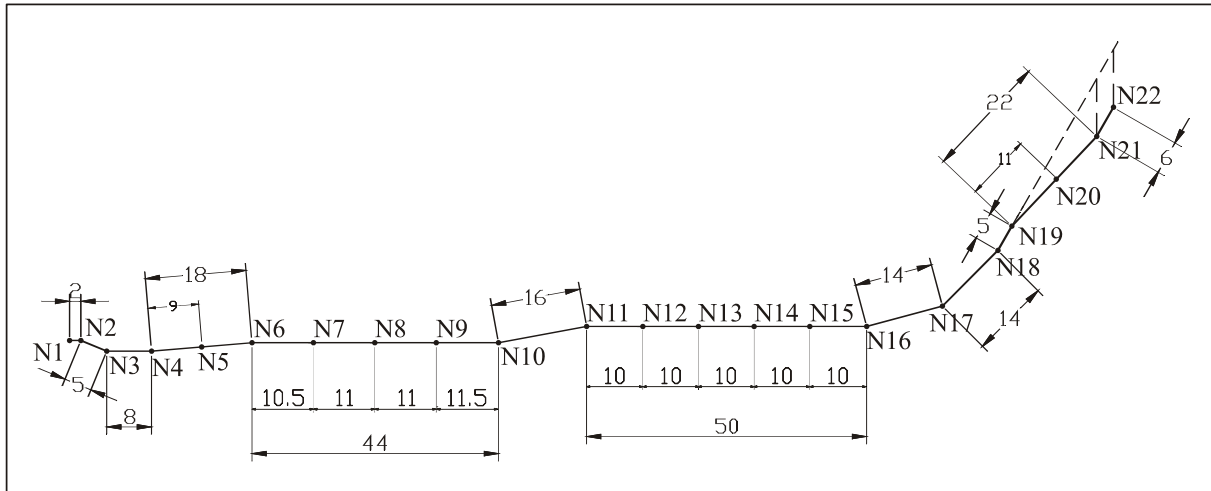


Fig. 4.20 Division of the transmission line according to the 22-point model

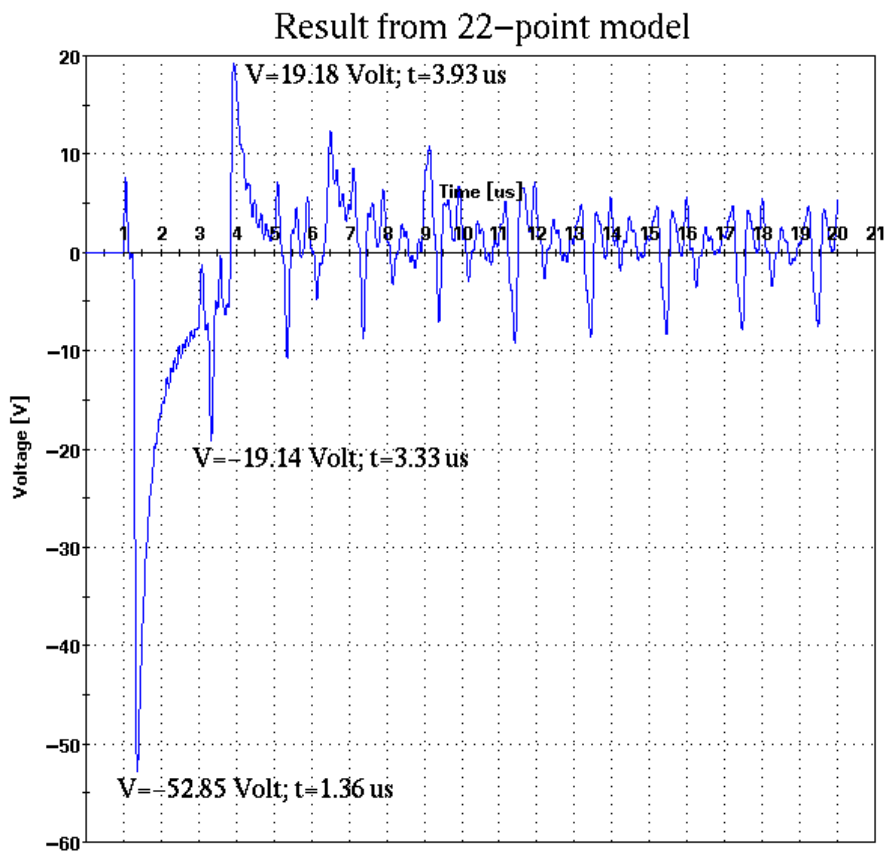
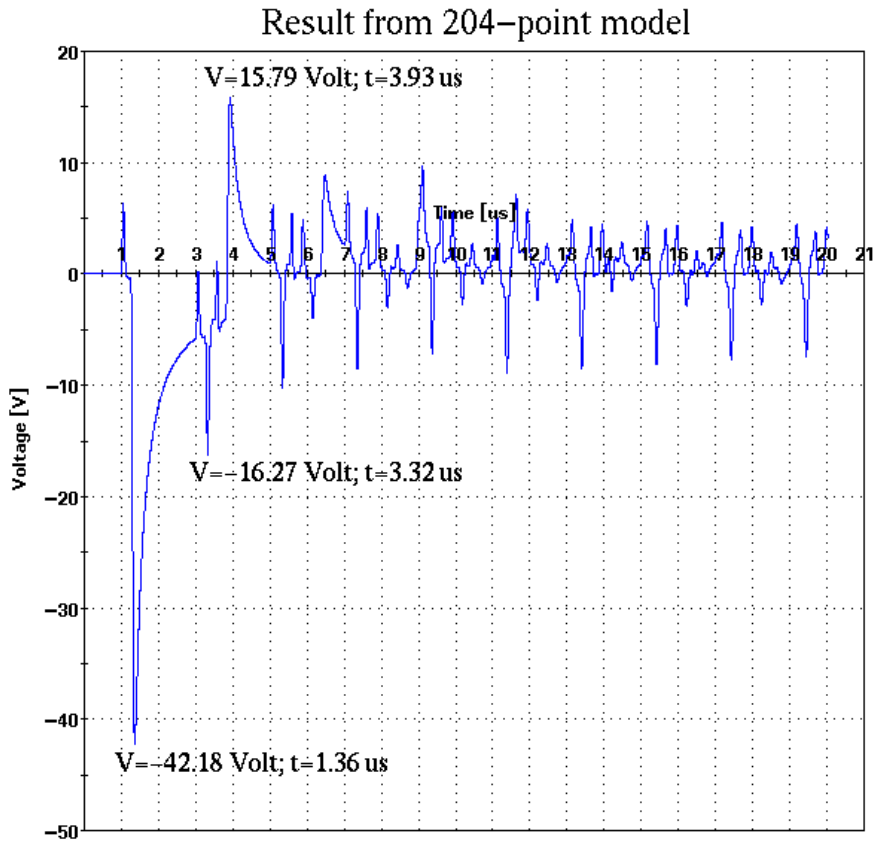
The reduction of the number of points used for modeling the line results in a faster time for a single calculation. With this model, one calculation takes only 21 min. The reduction of the number of sections affects also the number of the resistances which connect the bare copper conductors with the ground. In this case there are only 21; they are represented by eq. (4.12b). With the dimensions in Fig. 4.20, these resistances take values which lie in the range from 22 Ω to 93 Ω .

The results obtained by the two models are similar, if the curve patterns are compared, but different in the maximum values of the signal in these curves. This is due to the different number of points used for representing the line which affects the precision of the simulation. As mentioned above, the strongest influence of the signal at the far-end of the line is exerted by the current at the base of the lightning strike. Therefore, simulations with different current waveforms, but with the same values of all other parameters were performed. Both models were used in order to compare their results. Results obtained using three different current waveforms are shown in Fig. 4.21.

All the current waveforms have the same $I_{max}=13$ kA, but different risetimes, as described in the figure. A detailed comparison between these two models is made in Table 4.3. The values for the first two, respectively the first three peaks of each voltage curve representing the response at the far end of the line are specified and compared. This is achieved by introducing

the so-called correspondence coefficient k_{cor} between the two models as the ratio of the corresponding maximum values of the voltage at the far-end of the line.

a)



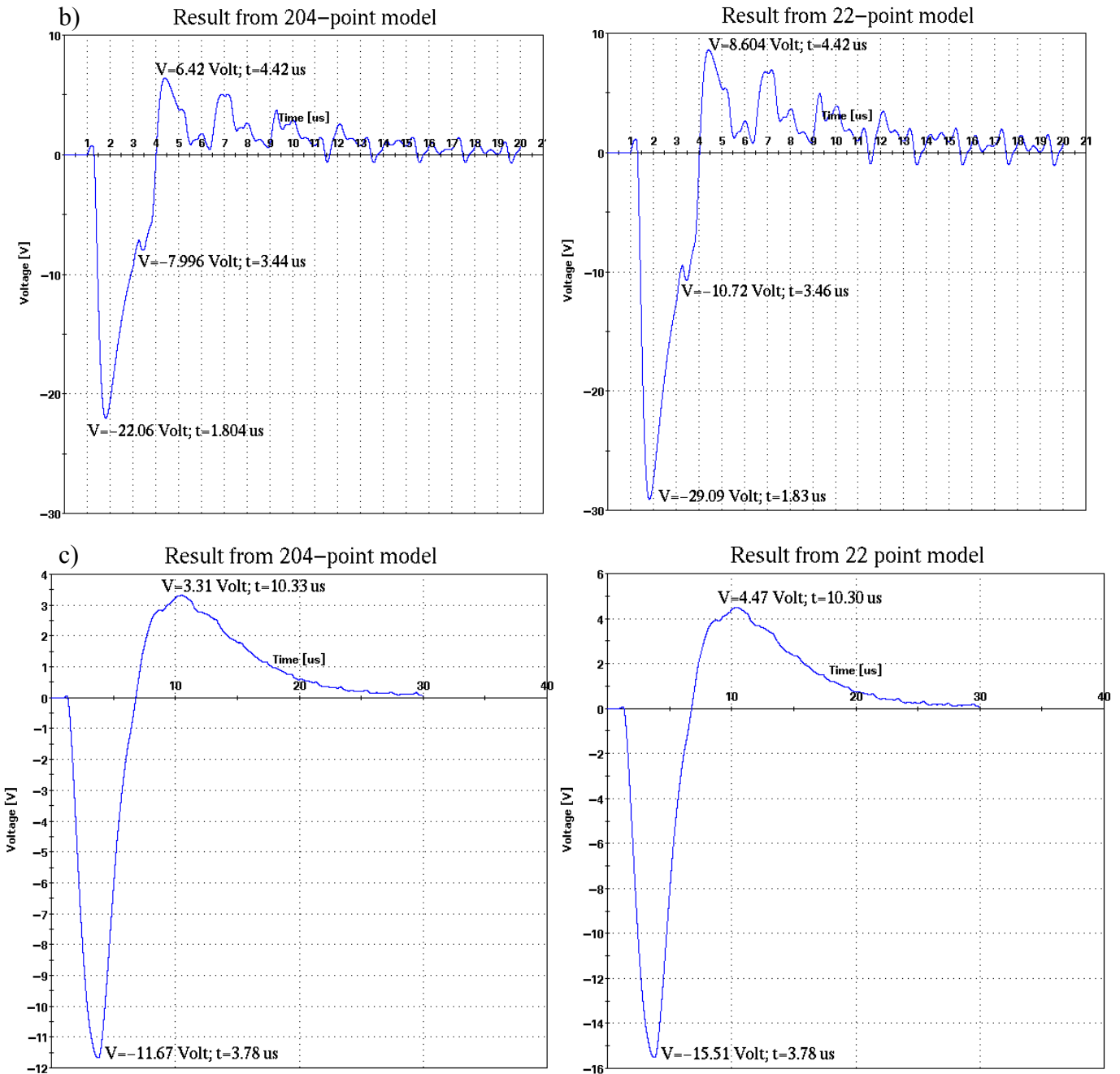


Fig. 4.21 Comparison of the results obtained with 22-point model and 204 point model: (a) simulations made with $I_{max}=13$ kA and $T_{rise}=0.22$ μ s; (b) simulations made with $I_{max}=13$ kA and $T_{rise}=1.1$ μ s; (c) simulations made with $I_{max}=13$ kA and $T_{rise}=4.5$ μ s;

The current waveforms take different values for the I_{max} and T_{rise} , as described above in Table 4.1. The first two peaks are taken from the results which are obtained when the lightning current injected at the beginning of the line has a rise time $T_{rise}=4.5$ μ s, because in these results only two peaks are observed, as is evident from Fig. 4.21.

Parameters of simulations	Values [Volts]		$k_{cor.}$	$1/k_{cor.}$
	22-point model	204-point model	22p/204p	204p/22p
$I_{max}=13$ kA, $T_{rise}=0.22$ μ s, $\epsilon_r=2.8$				
first peak ($t_{22}=1.36393$ μ s, $t_{204}=1.3621$ μ s;)	-52.8452	-42.1845	1.252716	0.7982655
second peak ($t_{22}=3.32999$ μ s, $t_{204}=3.3221$ μ s;)	-19.1374	-16.2767	1.1757543	0.8505178
third peak ($t_{22}=3.92547$ μ s, $t_{204}=3.92665$ μ s;)	19.1821	15.789	1.2149028	0.8231111
$I_{max}=13$ kA, $T_{rise}=0.7$ μ s, $\epsilon_r=2.8$				
first peak ($t_{22}=1.61011$ μ s, $t_{204}=1.5858$ μ s;)	-33.9038	-26.0688	1.3005509	0.768905
second peak ($t_{22}=3.41316$ μ s, $t_{204}=3.39778$ μ s;)	-12.5021	-9.19752	1.3592903	0.735678
third peak ($t_{22}=4.20158$ μ s, $t_{204}=4.17113$ μ s;)	10.2361	7.76199	1.3187469	0.7582956
$I_{max}=13$ kA, $T_{rise}=1.1$ μ s, $\epsilon_r=2.8$				
first peak ($t_{22}=1.82967$ μ s, $t_{204}=1.8045$ μ s;)	-29.0868	-22.0572	1.3186987	0.7583234
second peak ($t_{22}=3.45641$ μ s, $t_{204}=3.44434$ μ s;)	-10.7187	-7.99591	1.3405228	0.7459776
third peak ($t_{22}=4.41781$ μ s, $t_{204}=4.41644$ μ s;)	8.60425	6.41672	1.3409109	0.7457617
$I_{max}=13$ kA, $T_{rise}=4.5$ μ s, $\epsilon_r=2.8$				
first peak ($t_{22}=3.77909$ μ s, $t_{204}=3.77697$ μ s;)	-15.5129	-11.6659	1.3297645	0.7520128
second peak ($t_{22}=10.2994$ μ s, $t_{204}=10.328$ μ s;)	4.4699	3.30976	1.3505209	0.740455
$I_{max}=30$ kA, $T_{rise}=0.22$ μ s, $\epsilon_r=2.8$				
first peak ($t_{22}=1.36726$ μ s, $t_{204}=1.3621$ μ s;)	-120.345	-96.0864	1.2524665	0.7984245
second peak ($t_{22}=3.32999$ μ s, $t_{204}=3.3221$ μ s;)	-45.9282	-38.8126	1.1833322	0.8450712
third peak ($t_{22}=3.92547$ μ s, $t_{204}=3.92748$ μ s;)	41.644	34.4308	1.2094985	0.826789
$I_{max}=30$ kA, $T_{rise}=1.1$ μ s, $\epsilon_r=2.8$				
first peak ($t_{22}=1.82634$ μ s, $t_{204}=1.80367$ μ s;)	-66.9821	-50.8062	1.3183844	0.7585041
Second peak ($t_{22}=3.45641$ μ s, $t_{204}=3.44518$ μ s;)	-24.4201	-18.2147	1.3406809	0.7458897
third peak ($t_{22}=4.41116$ μ s, $t_{204}=4.40397$ μ s;)	19.7919	14.758	1.3410964	0.7456586
$I_{max}=30$ kA, $T_{rise}=4.5$ μ s, $\epsilon_r=2.8$				
first peak ($t_{22}=3.78575$ μ s, $t_{204}=3.78113$ μ s;)	-35.3536	-26.5862	1.3297726	0.7520083
second peak ($t_{22}=10.3925$ μ s, $t_{204}=10.3971$ μ s;)	10.2233	7.57623	1.3493915	0.7410748
$I_{max}=4.6$ kA, $T_{rise}=0.22$ μ s, $\epsilon_r=2.8$				
first peak ($t_{22}=1.36393$ μ s, $t_{204}=1.3621$ μ s;)	-18.6236	-14.8663	1.2527394	0.7982506
second peak ($t_{22}=3.32999$ μ s, $t_{204}=3.3221$ μ s;)	-6.36531	-5.45093	1.1677475	0.8563495
third peak ($t_{22}=3.92547$ μ s, $t_{204}=3.92665$ μ s;)	7.15897	5.86389	1.2208568	0.8190969
$I_{max}=4.6$ kA, $T_{rise}=1.1$ μ s, $\epsilon_r=2.8$				
first peak ($t_{22}=1.80971$ μ s, $t_{204}=1.80367$ μ s;)	-10.1899	-7.7367	1.3170861	0.7592518
second peak ($t_{22}=3.45308$ μ s, $t_{204}=3.44185$ μ s;)	-3.49861	-2.60839	1.341291	0.7455504
third peak ($t_{22}=4.41449$ μ s, $t_{204}=4.41146$ μ s;)	3.32595	2.48234	1.3398447	0.7463552
$I_{max}=4.6$ kA, $T_{rise}=4.5$ μ s, $\epsilon_r=2.8$				
first peak ($t_{22}=3.75248$ μ s, $t_{204}=3.75452$ μ s;)	-5.8024	-4.19635	1.3827255	0.7232094
second peak ($t_{22}=10.2328$ μ s, $t_{204}=10.2823$ μ s;)	1.70777	1.26645	1.3484701	0.7415811

Table 4.3 Comparison between the 22-point model and 204-point model and calculation of $k_{cor.}$

The values in the table show a good agreement of this coefficient for the different cases, especially when cases with the same rise times are considered.

From the results presented in the table it can be concluded that the 22-point model can be used for the stochastic simulation. The results can then be transformed to match the results from the 204-point model by just multiplying them by the correspondence coefficient, which can be formed as the arithmetic mean of the coefficients obtained as the ratio of the peaks for each case.

The main stochastic simulation of a direct lightning strike over the line is performed using the 22-point model. This is done by means of the Monte Carlo method [130]. It implies repeated trials, N on the whole, – each being carried out with a set of input quantities selected at random from the probability distribution of the input parameters presented in Table 4.2. In order to better simulate inhomogeneities along the line, a different set of input parameters for each section is used, i.e. in one trial the input parameters are chosen from the probability distributions shown in Table 4.2, but they are different for each section of the line.

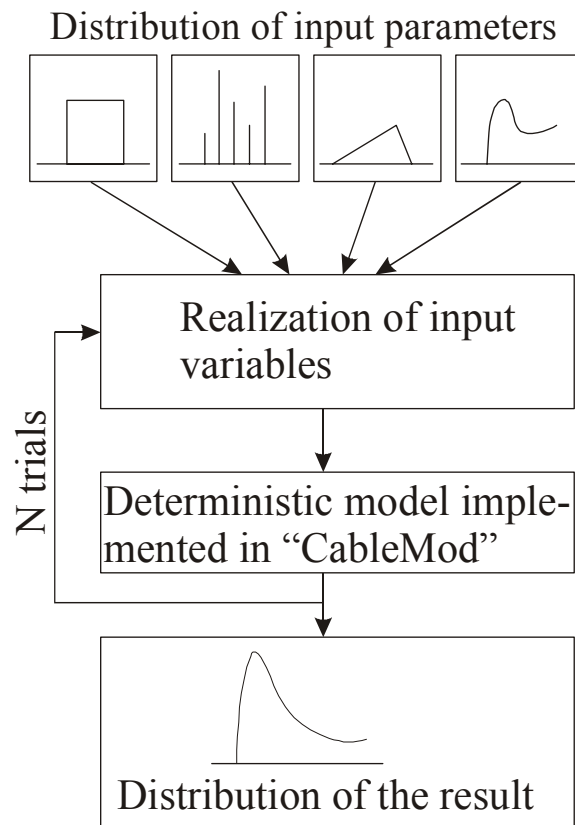


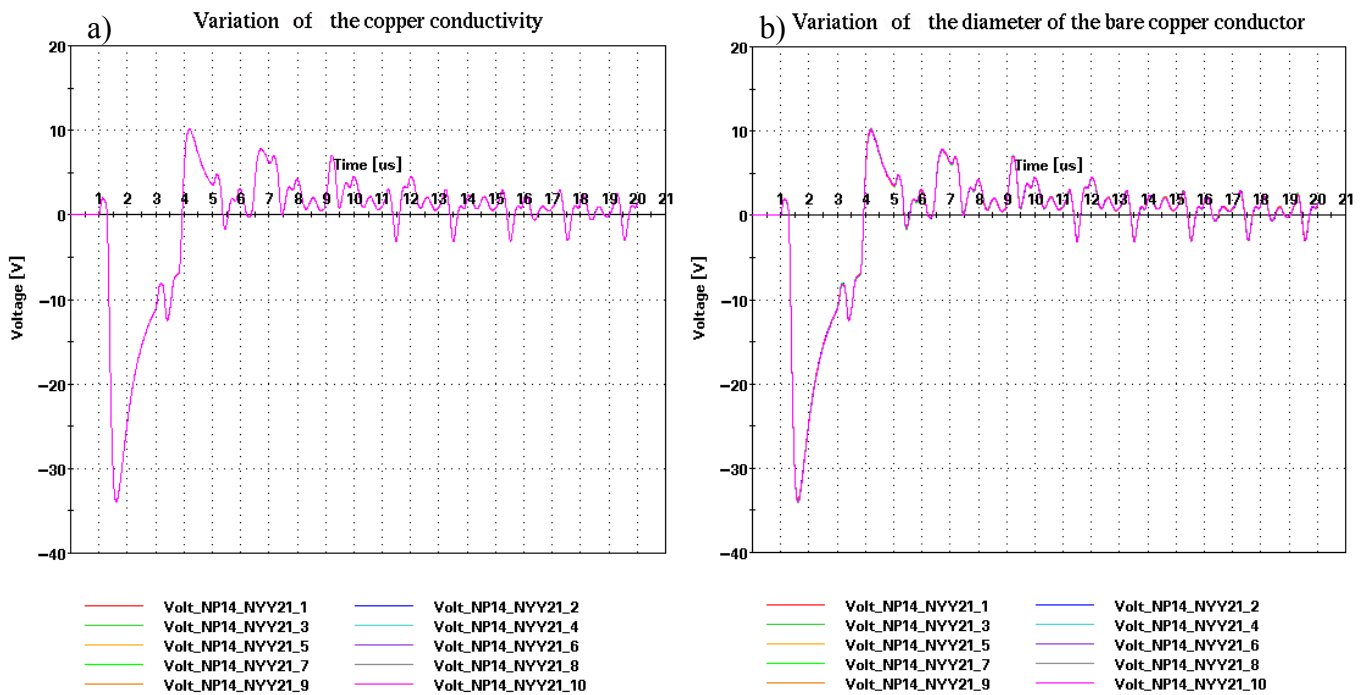
Fig. 4.22 Block-Diagram representation of Monte Carlo method used for stochastic simulation

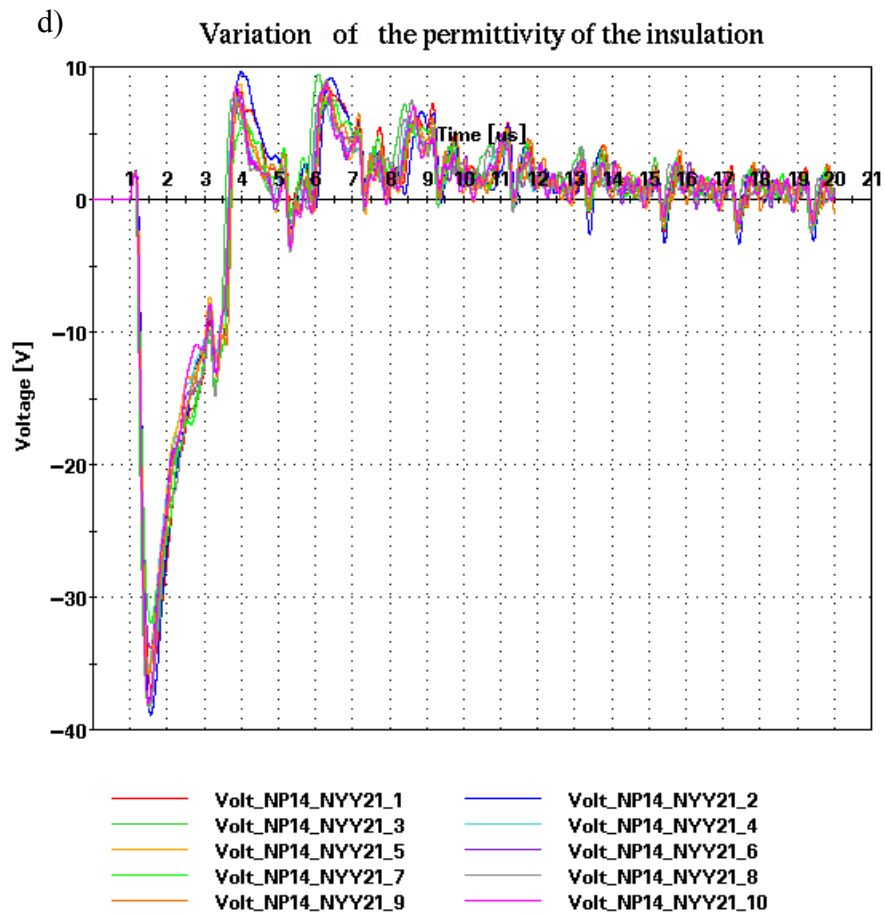
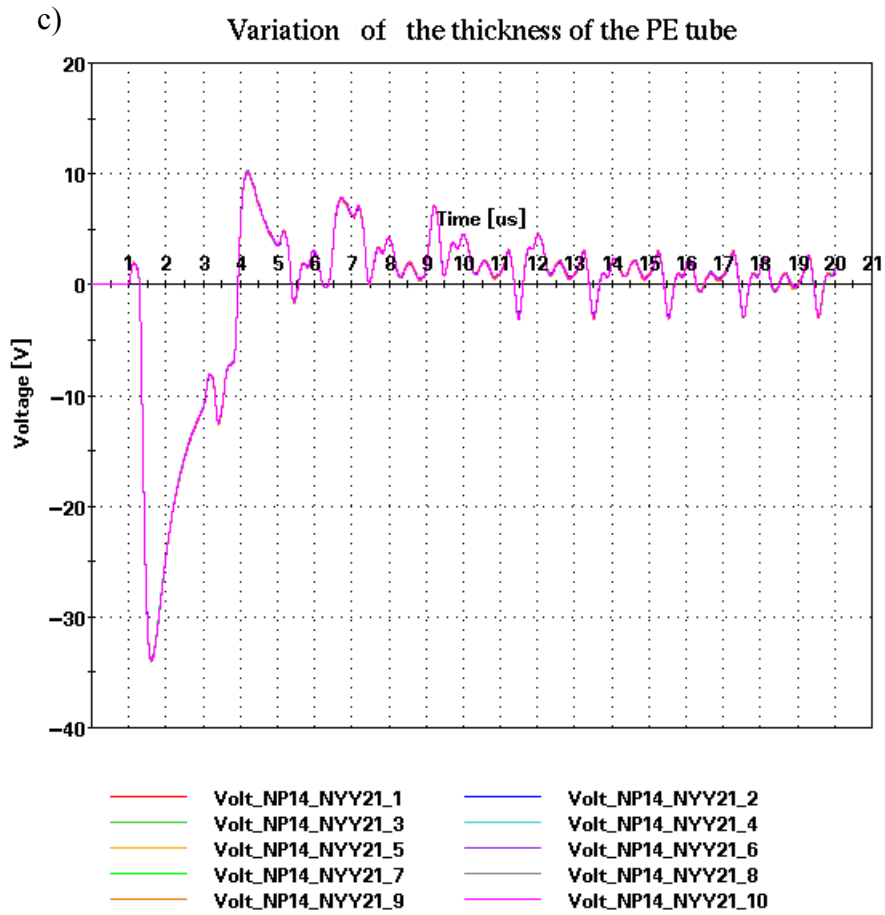
The simulation is conducted using the program “CableMod” again. The latter has a feature which enables one to choose whether fixed parameter or Monte Carlo analysis is to be performed. Of course, in the case of parameter or Monte Carlo analysis, the minimum and the maximum boundary or the probability distribution for the parameter of interest should be pointed out. By default, the program makes a fixed analysis where the given parameter is assigned a point (fixed) value. In order for stochastic analysis to be performed, a new model was developed taking into account the above considerations. Below, some of the results of the stochastic simulations are presented.

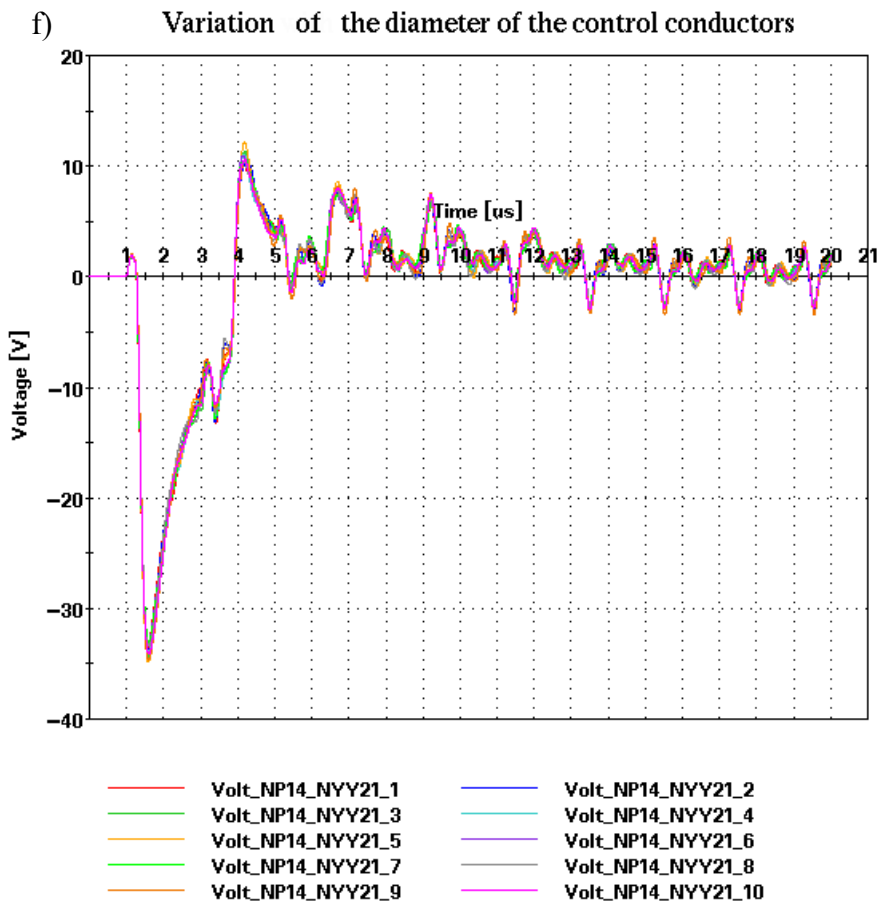
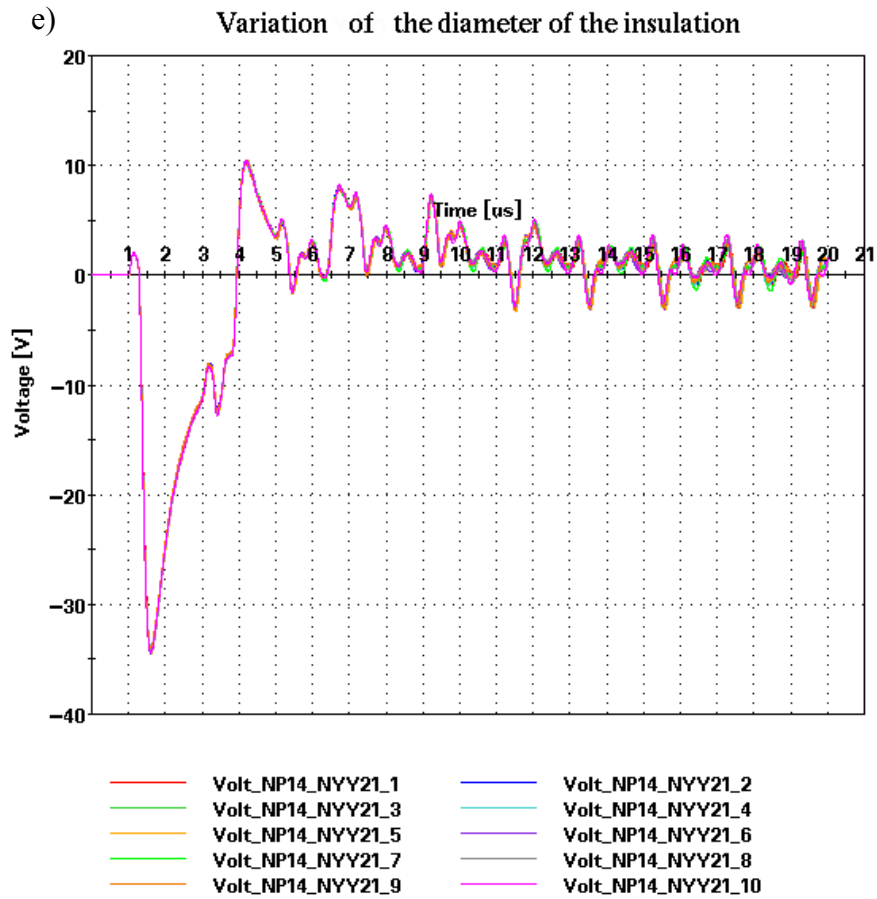
4.4.2.1 Partial stochastic simulation showing the influence of individual parameters

The first results show the influence of an individual parameter on the response at the far end of the line. The stochastic simulation in this case is only made with the number of the repeats $N=10$. In these repeats only a single parameter of interest varies. All other parameters are constant point values. Fig. 4.23a-h shows some of the results for this case.

The influence of some parameters, as for example the conductivity of the copper, the diameter of the bare copper conductors or the thickness of the PE tube is so small that the curves obtained from different trials almost coincide with one another.







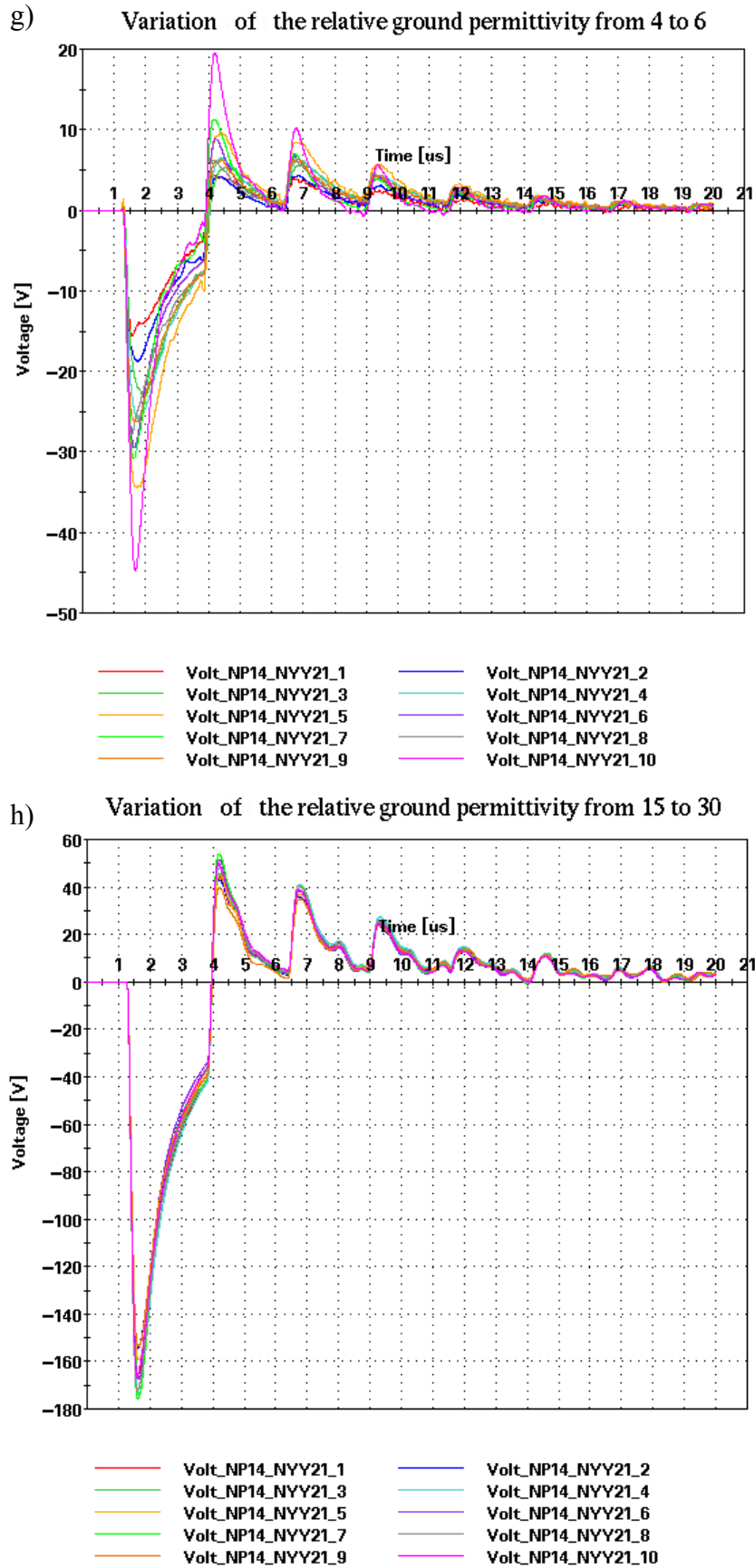


Fig. 4.23 Response at the far-end of the line. Stochastic simulation with single parameters

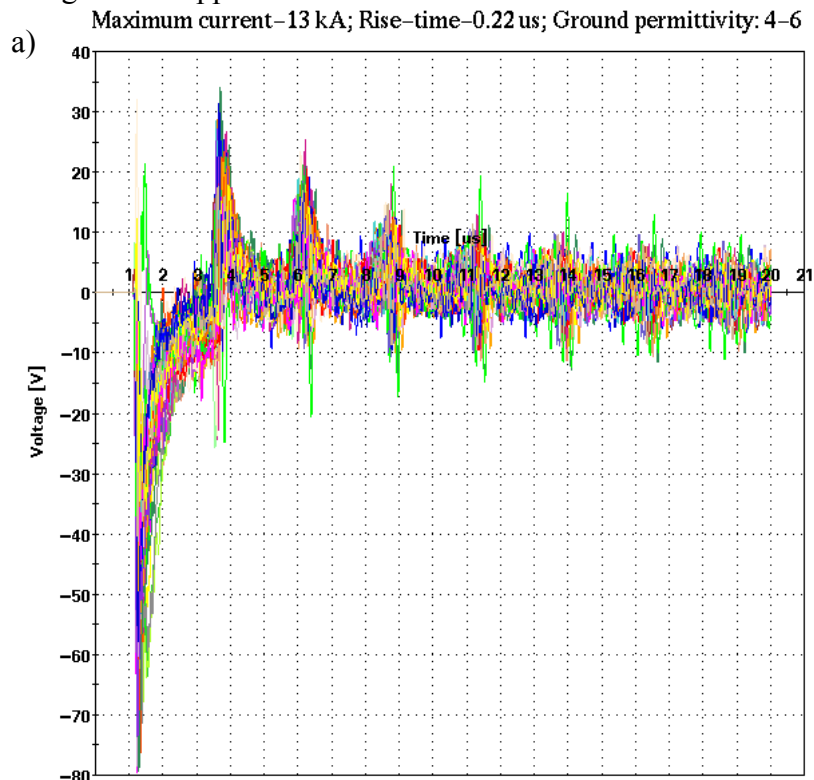
Number of Monte Carlo trials $N=10$, $I_{max}=13$ kA, $T_{rise}=0.7$ μ s

Other parameters, as for example the diameter of the conductors or the insulation, have a small influence on the induced voltage due to the fact that these parameters are the argument of a logarithm when defining the per-unit-length parameters, as shown in Appendix III. Therefore, the resulting values are smaller after taking the logarithm and their influence is not too big.

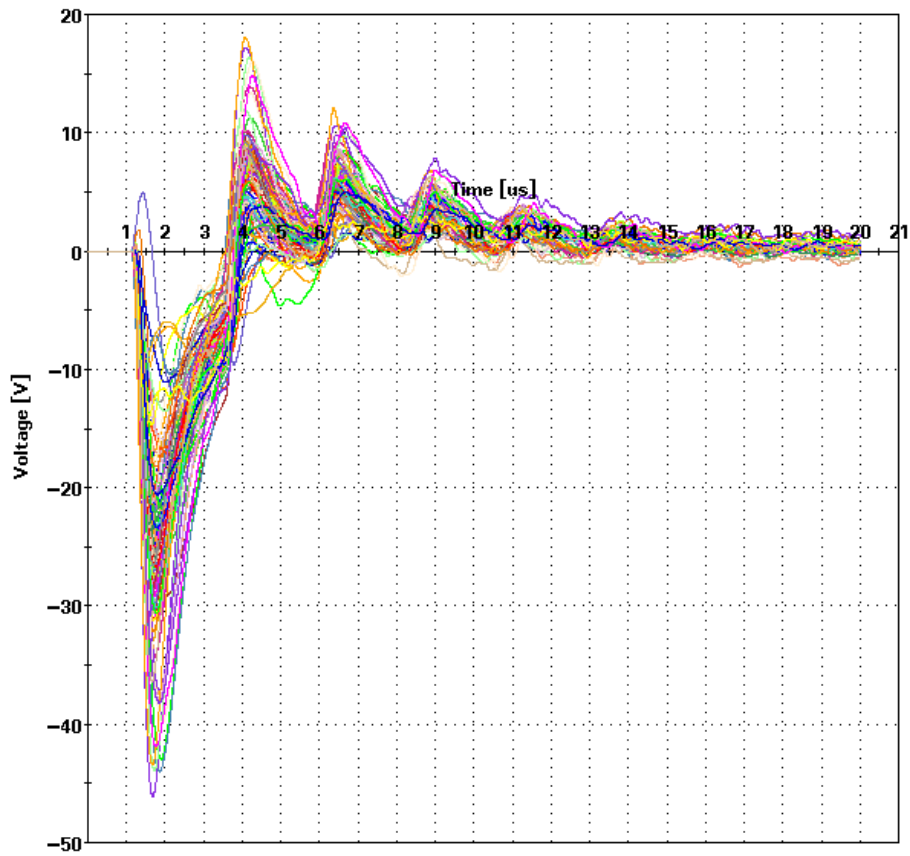
Calculations show that the parameter with the biggest influence on the response at the end of the line is the relative ground permittivity ϵ_r since this parameter appears in the logarithm as a factor in defining the per-unit-length parameters of the line. Therefore, simulations are carried out for two ranges of this parameter. Firstly, the weather is considered to be fine and the soil to be dry. The relative soil permittivity then lies between 4 and 6. Secondly, stormy weather and wet soil are assumed with a relative soil permittivity lying in the range from 15 to 30 [81].

4.4.2.2 Stochastic simulation with all parameters

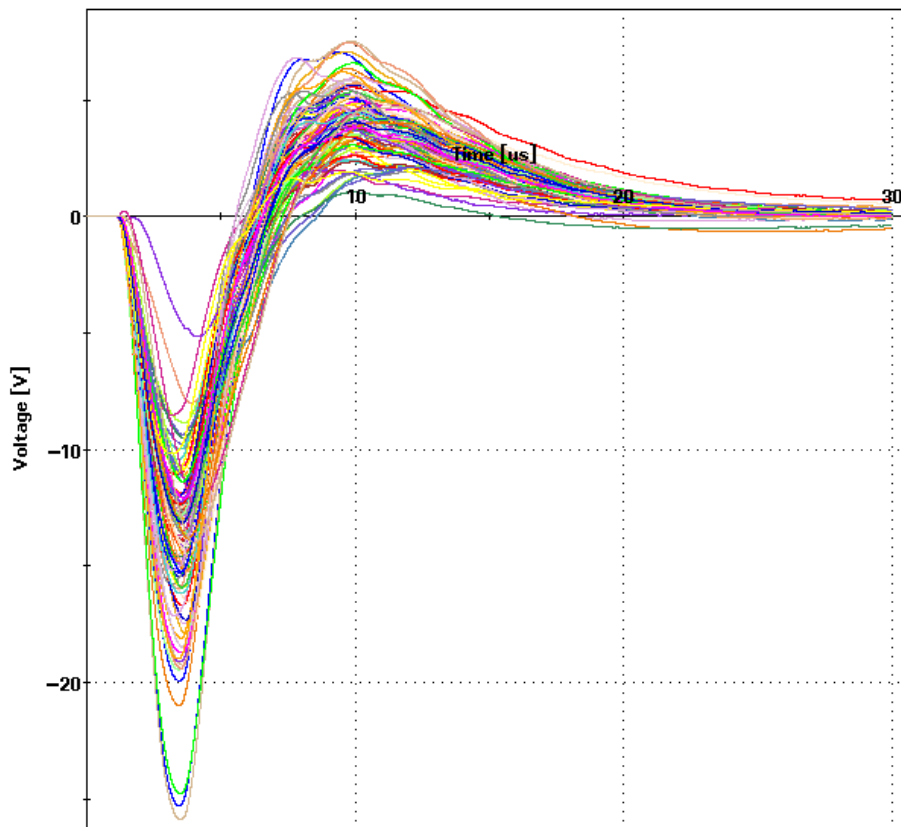
The results of the stochastic simulation with $N=100$ trials are shown in the Fig. 4.24a-f. Here, all parameters change simultaneously in every Monte Carlo trial according to their corresponding probability distributions, as presented in Table 4.2. The parameters of the lightning current waveform take the values shown in Table 4.1. In the figure below, the simulations with the maximum lightning current $I_{max}=13$ kA are presented. The results from all simulations are given in Appendix II.



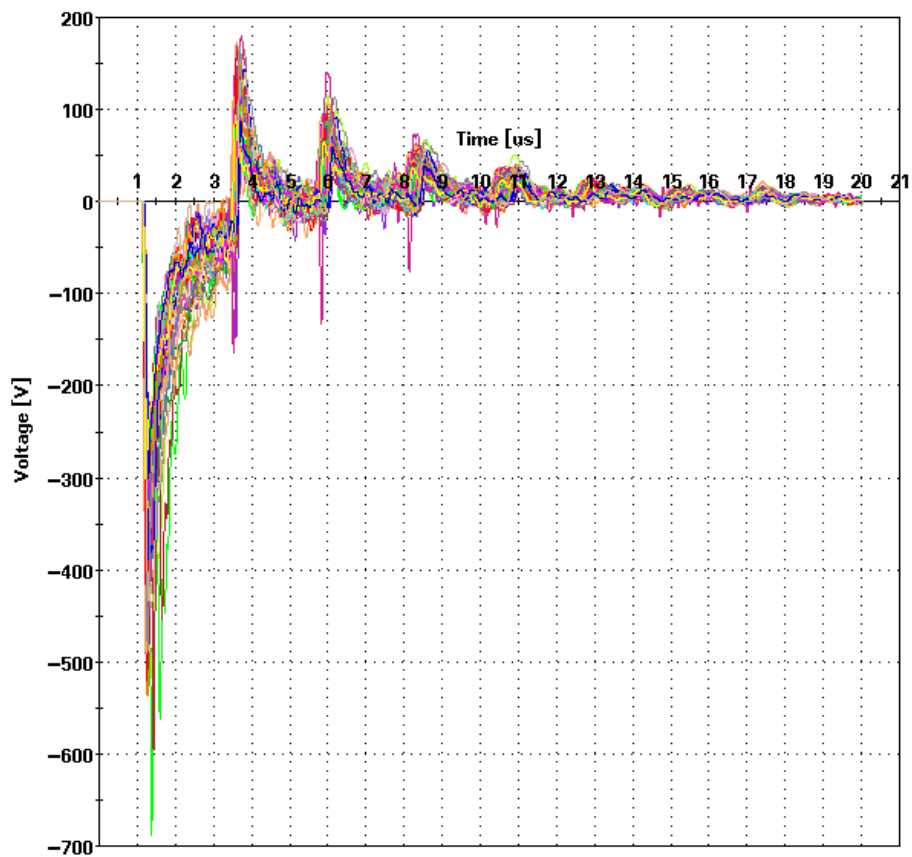
b) Maximum current–13 kA; Rise–time–1.1 us; Ground permittivity: 4–6



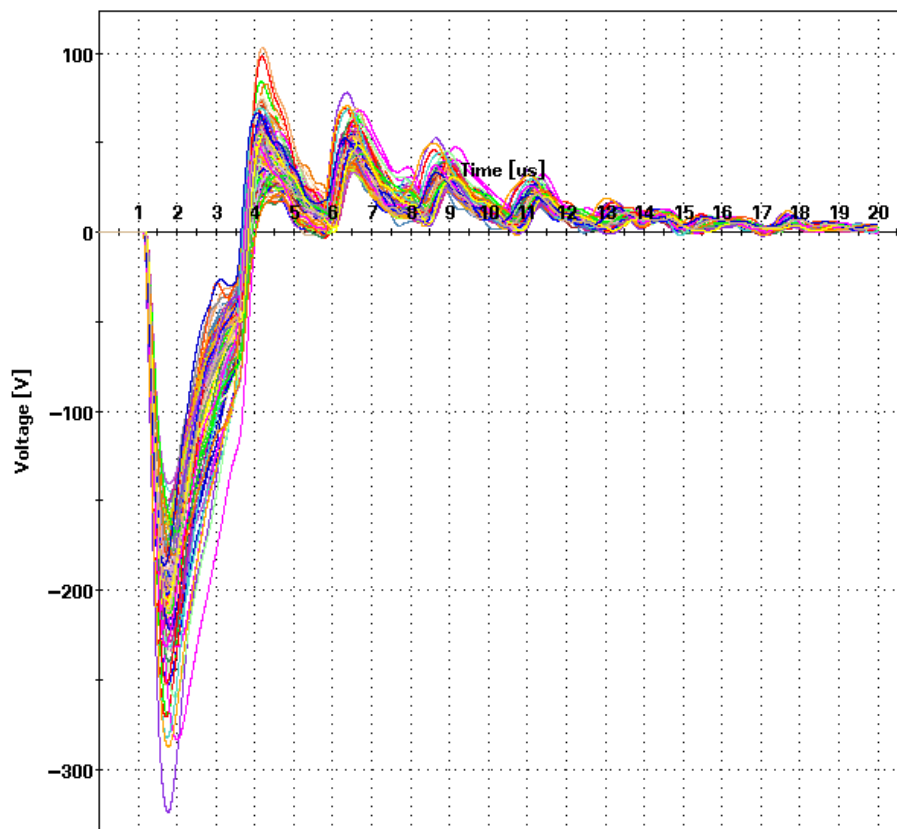
c) Maximum current–13 kA; Rise–time–4.5 us; Ground permittivity: 4–6



d) Maximum current–13 kA; Rise-time–0.22 us; Ground permittivity: 15–30



e) Maximum current–13 kA; Rise-time–1.1 us; Ground permittivity: 15–30



f) Maximum current–13 kA; Rise–time–4.5 μ s; Ground permittivity: 15–30

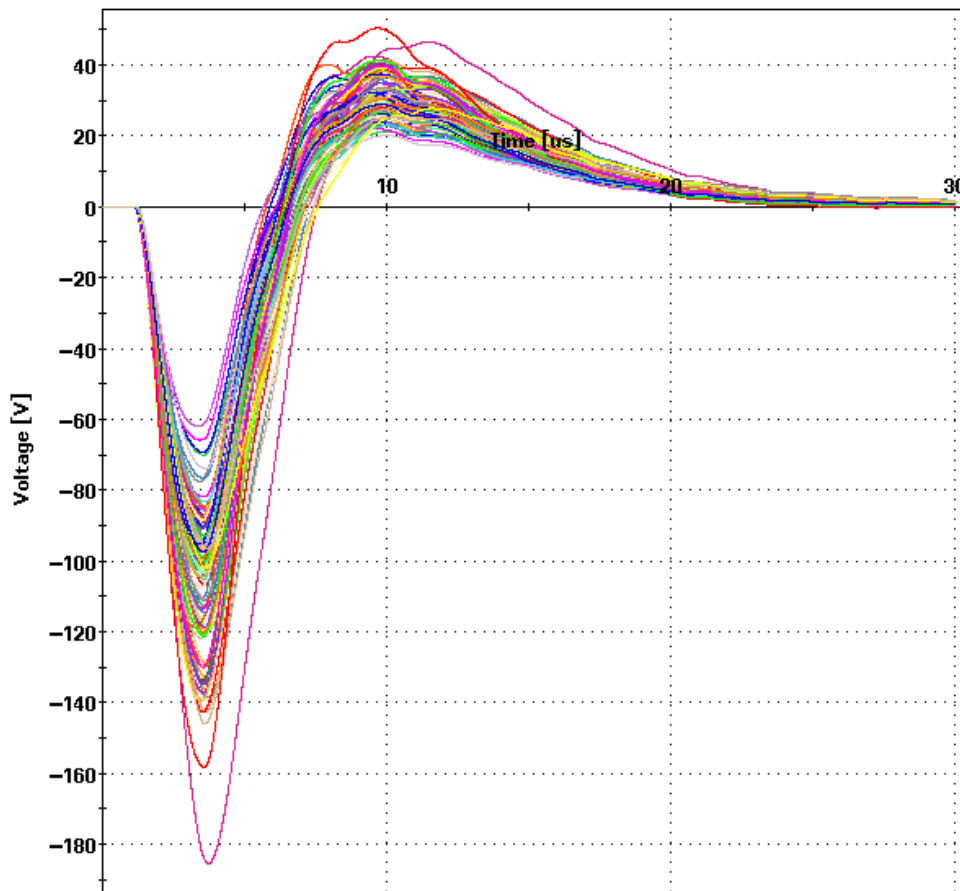


Fig. 4.24 Response at the far end of the line. Stochastic simulation with all parameters.

Number of Monte Carlo trials $N=100$, $I_{max}=13$ kA

The inclusion of stochastic effects shows that I_{max} , T_{rise} and the relative ground permittivity, ϵ_r , are the parameters with the biggest influence for the response at the far end of the line. T_{rise} which is responsible for the high frequency content of the spectrum in the frequency domain, influences both the maximum amplitude of the response and the shape of the curve. Shorter rise times, as for example $T_{rise} = 0.22 \mu$ s, make the response “sharper”, with more peaks, as can be seen from Fig. 4.24a and d. For a rise time of 4.5 μ s, the curve is almost smooth with two peaks only in the period from 0 to 30 μ s.

Further stochastic simulations show that similar results in the range of the maximum amplitude for the voltage at the far-end of the line are obtained with different combinations of the input parameters. A simulation made with the set of the input parameters $I_{max}=4.6$ kA, $T_{rise}=1.1 \mu$ s and $\epsilon_{r,g}=15-30$, presented in Appendix II, shows that the maximum voltage of

the response at the far end of the line is in the range from 40 V to 120 V. The same voltage response range is achieved for the simulation with input parameters $I_{max}=30$ kA, $T_{rise}=1.1$ μ s and $\epsilon_{r,g}=4-6$. However, the probability distributions for the maximum voltages in these two cases are different, as shown in the next section.

From the results presented above it is evident that in the case of wet soil (which is more likely during the thunderstorm activity), the voltage pulses with a magnitude 200 V, lasting for approximately 1 μ s are common events for the loads at the end of the line. The value of 200 V is far above the threshold operation voltages of digital devices. However, the damage threshold of electronic device is measured as the minimum power transferred through a terminal at which the device's characteristics are significantly and irreversibly altered. Typical damage thresholds of various electronic devices are given in Table 4.4. Values 10 to 100 times smaller are sufficient to cause temporary malfunction.

Components	Threshold destruction energies (mJ)
UHF diodes	$10^{-4} - 10^{-3}$
CMOS integrated circuits	$10^{-3} - 10^{-2}$
Low-power transistors	$10^{-3} - 10^{-1}$
Switching diodes	$10^{-2} - 10^{-1}$
Zener diodes	$10^{-1} - 10^{-2}$
Relays	1 – 100
Carbon resistors (0.25 W)	10

Table 4.4 Approximate values of threshold destruction energies for components subjected to pulses of duration equal or less than 1 μ s [30]

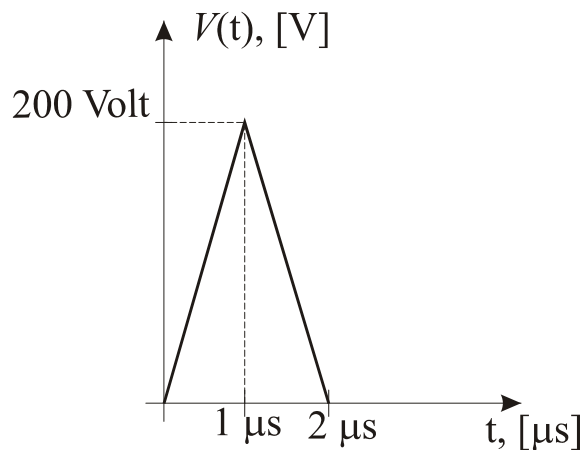


Fig. 4.25 Triangular voltage impulse

Assuming that a triangular impulse of 200 V illustrated in Fig. 4.25 with duration of 2 μ s, is passing through a resistor with $R=50 \Omega$. The energy absorbed by this resistor is calculated as

$$E = \int_0^{2\mu s} v(t)i(t)dt = \int_0^{2\mu s} \frac{v^2(t)}{R} dt = \frac{1}{R} \int_0^{2\mu s} v^2(t)dt \quad (4.15)$$

The calculation of this energy can be divided in two parts. First we can calculate the energy E_1 from 0 to 1 μ s and then the energy E_2 from 1 μ s to 2 μ s. With respect to Fig. 4.25 the triangular voltage impulse can be mathematically described as:

$$v(t) = \begin{cases} 200 \cdot 10^6 t, & 0 \leq t \leq 1\mu s \\ -200 \cdot 10^6 t + 400, & 1\mu s \leq t \leq 2\mu s \end{cases}$$

The calculation of the energies E_1 and E_2 is as follows

$$E_1 = \frac{1}{R} \int_0^{1\mu s} v^2(t)dt = \frac{1}{50} \int_0^{1\mu s} (200 \cdot 10^6 t)^2 dt = \frac{200^2 \cdot (10^6)^2}{50} \cdot \frac{t^3}{3} \Big|_0^{1\mu s} = 0,26(6) \text{ mJ}$$

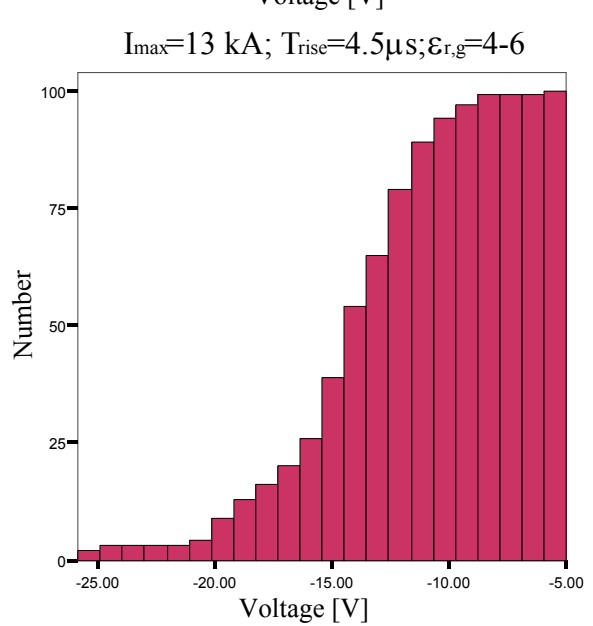
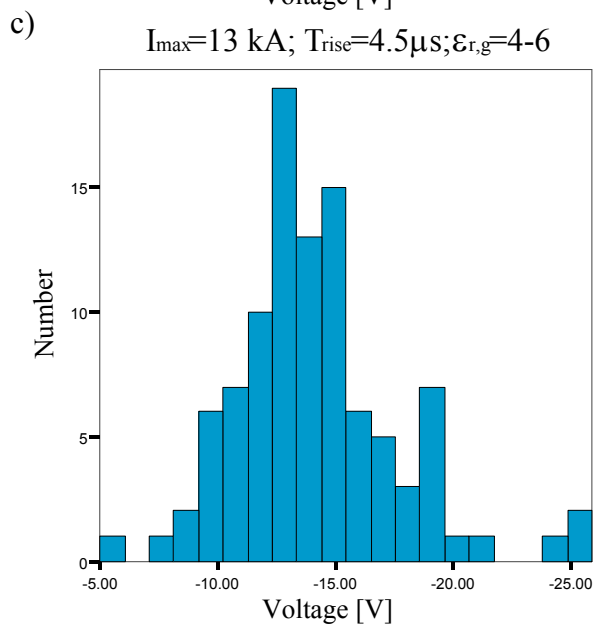
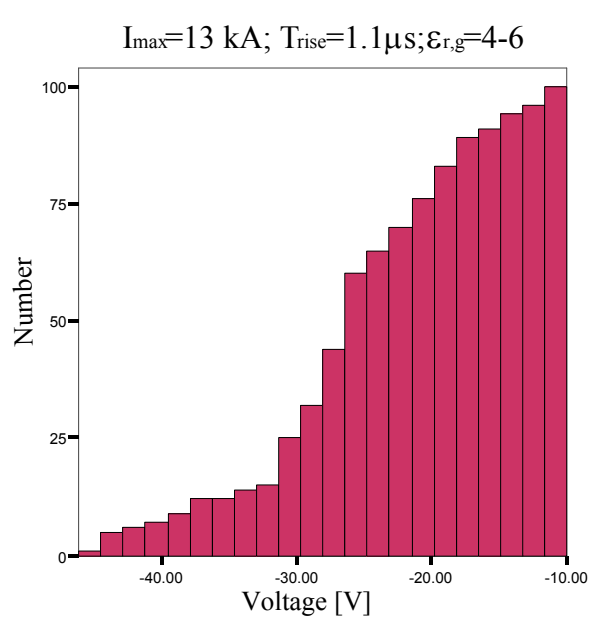
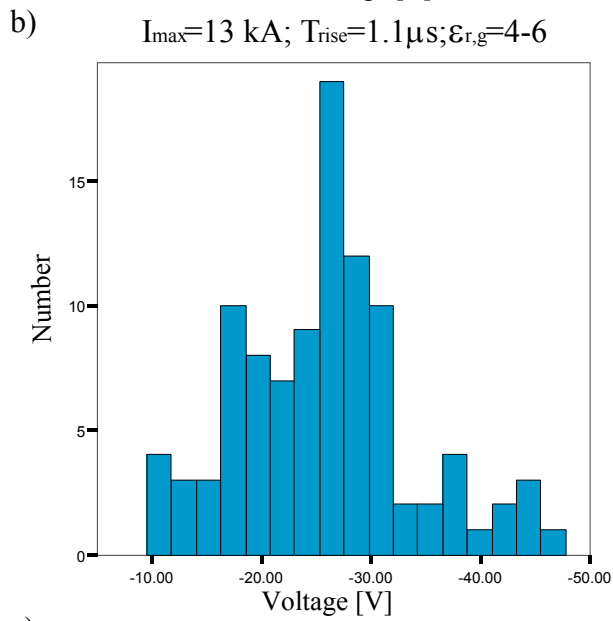
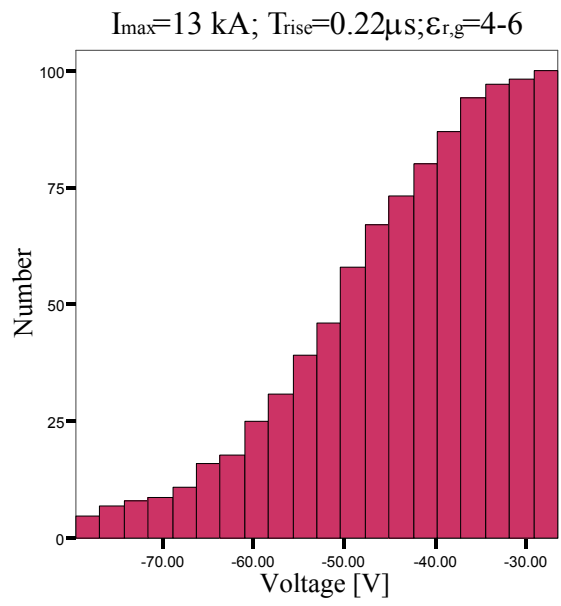
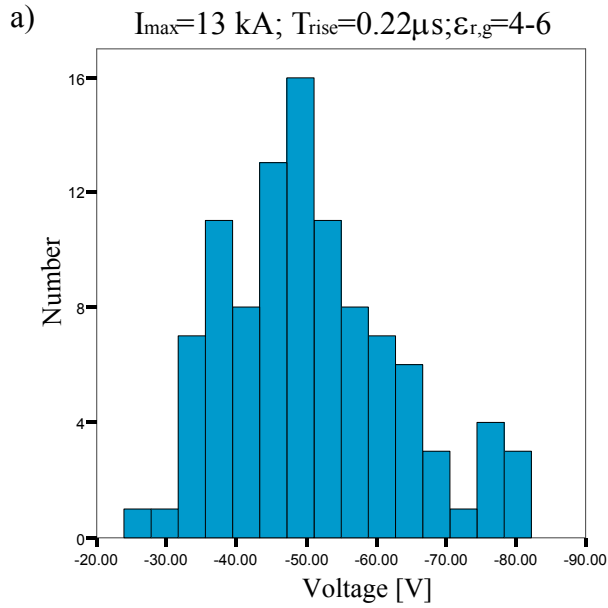
$$E_2 = \frac{1}{R} \int_{1\mu s}^{2\mu s} v^2(t)dt = \frac{1}{50} \int_{1\mu s}^{2\mu s} (-200 \cdot 10^6 t + 400)^2 dt = 0,26(6) \text{ mJ}$$

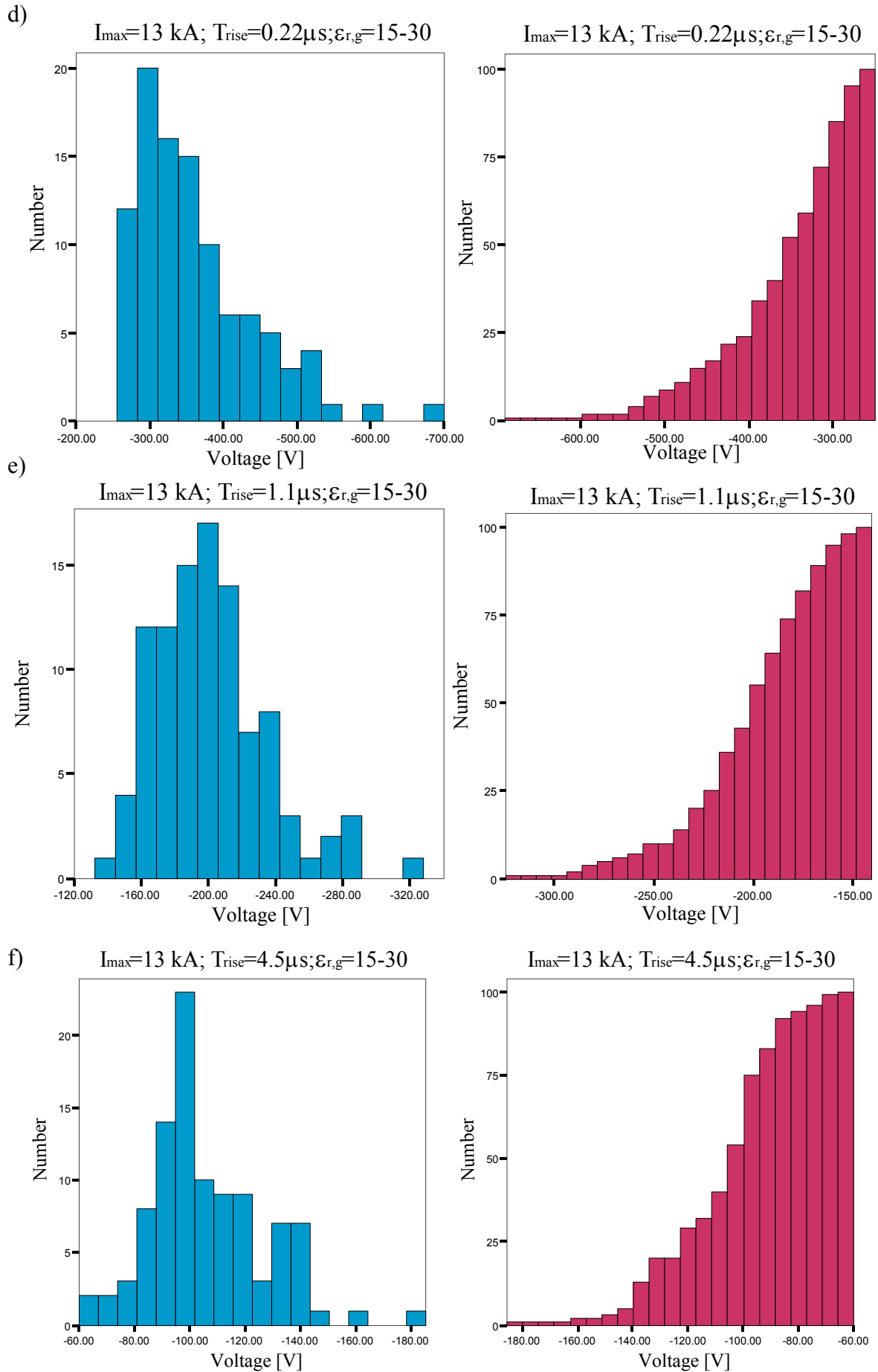
And the total energy absorbed by the element is $E = E_1 + E_2 = 0.53 \text{ mJ}$

This calculation shows that the voltage surges at the end of the line, obtained by the stochastic simulations presented above, are enough to destroy or to cause malfunction in the components stated in the table.

4.4.2.3 Evaluation of the stochastic results

In this section, the evaluation of the results shown above is introduced. Simulations with different sets of the input parameters are considered, which were shown in Fig. 4.24. The attention is concentrated on the first peak voltage of each curve in these simulations. Firstly, Fig. 4.26 depicts both histograms and cumulative histograms of this voltage for each simulation.





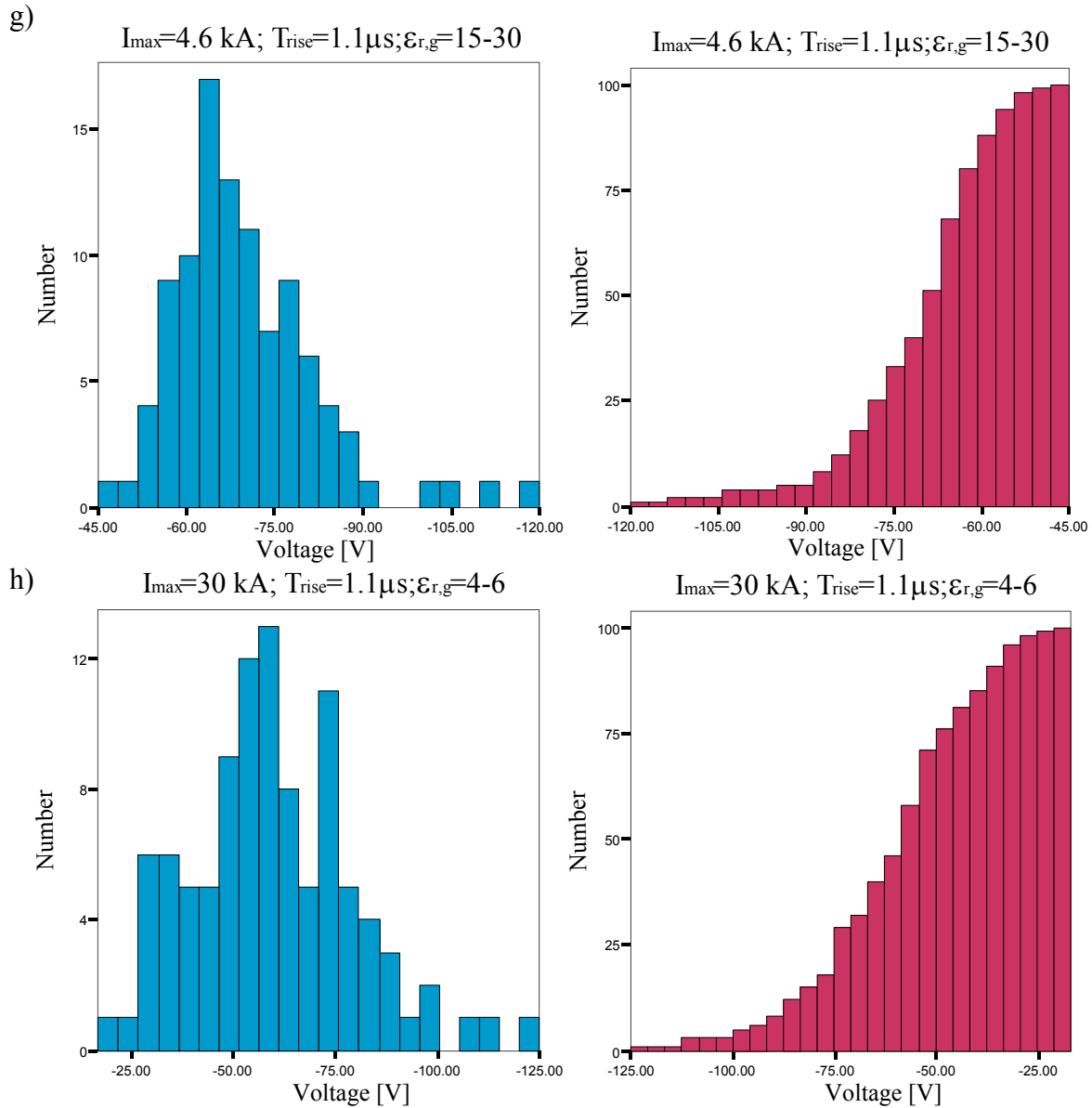


Fig. 4.26 Histograms of the peak voltage from the simulations with $N=100$ trials

Furthermore, for the evaluation of the distributions of the peak voltage, the Fortran program “ANPA” is used. The program estimates parameters of general types of probability distributions from input data. Table 4.5 gives the probability distributions implemented in “ANPA”.

No	Distribution	pdf of the distribution
1	Truncated Normal Distribution	$p(x) = \frac{1}{\left[1 - \Phi\left(-\frac{\mu}{\sigma}\right)\right] \sigma \sqrt{2\pi}} \cdot e^{-\frac{(x-\mu)^2}{2\sigma^2}} \quad x > 0$
2	Inverse Gaussian Distribution	$p(x) = \sqrt{\frac{a}{2\pi x^3}} \cdot e^{-\frac{a(x-s)^2}{2s^2x}} \quad x, a, s > 0$
3	Lognormal Distribution	$p(x) = \frac{1}{xs\sqrt{2\pi}} \cdot e^{-\frac{(\ln x - \mu)^2}{2s^2}} \quad x > 0$
4	Gamma Distribution	$p(x) = \frac{\eta}{\Gamma(b)} \cdot x^{b-1} \cdot e^{-\eta x} \quad x, b, \eta > 0$
5	Inverse Gamma Distribution	$p(x) = \frac{\beta^\alpha}{\Gamma(\alpha)} \cdot \left(\frac{1}{x}\right)^{\alpha+1} \cdot e^{-\frac{\beta}{x}} \quad x, \alpha, \beta > 0$
6	Weibull Distribution	$p(x) = \eta \cdot b \cdot (\eta \cdot x)^{b-1} \cdot e^{-(\eta \cdot x)^b} \quad x, b, \eta > 0$
7	Log-logistic Distribution	$p(x) = \frac{\delta \cdot e^\gamma \cdot x^{\delta-1}}{(1 + e^\gamma \cdot x^\delta)^2} \quad x, \delta > 0$

Table 4.5 Description of the probability distributions used in the program “ANPA”

The output of the program is an ASCII file where parameters of the pdf that represents each of the above distributions the best, based on a given input, are calculated. Using these parameters, a comparison between the different probability distributions for a given input dataset is made. The result of this comparison is a recommendation for the probability distribution that approximates the input values the best. The criterion for choosing the optimum distribution is the minimum squared difference between empirical and theoretical values, as well as between average values and the standard deviation.

Unfortunately the program has one limitation. Due to the fact that utilized probability distributions operate with positive variables only, the input dataset for the program should contain only positive values. As is evident from the above results, the first peak voltage in the stochastic simulations is negative. Therefore, as an input for the “ANPA” the absolute values of this voltage are used, assuming that the change of the sign of the values doesn’t change their probability distributions. Table 4.6 summarizes the probability distributions proposed by “ANPA” for the results shown above.

No	Parameters of the simulations	Suggested by “ANPA” distribution that the best approximates the input data	Parameters for the pdf of the distribution
1	$I_{\max}=13 \text{ kA}$, $T_{\text{rise}}=0.22 \text{ }\mu\text{s}$, $\epsilon_r=4-6$	Lognormal Distribution	$\mu=3.8999$, $s=0.241$
2	$I_{\max}=13 \text{ kA}$, $T_{\text{rise}}=1.1 \text{ }\mu\text{s}$, $\epsilon_r=4-6$	Truncated Normal Distribution	$\mu=25.63$, $\sigma=7.874$
3	$I_{\max}=13 \text{ kA}$, $T_{\text{rise}}=4.5 \text{ }\mu\text{s}$, $\epsilon_r=4-6$	Lognormal Distribution	$\mu=2.619$, $s=0.245$
4	$I_{\max}=13 \text{ kA}$, $T_{\text{rise}}=0.22 \text{ }\mu\text{s}$, $\epsilon_r=15-30$	Inverse Gamma Distribution	$\alpha=26.428$, $\beta=9166.8$
5	$I_{\max}=13 \text{ kA}$, $T_{\text{rise}}=1.1 \text{ }\mu\text{s}$, $\epsilon_r=15-30$	Inverse Gamma Distribution	$\alpha=45.597$, $\beta=8953.45$
6	$I_{\max}=13 \text{ kA}$, $T_{\text{rise}}=4.5 \text{ }\mu\text{s}$, $\epsilon_r=15-30$	Inverse Gamma Distribution	$\alpha=28.075$, $\beta=2873.3$
7	$I_{\max}=4.6 \text{ kA}$, $T_{\text{rise}}=1.1 \text{ }\mu\text{s}$, $\epsilon_r=15-30$	Inverse Gamma Distribution	$\alpha=43.22$, $\beta=2939.5$
8	$I_{\max}=30 \text{ kA}$, $T_{\text{rise}}=1.1 \text{ }\mu\text{s}$, $\epsilon_r=4-6$	Gamma Distribution	$b=8.406$, $\eta=0.1413$

Table 4.6 Probability distributions for the first peak voltage calculated by “ANPA” that the best approximate the results from the stochastic simulations

Graphically, the results from Table 4.6 are shown in Fig. 4.27.

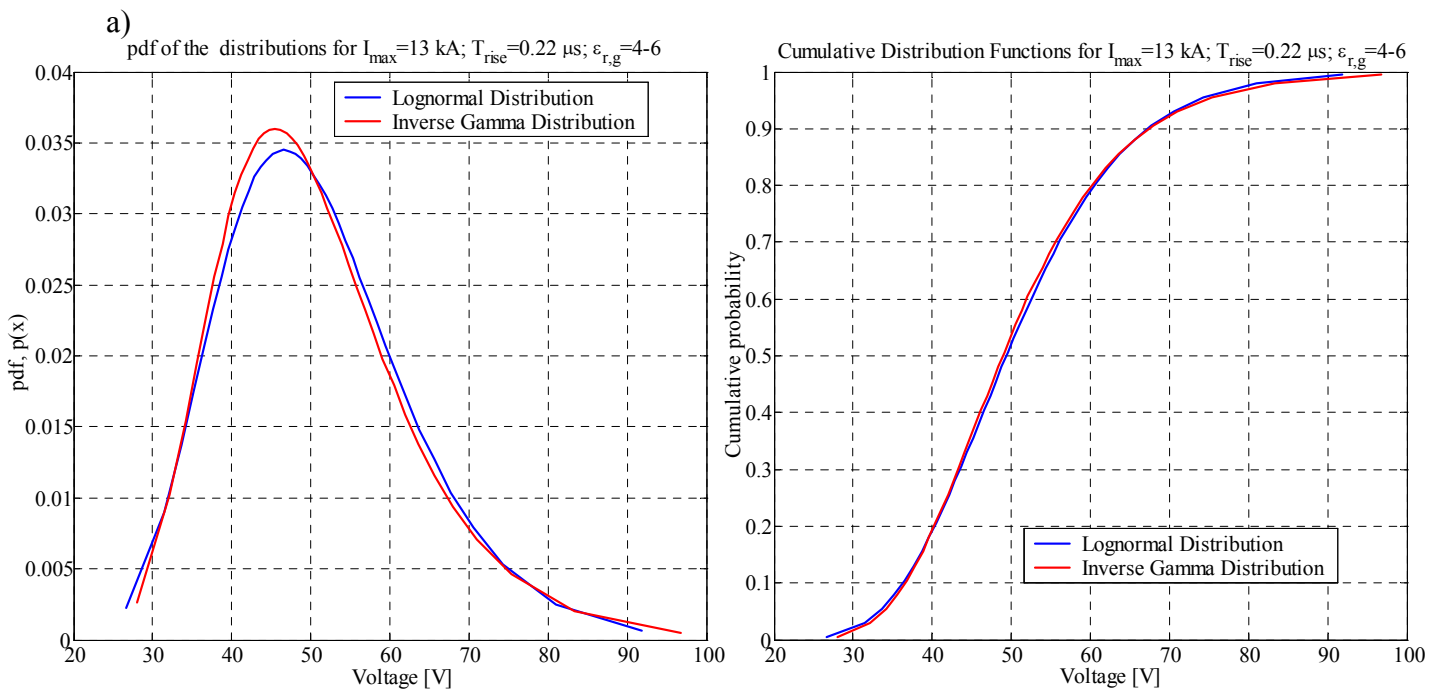
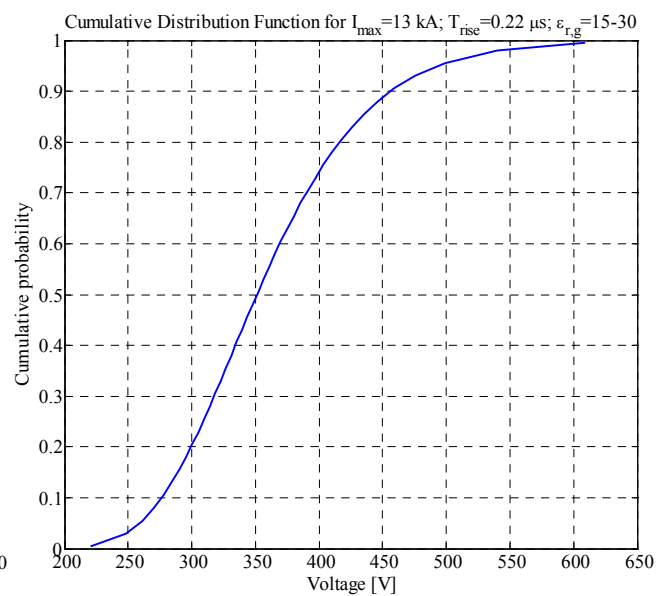
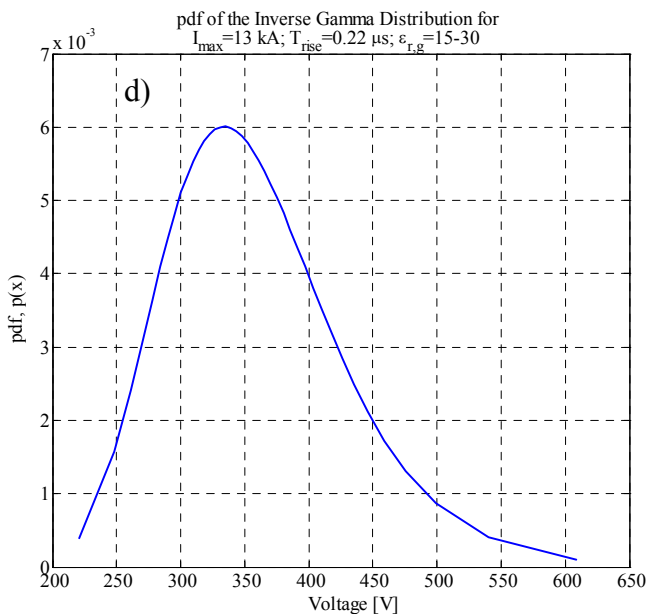
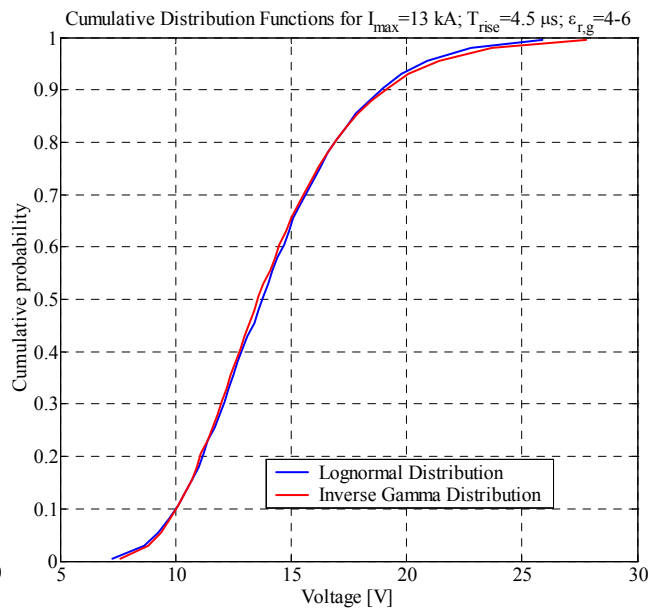
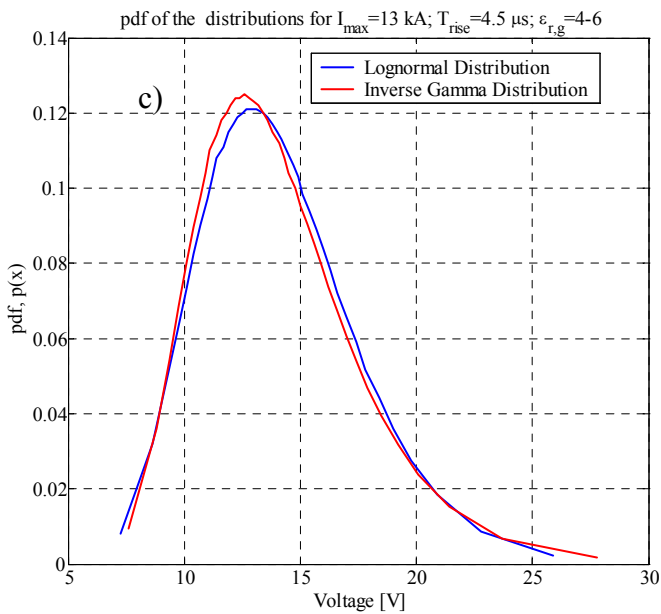
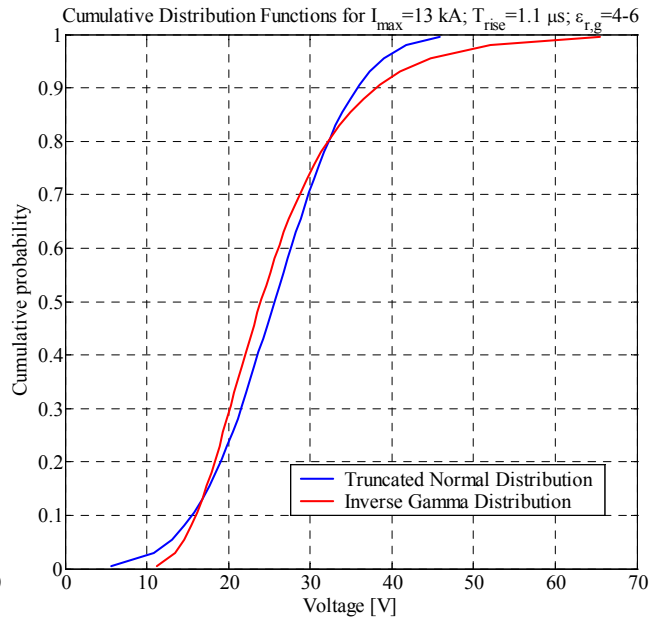
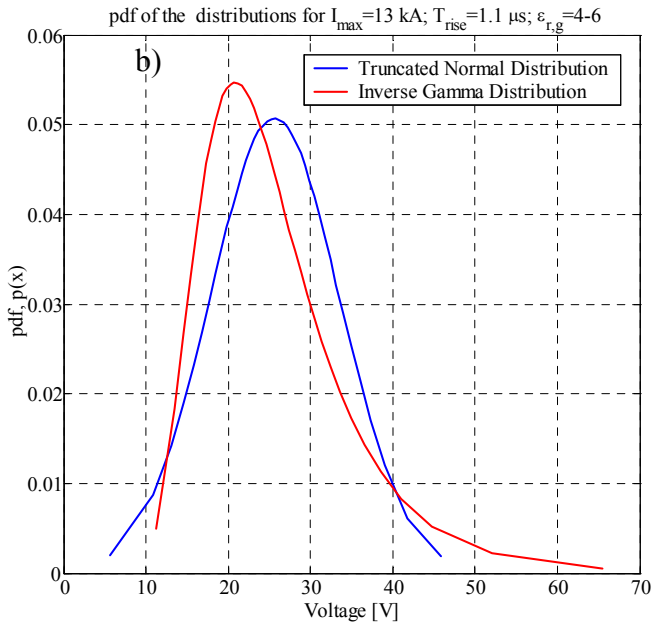
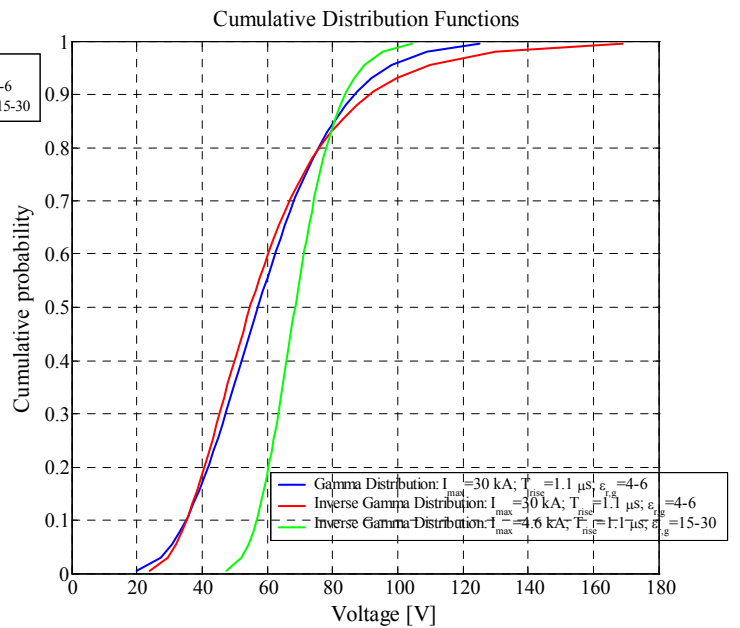
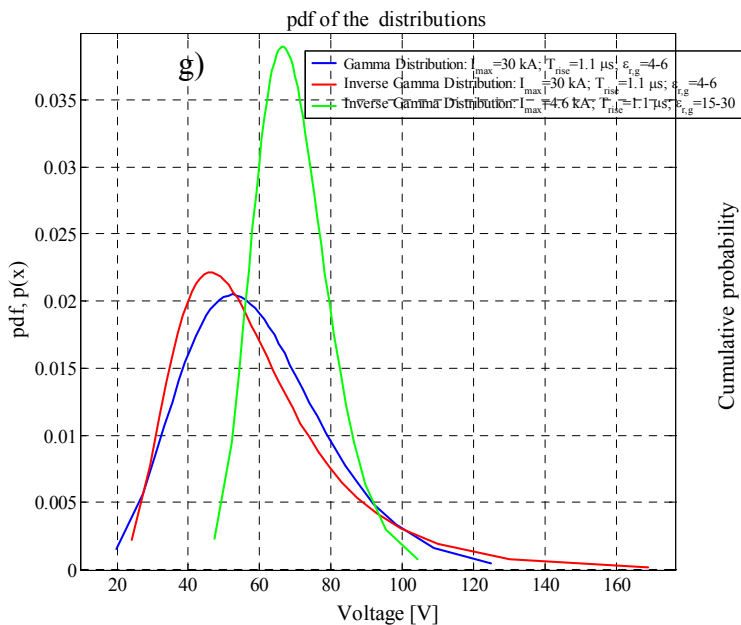
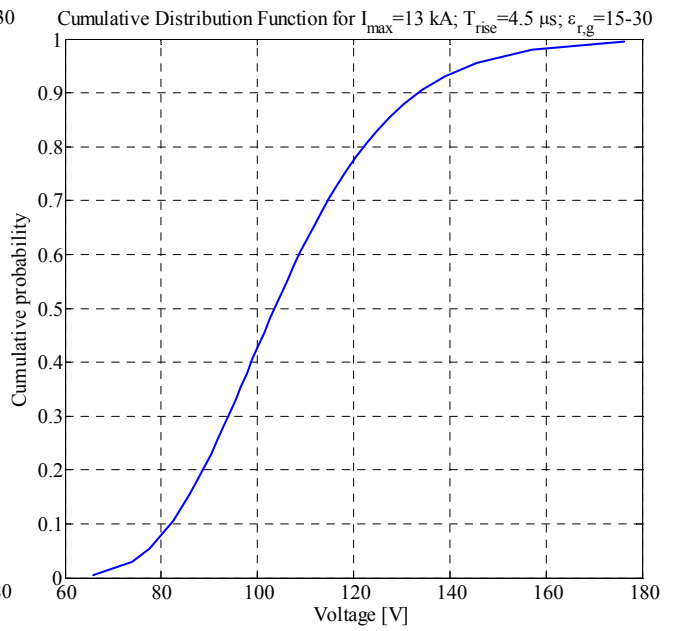
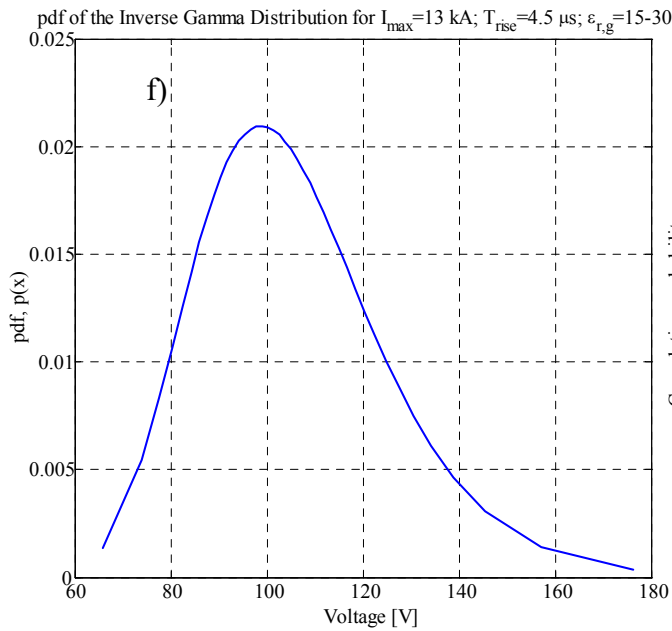
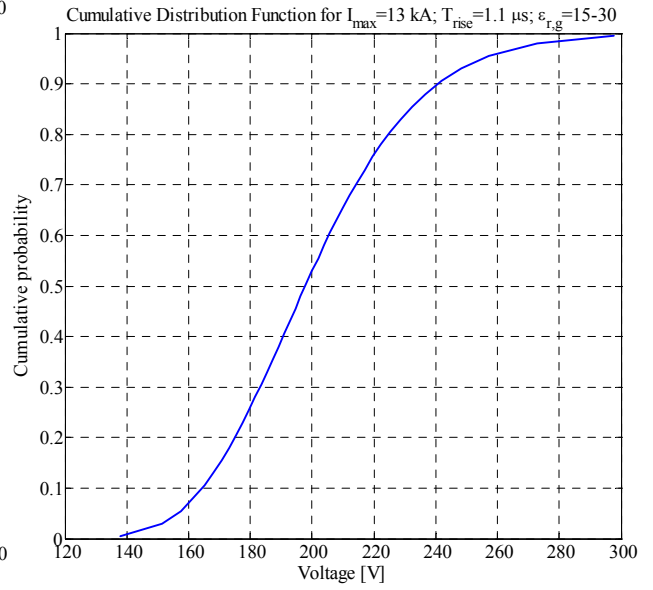
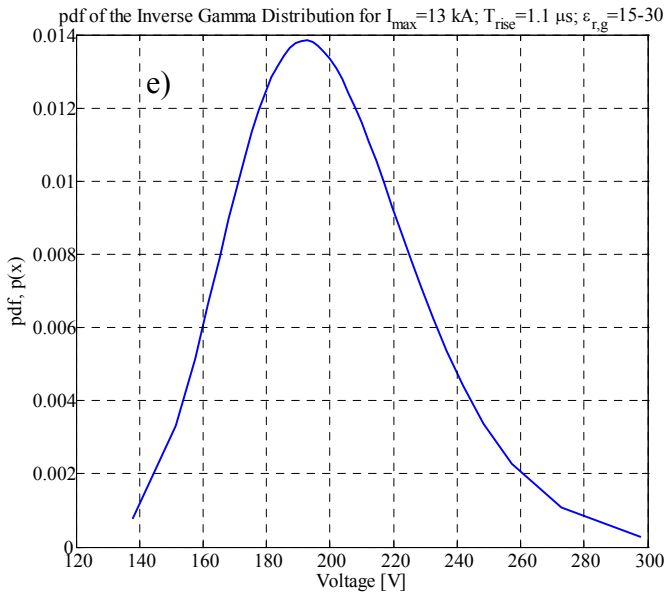


Fig. 4.27 Probability distributions of the peak voltage calculated by “ANPA”





As is evident from the above results, there is a tendency of the stochastic results being approximated best by the Inverse Gamma Distribution. In the plots where the suggested pdf is different from the latter, both are depicted – the proposed and Inverse Gamma distribution. It should be noted that in the case where the lognormal Distribution is proposed as the best approximation distribution, its curve almost coincides with the curve of the Inverse Gamma Distribution. So it can be concluded that from the eight distributions considered six can be well approximated by the Inverse Gamma Distribution.

Additionally, the evaluation of the second peak voltage which is positive, is performed with “ANPA”. Table 4.7 presents the corresponding results.

No	Parameters of the simulations	Suggested by “ANPA” distribution that the best approximates the input data	Parameters for the pdf of the distribution
1	$I_{\max}=13 \text{ kA}$, $T_{\text{rise}}=0.22 \text{ } \mu\text{s}$, $\epsilon_r=4-6$	Lognormal Distribution	$\mu=2.966$, $s=0.261$
2	$I_{\max}=13 \text{ kA}$, $T_{\text{rise}}=1.1 \text{ } \mu\text{s}$, $\epsilon_r=4-6$	Lognormal Distribution	$\mu=1.8795$, $s=0.4296$
3	$I_{\max}=13 \text{ kA}$, $T_{\text{rise}}=4.5 \text{ } \mu\text{s}$, $\epsilon_r=4-6$	Truncated Normal Distribution	$\mu=4.219$, $\sigma=1.311$
4	$I_{\max}=13 \text{ kA}$, $T_{\text{rise}}=0.22 \text{ } \mu\text{s}$, $\epsilon_r=15-30$	Inverse Gamma Distribution	$\alpha=17.328$, $\beta=1772.92$
5	$I_{\max}=13 \text{ kA}$, $T_{\text{rise}}=1.1 \text{ } \mu\text{s}$, $\epsilon_r=15-30$	Inverse Gamma Distribution	$\alpha=20.6366$, $\beta=1042.02$
6	$I_{\max}=13 \text{ kA}$, $T_{\text{rise}}=4.5 \text{ } \mu\text{s}$, $\epsilon_r=15-30$	Inverse Gamma Distribution	$\alpha=31.4991$, $\beta=951.21$
7	$I_{\max}=4.6 \text{ kA}$, $T_{\text{rise}}=1.1 \text{ } \mu\text{s}$, $\epsilon_r=15-30$	Lognormal Distribution	$\mu=2.974$, $s=0.2359$
8	$I_{\max}=30 \text{ kA}$, $T_{\text{rise}}=1.1 \text{ } \mu\text{s}$, $\epsilon_r=4-6$	Lognormal Distribution	$\mu=2.711$, $s=0.45$

Table 4.7 Probability distributions for the second peak voltage calculated by “ANPA” that the best approximate the results from the stochastic simulations

The results from the table confirm the conclusion that the peak voltages are best approximated either by the Inverse Gamma or by the Lognormal Distributions.

4.5 Determination of the expected lightning frequency as an initiating event

In section 4.4.2.2 it was shown that the current of the order of a few thousand amperes in the protective conductors could induce voltage surges in the control conductors which can destroy or bring out of order the devices connected at the end of the line. Typical damage thresholds of transistor-transistor logic (TTL) digital line drivers and receivers are shown in Fig. 4.28

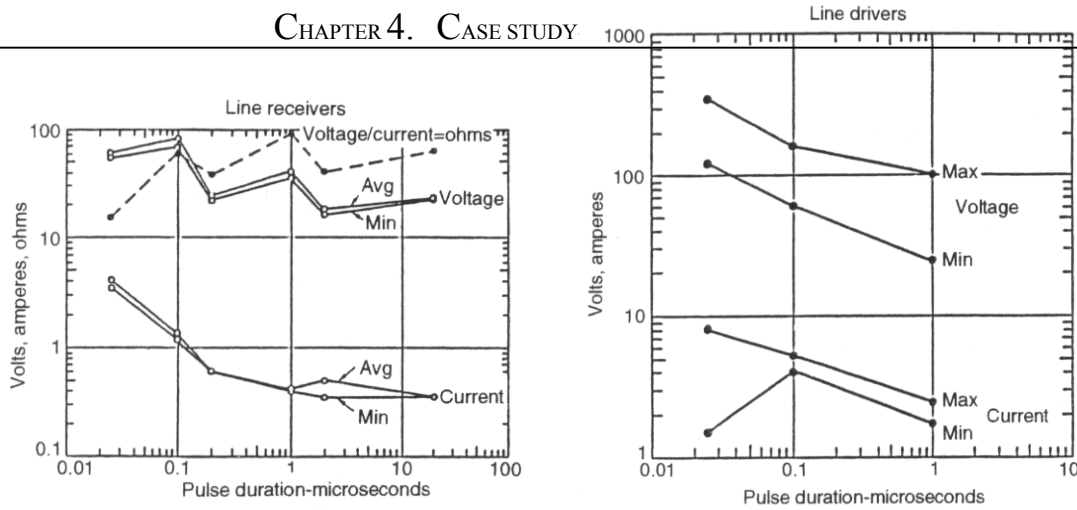


Fig. 4.28 Damage thresholds of typical TTL line drivers and receivers [115]

It is evident that the voltage surges presented above are higher than the maximum threshold levels introduced in the figure. Therefore, it can be concluded that any current pulse injected in the protective conductors whose amplitude is higher than a thousand amperes with a rise-time of the order of a few microseconds can lead to fatal consequences for the TTL devices connected to the end of the control conductors. Such current pulses can not only be produced by direct injection of lightning currents at the beginning of the line, as in the case shown in the previous section. It can also be induced by the voltage difference which exists in the ground due to a nearby lightning discharge, as illustrated in Fig. 4.29.

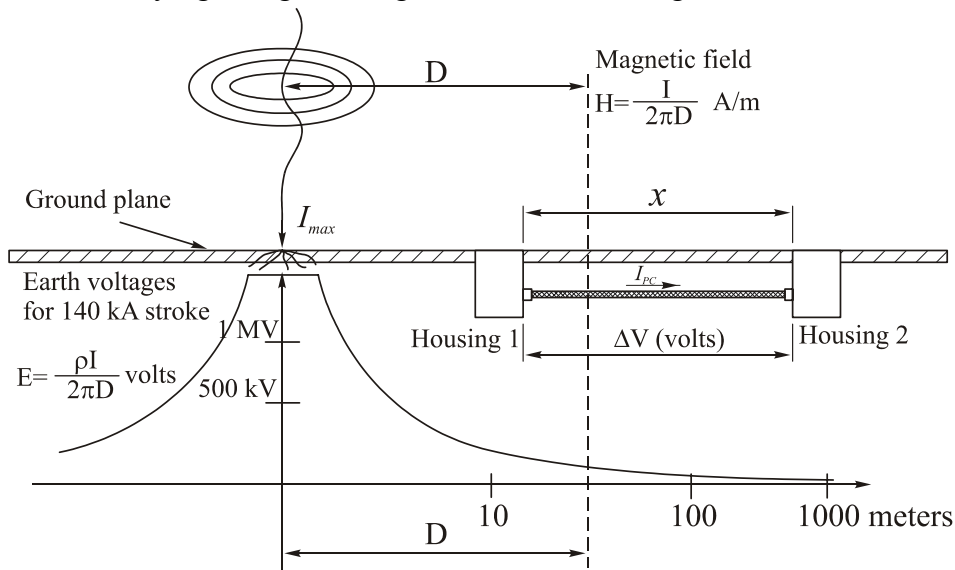


Fig. 4.29 Magnetic field and earth voltage potential difference which drives currents through cables. The earth voltage profile is shown for a 140 kA stroke into soil of 1000 Ω-m resistivity with D the distance from [115]

This is possible because the bare copper conductors are in direct contact with the ground. The earth voltage difference which is created in the ground by the injection of the lightning

current with a maximum amplitude I_{max} between the points D and $D+x$ away from the strike point can be calculated as [115]

$$\Delta V = \frac{\rho I_{max}}{2\pi} \left(\frac{1}{D} - \frac{1}{D+x} \right) \quad (4.16)$$

where ΔV is the voltage potential difference between points D and $D+x$ and ρ is the earth resistivity in $\Omega\cdot m$. Most lightning current stroke wave fronts are concave functions and for simplification can well be represented by a $(1 - \cos \omega t)$ function. If we want the function peak to be reached at $\pi/2$ radians (where the function equals one) in $2 \mu s$ (which represents a moderately severe rise time), ω is equal to 0.785×10^6 rad/sec.

The voltage difference ΔV will result in a current through the cable inductance L , as shown in the equivalent circuit of Fig. 4.30.

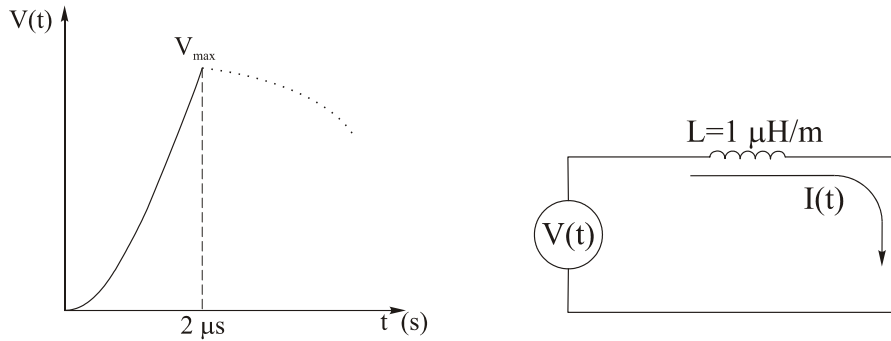


Fig. 4.30 Earth voltage waveform and equivalent circuit Adapted from [115]

Assuming an average soil voltage of $V(t)$ per meter of cable length between the two building is

$$V(t) = \frac{V_{max}}{x} (1 - \cos \omega t) \quad \text{for } 0 < t < 2\mu s \quad (4.17)$$

where V_{max} is the peak voltage ΔV obtained by eq.(4.16). Then, the current in inductor L is

$$I(t) = \frac{1}{L} \int_0^t V(\tau) d\tau \quad (4.18)$$

Substituting eq.(4.17) into eq.(4.18), the inductor current is

$$I(t) = \frac{1}{L} \int_0^t \frac{V_{max}}{x} (1 - \cos \omega \tau) d\tau \quad (4.19)$$

Performing the indicated integration with respect to time for $0 < t < 2\mu s$, the current becomes

$$I(t) = \frac{V_{max}}{Lx} \left(t - \frac{1}{\omega} \sin \omega t \right) \quad (4.20)$$

where ω equals 0.785×10^6 rad/sec for a peak current obtained at $2 \mu\text{s}$ and L is the conductor per-unit-length inductance equal to $1 \mu\text{H/m}$ [115].

Originally, the length of investigated line is 204 m. This value should be used in calculations if we assume that the lightning strikes in the vicinity of the beginning of the line. Because here it is accepted that the lightning can strike with equal probability along the whole length of the line, calculations are performed with an effective length x equal to 102 m. If the cable inductance per unit length is assumed to be $1 \mu\text{H/m}$, the peak current I_{PC} induced in the bare copper conductors at $t=2 \mu\text{s}$ can be calculated for various earth resistivities ρ and flash strike distances D by substituting the appropriate value of V obtained by eq.(4.16) into eq.(4.20). Two values for the maximum lightning current I_{max} are used in the calculations. The first value for I_{max} is 14 kA. A stroke of this magnitude or greater (including the first return stroke) can be expected to occur in about 95% of the cases. The second value is $I_{max}=140$ kA. A stroke of this magnitude may be expected to occur in about 1% of the cases. Fig. 4.31 presents the diagram of induced peak current I_{PC} in the bare copper conductors versus the distance from the strike point D . The rest of the parameters take the values described above.

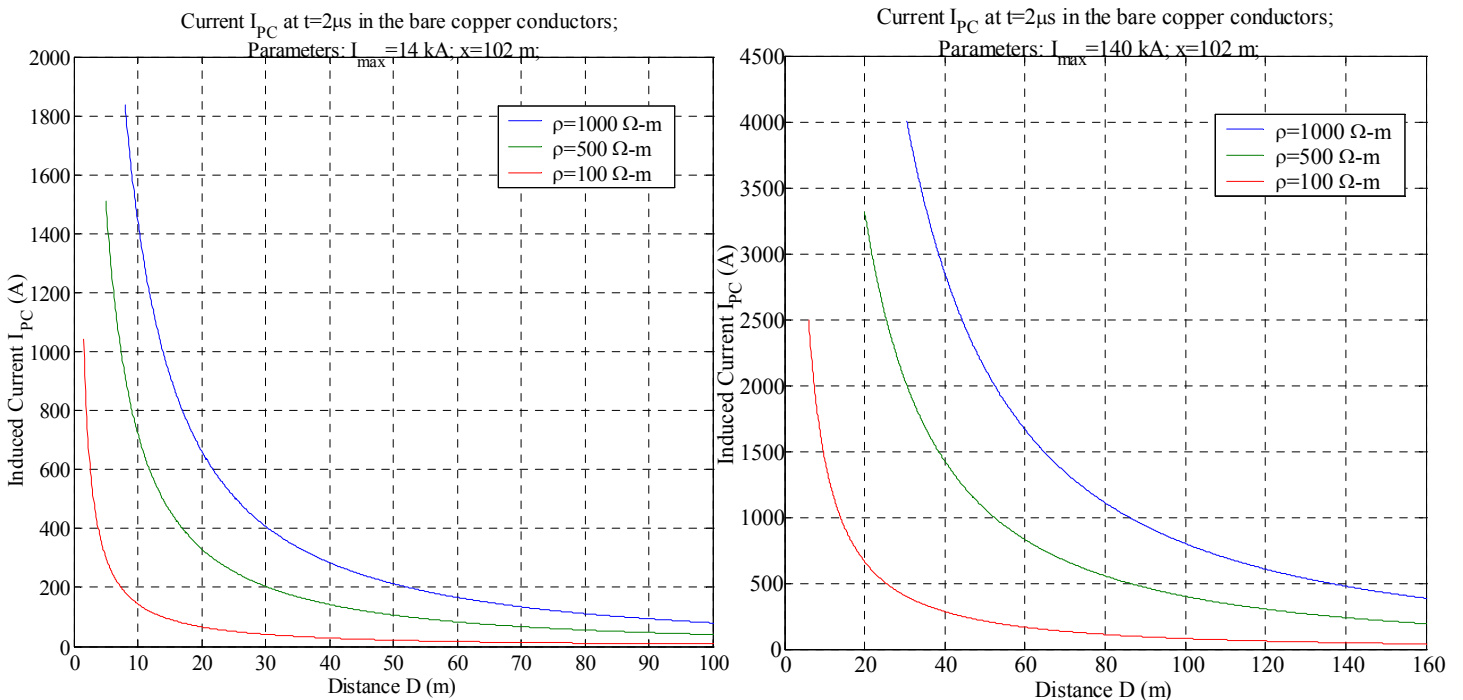


Fig. 4.31 Relationship between I_{PC} and D for different ρ and I_{max}

In what follows we assume that the current produced in the protective conductors whose peak amplitude is in the range of a thousand amperes can induce voltages in control conductors which can be considered as dangerous for the devices connected to the end of the line. From the above

diagrams we can conclude that a lightning flash which occurs within the distance D shorter than 15 m for a stroke with $I_{max} = 14$ kA and 80 m for a stroke with $I_{max} = 140$ kA from the line route can lead to potential malfunction or destruction of the devices at the end of the line.

This enables one to calculate the area surrounding the line which can be considered as critical for the operation of the equipment in the case of a lightning strike there. This critical area S_C can be approximated by a rectangle with one side equal to the line length and the other side equal to two times the distance mentioned above for the strike with $I_{max} = 14$ kA and $I_{max} = 140$ kA respectively, as illustrated in Fig. 4.32.

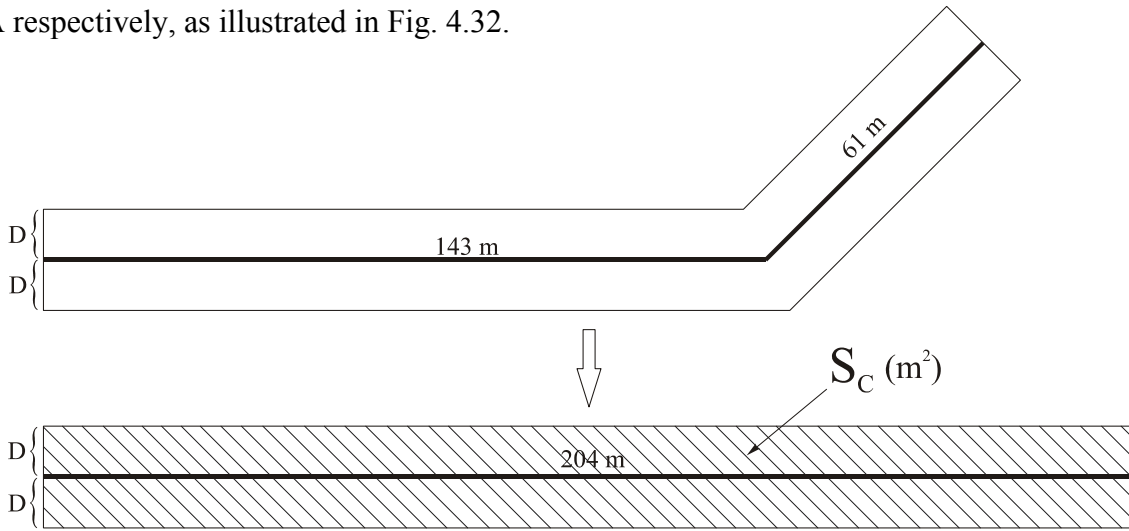


Fig. 4.32 Defining the critical area S_C for the investigated transmission line

Hence, in the case of a lightning strike with $I_{max} = 14$ kA this critical ground surface is

$$S_{C, I_{max}=14kA} = 204m \times 30m = 6120m^2$$

and in the case of lightning strike with $I_{max} = 140$ kA the critical ground surface is

$$S_{C, I_{max}=140kA} = 204m \times 160m = 32640m^2$$

Knowing the critical area S_C enables one to calculate the expected frequency of lightning strikes F_L which can cause undesired consequences in the devices at the end of the line. It is given by the following equation

$$F_L = N_d \cdot S_C \cdot P_{I_{max}} \quad (4.21)$$

where

N_d - density of lightning flashes to the ground expressed by the number of strokes per km^2 per year;

S_C - critical area (km^2);

$P_{I_{max}}$ - probability of occurrence of a lightning stroke with maximum current bigger than I_{max} ;

From Fig. 3.31 we can determine that the keraunic level of the area, where the line is situated is 30. Using eq. (3.37) the density of the lightning flashes to the ground for this area is

$$N_d = 0.04 \times 30^{1.25} = 2.81$$

The expected lightning frequency for the strokes with $I_{max} > 14$ kA and $I_{max} > 140$ kA respectively is

$$F_{L, I_{max} > 14 \text{ kA}} = 2.81 \times \frac{6120}{10^6} \times 0.95 = 1.634 \times 10^{-2} \text{ a}^{-1}$$

$$F_{L, I_{max} > 140 \text{ kA}} = 2.81 \times \frac{32640}{10^6} \times 0.01 = 0.92 \times 10^{-3} \text{ a}^{-1}$$

The interpretation of these results is that we can expect approximately 1.6 times per 100 years a disturbance in the line due to the strike with the maximum current bigger than 14 kA and less than 1 time per 1000 years disturbance in the line due to the strike with maximum current bigger than 140 kA.

With the model presented above, Monte Carlo simulation was performed. The following input parameters were considered as random variables which were described by probability distributions: maximum lightning current – I_{max} , earth resistivity – ρ , length of the line – x and density of the lightning flashes to the ground – N_d .

Using this approach enables us to find the expected lightning frequency as initiating event F_L not as a single value, but as a probability distribution.

Treating the input parameters as random variables is important because changing the length of the line in the model, for example, represents different lightning strike points in the area of the line. Thus varying the input parameters, more realistic results for F_L can be obtained.

Here the distance from the strike point D is defined again as the distance which can cause peak current in protective conductors I_{PC} bigger than 1000 A. Using this distance, the critical area S_C is calculated.

For a given maximum lightning current I_{max} , the probability of occurrence of a lightning stroke with peak current bigger than I_{max} is calculated by integration of the pdf function of I_{max} .

The probability distributions of the input parameters used in Monte Carlo simulation are given in Table 4.8.

Quantity	Unit	Type of distribution	μ	σ
Maximum lightning current – I_{max}	kA	lognormal	3.4	0.6
Uniform distribution			min	max
Earth resistivity – ρ	Ω -m	rectangular	10	1000
Length of the line – x	m	rectangular	102	204
Density of the lightning flashes to the ground – N_d	km^2yr^{-1}	rectangular	1	4

Table 4.8 Probability distributions of the input parameters

The simulation was performed with $N=10000$ Monte Carlo trials. The histogram of the result is shown in Fig. 4.33.

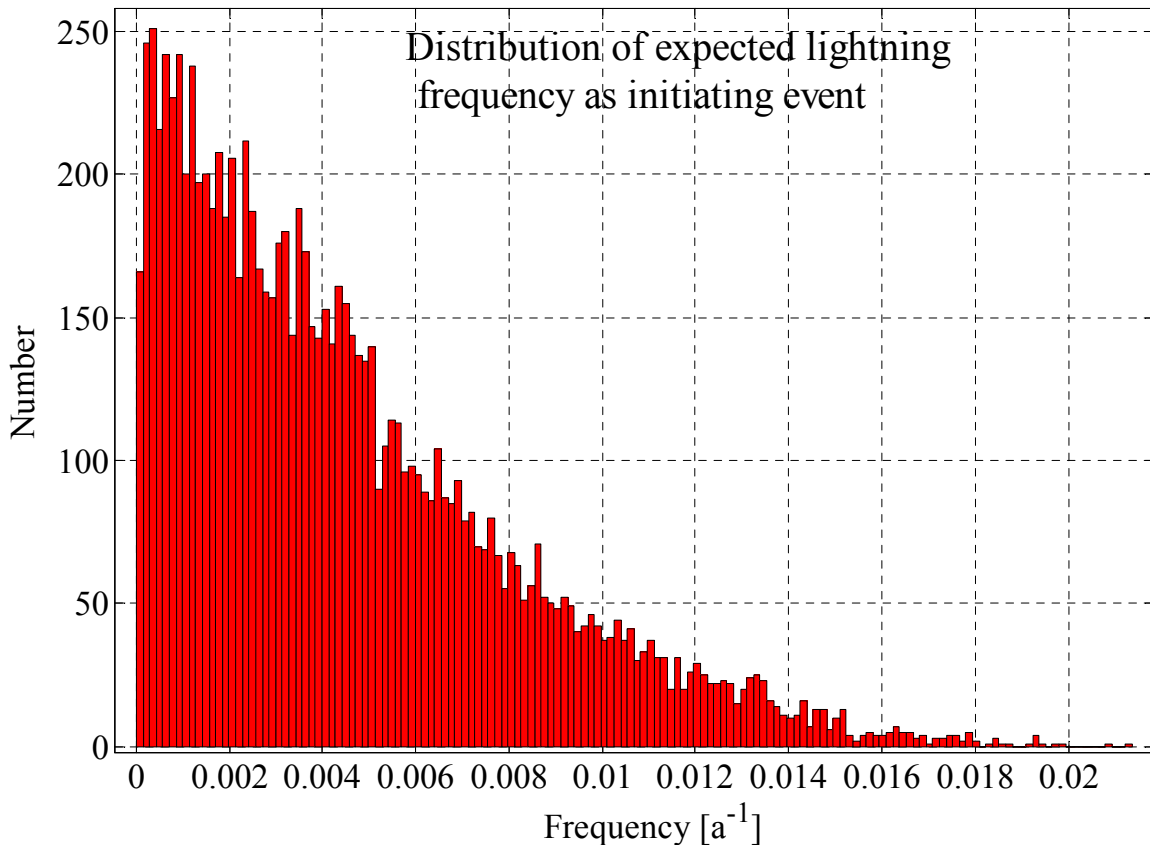


Fig. 4.33 Histogram of expected lightning frequency as initiating event

Using again the program “ANPA”, evaluation of the result was made. The proposed distribution that best approximates the result is Weibull distribution, which pdf function is given in Fig. 4.34.

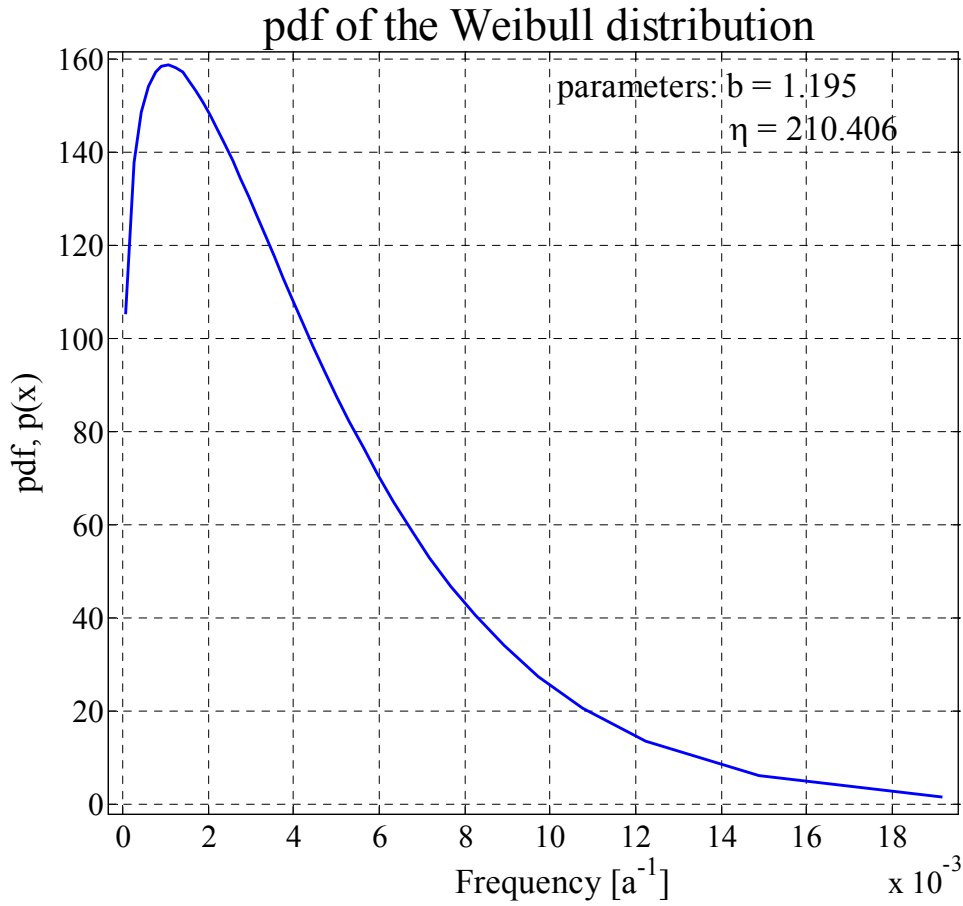


Fig. 4.34 Probability distribution of the expected lightning frequency calculated by “ANPA”

Of course, the stipulation here is that calculations for the frequency presented above concern the simplest case of unshielded cables. It is desirable that further investigations of this topic include the determination of the corresponding frequency for shielded cables as well.

From the above calculations it is obvious that in some cases, the frequency of lightning flashes considered as an initiating event which can lead to undesired consequences is bigger compared to the frequency of occurrence of other initiating events as, for example, small leakages in the main cooling pipeline whose frequency ranges from 9.0×10^{-5} to $2.8 \times 10^{-3} \text{ a}^{-1}$. Therefore, “barriers” should be used whose purpose is to decrease this frequency. In our case, such barriers are, for example, utilization of shielded cables or installation of current and voltage surge arrestors at the ends of the line.

Chapter 5

5. Summary and outlook

The emphasis of the present work lies on the electromagnetic interaction of lightning with a low-voltage transmission line located under the ground. The stochastic nature of some of the parameters involved such as, for example, the conductors and insulation diameters, properties of the surrounding soil and properties of the conductors and insulation are also taken into account.

In order to simulate the impact of the lightning stroke over the transmission line, an appropriate lightning stroke model was developed. The advantage of this model is that it simulates and enables one to compare both aboveground and underground electromagnetic fields produced by lightning. It was determined that although some differences between this model and models used by other authors [25], due to high flexibility in adjusting some of the input parameters, a very good agreement between the results computed by the program “LEMFieldE” and the results published in the literature was achieved. This allows one to use “LEMFieldE” in further simulations.

In simulating the interaction of lightning with the transmission line two basic cases are considered. They were chosen in such a way as to embrace different mechanisms of interactions of the lightning with the transmission line. In the case of the electromagnetic field coupling, it was confirmed that if the line is located under the ground it is protected sufficiently from the consequences caused by lightning. In this case, the surge at the end of the line cannot influence the normal operation of the devices at its end. It was shown that in the case when the lightning current is injected in the protective conductors which can be considered as a part of the line, the surges are strong enough to cause damage or malfunctions

in the devices at the line ends. So, any strike can be considered as dangerous along the length of the line which can cause the propagation of the lightning current into the protective conductors. These conductors, although intended for lightning protection, cannot shield the control conductors from the current surges caused by crosstalk between them and the high lightning current that flows in the protective conductors.

The stochastic simulations conducted have shown that the lightning current and the properties of the soil are the factors with the biggest influence for the response at the far-end of the line. In this case, materials with small value of the relative electric permittivity ϵ_r should be used to fill in the space between the protective and control conductors. Also engineering solutions which maintain the humidity level of the soil as low as possible in the channel of the line are worth being implemented. The smaller the relative permittivity of the ground, the lower the surge at the end of the line.

It should be mentioned that simulation is performed with control conductors of a very simple type. They don't have braided or any other form of metallic shield which can mitigate the effect of the crosstalk. Although rare, such cables are still in use in low-voltage transmission lines due to their low price. Further investigation of the subject can include the development of a model where the control conductors are replaced by shielded cables in order to examine how the inclusion of the shielded wires will reduce the surge at the end of the line.

Bibliography

- [1] Abdel-Rahman, M., Janischewskyj, W., Hussein, A.M., Rachidi, F. and Chang, J.S.: Statistical analysis of magnetic fields due to CN Tower multistroke flashes. *Proc. of the 24th International Conference on Lightning Protection (ICLP)*, Birmingham, United Kingdom, 1998, pp. 107-112.
- [2] Abramowitz, M. and Stegun, I.A.: *Handbook of mathematical functions, with formulas, graphs, and mathematical tables*, Dover Publications, New York, 1972, xiv, 1046 p. pp.
- [3] Agrawal, A.K., Price, H.J. and Gurbaxani, S.H.: Transient response of multiconductor transmission lines excited by a nonuniform electromagnetic field, *IEEE Transactions on Electromagnetic Compatibility*, 22 (1980) 119-129.
- [4] Amoroso, V. and Lattarulo, F.: The Electromagnetic Field of an Improved Lightning Return-Stroke Representation, *IEEE Transactions on Electromagnetic Compatibility*, 35 (1993) 317-328.
- [5] Andreasson, T. and Skansholm, J.: *Getting started with UNIX and X*, Addison-Wesley Pub. Co, Wokingham, Eng. ; Reading, Mass., 1993, xi, 271 p. pp.
- [6] Antonini, G., Cristina, S. and Orlandi, A.: PEEC modeling of lightning protection systems and coupling to coaxial cables, *IEEE Transactions on Electromagnetic Compatibility*, 40 (1998) 481-491.
- [7] Antonini, G. and Orlandi, A.: Lightning-induced effects on lossy MTL terminated on arbitrary loads: A wavelet approach, *IEEE Transactions on Electromagnetic Compatibility*, 42 (2000) 181-189.
- [8] Asakawa, A., Miyake, K., Yokoyama, S., Shindo, T., Yokota, T. and Sakai, T.: Two types of lightning discharges to a high stack on the coast of the Sea of Japan in winter, *IEEE Transactions on Power Delivery*, 12 (1997) 1222-1231.
- [9] Barlow, R. and Barnett, A.R.: *Computing for scientists: principles of programming with Fortran 90 and C++*, John Wiley & Sons, Chichester, 1998.
- [10] Bellan, D. and Pignari, S.: A probabilistic model for the response of an electrically short two-conductor transmission line driven by a random plane wave field, *IEEE Transactions on Electromagnetic Compatibility*, 43 (2001) 130-139.
- [11] Berger, K.: Novel Observation on Lightning Discharges: Results of Research on Mount San Salvatore, *J. Franklin Inst.*, 283 (1967) 478-525.
- [12] Berger, K.: Blitzstrom - Parameter von Aufwärtsblitzen, *Bull. Schweiz. Elektrotech.*, 69 (1978) 353-360.
- [13] Berger, K., Anderson, R.B. and Kröniger, H.: Parameters of lightning flashes, *Electra*, 41 (1975) 23-37.
- [14] Berger, K. and Vogelsanger, E.: Messungen und Resultate der Blitzforschung der Jahre 1955-1963 auf dem Monte San Salvatore, *Bull. Schweiz. Elektrotech.*, 56 (1965) 2-22.

-
- [15] Berger, K. and Vogelsanger, E.: Photographische Blitzuntersuchungen der Jahre 1955-1965 auf dem Monte San Salvatore, *Bull. Schweiz. Elektrotech.*, 57 (1966) 599-620.
- [16] Blitz Planer, DEHN + SÖHNE GmbH, Neumarkt, Germany, 2001.
- [17] Bruce, C.E.R. and Golde, R.H.: The lightning discharge, *J. Inst. Elect. Eng. - Pt. 2*, 88 (1941) 487-520.
- [18] CableMod Version 2.0: User's Manual, SimLab Software GmbH-Munich, Germany, 2002.
- [19] Chemical Rubber Company: *CRC standard mathematical tables and formulae*, 30th edn., CRC Press, Boca Raton, 1996, 812 pp.
- [20] Chivers, I.D. and Sleightholme, J.: *Introducing Fortran 90*, Springer-Verlag, Berlin; London, 1995.
- [21] Cooray, V.: Horizontal fields generated by return strokes, *Radio Science*, 27 (1992) 529-537.
- [22] Cooray, V.: A model for subsequent return strokes, *Journal of Electrostatics*, 30 (1993) 343-354.
- [23] Cooray, V.: Calculating Lightning-Induced Overvoltages in Power-Lines - a Comparison of Two Coupling Models, *IEEE Transactions on Electromagnetic Compatibility*, 36 (1994) 179-182.
- [24] Cooray, V.: Predicting the spatial and temporal variation of the electromagnetic fields, currents, and speeds of subsequent return strokes, *IEEE Transactions on Electromagnetic Compatibility*, 40 (1998) 427-435.
- [25] Cooray, V.: Underground electromagnetic fields generated by the return strokes of lightning flashes, *IEEE Transactions on Electromagnetic Compatibility*, 43 (2001) 75-84.
- [26] Cooray, V. and Perez, H.: Some Features of Lightning Flashes Observed in Sweden, *Journal of Geophysical Research-Atmospheres*, 99 (1994) 10683-10688.
- [27] Cooray, V. and Scuka, V.: Lightning-induced overvoltages in power lines: Validity of various approximations made in overvoltage calculations, *IEEE Transactions on Electromagnetic Compatibility*, 40 (1998) 355-363.
- [28] D'Amore, M. and Sarto, M.S.: Theory of field-excited networks, *IEEE Transactions on Electromagnetic Compatibility*, 38 (1996) 212-220.
- [29] Datta, B.N.: *Numerical linear algebra and applications*, Brooks/Cole Pub., Pacific Grove, 1995, xxii, 680 p. pp.
- [30] Degauque, P. and Hamelin, J.: *Electromagnetic compatibility*, Oxford University Press, Oxford [England]; New York, 1993, xxvi, 652 p. pp.
- [31] Diendorfer, G.: Induced voltage on an overhead line due to nearby lightning, *IEEE Transactions on Electromagnetic Compatibility*, 32 (1990) 292-299.
- [32] Diendorfer, G., Schulz, W. and Rakov, V.A.: Lightning characteristics based on data from the Austrian lightning locating system, *IEEE Transactions on Electromagnetic Compatibility*, 40 (1998) 452-464.
- [33] Djordjevic, A.R. and Artech House Inc.: *LINPAR for Windows matrix parameters for multiconductor transmission lines*. Artech House, Boston, 1999.
- [34] Djordjevic, A.R. and Sarkar, T.K.: Analysis of time response of lossy multiconductor transmission line networks, *IEEE Transactions on Microwave Theory and Techniques*, 35 (1987) 898-908.
- [35] Djordjevic, A.R., Sarkar, T.K. and Harrington, R.F.: Analysis of lossy transmission lines with arbitrary nonlinear terminal networks, *IEEE Transactions on Microwave Theory and Techniques*, 34 (1986) 660-666.
- [36] Djordjevic, A.R., Sarkar, T.K. and Harrington, R.F.: Time-Domain Response of Multiconductor Transmission Lines, *Proceedings of the IEEE*, 75 (1987) 743-764.
- [37] Dubi, A.: *Monte Carlo applications in systems engineering*, Wiley, Chichester [West Sussex, England]; New York, 2000, xxi, 266 p. pp.

- [38] Erdin, I., Dounavis, A., Achar, R. and Nakhla, M.S.: A SPICE model for incident field coupling to lossy multiconductor transmission lines, *IEEE Transactions on Electromagnetic Compatibility*, 43 (2001) 485-494.
- [39] Eriksson, A.J.: An improved electrogeometric model for transmission line shielding analysis, *IEEE Transactions on Power Delivery*, 2 (1987) 873-886.
- [40] Faria, J.A.B.: *Multiconductor transmission-line structures: modal analysis techniques*, Wiley, New York, 1993, viii, 203 p. pp.
- [41] Fisher, R.J., Schnetzer, G.H., Thottappillil, R., Rakov, V.A., Uman, M.A. and Goldberg, J.D.: Parameters of Triggered-Lightning Flashes in Florida and Alabama, *Journal of Geophysical Research-Atmospheres*, 98 (1993) 22887-22902.
- [42] Fuchs, F., Landers, E.U., Schmid, R. and Wiesinger, J.: Lightning current and magnetic field parameters caused by lightning strikes to tall structures relating to interference of electronic systems, *IEEE Transactions on Electromagnetic Compatibility*, 40 (1998) 444-451.
- [43] Galvan, A., Cooray, V. and Scuka, V.: Interaction of electromagnetic fields from cloud and ground lightning flashes with an artificial low-voltage power installation, *IEEE Transactions on Electromagnetic Compatibility*, 41 (1999) 250-257.
- [44] Galvan, A., Cooray, V. and Thottappillil, R.: A technique for the evaluation of lightning-induced voltages in complex low-voltage power-installation networks, *IEEE Transactions on Electromagnetic Compatibility*, 43 (2001) 402-409.
- [45] Gardner, R.L.: *Lightning electromagnetics*, Hemisphere Pub., New York, 1990, x, 540 p. pp.
- [46] Gehrke, W.: *Fortran 95 language guide*, Springer, London; New York, 1996.
- [47] Georgiadis, N., Rubinstein, M., Uman, M.A., Medelius, P.J. and Thomson, E.M.: Lightning-induced voltages at both ends of a 448-m power distribution line, *IEEE Transactions on Electromagnetic Compatibility*, 34 (1992) 451-460.
- [48] Gomes, C. and Cooray, V.: Concepts of lightning return stroke models, *IEEE Transactions on Electromagnetic Compatibility*, 42 (2000) 82-96.
- [49] Goudos, S.K., Vafiadis, E.E. and Sahalos, J.N.: Monte Carlo simulation for the prediction of the emission level from multiple sources inside shielded enclosures, *IEEE Transactions on Electromagnetic Compatibility*, 44 (2002) 291-308.
- [50] Granzow, K.D.: *Digital transmission lines: computer modelling and analysis*, Oxford University Press, Oxford; New York, 1998, xx, 341 p. pp.
- [51] Grcev, L.D.: Computer analysis of transient voltages in large grounding systems, *IEEE Transactions on Power Delivery*, 11 (1996) 815-823.
- [52] Grcev, L.D. and Heimbach, M.: Frequency dependent and transient characteristics of substation grounding systems, *IEEE Transactions on Power Delivery*, 12 (1997) 172-178.
- [53] Guerrieri, S., Nucci, C.A., Rachidi, F. and Rubinstein, M.: On the influence of elevated strike objects on directly measured and indirectly estimated lightning currents, *IEEE Transactions on Power Delivery*, 13 (1998) 1543-1555.
- [54] Harman, T.L., Dabney, J. and Richert, N.: *Advanced engineering mathematics using MATLAB V.4*, PWS Pub. Co., Boston, 1997, xxxix, 643 p. pp.
- [55] Hauptmanns, U.: Uncertainty and the calculation of safety-related parameters for chemical reactions, *Journal of Loss Prevention in the Process Industries*, 10 (1997) 243-247.
- [56] Hauptmanns, U. and Grosskopf, M.: Accounting for stochastic quantities in calculating interference voltages, *Journal of Loss Prevention in the Process Industries*, 14 (2001) 11-16.

- [57] Heidler, F.: Traveling current source model for LEMP calculation. *Proc. of the 6th Int. Zurich Symp. Electromagn. Compat.*, Zurich, Switzerland, 1985, pp. 157-162.
- [58] Heidler, F. and Hopf, C.: Measurement results of the electric fields in cloud-to-ground lightning in nearby Munich, Germany, *IEEE Transactions on Electromagnetic Compatibility*, 40 (1998) 436-443.
- [59] Heimbach, M. and Greev, L.D.: Grounding system analysis in transients programs applying electromagnetic field approach, *IEEE Transactions on Power Delivery*, 12 (1997) 186-193.
- [60] Hermosillo, V.F. and Cooray, V.: Calculation of Fault Rates of Overhead Power Distribution Lines Due to Lightning-Induced Voltages Including the Effect of Ground Conductivity, *IEEE Transactions on Electromagnetic Compatibility*, 37 (1995) 392-399.
- [61] Hoidalén, H.K., Sletbak, J. and Henriksen, T.: Ground effects on induced voltages from nearby lightning, *IEEE Transactions on Electromagnetic Compatibility*, 39 (1997) 269-278.
- [62] Holt, R. and Nguyen, T.T.: Monte Carlo estimation of the rates of lightning strikes on power lines, *Electric Power Systems Research*, 49 (1999) 201-210.
- [63] Hubert, P., Laroche, P., Berard, A.E. and Barret, L.: Triggered lightning in New Mexico, *Journal of Geophysical Research*, 89 (1984) 2511-2521.
- [64] Hussein, A.M., Janischewskyj, W., Chang, J.S., Shostak, V., Chisholm, W.A., Dzurevych, P. and Kawasaki, Z.I.: Simultaneous Measurement of Lightning Parameters for Strokes to the Toronto-Canadian-National-Tower, *Journal of Geophysical Research-Atmospheres*, 100 (1995) 8853-8861.
- [65] Janischewskyj, W., Hussein, A.M. and Chang, J.S.: Characteristics of CN Tower multistroke flashes. *Proc. of the 10th International Symposium on High Voltage Engineering*, Montreal, Quebec, Canada, 1997, pp. 29-34.
- [66] Janischewskyj, W., Hussein, A.M., Shostak, V., Rusan, I., Li, J.X. and Chang, J.S.: Statistics of lightning strikes to the Toronto Canadian National Tower (1978-1995), *IEEE Transactions on Power Delivery*, 12 (1997) 1210-1221.
- [67] Janischewskyj, W., Shostak, V. and Hussein, A.M.: Comparison of lightning electromagnetic field characteristics of first and subsequent return strokes to a tall tower: 1. Magnetic field. *Proc. of the 24th International Conference on Lightning Protection (ICLP)*, Birmingham, United Kingdom, 1998, pp. 245-251.
- [68] Johnson, N.L., Kotz, S. and Balakrishnan, N.: *Continuous univariate distributions*, 2nd edn., Wiley, New York, 1994.
- [69] Kijima, H.: Earth-resistance estimation instrument. *Proc. of the 21st International Conference on Lightning Protection (ICLP)*, Berlin, Germany, 1992, pp. 145-150.
- [70] Kinney, J.J.: *Probability: an introduction with statistical applications*, John Wiley & Sons, New York, 1997, xiv, 513 p. pp.
- [71] Kitagawa, N., Brook, M. and Workman, J.: Continuing currents in cloud-to-ground lightning discharges, *Journal of Geophysical Research*, 67 (1962) 637-647.
- [72] Klein, M., Kiehl, P., Breutmann, N. and DIN-Deutsches Institut für Normung: *Einführung in die DIN-Normen*, 13., neubearb. und erw. Aufl. edn., B. G. Teubner, Beuth Verlag, Stuttgart, Berlin, Wien, 2001, 1208 pp.
- [73] Krider, E.P., Leteinturier, C. and Willett, J.C.: Submicrosecond field variations in natural lightning processes, *Res. Lett. Atmos. Electr.*, 12 (1992) 3-9.
- [74] Lapohos, T., LoVetri, J. and Seregelyi, J.: External field coupling to MTL networks with nonlinear junctions: Numerical modeling and experimental validation, *IEEE Transactions on Electromagnetic Compatibility*, 42 (2000) 16-28.

- [75] LAPP KABEL-Katalog 2001, U. I. LAPP GmbH, Stuttgart, Germany.
- [76] Leteinturier, C., Hamelin, J. and Berard, A.E.: Submicrosecond characteristics of lightning return-stroke currents, *IEEE Transactions on Electromagnetic Compatibility*, 33 (1991) 351-357.
- [77] Leteinturier, C., Weidman, C. and Hamelin, J.: Current and electric field derivatives in triggered lightning return strokes, *Journal of Geophysical Research*, 95 (1990) 811-828.
- [78] Lin, Y.T., Uman, M.A., Tiller, J.A., Brantley, R.D., Beasley, W.H., Krider, E.P. and Weidman, C.: Characterization of Lightning Return Stroke Electric and Magnetic Fields from Simultaneous Two-Station Measurements, *Journal of Geophysical Research*, 84 (1979) 6307-6314.
- [79] Liu, Y.Q., Zitnik, M. and Thottappillil, R.: An improved transmission-line model of grounding system, *IEEE Transactions on Electromagnetic Compatibility*, 43 (2001) 348-355.
- [80] Loyka, S.L.: On calculation of the ground transient resistance of overhead lines, *IEEE Transactions on Electromagnetic Compatibility*, 41 (1999) 193-195.
- [81] Martinez, A. and Byrnes, A.P.: Modeling Dielectric-constant values of Geologic Materials: An Aid to Ground-Penetrating Radar Data Collection and Interpretation. Current Research in Earth Science, Kansas Geological Survey, Bulletin 247, Kansas City (Pennsylvanian), 2001.
- [82] Mata, C.T., Fernandez, M.I., Rakov, V.A. and Uman, M.A.: EMTP modeling of a triggered-lightning strike to the phase conductor of an overhead distribution line, *IEEE Transactions on Power Delivery*, 15 (2000) 1175-1181.
- [83] Mendenhall, W. and Sincich, T.: *Statistics for engineering and the sciences*, 4th edn., Prentice-Hall, Englewood Cliffs, N.J., 1995, xvii, 1182 p. pp.
- [84] Miki, M., Rakov, V.A., Rambo, K.J., Schnetzer, G.H. and Uman, M.A.: Electric fields near triggered lightning channels measured with Pockels sensors, *Journal of Geophysical Research-Atmospheres*, 107 (2002) -.
- [85] Moore, H.G. and Yaqub, A.: *A first course in linear algebra with applications*, 3rd edn., Academic Press, San Diego, 1998.
- [86] Motoyama, H., Janischewskyj, W., Hussein, A.M., Rusan, R., Chisholm, W.A. and Chang, J.S.: Electromagnetic field radiation model for lightning strokes to tall structures, *IEEE Transactions on Power Delivery*, 11 (1996) 1624-1632.
- [87] Mousa, A.M. and Srivastava, K.D.: Modelling of power lines in lightning incidence calculations, *IEEE Transactions on Power Delivery*, 5 (1990) 303-310.
- [88] Newman, M.M., Stahmann, J.R., Robb, J.D., Lewis, S.G., Martin, S.G. and Zinn, S.V.: Triggered Lightning Strokes at Very Close Range, *Journal of Geophysical Research*, 72 (1967) 4761-4764.
- [89] Nitsch, J., Baum, C.E. and Strum, R.: Analytical treatment of uniform multiconductor transmission lines, *IEEE Transactions on Electromagnetic Compatibility*, 35 (1993) 285-294.
- [90] Nucci, C.A., Guerrieri, S., de Barros, M.T.C. and Rachidi, F.: Influence of corona on the voltages induced by nearby lightning on overhead distribution lines, *IEEE Transactions on Power Delivery*, 15 (2000) 1265-1273.
- [91] Nucci, C.A., Mazzetti, C., Rachidi, F. and Ianoz, M.: On lightning return stroke models for LEMP calculations. *Proc. of the 19th Int. Conf. Lightning Protection*, Graz, Austria, 1988.
- [92] Nucci, C.A., Rachidi, F., Ianoz, M., Mazzetti, C., Chowdhuri, P. and Darveniza, M.: Comparison of Two Coupling Models for Lightning-Induced Overvoltage Calculations, *IEEE Transactions on Power Delivery*, 10 (1995) 330-339.
- [93] Nucci, C.A., Rachidi, F., Ianoz, M.V. and Mazzetti, C.: Lightning-induced voltages on overhead lines, *IEEE Transactions on Electromagnetic Compatibility*, 35 (1993) 75-86.

-
- [94] Omid, M., Kami, Y. and Hayakawa, M.: Field coupling to nonuniform and uniform transmission lines, *IEEE Transactions on Electromagnetic Compatibility*, 39 (1997) 201-211.
- [95] Orlandi, A., Mazzetti, C., Flisowski, Z. and Yarmarkin, M.: Systematic approach for the analysis of the electromagnetic environment inside a building during lightning strike, *IEEE Transactions on Electromagnetic Compatibility*, 40 (1998) 521-535.
- [96] Orlandi, A. and Paul, C.R.: FDTD analysis of lossy, multiconductor transmission lines terminated in arbitrary loads, *IEEE Transactions on Electromagnetic Compatibility*, 38 (1996) 388-399.
- [97] Paletta, L., Parmantier, J.P., Issac, F., Dumas, P. and Alliot, J.C.: Susceptibility analysis of wiring in a complex system combining a 3-D solver and a transmission-line network simulation, *IEEE Transactions on Electromagnetic Compatibility*, 44 (2002) 309-317.
- [98] Paul, C.R.: Frequency Response of Multiconductor Transmission Lines Illuminated by an Electromagnetic Field, *IEEE Transactions on Electromagnetic Compatibility*, 18 (1976) 183-190.
- [99] Paul, C.R.: Effects of Pigtailed Crosstalk to Braided-Shield Cables, *IEEE Transactions on Electromagnetic Compatibility*, 22 (1980) 161-172.
- [100] Paul, C.R.: Computation of Crosstalk in a Multiconductor Transmission Line, *IEEE Transactions on Electromagnetic Compatibility*, 23 (1981) 352-358.
- [101] Paul, C.R.: Transmission-Line Modeling of Shielded Wires for Crosstalk Prediction, *IEEE Transactions on Electromagnetic Compatibility*, 23 (1981) 345-351.
- [102] Paul, C.R.: *Analysis of linear circuits*, McGraw-Hill, New York, 1989, xxi, 792 p. pp.
- [103] Paul, C.R.: Literal Solution for Time-Domain Crosstalk on Lossless Transmission Lines, *IEEE Transactions on Electromagnetic Compatibility*, 34 (1992) 433-444.
- [104] Paul, C.R.: *Introduction to electromagnetic compatibility*, Wiley, New York, 1992, xvii, 765 p. pp.
- [105] Paul, C.R.: A SPICE Model for Multiconductor Transmission Lines Excited by an Incident Electromagnetic Field, *IEEE Transactions on Electromagnetic Compatibility*, 36 (1994) 342-354.
- [106] Paul, C.R.: *Analysis of multiconductor transmission lines*, Wiley, New York, 1994, xvii, 559 p. pp.
- [107] Paul, C.R.: Literal Solutions for the Time-Domain Response of a Two-Conductor Transmission-Line Excited by an Incident Electromagnetic Field, *IEEE Transactions on Electromagnetic Compatibility*, 37 (1995) 241-251.
- [108] Paul, C.R. and Bowles, B.: Symbolic Solution of the Multiconductor Transmission-Line Equations for Lines Containing Shielded Wires, *IEEE Transactions on Electromagnetic Compatibility*, 33 (1991) 149-162.
- [109] Paul, C.R. and Feather, A.E.: Computation of the Transmission Line Inductance and Capacitance Matrices from the Generalized Capacitance Matrix, *IEEE Transactions on Electromagnetic Compatibility*, 18 (1976) 175-183.
- [110] Paul, C.R. and McKnight, J.W.: Prediction of Crosstalk Involving Twisted Pairs of Wires - Part I: A Transmission-Line Model for Twisted-Wire Pairs, *IEEE Transactions on Electromagnetic Compatibility*, 21 (1979) 92-105.
- [111] Paul, C.R. and McKnight, J.W.: Prediction of Crosstalk Involving Twisted Pairs of Wires - Part II: A Simplified Low-Frequency Prediction Model, *IEEE Transactions on Electromagnetic Compatibility*, 21 (1979) 105-114.
- [112] Paul, C.R., Whites, K.W. and Nasar, S.A.: *Introduction to electromagnetic fields*, 3rd edn., WCB/McGraw-Hill, Boston, 1998, xx, 758 p. pp.
- [113] Peier, D.: *Elektromagnetische Verträglichkeit*, Hüthig Buch Verlag, Heidelberg, Germany, 1990, 222 pp.

- [114] Perez, H., Pislser, E., Cooray, V. and Scuka, V.: Lightning current statistics accomplished with the data collected by lightning localization networks. *Proc. of the 21st International Conference on Lightning Protection (ICLP)*, Berlin, Germany, 1992, pp. 343-349.
- [115] Perez, R.: *Handbook of electromagnetic compatibility*, Academic Press, San Diego, 1995, xvii, 1098 p. pp.
- [116] Poppe, G.P.M. and Wijers, C.M.J.: More efficient computation of the complex error function, *ACM Transactions on Mathematical Software*, 6 (1990) 38-46.
- [117] Press, W.H.: *Numerical recipes in FORTRAN: the art of scientific computing*, 2nd edn., Cambridge University Press, Cambridge [England] ; New York, NY, USA, 1992, xxvi, 963 p. pp.
- [118] Probst, S. and Flaxa, R.: *The power Linux: Linux 2.0, LST-distribution 2.2*, International edn., Springer, Berlin ; New York, 1997, vi, 196 p. pp.
- [119] Rachidi, F., Janischewskyj, W., Hussein, A.M., Nucci, C.A., Guerrieri, S., Kordi, B. and Chang, J.S.: Current and electromagnetic field associated with lightning-return strokes to tall towers, *IEEE Transactions on Electromagnetic Compatibility*, 43 (2001) 356-367.
- [120] Rachidi, F., Nucci, C.A., Ianoz, M. and Mazzetti, C.: Influence of a lossy ground on lightning-induced voltages on overhead lines, *IEEE Transactions on Electromagnetic Compatibility*, 38 (1996) 250-264.
- [121] Rakov, V.A.: Transient response of a tall object to lightning, *IEEE Transactions on Electromagnetic Compatibility*, 43 (2001) 654-661.
- [122] Rakov, V.A. and Dulzon, A.A.: Calculated electromagnetic fields of lightning return stroke, *Tekh. Elektrodinam.*, 1 (1987) 87-89.
- [123] Rakov, V.A. and Uman, M.A.: Long continuing current in negative lightning ground flashes, *Journal of Geophysical Research*, 95 (1990) 5455-5470.
- [124] Rakov, V.A. and Uman, M.A.: Some Properties of Negative Cloud-to-Ground Lightning Flashes Versus Stroke Order, *Journal of Geophysical Research*, 95 (1990) 5447-5453.
- [125] Rakov, V.A. and Uman, M.A.: Review and evaluation of lightning return stroke models including some aspects of their application, *IEEE Transactions on Electromagnetic Compatibility*, 40 (1998) 403-426.
- [126] Rakov, V.A., Uman, M.A., Rambo, K.J., Fernandez, M.I., Fisher, R.J., Schnetzer, G.H., Thottappillil, R., Eybert-Berard, A., Berlandis, J.P., Lalande, P., Bonamy, A., Laroche, P. and Bondiou-Clergerie, A.: New insights into lightning processes gained from triggered-lightning experiments in Florida and Alabama, *Journal of Geophysical Research-Atmospheres*, 103 (1998) 14117-14130.
- [127] Rakov, V.A., Uman, M.A. and Thottappillil, R.: Review of Lightning Properties from Electric Field and TV Observations, *Journal of Geophysical Research-Atmospheres*, 99 (1994) 10745-10750.
- [128] Ramo, S., Whinnery, J.R. and Van Duzer, T.: *Fields and waves in communication electronics*, 3rd edn., Wiley, New York, 1994, xix, 844 p. pp.
- [129] Rashid, M.H.: *SPICE for circuits and electronics using PSpice*, 2nd edn., Prentice Hall, Englewood Cliffs, N.J., 1995, xviii, 364 p. pp.
- [130] Ripley, B.D.: *Stochastic simulation*, Wiley, New York, 1987, xi, 237 p. pp.
- [131] Rizk, F.A.M.: Modeling of transmission line exposure to direct lightning strokes, *IEEE Transactions on Power Delivery*, 5 (1990) 1983-1997.
- [132] Rubinstein, M.: An approximate formula for the calculation of the horizontal electric field from lightning at close, intermediate, and long range, *IEEE Transactions on Electromagnetic Compatibility*, 38 (1996) 531-535.
- [133] Rubinstein, M., Rachidi, F., Uman, M.A., Thottappillil, R., Rakov, V.A. and Nucci, C.A.: Characterization of Vertical Electric Fields 500 m and 30 m from Triggered Lightning, *Journal of Geophysical Research-Atmospheres*, 100 (1995) 8863-8872.

- [134] Rubinstein, M., Uman, M.A., Medelius, P.J. and Thomson, E.M.: Measurements of the Voltage Induced on an Overhead Power Line 20 m from Triggered Lightning, *IEEE Transactions on Electromagnetic Compatibility*, 36 (1994) 134-140.
- [135] Rubinstein, R.Y. and Melamed, B.: *Modern simulation and modeling*, Wiley, New York, 1998, xvii, 352 p. pp.
- [136] Sadovic, S., Joulie, R., Tartier, S. and Brocard, E.: Use of line surge arresters for the improvement of the lightning performance of 63 kV and 90 kV shielded and unshielded transmission lines, *IEEE Transactions on Power Delivery*, 12 (1997) 1232-1240.
- [137] Schoene, J., Uman, M.A., Rakov, V.A., Kodali, V., Rambo, K.J. and Schnetzer, G.H.: Statistical characteristics of the electric and magnetic fields and their time derivatives 15 m and 30 m from triggered lightning, *Journal of Geophysical Research-Atmospheres*, 108 (2003) -.
- [138] Shiran, S., Reiser, B. and Haim, C.: A probabilistic model for the evaluation of coupling between transmission lines, *IEEE Transactions on Electromagnetic Compatibility*, 35 (1993) 387-393.
- [139] Stern, R.B.: Time domain calculation of electric field penetration through metallic shields, *IEEE Transactions on Electromagnetic Compatibility*, 30 (1988) 307-311.
- [140] Technical Documentation, KGG, Germany.
- [141] Tesche, F.M. and Barnes, P.R.: Transient Response of a Distribution Circuit Recloser and Control Unit to a High-Altitude electromagnetic Pulse (HEMP) and Lightning, *IEEE Transactions on Electromagnetic Compatibility*, 32 (1990) 113-124.
- [142] Tesche, F.M., Ianoz, M. and Karlsson, T.: *EMC analysis methods and computational models*, John Wiley & Sons, Inc., New York, 1997, xxvi, 623 p. pp.
- [143] Tesche, F.M., Kalin, A.W., Brandli, B., Reusser, B., Ianoz, M., Tabara, D. and Zweijacker, P.: Estimates of lightning-induced voltage stresses within buried shielded conduits, *IEEE Transactions on Electromagnetic Compatibility*, 40 (1998) 492-504.
- [144] Thomson, E.M.: The Dependence of Lightning Return Stroke Characteristics on Latitude, *Journal of Geophysical Research*, 85 (1980) 1050-1056.
- [145] Thomson, E.M., Galib, M.A., Uman, M.A., Beasley, W.H. and Master, M.J.: Some Features of Stroke Occurrence in Florida Lightning Flashes, *Journal of Geophysical Research*, 89 (1984) 4910-4916.
- [146] Thottappillil, R.: Electromagnetic pulse environment of cloud-to-ground lightning for EMC studies, *IEEE Transactions on Electromagnetic Compatibility*, 44 (2002) 203-213.
- [147] Thottappillil, R. and Uman, M.A.: Comparison of Lightning Return-Stroke Models, *Journal of Geophysical Research-Atmospheres*, 98 (1993) 22903-22914.
- [148] Tröscher, M., Englmaier, A. and Scholl, B.: EMC simulation of complex cable harnesses for industrial applications. SimLab Software GmbH-Munich, BMW AG-Munich.
- [149] Tsaliovich, A.B.: *Cable shielding for electromagnetic compatibility*, Chapman & Hall, New York, 1995, xv, 469 p. pp.
- [150] Tuinenga, P.W.: *SPICE: a guide to circuit simulation and analysis using PSpice*, 3rd edn., Prentice Hall, Englewood Cliffs, N.J., 1995, xvi, 288 p. pp.
- [151] Uman, M.A.: *The lightning discharge*, Academic Press, Orlando, 1987, xii, 377 pp.
- [152] Uman, M.A. and Krider, E.P.: Natural and artificially initiated lightning, *Science*, 246 (1989) 457-464.
- [153] Uman, M.A. and McLain, D.K.: Magnetic field of the lightning return stroke, *Journal of Geophysical Research*, 74 (1969) 6899-6910.

-
- [154] Uman, M.A., Rakov, V.A., Schnetzer, G.H., Rambo, K.J., Crawford, D.E. and Fisher, R.J.: Time derivative of the electric field 10, 14, and 30 m from triggered lightning strokes, *Journal of Geophysical Research-Atmospheres*, 105 (2000) 15577-15595.
- [155] Uman, M.A., Schoene, J., Rakov, V.A., Rambo, K.J. and Schnetzer, G.H.: Correlated time derivatives of current, electric field intensity, and magnetic flux density for triggered lightning at 15 m, *Journal of Geophysical Research-Atmospheres*, 107 (2002) -.
- [156] Varbanov, V., Hauptmanns, U., Wollenberg, G. and Steinmetz, T.: Untersuchungen zur Einkopplung von Blitzschlägen in Sicherheitssysteme. 6. *Fachtagung Anlagen-, Arbeits- und Umweltsicherheit*, Köthen, Germany, 2002.
- [157] Varbanov, V., Hauptmanns, U., Wollenberg, G. and Steinmetz, T.: Potential lightning impact on safety systems, *Journal of the University of Chemical Technology and Metallurgy*, XXXVIII (2003) 565-570.
- [158] Varbanov, V., Hauptmanns, U., Wollenberg, G., Steinmetz, T. and Zander, R.: Stochastic Effects of Potential Lightning Impact on Safety Systems. *Proc. of the International Conference on Probabilistic Safety Assessment and Management (PSAM 7)*, Berlin, Germany, 2004.
- [159] Von Hippel, A.R.: *Dielectric materials and applications*, Artech House, Boston, 1995, xii, 438 p. pp.
- [160] Wait, J.R.: Concerning the horizontal electric field of lightning, *IEEE Transactions on Electromagnetic Compatibility*, 39 (1997) 186-186.
- [161] Wiebke, D.: *Untersuchung des statistischen Zusammenhanges zwischen Blitzdichte und Niederschlagsmenge*, Diplomarbeit, Institut für Meteorologie und Klimatologie der Universität Hannover; Hannover, 2000.
- [162] Williams, T.: *EMC for product designers*, Newnes, Oxford; Boston, 1992, xiv, 255 p. pp.
- [163] Zwillinger, D. and Kokoska, S.: *CRC standard probability and statistics tables and formulae*, Chapman & Hall/CRC, Boca Raton, 2000, 554 pp.

Appendix I

"LEMFielDE" source code (Lightning ElectroMagnetic Field code using MTLE current distribution model)

```

C
C
C   Program LEMFIELDE
C
C*****
C
C   PROGRAM TO COMPUTE FIELDS PRODUCED BY A LIGHTNING STRIKE ABOVE
C   THE GROUND AT A HEIGHT z AND A DISTANCE r FROM THE LIGHTNING
C   ALSO CALCULATES THE FIELDS AT A DISTANCE D AND DEPTH s UNDER THE GROUND
C   THIS PROGRAM USES MTLE MODEL (modified transmission line with exponential
C   attenuation of a current in lightning channel)
C   THE INPUT DATA ARE READ FROM THE FILE "LEMFIELD.DAT"
C   THE OUTPUT DATA ARE WRITTEN IN DIFFERENT FILES - A SEPARATE FILE FOR EACH
C   COMPONENT OF THE PRODUCED FIELD. ONE FILE FOR THE USED INPUT PARAMETERS
C   AND ONE FILE FOR THE CURRENT WAVEFORM AT THE BASE OF THE LIGHTNING.
C
C*****
C
C
C   IMPLICIT DOUBLE PRECISION (A-H, O-Z)
*
*   DOUBLE PRECISION CUR(4096), XZ, XR, H
*
REAL    EPSR, SG, W, F, Sx,
1      PI, CV, EPS, XMU,
2      TMAXX, TMAX, DT, DF,
3      S(1024)
*
COMPLEX*16  CURSPEC(4096), EZ_PERSPEC(4096), HFI_PERSPEC(4096),
1          ER_PERSPEC(4096), ER_REALSPEC(4096),
2          EZ_PTEMP, HFI_PTEMP, ER_PTEMP, ER_RTEMP, HFI_PTEMPZ0,
3          EZ_ITEMP, HFI_ITEMP, ER_ITEMP, HFI_ITEMPZ0,
4          EZ_RSPEC_S0(4096), HFI_RSPEC_S0(4096), ER_RSPEC_S0(4096),
5          EZ_RSPEC_Sx(4096), HFI_RSPEC_Sx(4096), ER_RSPEC_Sx(4096),
6          EZ_RTEMP_S0, HFI_RTEMP_S0, ER_RTEMP_S0, EZ_ITEMP_S0,
7          EZ_RTEMP_Sx, HFI_RTEMP_Sx, ER_RTEMP_Sx, HFI_ITEMP_S0
*
COMPLEX    CJ, WT, GAMA0, GAMA
C
C-----
C
INTERFACE
SUBROUTINE CIMPSC(A,B,E,MAXI,XINTG,XIP)
  INTEGER,    INTENT(IN)  :: MAXI
  DOUBLE PRECISION, INTENT(IN)  :: A,B,E
  COMPLEX*16,  INTENT(OUT)  :: XIP
  INTERFACE
    SUBROUTINE XINTG(Z,FZ)
      DOUBLE PRECISION, INTENT(IN)  :: Z
      COMPLEX*16,    INTENT(OUT)  :: FZ
    END SUBROUTINE XINTG
  END INTERFACE
END SUBROUTINE CIMPSC
END INTERFACE
C
INTERFACE
SUBROUTINE EZ_FUNC(ZPRIM,FEZ)
  DOUBLE PRECISION, INTENT(IN)  :: ZPRIM
  COMPLEX*16,    INTENT(OUT)  :: FEZ
END SUBROUTINE EZ_FUNC
C
SUBROUTINE HF_FUNC(ZPRIM,FHF)
  DOUBLE PRECISION, INTENT(IN)  :: ZPRIM
  COMPLEX*16,    INTENT(OUT)  :: FHF
END SUBROUTINE HF_FUNC
C
SUBROUTINE HF_FUNCZEROZ(ZPRIM,FHF)
  DOUBLE PRECISION, INTENT(IN)  :: ZPRIM
  COMPLEX*16,    INTENT(OUT)  :: FHF
END SUBROUTINE HF_FUNCZEROZ
C
SUBROUTINE ER_FUNC(ZPRIM,FER)
  DOUBLE PRECISION, INTENT(IN)  :: ZPRIM

```

```

        COMPLEX*16,    INTENT(OUT) :: FER
    END SUBROUTINE ER_FUNC
END INTERFACE
C ADDING COORAY -----
INTERFACE
SUBROUTINE EZ_FUNC_S0(ZPRIM,FEZ)
    DOUBLE PRECISION, INTENT(IN) :: ZPRIM
    COMPLEX*16,    INTENT(OUT) :: FEZ
END SUBROUTINE EZ_FUNC_S0
C
SUBROUTINE HF_FUNC_S0(ZPRIM,FHF)
    DOUBLE PRECISION, INTENT(IN) :: ZPRIM
    COMPLEX*16,    INTENT(OUT) :: FHF
END SUBROUTINE HF_FUNC_S0
END INTERFACE
C
C-----
C
Common /PCONS/  PI, CV, EPS, XMU, CJ
Common /CURPARM/  CI01, CI02, T11, T21, T12, T22, NN1, NN2
Common /CHANNEL/  HT, CHVEL, XLAM, H, XZ, XR, W
Common /EARTH/    EPSR, SG
Common /UNDERGR/  GAMA0, GAMA
C
C-----
C
Call GETTIM(IHR,IMIN,ISEC,I100TH)
TIM1 = 60. * (60.*IHR+IMIN) + ISEC + I100TH / 100.

PI = 2. * ASIN(1.E0)
CV = 3.0E8
EPS = 1. / (36.*PI) * 1.0E-9
XMU = 4. * PI * 1.0E-7
CJ = CMPLX(0.E0,1.E0)
C  Z0 = 120. * PI
C-----
C
Open (Unit=1,File='LEMFIELD.DAT',Status='OLD')
Read (1,*) XZ, XR, Sx
Read (1,*) EPSR, SG
Read (1,*) M1, TMAXX
Read (1,*) CI01, T11, T21, NN1
Read (1,*) CI02, T12, T22, NN2
Read (1,*) CHVEL, XLAM, H
Close (1)
*-----
C DEFINE OR SCALE PARMETERS
*-----
TMAX = 4. * TMAXX * 1.E-6
M = M1 + 2
NP = 2 ** M
N2 = NP / 2
DT = TMAX / FLOAT(NP-1)
DF = 1.0 / TMAX
FMAX = DF * (N2-1)
CHVEL = CV * CHVEL
XLAM = XLAM * 1000.
HT = 1.0 * XLAM
H = H * 1000.
H1 = -H
H0 = 0.D0
C  Parameters for the precision and iteration for numerical integration
E1 = 1.D-4
MAXI1 = 25
C-----
C
CI01 = CI01 * 1000.
CI02 = CI02 * 1000.
T11 = T11 * 1.D-6
T12 = T12 * 1.D-6
T21 = T21 * 1.D-6
T22 = T22 * 1.D-6
*-----
C OUTPUT THE INPUT VALUES FOR COMPARG FOR ERROR
*-----
Open (Unit=1,File='LEMFielD.out',Status='UNKNOWN')
Write (1,501) XZ, XR, Sx
501  Format ('Distance from the ground is: ', 1PE14.5/,
1      'Distance from the lightning is: ', 1PE14.5/,
2      'Depth under the ground is: ', 1PE14.5)
Write (1,502) EPSR, SG
502  Format ('Ground parameters are: EPSR=', 1PE14.5, 'SIGM=', 1PE14.5)
Write (1,503) M, TMAXX
503  Format ('M=', I3, ' Tmax=', 1PE14.5)
Write (1,504) CI01, T11, T21, NN1
504  Format ('CI01=', 1PE14.5, ' A, T11=', 1PE14.5, ' micro_s, T21=',
1      1PE14.5, ' micro_s, N1=', I2)
Write (1,505) CI02, T12, T22, NN2

```

```

505 Format ('CI02=', IPE14.5, ' A, T12=', IPE14.5, ' micro_s, T22=',
1 IPE14.5, ' micro_s, N2=', I2)
Write (1,506) CHVEL, XLAM, H
506 Format ('Velocity in channel is: ', IPE14.5, ' m/s',/,
1 'Channel attenuation is: ', IPE14.5, ' m'/,
2 'Channel height is: ', IPE14.5, ' m')
Close (1)
*
C DETERMINE THE TRANSIENT LIGHTNING CHANNEL CURRENT AT THE BASE
*
Call LIGHTCUR(NP,TMAX,CUR)
C OUTPUT THE TRANSIENT CURRENT
Open (Unit=1,File='CH_CURT.TIM',Status='UNKNOWN')
Write (1,*) 'LIGHTNING CHANNEL CURRENT AT THE BASE'
Do 10 I = 1, NP / 4
T = DT * (I-1)
Write (1,5000) T, CUR(I)
10 Continue
Close (1)

Write (*,*) 'Computing channel current spectrum'
C DEFINE DRIVING SPECTRA
Do 20 I = 1, NP
CURSPEC(I) = CMPLX(CUR(I),0.D0)
20 Continue
IFS = -2
Call FORT(CURSPEC,DT,DF,M,S,IFS,IFERR)
C OUTPUT THE BASE CURRENT SPECTRA
Open (Unit=1,File='CH_CURF.FRQ',Status='UNKNOWN')
Write (1,*) 'LIGHTNING CHANNEL CURRENT SPECTRA AT THE BASE'
Do 30 I = 1, N2
F = DF * (I-1)
Write (1,5000) F, CURSPEC(I)
30 Continue
Close (1)
*
C OUTPUT THE SPECTRAL RESPONSES
*
Open (1,File='EZ_PERF.FRQ')
Open (2,File='HFI_PERF.FRQ')
Open (3,File='ER_REALF.FRQ')
C ADDING COORAY -----
Open (7,File='EZ_RS0F.FRQ')
Open (8,File='HFI_RS0F.FRQ')
Open (9,File='ER_RS0F.FRQ')
Open (10,File='EZ_RSx F.FRQ')
Open (11,File='HFI_RSx F.FRQ')
Open (12,File='ER_RSx F.FRQ')
C -----
Write (1,*) 'VERTICAL ELECTRIC FIELD IN FREQUENCY DOMAIN AT'
1 ', HEIGHT ', XZ, ' m AND DISTANCE ', XR, ' m IS:'
Write (2,*) 'HORIZONTAL MAGNETIG FIELD IN FREQUENCY DOMAIN AT'
1 ', HEIGHT ', XZ, ' m AND DISTANCE ', XR, ' m IS:'
Write (3,*) 'HORIZONTAL ELECTRIC FIELD IN FREQUENCY DOMAIN AT'
1 ', HEIGHT ', XZ, ' m AND DISTANCE ', XR, ' m IS:'
C ADDING COORAY -----
Write (7,*) 'VERTICAL ELECTRIC FIELD IN FREQUENCY DOMAIN AT'
1 ', THE GROUND LEVEL AND DISTANCE ', XR, ' m FROM'
2 ', THE LIGHTNING CHANNEL ACCORDING COORAY IS:'
Write (8,*) 'HORIZONTAL MAGNETIG FIELD IN FREQUENCY DOMAIN AT'
1 ', THE GROUND LEVEL AND DISTANCE ', XR, ' m FROM'
2 ', THE LIGHTNING CHANNEL ACCORDING COORAY IS:'
Write (9,*) 'HORIZONTAL ELECTRIC FIELD IN FREQUENCY DOMAIN AT'
1 ', THE GROUND LEVEL AND DISTANCE ', XR, ' m FROM'
2 ', THE LIGHTNING CHANNEL ACCORDING COORAY IS:'
Write (10,*) 'VERTICAL ELECTRIC FIELD IN FREQUENCY DOMAIN ', Sx
1 ', m UNDER THE GROUND AND DISTANCE ', XR, ' m FROM'
2 ', THE LIGHTNING CHANNEL ACCORDING COORAY IS:'
Write (11,*) 'HORIZONTAL MAGNETIG FIELD IN FREQUENCY DOMAIN ', Sx
1 ', m UNDER THE GROUND AND DISTANCE ', XR, ' m FROM'
2 ', THE LIGHTNING CHANNEL ACCORDING COORAY IS:'
Write (12,*) 'HORIZONTAL ELECTRIC FIELD IN FREQUENCY DOMAIN ', Sx
1 ', m UNDER THE GROUND AND DISTANCE ', XR, ' m FROM'
2 ', THE LIGHTNING CHANNEL ACCORDING COORAY IS:'
C -----
C
C MAIN FREQUENCY LOOP -----
C
Write (*,*) 'Computing the spectrum ...'
Write (*,*) ''
Do 40 I = 1, N2
EZ_PTEMP = CMPLX(0.D0,0.D0)
HFI_PTEMP = CMPLX(0.D0,0.D0)
ER_PTEMP = CMPLX(0.D0,0.D0)
ER_RTEMP = CMPLX(0.D0,0.D0)
C ADDING COORAY -----

```



```

EZ_RTEMP_S0 = CMPLX(0.D0,0.D0)
HFI_RTEMP_S0 = CMPLX(0.D0,0.D0)
ER_RTEMP_S0 = CMPLX(0.D0,0.D0)
EZ_RTEMP_Sx = CMPLX(0.D0,0.D0)
HFI_RTEMP_Sx = CMPLX(0.D0,0.D0)
ER_RTEMP_Sx = CMPLX(0.D0,0.D0)
C -----
F = DF * (I-1)
  If (I.NE.1) Then
    W = 2. * PI * F
C -----
PERCENT = FLOAT(I) / FLOAT(N2) * 100.
Write (*,5100) PERCENT
C -----
C DEFINING GAMA0 AND GAMA -----
GAMA0 = CJ*W/CV
GAMA = CSQRT(CJ*W*XMU*SG - W**2*XMU*EPSR*EPS)
C -----
C COMPUTE THE FIELDS -----
Call CIMPSC(H1,H,E1,MAXI1,EZ_FUNC,EZ_ITEMP)
Call CIMPSC(H1,H,E1,MAXI1,HF_FUNC,HFI_ITEMP)
Call CIMPSC(H1,H,E1,MAXI1,ER_FUNC,ER_ITEMP)
Call CIMPSC(H1,H,E1,MAXI1,HF_FUNCZEROZ,HFI_ITEMPZO)
C ADDING COORAY -----
Call CIMPSC(H0,H,E1,MAXI1,EZ_FUNC_S0,EZ_ITEMP_S0)
Call CIMPSC(H0,H,E1,MAXI1,HF_FUNC_S0,HFI_ITEMP_S0)
C -----
EZ_PTEMP = CURSPEC(I)*EZ_ITEMP/(4.*PI*EPS)
HFI_PTEMP = CURSPEC(I)*HFI_ITEMP/(4.*PI)
ER_PTEMP = CURSPEC(I)*ER_ITEMP/(4.*PI*EPS)
HFI_PTEMPZO = CURSPEC(I)*HFI_ITEMPZO/(4.*PI)
C WAVE TILT EXPRESSION -----
WT = CV*XMU/CSQRT(EPSR+SG/(CJ*W*EPS))
ER_RTEMP = ER_PTEMP-HFI_PTEMPZO*WT
C COMPUTING THE FIELD ON AND UNDER THE GROUND ACCORDING TO COORAY -----
EZ_RTEMP_S0 = CURSPEC(I)*EZ_ITEMP_S0/(4.*PI*EPS)
HFI_RTEMP_S0 = CURSPEC(I)*HFI_ITEMP_S0/(4.*PI)
ER_RTEMP_S0 = CV*HFI_RTEMP_S0*XMU*GAMA0/GAMA
EZ_RTEMP_Sx = EZ_RTEMP_S0*CEXP(-GAMA*Sx)*EPS/
1 (SG+CJ*W*EPS*EPSR)
  HFI_RTEMP_Sx = HFI_RTEMP_S0*CEXP(-GAMA*Sx)
  ER_RTEMP_Sx = ER_RTEMP_S0*CEXP(-GAMA*Sx)
C -----
End If
C -----
Write (1,5000) F, EZ_PTEMP
Write (2,5000) F, HFI_PTEMP
Write (3,5000) F, ER_RTEMP
C ADDING COORAY -----
Write (7,5000) F, EZ_RTEMP_S0
Write (8,5000) F, HFI_RTEMP_S0
Write (9,5000) F, ER_RTEMP_S0
Write (10,5000) F, EZ_RTEMP_Sx
Write (11,5000) F, HFI_RTEMP_Sx
Write (12,5000) F, ER_RTEMP_Sx
C -----
EZ_PERSPEC(I) = EZ_PTEMP
HFI_PERSPEC(I) = HFI_PTEMP
ER_PERSPEC(I) = ER_PTEMP
ER_REALSPEC(I) = ER_RTEMP
C ADDING COORAY -----
EZ_RSPEC_S0(I) = EZ_RTEMP_S0
HFI_RSPEC_S0(I) = HFI_RTEMP_S0
ER_RSPEC_S0(I) = ER_RTEMP_S0
EZ_RSPEC_Sx(I) = EZ_RTEMP_Sx
HFI_RSPEC_Sx(I) = HFI_RTEMP_Sx
ER_RSPEC_Sx(I) = ER_RTEMP_Sx
C -----
40 Continue
Close (1)
Close (2)
Close (3)
C ADDING COORAY -----
Close (7)
Close (8)
Close (9)
Close (10)
Close (11)
Close (12)
* -----
C FILL COMPLEX CONJUGATE PARTS OF THE SPECTRA
* -----
NN = N2 + 2
Do 50 I = NN, NP
  J = NP + 2 - I
  EZ_PERSPEC(I) = CONJG(EZ_PERSPEC(J))

```

```

HFI_PERSPEC(I) = CONJG(HFI_PERSPEC(J))
ER_REALSPEC(I) = CONJG(ER_REALSPEC(J))
C ADDING COORAY -----
EZ_RSPEC_S0(I) = CONJG(EZ_RSPEC_S0(J))
HFI_RSPEC_S0(I) = CONJG(HFI_RSPEC_S0(J))
ER_RSPEC_S0(I) = CONJG(ER_RSPEC_S0(J))
EZ_RSPEC_Sx(I) = CONJG(EZ_RSPEC_Sx(J))
HFI_RSPEC_Sx(I) = CONJG(HFI_RSPEC_Sx(J))
ER_RSPEC_Sx(I) = CONJG(ER_RSPEC_Sx(J))
C -----
50 Continue
EZ_PERSPEC(N2+1) = CMPLX(REAL(EZ_PERSPEC(N2)),0.D0)
HFI_PERSPEC(N2+1) = CMPLX(REAL(HFI_PERSPEC(N2)),0.D0)
ER_REALSPEC(N2+1) = CMPLX(REAL(ER_REALSPEC(N2)),0.D0)
C ADDING COORAY -----
EZ_RSPEC_S0(N2+1) = CMPLX(REAL(EZ_RSPEC_S0(N2)),0.D0)
HFI_RSPEC_S0(N2+1) = CMPLX(REAL(HFI_RSPEC_S0(N2)),0.D0)
ER_RSPEC_S0(N2+1) = CMPLX(REAL(ER_RSPEC_S0(N2)),0.D0)
EZ_RSPEC_Sx(N2+1) = CMPLX(REAL(EZ_RSPEC_Sx(N2)),0.D0)
HFI_RSPEC_Sx(N2+1) = CMPLX(REAL(HFI_RSPEC_Sx(N2)),0.D0)
ER_RSPEC_Sx(N2+1) = CMPLX(REAL(ER_RSPEC_Sx(N2)),0.D0)
* -----
C TRANSFORM FIELDS INTO TIME DOMAIN
* -----
IFS = 2
Call FORT(EZ_PERSPEC,DT,DF,M,S,IFS,IFERR)
Call FORT(HFI_PERSPEC,DT,DF,M,S,IFS,IFERR)
Call FORT(ER_REALSPEC,DT,DF,M,S,IFS,IFERR)
C ADDING COORAY -----
Call FORT(EZ_RSPEC_S0,DT,DF,M,S,IFS,IFERR)
Call FORT(HFI_RSPEC_S0,DT,DF,M,S,IFS,IFERR)
Call FORT(ER_RSPEC_S0,DT,DF,M,S,IFS,IFERR)
Call FORT(EZ_RSPEC_Sx,DT,DF,M,S,IFS,IFERR)
Call FORT(HFI_RSPEC_Sx,DT,DF,M,S,IFS,IFERR)
Call FORT(ER_RSPEC_Sx,DT,DF,M,S,IFS,IFERR)
C OUTPUT THE TRANSIENT FIELDS -----
Open (1,File='EZ_PERT.TIM')
Open (2,File='HFI_PERT.TIM')
Open (3,File='ER_REALT.TIM')
C ADDING COORAY -----
Open (7,File='EZ_RS0T.TIM')
Open (8,File='HFI_RS0T.TIM')
Open (9,File='ER_RS0T.TIM')
Open (10,File='EZ_RSxT.TIM')
Open (11,File='HFI_RSxT.TIM')
Open (12,File='ER_RSxT.TIM')
C -----
Write (1,*) 'TIME DOMAIN VERTICAL ELECTRIC FIELD AT HIGHT ', XZ,
1      ', m AND DISTANCE ', XR, ' m IS:'
Write (2,*) 'TIME DOMAIN HORIZONTAL MAGNETIC FIELD AT HIGHT ', XZ,
1      ', m AND DISTANCE ', XR, ' m IS:'
Write (3,*) 'TIME DOMAIN HORIZONTAL ELECTRIC FIELD AT HIGHT ', XZ,
1      ', m AND DISTANCE ', XR, ' m IS:'
C ADDING COORAY -----
Write (7,*) 'TIME DOMAIN VERTICAL ELECTRIC FIELD AT
1      ', ' THE GROUND LEVEL AND DISTANCE ', XR, ' m FROM'
2      ', ' THE LIGHTNING CHANNEL ACCORDING COORAY IS:'
Write (8,*) 'TIME DOMAIN HORIZONTAL MAGNETIG FIELD AT
1      ', ' THE GROUND LEVEL AND DISTANCE ', XR, ' m FROM'
2      ', ' THE LIGHTNING CHANNEL ACCORDING COORAY IS:'
Write (9,*) 'TIME DOMAIN HORIZONTAL ELECTRIC FIELD AT
1      ', ' THE GROUND LEVEL AND DISTANCE ', XR, ' m FROM'
2      ', ' THE LIGHTNING CHANNEL ACCORDING COORAY IS:'
Write (10,*) 'TIME DOMAIN VERTICAL ELECTRIC FIELD ', Sx
1      ', m UNDER THE GROUND AND DISTANCE ', XR, ' m FROM'
2      ', ' THE LIGHTNING CHANNEL ACCORDING COORAY IS:'
Write (11,*) 'TIME DOMAIN HORIZONTAL MAGNETIG FIELD ', Sx
1      ', m UNDER THE GROUND AND DISTANCE ', XR, ' m FROM'
2      ', ' THE LIGHTNING CHANNEL ACCORDING COORAY IS:'
Write (12,*) 'TIME DOMAIN HORIZONTAL ELECTRIC FIELD ', Sx
1      ', m UNDER THE GROUND AND DISTANCE ', XR, ' m FROM'
2      ', ' THE LIGHTNING CHANNEL ACCORDING COORAY IS:'
C -----
Do 60 I = 1, NP / 4
T = DT * (I-1)
Write (1,5000) T, REAL(EZ_PERSPEC(I))
Write (2,5000) T, REAL(HFI_PERSPEC(I))
Write (3,5000) T, REAL(ER_REALSPEC(I))
C ADDING COORAY -----
Write (7,5000) T, REAL(EZ_RSPEC_S0(I))
Write (8,5000) T, REAL(HFI_RSPEC_S0(I))
Write (9,5000) T, REAL(ER_RSPEC_S0(I))
Write (10,5000) T, REAL(EZ_RSPEC_Sx(I))
Write (11,5000) T, REAL(HFI_RSPEC_Sx(I))
Write (12,5000) T, REAL(ER_RSPEC_Sx(I))
C -----

```

```

60 Continue
  Close (1)
  Close (2)
  Close (3)
C ADDING COORAY -----
  Close (7)
  Close (8)
  Close (9)
  Close (10)
  Close (11)
  Close (12)
C -----
C THIS IS THE END OF THE PROGRAMM
C -----
  Call GETTIM(IHR,IMIN,ISEC,I100TH)
  TIM2 = 60. * (60.*IHR+IMIN) + ISEC + I100TH / 100.
  TT = TIM2 - TIM1
  TT = TT / 60.
  Write (*,*) 'TOTAL COMPUTATION TIME =', TT, ' Min.'
  Stop
5000 Format (3E14.5)
5100 Format ('+',Percentage complete --> ',F5.1)
  End
C
C
C -----
C FROM HERE BEGIN THE SUBROUTINES
C -----
C
C
C*****
  Subroutine LIGHTCUR(NP,TMAX,CUR)
C
C SUBROUTINE TO COMPUTE THE TRANSIENT LIGHTNING CHANNEL RETURN CURRENT
C AT THE BASE
C
C*****
C
  IMPLICIT DOUBLE PRECISION (A-H, O-Z)
  REAL TMAX
C
  Common /CURPARM/ CI01, CI02, T11, T21, T12, T22, NN1, NN2
  Dimension CUR(*)
* -----
  DT = TMAX / (NP-1)
  N2 = NP / 2
  Do 10 I = 1, N2
    T = DT * (I-1)
    Call WVFORM(T,CI01,T11,T21,NN1,F1)
    Call WVFORM(T,CI02,T12,T22,NN2,F2)
    CUR(I) = F1 + F2
    If (I.GT.N2/2) CUR(I) = 0.D0
    CUR(N2+I) = -CUR(I)
  10 Continue

  Return
  End
C
C*****
C
C
  Subroutine WVFORM(T,CI0,T1,T2,N,TT)
C
C FUNCTION TO DEFINE THE CHANNEL WAVEFORM COMPONENT
C
C*****
C
  IMPLICIT DOUBLE PRECISION (A-H, O-Z)
C
  TT = 0.D0
  ETA = DEXP(-(T1/T2)*(N*T2/T1))*(1./FLOAT(N))
  TT = CI0 / ETA * ((T/T1)**N) / (1+(T/T1)**N)
  TT = TT * DEXP(-T/T2)

  Return
  End
C
C
C
C*****
C
  Subroutine CIMPSC(A,B,E,MAXI,XINTG,XIP)
C
C NUMERICAL INTEGRATION ROUTINE - FOR A COMPLEX FUNCTION
C
C Originally XINTG is assumed to be a function,

```

```

C Here it is redesigned to be a subroutine
C Also here all variables are of type DOUBLE PRECISION or COMPLEX*16
C
C*****
C
C IMPLICIT DOUBLE PRECISION (A-H, O-Z)
C
C Complex FAFB, XIP, XJ, FNEWX, XI, S, XINTG
C
C COMPLEX*16 FAFB, XIP, XJ, FNEWX, XI, S, ZA, ZB, ZNEW
C-----
C INTERFACE
C SUBROUTINE XINTG(Z,FZ)
C DOUBLE PRECISION, INTENT(IN) :: Z
C COMPLEX*16, INTENT(OUT) :: FZ
C END SUBROUTINE XINTG
C END INTERFACE
C
C-----
C FAFB = XINTG(A) + XINTG(B)
C
C CALL XINTG(A,ZA)
C CALL XINTG(B,ZB)
C FAFB = ZA + ZB
C-----
C
C XH = B - A
C XIR = XH * .5
C XJ = XIR * FAFB
C XNEW = A + XIR
C XHA = XIR / 3.
C INDEX = 0
C-----
C 10 FNEWX = XINTG(XNEW)
C-----
C 10 CALL XINTG(XNEW,ZNEW)
C FNEWX = ZNEW
C-----
C
C If (INDEX.GT.0) Go To 40
C INDEX = 1
C XI = XHA * (FAFB+FNEWX*4.)
C 20 XJ = (XJ+XI*3.) * .25
C INDEX = INDEX + 1
C If (INDEX.GT.MAXI) Then
C Write (*,*) 'CAUTION, CIMPS NOT CONVERGED!'
C Go To 50
C End If
C XH = XH * .5
C XNEW = A + XH * .5
C S = (0.D0,0.D0)
C 30 If (XNEW.LT.B) Go To 10
C XIP = (XJ+XH*2.*S) / 3.
C If (CABS(XIP-XI).LT.CABS(E*XIP)) Go To 30
C THE ABOVE CONDITION IS REPLACED BY THE FOLLOWING:
C COND1 = DSQRT((REAL(XIP-XI))**2+(AIMAG(XIP-XI))**2)
C COND2 = DSQRT((REAL(E*XIP))**2+(AIMAG(E*XIP))**2)
C If (COND1.LT.COND2) Go To 50
C XI = XIP
C Go To 20
C 40 S = S + FNEWX
C XNEW = XNEW + XH
C Go To 30
C 50 Return
C End
C
C
C
C*****
C
C Subroutine EZ_FUNC(ZPRIM,FEZ)
C
C FUNCTION TO DEFINE E_Z FIELD
C
C*****
C
C
C IMPLICIT DOUBLE PRECISION (A-H, O-Z)
C
C *
C DOUBLE PRECISION ZPRIM
C REAL W, PI, CV, EPS, XMU
C COMPLEX*16 FEZ, F1, F3
C COMPLEX CJ
C
C *
C Common /PCONS/ PI, CV, EPS, XMU, CJ
C Common /CHANNEL/ HT, CHVEL, XLAM, H, XZ, XR, W
C

```

```

C-----
C
C   ZZ = DABS(ZPRIM)
C   ZS = XZ-ZPRIM
C   R0 = DSQRT(XR**2+ZS**2)
C-----
C   F1 = (2*ZS**2-XR**2)/(CJ*W*R0**5)
C   F2 = (2*ZS**2-XR**2)/(CV*R0**4)
C   F3 = (CJ*W*XR**2)/(CV**2*R0**3)
C-----
C   FEZ = DEXP(-ZZ/XLAM)*CEXP(-CJ*W*ZZ/CHVEL)*CEXP(-CJ*W*R0/CV)*
C   1   (F1+F2-F3)
C   THE ABOVE EXPRESSION IS REPLACED BY:
C   FEZ = DEXP(-ZZ/XLAM)*(DCOS(W*ZZ/CHVEL)-CJ*DSIN(W*ZZ/CHVEL))*
C   1   (DCOS(W*R0/CV)-CJ*DSIN(W*R0/CV))*(F1+F2-F3)
C-----
C   Return
C   End
C
C
C
C*****
C
C
C   Subroutine HF_FUNC(ZPRIM,FHF)
C
C FUNCTION TO DEFINE H_FI FIELD
C
C*****
C
C
C   IMPLICIT DOUBLE PRECISION (A-H, O-Z)
*
*   DOUBLE PRECISION ZPRIM
*   REAL           W, PI, CV, EPS, XMU
*   COMPLEX*16     FHF, F2
*   COMPLEX        CJ
*
*   Common /PCONS/  PI, CV, EPS, XMU, CJ
*   Common /CHANNEL/ HT, CHVEL, XLAM, H, XZ, XR, W
C-----
C
C   ZZ = DABS(ZPRIM)
C   ZS = XZ-ZPRIM
C   R0 = DSQRT(XR**2+ZS**2)
C-----
C   F1 = XR/R0**3
C   F2 = (CJ*W*XR)/(CV*R0**2)
C-----
C   FEZ = DEXP(-ZZ/XLAM)*CEXP(-CJ*W*ZZ/CHVEL)*CEXP(-CJ*W*R0/CV)*
C   1   (F1+F2)
C   THE ABOVE EXPRESSION IS REPLACED BY:
C   FHF = DEXP(-ZZ/XLAM)*(DCOS(W*ZZ/CHVEL)-CJ*DSIN(W*ZZ/CHVEL))*
C   1   (DCOS(W*R0/CV)-CJ*DSIN(W*R0/CV))*(F1+F2)
C-----
C   Return
C   End
C
C
C
C*****
C
C
C   Subroutine HF_FUNCZEROZ(ZPRIM,FHF)
C
C FUNCTION TO DEFINE H_FI FIELD AT THE GROUND WHERE Z=0
C
C*****
C
C
C   IMPLICIT DOUBLE PRECISION (A-H, O-Z)
*
*   DOUBLE PRECISION ZPRIM
*   REAL           W, PI, CV, EPS, XMU
*   COMPLEX*16     FHF, F2
*   COMPLEX        CJ
*
*   Common /PCONS/  PI, CV, EPS, XMU, CJ
*   Common /CHANNEL/ HT, CHVEL, XLAM, H, XZ, XR, W
C-----
C
C   ZZ = DABS(ZPRIM)
C   ZS = XZ-ZPRIM
C   ZS = ZPRIM

```

```

R0 = DSQRT(XR**2+ZS**2)
C -----
C F1 = XR/R0**3
C F2 = (CJ*W*XR)/(CV*R0**2)
C -----
C FEZ = DEXP(-ZZ/XLAM)*CEXP(-CJ*W*ZZ/CHVEL)*CEXP(-CJ*W*R0/CV)*
C 1 (F1+F2)
C THE ABOVE EXPRESSION IS REPLACED BY:
C FHF = DEXP(-ZZ/XLAM)*(DCOS(W*ZZ/CHVEL)-CJ*DSIN(W*ZZ/CHVEL))*
C 1 (DCOS(W*R0/CV)-CJ*DSIN(W*R0/CV))*(F1+F2)
C -----
C Return
C End
C
C
C
C*****
C
C Subroutine ER_FUNC(ZPRIM,FER)
C
C FUNCTION TO DEFINE E_R FIELD - GROUND PERFEC CONDUCTOR
C
C*****
C
C
C IMPLICIT DOUBLE PRECISION (A-H, O-Z)
*
DOUBLE PRECISION ZPRIM
REAL W, PI, CV, EPS, XMU
COMPLEX*16 FER, F1, F3
COMPLEX CJ
*
Common /PCONS/ PI, CV, EPS, XMU, CJ
Common /CHANNEL/ HT, CHVEL, XLAM, H, XZ, XR, W
C
C -----
C
C ZZ = DABS(ZPRIM)
C ZS = XZ-ZPRIM
C R0 = DSQRT(XR**2+ZS**2)
C -----
C F1 = (3*XR*ZS)/(CJ*W*R0**5)
C F2 = (3*XR*ZS)/(CV*R0**4)
C F3 = (CJ*W*XR*ZS)/(CV**2*R0**3)
C -----
C FEZ = DEXP(-ZZ/XLAM)*CEXP(-CJ*W*ZZ/CHVEL)*CEXP(-CJ*W*R0/CV)*
C 1 (F1+F2+F3)
C THE ABOVE EXPRESSION IS REPLACED BY:
C FER = DEXP(-ZZ/XLAM)*(DCOS(W*ZZ/CHVEL)-CJ*DSIN(W*ZZ/CHVEL))*
C 1 (DCOS(W*R0/CV)-CJ*DSIN(W*R0/CV))*(F1+F2+F3)
C -----
C Return
C End
C
C
C
C -----
C From here begin formulas for the function under the integral
C for the field under the ground
C -----
C
C
C
C*****
C
C Subroutine EZ_FUNC_S0(ZPRIM,FEZ)
C
C FUNCTION TO DEFINE E_Z FIELD ON THE GROUND ACCORDING COORAY'S FORMULA
C
C*****
C
C
C IMPLICIT DOUBLE PRECISION (A-H, O-Z)
*
DOUBLE PRECISION ZPRIM
REAL W, PI, CV, EPS, XMU, EPSR, SG,
C 1 SIN_TITA, COS_TITA, R04
COMPLEX*16 FEZ, F_SOM, JWS016, F_JWS016, F1, F2
COMPLEX CJ, GAMA0, GAMA, DELTA, GE, WS0, JWS0
*
*
*
Common /PCONS/ PI, CV, EPS, XMU, CJ
Common /CHANNEL/ HT, CHVEL, XLAM, H, XZ, XR, W

```

```

Common /EARTH/  EPSR, SG
Common /UNDERGR/  GAMA0, GAMA
C
C-----
C
ZZ = DABS(ZPRIM)
C  ZS = XZ-ZPRIM
R0 = DSQRT(XR**2+ZPRIM**2)
R04 = SNGL(R0)
SIN_TITA8 = ZPRIM/R0
COS_TITA8 = XR/R0
SIN_TITA = SNGL(SIN_TITA8)
COS_TITA = SNGL(COS_TITA8)
DELTA = (GAMA0/GAMA)*CSQRT(1-(GAMA0/GAMA)**2*COS_TITA**2)
GE = (SIN_TITA-DELTA)/(SIN_TITA+DELTA)
C-----
WS0 = -(GAMA0*R04/2)*(SIN_TITA+DELTA)**2
JWS0 = CJ*CSQRT(WS0)
JWS016 = JWS0
Call ERFCC(JWS016,F_JWS016)
F_SOM = 1-CJ*CSQRT(PI*WS0)*CEXP(-WS0)*F_JWS016
C-----
F1 = CJ*W*COS_TITA**2/(CV**2*R0)
F2 = (1+GE) + (1-GE)*F_SOM
C-----
C  FEZ = DEXP(-ZZ/XLAM)*CEXP(-CJ*W*ZZ/CHVEL)*CEXP(-CJ*W*R0/CV)*
C  1  (F1+F2-F3)
C  THE ABOVE EXPRESSION IS REPLACED BY:
FEZ = DEXP(-ZZ/XLAM)*(DCOS(W*ZZ/CHVEL)-CJ*DSIN(W*ZZ/CHVEL))*
1  (DCOS(W*R0/CV)-CJ*DSIN(W*R0/CV))*F1*F2
C-----
Return
End
C
C
C
C*****
C
C
C  Subroutine HF_FUNC_S0(ZPRIM,FHF)
C
C FUNCTION TO DEFINE H_FI FIELD ON THE GROUND ACCORDING COORAY'S FORMULA
C
C*****
C
C
C  IMPLICIT DOUBLE PRECISION (A-H, O-Z)
*
DOUBLE PRECISION ZPRIM
REAL W, PI, CV, EPS, XMU, EPSR, SG,
1 SIN_TITA, COS_TITA, R04
COMPLEX*16 FHF, F_SOM, JWS016, F_JWS016, F1, F2
COMPLEX CJ, GAMA0, GAMA, DELTA, GE, WS0, JWS0
*
*
*
Common /PCONS/  PI, CV, EPS, XMU, CJ
Common /CHANNEL/  HT, CHVEL, XLAM, H, XZ, XR, W
Common /EARTH/  EPSR, SG
Common /UNDERGR/  GAMA0, GAMA
C
C-----
C
ZZ = DABS(ZPRIM)
C  ZS = XZ-ZPRIM
R0 = DSQRT(XR**2+ZPRIM**2)
R04 = SNGL(R0)
SIN_TITA8 = ZPRIM/R0
COS_TITA8 = XR/R0
SIN_TITA = SNGL(SIN_TITA8)
COS_TITA = SNGL(COS_TITA8)
DELTA = (GAMA0/GAMA)*CSQRT(1-(GAMA0/GAMA)**2*COS_TITA**2)
GE = (SIN_TITA-DELTA)/(SIN_TITA+DELTA)
C-----
WS0 = -(GAMA0*R04/2)*(SIN_TITA+DELTA)**2
JWS0 = CJ*CSQRT(WS0)
JWS016 = JWS0
Call ERFCC(JWS016,F_JWS016)
F_SOM = 1-CJ*CSQRT(PI*WS0)*CEXP(-WS0)*F_JWS016
C-----
F1 = CJ*W*COS_TITA/(CV*R0)
F2 = (1+GE) + (1-GE)*F_SOM
C-----
C  FEZ = DEXP(-ZZ/XLAM)*CEXP(-CJ*W*ZZ/CHVEL)*CEXP(-CJ*W*R0/CV)*
C  1  (F1+F2-F3)
C  THE ABOVE EXPRESSION IS REPLACED BY:

```

```

FHF = DEXP(-ZZ/XLAM)*(DCOS(W*ZZ/CHVEL)-CJ*DSIN(W*ZZ/CHVEL))*
1 (DCOS(W*R0/CV)-CJ*DSIN(W*R0/CV))*F1*F2
-----
C
C Return
C End
C
C
C
C-----
C
C
C COMPLEMENTARY ERROR FUNCTION OF A COMPLEX ARGUMENT
C
C-----
C
C Last change: VDV 29 Oct 2001 9:28 pm
C *****
C Subroutine for computing complementary error function of a complex argument
C ZI - INPUT COMPLEX NUMBER
C WZC - COMPUTED OUPUT RESULT
C ALL NUMERICAL VARIABLES ARE DOUBLE PRECISION
C *****
C SUBROUTINE ERFCC(ZI, WZC)
C USES WOFZ SUBROUTINE
C COMPLEX*16 ZI, WZC, WZ, CJ
C DOUBLE PRECISION XP, YP, WU, WV
C LOGICAL FLAG
*
C CJ = CMPLX(0.D0,1.D0)
C XP = REAL(ZI)
C YP = AIMAG(ZI)
*
C CALL WOFZ(YP,XP,WU,WV,FLAG)
C WZ = CMPLX(WU,-WV)
*
C WZC = DEXP(YP**2-XP**2)*(DCOS(2*XP*YP)-CJ*DSIN(2*XP*YP)) * WZ
*
C RETURN
C END
C
C-----
C
C ALGORITHM 680, COLLECTED ALGORITHMS FROM ACM.
C THIS WORK PUBLISHED IN TRANSACTIONS ON MATHEMATICAL SOFTWARE,
C VOL. 16, NO. 1, PP. 47.
C SUBROUTINE WOFZ(XI, YI, U, V, FLAG)
C
C GIVEN A COMPLEX NUMBER Z = (XI,YI), THIS SUBROUTINE COMPUTES
C THE VALUE OF THE FADDEEVA-FUNCTION W(Z) = EXP(-Z**2)*ERFC(-I*Z),
C WHERE ERFC IS THE COMPLEX COMPLEMENTARY ERROR-FUNCTION AND I
C MEANS SQRT(-1).
C THE ACCURACY OF THE ALGORITHM FOR Z IN THE 1ST AND 2ND QUADRANT
C IS 14 SIGNIFICANT DIGITS; IN THE 3RD AND 4TH IT IS 13 SIGNIFICANT
C DIGITS OUTSIDE A CIRCULAR REGION WITH RADIUS 0.126 AROUND A ZERO
C OF THE FUNCTION.
C ALL REAL VARIABLES IN THE PROGRAM ARE DOUBLE PRECISION.
C
C
C THE CODE CONTAINS A FEW COMPILER-DEPENDENT PARAMETERS :
C RMAXREAL = THE MAXIMUM VALUE OF RMAXREAL EQUALS THE ROOT OF
C RMAX = THE LARGEST NUMBER WHICH CAN STILL BE
C IMPLEMENTED ON THE COMPUTER IN DOUBLE PRECISION
C FLOATING-POINT ARITHMETIC
C RMAXEXP = LN(RMAX) - LN(2)
C RMAXGONI = THE LARGEST POSSIBLE ARGUMENT OF A DOUBLE PRECISION
C GONIOMETRIC FUNCTION (DCOS, DSIN, ...)
C THE REASON WHY THESE PARAMETERS ARE NEEDED AS THEY ARE DEFINED WILL
C BE EXPLAINED IN THE CODE BY MEANS OF COMMENTS
C
C
C PARAMETER LIST
C XI = REAL PART OF Z
C YI = IMAGINARY PART OF Z
C U = REAL PART OF W(Z)
C V = IMAGINARY PART OF W(Z)
C FLAG = AN ERROR FLAG INDICATING WHETHER OVERFLOW WILL
C OCCUR OR NOT; TYPE LOGICAL;
C THE VALUES OF THIS VARIABLE HAVE THE FOLLOWING
C MEANING :
C FLAG=.FALSE. : NO ERROR CONDITION
C FLAG=.TRUE. : OVERFLOW WILL OCCUR, THE ROUTINE
C BECOMES INACTIVE
C XI, YI ARE THE INPUT-PARAMETERS
C U, V, FLAG ARE THE OUTPUT-PARAMETERS
C
C FURTHERMORE THE PARAMETER FACTOR EQUALS 2/SQRT(PI)
C

```



```

C THE ROUTINE IS NOT UNDERFLOW-PROTECTED BUT ANY VARIABLE CAN BE
C PUT TO 0 UPON UNDERFLOW;
C
C REFERENCE - GPM POPPE, CMJ WIJERS; MORE EFFICIENT COMPUTATION OF
C THE COMPLEX ERROR-FUNCTION, ACM TRANS. MATH. SOFTWARE.
C
*
*
*
* IMPLICIT DOUBLE PRECISION (A-H, O-Z)
*
LOGICAL A, B, FLAG
PARAMETER (FACTOR = 1.12837916709551257388D0,
* RMAXREAL = 0.5D+154,
* RMAXEXP = 708.503061461606D0,
* RMAXGONI = 3.53711887601422D+15)
*
FLAG = .FALSE.
*
XABS = DABS(XI)
YABS = DABS(YI)
X = XABS/6.3
Y = YABS/4.4
*
C
C THE FOLLOWING IF-STATEMENT PROTECTS
C QRHO = (X**2 + Y**2) AGAINST OVERFLOW
C
IF ((XABS.GT.RMAXREAL).OR.(YABS.GT.RMAXREAL)) GOTO 100
*
QRHO = X**2 + Y**2
*
XABSQ = XABS**2
XQUAD = XABSQ - YABS**2
YQUAD = 2*XABS*YABS
*
A = QRHO.LT.0.085264D0
*
IF (A) THEN
C
C IF (QRHO.LT.0.085264D0) THEN THE FADDEEVA-FUNCTION IS EVALUATED
C USING A POWER-SERIES (ABRAMOWITZ/STEGUN, EQUATION (7.1.5), P.297)
C N IS THE MINIMUM NUMBER OF TERMS NEEDED TO OBTAIN THE REQUIRED
C ACCURACY
C
QRHO = (1-0.85*Y)*DSQRT(QRHO)
N = IDNINT(6 + 72*QRHO)
J = 2*N+1
XSUM = 1.0/J
YSUM = 0.0D0
DO 10 I=N, 1, -1
J = J - 2
XAUX = (XSUM*XQUAD - YSUM*YQUAD)/I
YSUM = (XSUM*YQUAD + YSUM*XQUAD)/I
XSUM = XAUX + 1.0/J
10 CONTINUE
U1 = -FACTOR*(XSUM*YABS + YSUM*XABS) + 1.0
V1 = FACTOR*(XSUM*XABS - YSUM*YABS)
DAUX = DEXP(-XQUAD)
U2 = DAUX*DCOS(YQUAD)
V2 = -DAUX*DSIN(YQUAD)
*
U = U1*U2 - V1*V2
V = U1*V2 + V1*U2
*
ELSE
C
C IF (QRHO.GT.1.0) THEN W(Z) IS EVALUATED USING THE LAPLACE
C CONTINUED FRACTION
C NU IS THE MINIMUM NUMBER OF TERMS NEEDED TO OBTAIN THE REQUIRED
C ACCURACY
C
C IF ((QRHO.GT.0.085264D0).AND.(QRHO.LT.1.0)) THEN W(Z) IS EVALUATED
C BY A TRUNCATED TAYLOR EXPANSION, WHERE THE LAPLACE CONTINUED FRACTION
C IS USED TO CALCULATE THE DERIVATIVES OF W(Z)
C KAPN IS THE MINIMUM NUMBER OF TERMS IN THE TAYLOR EXPANSION NEEDED
C TO OBTAIN THE REQUIRED ACCURACY
C NU IS THE MINIMUM NUMBER OF TERMS OF THE CONTINUED FRACTION NEEDED
C TO CALCULATE THE DERIVATIVES WITH THE REQUIRED ACCURACY
C
IF (QRHO.GT.1.0) THEN
H = 0.0D0
KAPN = 0
QRHO = DSQRT(QRHO)

```

```

    NU = IDINT(3 + (1442/(26*QRHO+77)))
ELSE
    QRHO = (1-Y)*DSQRT(1-QRHO)
    H = 1.88*QRHO
    H2 = 2*H
    KAPN = IDNINT(7 + 34*QRHO)
    NU = IDNINT(16 + 26*QRHO)
ENDIF
*
    B = (H.GT.0.0)
*
    IF (B) QLAMBDA = H2**KAPN
*
    RX = 0.0
    RY = 0.0
    SX = 0.0
    SY = 0.0
*
    DO 11 N=NU, 0, -1
    NP1 = N + 1
    TX = YABS + H + NP1*RX
    TY = XABS - NP1*RY
    C = 0.5/(TX**2 + TY**2)
    RX = C*TX
    RY = C*TY
    IF ((B).AND.(N.LE.KAPN)) THEN
    TX = QLAMBDA + SX
    SX = RX*TX - RY*SY
    SY = RY*TX + RX*SY
    QLAMBDA = QLAMBDA/H2
    ENDIF
11 CONTINUE
*
    IF (H.EQ.0.0) THEN
    U = FACTOR*RX
    V = FACTOR*RY
    ELSE
    U = FACTOR*SX
    V = FACTOR*SY
    END IF
*
    IF (YABS.EQ.0.0) U = DEXP(-XABS**2)
*
    END IF
*
*
C
C EVALUATION OF W(Z) IN THE OTHER QUADRANTS
C
*
    IF (YI.LT.0.0) THEN
*
    IF (A) THEN
    U2 = 2*U2
    V2 = 2*V2
    ELSE
    XQUAD = -XQUAD
    *
    C
    C THE FOLLOWING IF-STATEMENT PROTECTS 2*EXP(-Z**2)
    C AGAINST OVERFLOW
    C
    IF ((YQUAD.GT.RMAXGONI).OR.
    * (XQUAD.GT.RMAXEXP)) GOTO 100
*
    W1 = 2*DEXP(XQUAD)
    U2 = W1*DCOS(YQUAD)
    V2 = -W1*DSIN(YQUAD)
    END IF
*
    U = U2 - U
    V = V2 - V
    IF (XI.GT.0.0) V = -V
    ELSE
    IF (X1.LT.0.0) V = -V
    END IF
*
    RETURN
*
100 FLAG = .TRUE.
    RETURN
    END
*
-----
C
C
C

```

```

C
C
C Subroutine FORT(A,DT,DF,M,S,IFS,IFERR)
C-----
C
C SUBROUTINE TO PERFORM A FFT OPERATION ON A COMPLEX-VALUED
C VECTOR A(N) .
C
C INPUT DATA ...
C M = POWER OF 2 TO DEFINE # OF POINTS
C A(M) = NO OF COMPLEX VALUES TO BE TRANSFORMED
C DT = TIME INCREMENT OF DATA
C DF = FREQUENCY DOMAIN INCREMENT
C S(M) = DUMMY ARRAY DEFINED ONCE FOR A FIXED M AND USED IN
C SUBSEQUENT CALCULATIONS
C IFS = 0 TO DEFINE THE S ARRAY
C = -2 FOR TIME TO FREQUENCY TRANSFORM
C = 2 FOR FREQUENCY TO TIME TRANSFORM
C
C OUTPUT DATA ...
C A(M) = TRANSFORM OF INPUT ARRAY
C IFERR = 1 IF AN ERROR HAS OCCURRED
C-----
C
C Dimension A(1), S(1), K(14)
*
C DOUBLE PRECISION A
*
C Equivalence (K(13),K1), (K(12),K2), (K(11),K3), (K(10),K4)
C Equivalence (K(9),K5), (K(8),K6), (K(7),K7), (K(6),K8), (K(5),K9)
C Equivalence (K(4),K10), (K(3),K11), (K(2),K12), (K(1),K13), (
C * K(1),N2)
C If (M.GT.0) Then
C If (M.LE.13) Go To 30
C End If
10 IFERR = 1
20 Return
30 IFERR = 0
N = 2 ** M
C If (IABS(IFS).LE.1) Go To 330
C If (N.GT.NP) Then
C IFERR = 1
C Go To 330
C End If
40 K(1) = N + N
C Do 50 L = 2, M
C K(L) = K(L-1) / 2
50 Continue
C Do 60 L = M, 12
C K(L+1) = 2
60 Continue
IJ = 2
C Do 190 J1 = 2, K1, 2
C Do 180 J2 = J1, K2, K1
C Do 170 J3 = J2, K3, K2
C Do 160 J4 = J3, K4, K3
C Do 150 J5 = J4, K5, K4
C Do 140 J6 = J5, K6, K5
C Do 130 J7 = J6, K7, K6
C Do 120 J8 = J7, K8, K7
C Do 110 J9 = J8, K9, K8
C Do 100 J10 = J9, K10, K9
C Do 90 J11 = J10, K11, K10
C Do 80 J12 = J11, K12, K11
C Do 70 JI = J12, K13, K12
C If (I.L.T.JI) Then
C T = A(IJ-1)
C A(IJ-1) = A(JI-1)
C A(JI-1) = T
C T = A(IJ)
C A(IJ) = A(JI)
C A(JI) = T
C End If
C IJ = IJ + 2
70 Continue
80 Continue
90 Continue
100 Continue
110 Continue
120 Continue
130 Continue
140 Continue
150 Continue
160 Continue
170 Continue

```

```

180 Continue
190 Continue
  If (IFS) 200, 10, 220
200 FN = N
  Do 210 I = 1, N
    A(2*I-1) = A(2*I-1) / FN
    A(2*I) = -A(2*I) / FN
210 Continue
220 Do 230 I = 1, N, 2
  T = A(2*I-1)
  A(2*I-1) = T + A(2*I+1)
  A(2*I+1) = T - A(2*I+1)
  T = A(2*I)
  A(2*I) = T + A(2*I+2)
  A(2*I+2) = T - A(2*I+2)
230 Continue
  If (M-1) 10, 20, 240
240 LEXP1 = 2
  LEXP = 8
  NPL = 2 ** MT
  Do 280 L = 2, M
  Do 250 I = 2, N2, LEXP
    I1 = I + LEXP1
    I2 = I1 + LEXP1
    I3 = I2 + LEXP1
    T = A(I-1)
    A(I-1) = T + A(I2-1)
    A(I2-1) = T - A(I2-1)
    T = A(I)
    A(I) = T + A(I2)
    A(I2) = T - A(I2)
    T = -A(I3)
    TI = A(I3-1)
    A(I3-1) = A(I1-1) - T
    A(I3) = A(I1) - TI
    A(I1-1) = A(I1-1) + T
    A(I1) = A(I1) + TI
250 Continue
  If (L.GT.2) Then
    KLAST = N2 - LEXP
    JJ = NPL
    Do 270 J = 4, LEXP1, 2
      NPJJ = NT - JJ
      UR = S(NPJJ)
      UI = S(JJ)
      ILAST = J + KLAST
      Do 260 I = J, ILAST, LEXP
        I1 = I + LEXP1
        I2 = I1 + LEXP1
        I3 = I2 + LEXP1
        T = A(I2-1) * UR - A(I2) * UI
        TI = A(I2-1) * UI + A(I2) * UR
        A(I2-1) = A(I-1) - T
        A(I2) = A(I) - TI
        A(I-1) = A(I-1) + T
        A(I) = A(I) + TI
        T = -A(I3-1) * UI - A(I3) * UR
        TI = A(I3-1) * UR - A(I3) * UI
        A(I3-1) = A(I1-1) - T
        A(I3) = A(I1) - TI
        A(I1-1) = A(I1-1) + T
        A(I1) = A(I1) + TI
260 Continue
      JJ = JJ + NPL
270 Continue
    End If
    LEXP1 = LEXP1 + LEXP1
    LEXP = LEXP + LEXP
    NPL = NPL / 2
280 Continue
  If (IFS) 290, 10, 310
290 Do 300 I = 1, N
  A(2*I-1) = A(2*I-1) * FLOAT(N-1) * DT
  A(2*I) = -A(2*I) * FLOAT(N-1) * DT
300 Continue
  Go To 20
310 Do 320 I = 1, N
  A(2*I) = A(2*I) * DF
  A(2*I-1) = A(2*I-1) * DF
320 Continue
  Go To 20
C
C DEFINE S VECTOR
C
330 NP = N
  MP = M

```

```

NT = N / 4
MT = M - 2
If (MT.GT.0) Then
  THETA = .7853981634
  JSTEP = NT
  JDIF = NT / 2
  S(JDIF) = SIN(THETA)
  If (MT.GE.2) Then
    Do 350 L = 2, MT
      THETA = THETA * .5
      JSTEP2 = JSTEP
      JSTEP = JDIF
      JDIF = JDIF / 2
      S(JDIF) = SIN(THETA)
      JC1 = NT - JDIF
      S(JC1) = COS(THETA)
      JLAST = NT - JSTEP2
      If (JLAST.GE.JSTEP) Then
        Do 340 J = JSTEP, JLAST, JSTEP
          JC = NT - J
          JD = J + JDIF
          S(JD) = S(J) * S(JC1) + S(JDIF) * S(JC)
340      Continue
        End If
350      Continue
      End If
    End If
  End If
  If (IFS) 40, 20, 40
  End
C -----
C
C
C

```

LEMFIELD.DAT - “LEMField” input data file

0.001	5000.0	1.0		-Height of the observer - (m), distance from the lightning - (m) and depth below the ground - (m)
5.0	0.005			-Epsr and Sigma (S/m) of the earth
10	60.0			-Specification for the time and number of points for FFT
11.7	0.25	2.5	2	-Variables describing lightning channel at the base - first function
6.5	2.1	230.0	2	-Variables describing lightning channel at the base - second function
0.633333333333	2.0	7.0		-Characteristics of the lightning channel, km

DIM.DAT - “LEMFieDE_M” input data file

DIM.DAT									
First conductor					Second conductor				
$\alpha_r = \arccos(x_i/r_i)$					$\alpha_r = \arccos(x_i/r_i)$				
r_1 (m)	s_1 (m)	$\alpha_1(^{\circ})$	$\alpha_2(^{\circ})$	$\cos(\alpha_r)$	r_2 (m)	s_2 (m)	$\alpha_1(^{\circ})$	$\alpha_2(^{\circ})$	$\cos(\alpha_r)$
342.7802373	2.05	15.000	0.000	0.999999929	342.7791371	2.05	15.000	0.000	0.999999924
343.746358	2.05	15.000	0.000	0.999999362	343.7452608	2.05	15.000	0.000	0.999999349
344.7126718	2.05	15.000	0.000	0.999998238	344.7115778	2.05	15.000	0.000	0.999998216
345.6791773	2.05	15.000	0.000	0.999996566	345.6780863	2.05	15.000	0.000	0.999996535
346.6458728	2.05	15.000	0.000	0.999994356	346.6447849	2.05	15.000	0.000	0.999994316
347.6127567	2.05	15.000	0.000	0.999991615	347.6116718	2.05	15.000	0.000	0.999991567
348.5798275	2.05	15.000	0.000	0.999988354	348.5787456	2.05	15.000	0.000	0.999988297
349.5470836	2.05	15.000	0.000	0.99998458	349.5460047	2.05	15.000	0.000	0.999984515
350.5145235	2.05	15.000	0.000	0.999980303	350.5134475	2.05	15.000	0.000	0.99998023
351.4821456	2.05	15.000	0.000	0.999975531	351.4810726	2.05	15.000	0.000	0.999975449
352.4499485	2.05	15.000	0.000	0.999970273	352.4488785	2.05	15.000	0.000	0.999970183
353.4179306	2.05	15.000	0.000	0.999964536	353.4168635	2.05	15.000	0.000	0.999964438
354.3860906	2.05	15.000	0.000	0.999958329	354.3850264	2.05	15.000	0.000	0.999958222
355.3544269	2.05	15.000	0.000	0.999951659	355.3533656	2.05	15.000	0.000	0.999951545
356.1960067	2.05	45.000	0.000	0.999937666	356.1930303	2.05	45.000	0.000	0.99993757
356.9116493	2.05	45.000	0.000	0.999913875	356.9086789	2.05	45.000	0.000	0.999913763
357.628656	2.05	45.000	0.000	0.999886365	357.6256916	2.05	45.000	0.000	0.999886236
358.3470188	2.05	45.000	0.000	0.999855182	358.3440603	2.05	45.000	0.000	0.999855037
359.0667293	2.05	45.000	0.000	0.999820371	359.0637767	2.05	45.000	0.000	0.999820209
359.7877795	2.05	45.000	0.000	0.999781976	359.7848329	2.05	45.000	0.000	0.999781798
360.5101615	2.05	45.000	0.000	0.999740042	360.5072208	2.05	45.000	0.000	0.999739848
361.2338671	2.05	45.000	0.000	0.999694613	361.2309323	2.05	45.000	0.000	0.999694402
361.9588885	2.05	45.000	0.000	0.999645731	361.9559596	2.05	45.000	0.000	0.999645504
362.6852178	2.05	45.000	0.000	0.99959344	362.6822947	2.05	45.000	0.000	0.999593196
363.4128471	2.05	45.000	0.000	0.999537782	363.4099299	2.05	45.000	0.000	0.999537523
364.1417686	2.05	45.000	0.000	0.9994788	364.1388572	2.05	45.000	0.000	0.999478525
364.8719747	2.05	45.000	0.000	0.999416535	364.8690691	2.05	45.000	0.000	0.999416244
365.6034575	2.05	45.000	0.000	0.999351029	365.6005577	2.05	45.000	0.000	0.999350722
366.2362736	2.05	60.000	0.000	0.999273628	366.2326708	2.05	60.000	0.000	0.999273392
366.7698894	2.05	60.000	0.000	0.999183032	366.7662918	2.05	60.000	0.000	0.999182781
367.3054525	2.05	60.000	0.000	0.999087401	367.3018601	2.05	60.000	0.000	0.999087136
367.8429543	2.05	60.000	0.000	0.998986784	367.8393672	2.05	60.000	0.000	0.998986504
368.3823865	2.05	60.000	0.000	0.998881226	368.3788046	2.05	60.000	0.000	0.998880931
368.923151	2.082954091	60.000	3.779	0.998770897	368.9195743	2.082954091	60.000	3.779	0.998770587
369.465233	2.148862274	60.000	3.779	0.998655858	369.4616616	2.148862274	60.000	3.779	0.998655533
370.0092118	2.214770457	60.000	3.779	0.998536037	370.0056456	2.214770457	60.000	3.779	0.998535697
370.5550789	2.280678639	60.000	3.779	0.998411481	370.551518	2.280678639	60.000	3.779	0.998411126
371.1028261	2.346586822	60.000	3.779	0.998282233	371.0992705	2.346586822	60.000	3.779	0.998281863
371.652445	2.412495004	60.000	3.779	0.998148339	371.6488946	2.412495004	60.000	3.779	0.998147955
372.2039273	2.478403187	60.000	3.779	0.998009844	372.2003822	2.478403187	60.000	3.779	0.998009445
372.7572648	2.54431137	60.000	3.779	0.997866793	372.753725	2.54431137	60.000	3.779	0.997866379
373.3124493	2.610219552	60.000	3.779	0.997719229	373.3089147	2.610219552	60.000	3.779	0.9977188

APPENDIX I “LEMF_{FIELD}E” SOURCE CODE AND INPUT DATA FILES

373.8694724	2.676127735	60.000	3.779	0.997567198	373.865943	2.676127735	60.000	3.779	0.997566754
374.4283259	2.742035917	60.000	3.779	0.997410743	374.4248019	2.742035917	60.000	3.779	0.997410285
374.9890018	2.8079441	60.000	3.779	0.997249908	374.985483	2.8079441	60.000	3.779	0.997249435
375.5514918	2.873852283	60.000	3.779	0.997084737	375.5479783	2.873852283	60.000	3.779	0.997084249
376.1157878	2.939760465	60.000	3.779	0.996915273	376.1122796	2.939760465	60.000	3.779	0.99691477
376.6818817	3.005668648	60.000	3.779	0.99674156	376.6783787	3.005668648	60.000	3.779	0.996741042
377.2497653	3.071576831	60.000	3.779	0.996563639	377.2462676	3.071576831	60.000	3.779	0.996563107
377.8194307	3.137485013	60.000	3.779	0.996381555	377.8159383	3.137485013	60.000	3.779	0.996381008
378.3908697	3.203393196	60.000	3.779	0.99619535	378.3873826	3.203393196	60.000	3.779	0.996194787
378.9640744	3.269301378	60.000	3.779	0.996005065	378.9605926	3.269301378	60.000	3.779	0.996004488
379.5390367	3.335209561	60.000	3.779	0.995810744	379.5355602	3.335209561	60.000	3.779	0.995810152
380.1157487	3.401117744	60.000	3.779	0.995612428	380.1122774	3.401117744	60.000	3.779	0.995611821
380.6942024	3.467025926	60.000	3.779	0.995410158	380.6907364	3.467025926	60.000	3.779	0.995409537
381.2751953	3.5	60.000	0.000	0.995203687	381.2717346	3.5	60.000	0.000	0.995203051
381.858381	3.5	60.000	0.000	0.994993167	381.8549255	3.5	60.000	0.000	0.994992517
382.4432922	3.5	60.000	0.000	0.994778802	382.439842	3.5	60.000	0.000	0.994778137
383.0299209	3.5	60.000	0.000	0.994560632	383.026476	3.5	60.000	0.000	0.994559951
383.6182593	3.5	60.000	0.000	0.994338697	383.6148197	3.5	60.000	0.000	0.994338002
384.2082995	3.5	60.000	0.000	0.994113038	384.2048652	3.5	60.000	0.000	0.994112329

Per-unit-length parameter matrices as calculated by the program "CableMod" for one of the sections of the line in the case of the crosstalk computations

```

*****
***** RESULT *****
*****

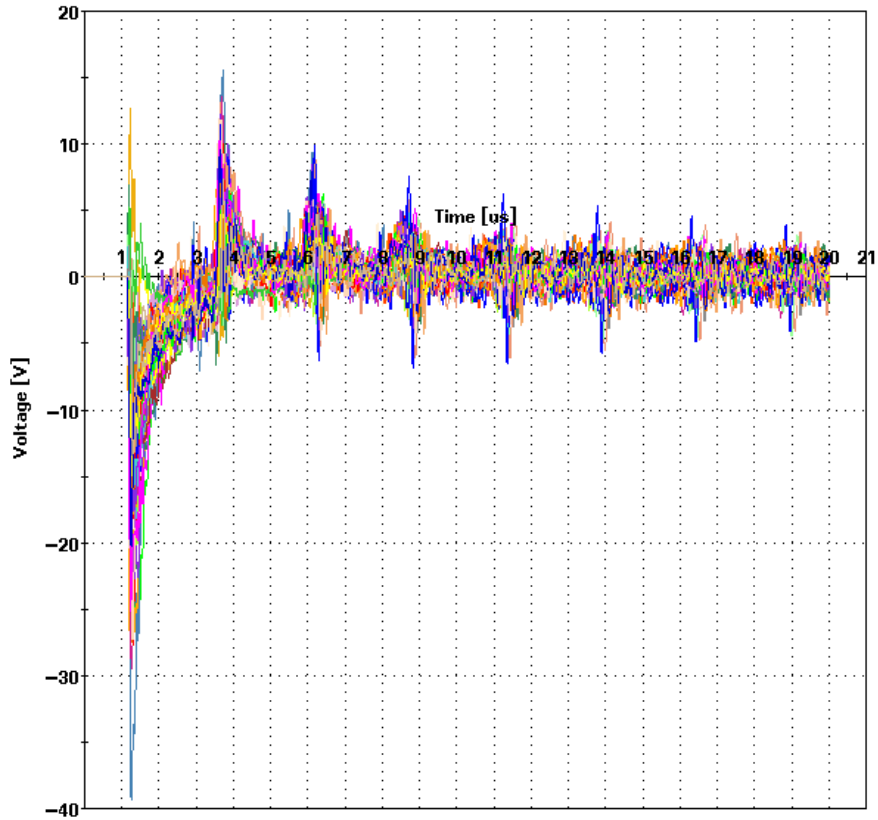
** SimLab Model
** System: NR1_NR2
** Order of Conductors:
** 1 : LNYR_R1R2_1stw
** 2 : LNYR_R1R2_2ndw
** 3 : LNYR_R1R2_3thw
** 4 : LNYR_R1R2_4thw
** 5 : LCuB1_R1R2
** 6 : LCuB2_R1R2
** 7 : LCuB3_R1R2
** 8 : LCuB4_R1R2
** 9 : LCuB5_R1R2
.MODEL NR1_NR2 NTL=9
+
+ C(1,1)=7.64e-13 C(1,2)=4.84e-11 C(1,3)=9.01e-12 C(1,4)=4.85e-11 C(1,5)=9.72e-13
+ C(1,6)=1.41e-12 C(1,7)=1.93e-12 C(1,8)=9.23e-13 C(1,9)=7.01e-13
+ C(2,1)=4.84e-11 C(2,2)=7.64e-13 C(2,3)=4.85e-11 C(2,4)=9.01e-12 C(2,5)=7.01e-13
+ C(2,6)=9.23e-13 C(2,7)=1.93e-12 C(2,8)=1.41e-12 C(2,9)=9.72e-13
+ C(3,1)=9.01e-12 C(3,2)=4.85e-11 C(3,3)=8.80e-13 C(3,4)=4.85e-11 C(3,5)=1.03e-12
+ C(3,6)=8.15e-13 C(3,7)=1.19e-12 C(3,8)=1.25e-12 C(3,9)=1.32e-12
+ C(4,1)=4.85e-11 C(4,2)=9.01e-12 C(4,3)=4.85e-11 C(4,4)=8.80e-13 C(4,5)=1.32e-12
+ C(4,6)=1.25e-12 C(4,7)=1.19e-12 C(4,8)=8.15e-13 C(4,9)=1.03e-12
+ C(5,1)=9.72e-13 C(5,2)=7.01e-13 C(5,3)=1.03e-12 C(5,4)=1.32e-12 C(5,5)=7.81e-12
+ C(5,6)=8.50e-12 C(5,7)=3.61e-12 C(5,8)=3.00e-12 C(5,9)=5.41e-12
+ C(6,1)=1.41e-12 C(6,2)=9.23e-13 C(6,3)=8.15e-13 C(6,4)=1.25e-12 C(6,5)=8.50e-12
+ C(6,6)=5.60e-12 C(6,7)=1.42e-11 C(6,8)=4.71e-12 C(6,9)=3.00e-12
+ C(7,1)=1.93e-12 C(7,2)=1.93e-12 C(7,3)=1.19e-12 C(7,4)=1.19e-12 C(7,5)=3.61e-12
+ C(7,6)=1.42e-11 C(7,7)=3.70e-12 C(7,8)=1.42e-11 C(7,9)=3.61e-12
+ C(8,1)=9.23e-13 C(8,2)=1.41e-12 C(8,3)=1.25e-12 C(8,4)=8.15e-13 C(8,5)=3.00e-12
+ C(8,6)=4.71e-12 C(8,7)=1.42e-11 C(8,8)=5.60e-12 C(8,9)=8.50e-12
+ C(9,1)=7.01e-13 C(9,2)=9.72e-13 C(9,3)=1.32e-12 C(9,4)=1.03e-12 C(9,5)=5.41e-12
+ C(9,6)=3.00e-12 C(9,7)=3.61e-12 C(9,8)=8.50e-12 C(9,9)=7.81e-12
+
+ L(1,1)=1.77e-06 L(1,2)=1.52e-06 L(1,3)=1.46e-06 L(1,4)=1.52e-06 L(1,5)=8.04e-07
+ L(1,6)=8.89e-07 L(1,7)=9.57e-07 L(1,8)=8.84e-07 L(1,9)=8.01e-07
+ L(2,1)=1.52e-06 L(2,2)=1.77e-06 L(2,3)=1.52e-06 L(2,4)=1.46e-06 L(2,5)=8.01e-07
+ L(2,6)=8.84e-07 L(2,7)=9.57e-07 L(2,8)=8.89e-07 L(2,9)=8.04e-07
+ L(3,1)=1.46e-06 L(3,2)=1.52e-06 L(3,3)=1.77e-06 L(3,4)=1.52e-06 L(3,5)=8.03e-07
+ L(3,6)=8.80e-07 L(3,7)=9.48e-07 L(3,8)=8.84e-07 L(3,9)=8.07e-07
+ L(4,1)=1.52e-06 L(4,2)=1.46e-06 L(4,3)=1.52e-06 L(4,4)=1.77e-06 L(4,5)=8.07e-07
+ L(4,6)=8.84e-07 L(4,7)=9.48e-07 L(4,8)=8.80e-07 L(4,9)=8.03e-07
+ L(5,1)=8.04e-07 L(5,2)=8.01e-07 L(5,3)=8.03e-07 L(5,4)=8.07e-07 L(5,5)=1.52e-06
+ L(5,6)=7.98e-07 L(5,7)=7.52e-07 L(5,8)=7.04e-07 L(5,9)=6.94e-07
+ L(6,1)=8.89e-07 L(6,2)=8.84e-07 L(6,3)=8.80e-07 L(6,4)=8.84e-07 L(6,5)=7.98e-07
+ L(6,6)=1.50e-06 L(6,7)=9.48e-07 L(6,8)=8.10e-07 L(6,9)=7.04e-07
+ L(7,1)=9.57e-07 L(7,2)=9.57e-07 L(7,3)=9.48e-07 L(7,4)=9.48e-07 L(7,5)=7.52e-07
+ L(7,6)=9.48e-07 L(7,7)=1.50e-06 L(7,8)=9.48e-07 L(7,9)=7.52e-07
+ L(8,1)=8.84e-07 L(8,2)=8.89e-07 L(8,3)=8.84e-07 L(8,4)=8.80e-07 L(8,5)=7.04e-07
+ L(8,6)=8.10e-07 L(8,7)=9.48e-07 L(8,8)=1.50e-06 L(8,9)=7.98e-07
+ L(9,1)=8.01e-07 L(9,2)=8.04e-07 L(9,3)=8.07e-07 L(9,4)=8.03e-07 L(9,5)=6.94e-07
+ L(9,6)=7.04e-07 L(9,7)=7.52e-07 L(9,8)=7.98e-07 L(9,9)=1.52e-06
+
+ R(1)=4.45e-03 R(2)=4.45e-03 R(3)=4.45e-03 R(4)=4.45e-03 R(5)=2.51e-04 R(6)=2.51e-04
+ R(7)=2.51e-04 R(8)=2.51e-04 R(9)=2.51e-04
+
+ D(1)=1.44e+04 D(2)=1.44e+04 D(3)=1.44e+04 D(4)=1.44e+04 D(5)=8.10e+02 D(6)=8.10e+02
+ D(7)=8.10e+02 D(8)=8.10e+02 D(9)=8.10e+02

```

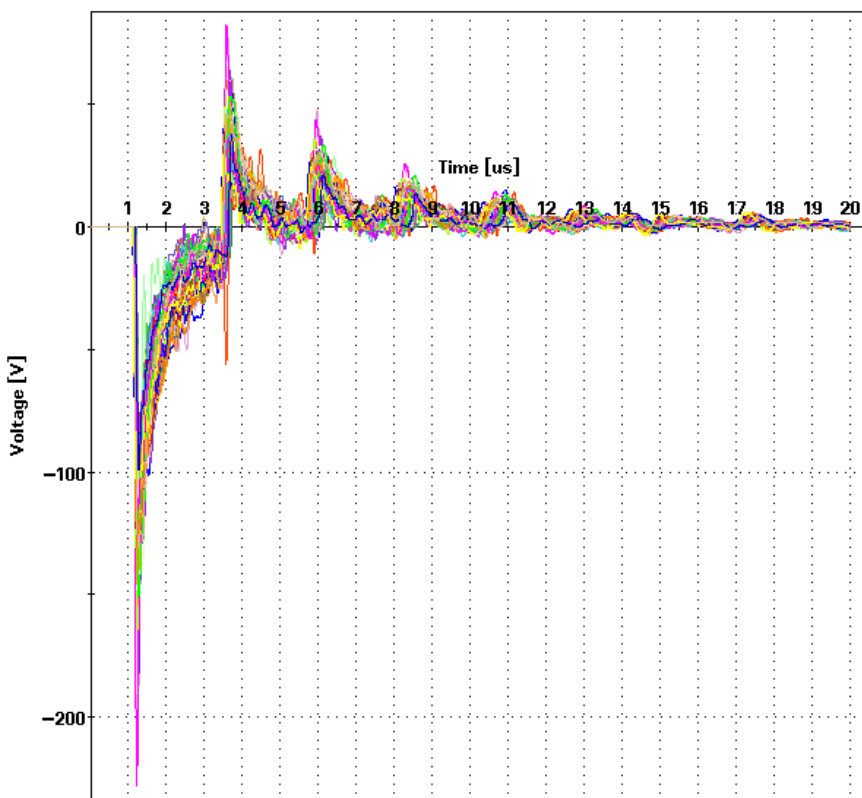

Appendix II

Complete results from the stochastic simulation of direct lightning strike

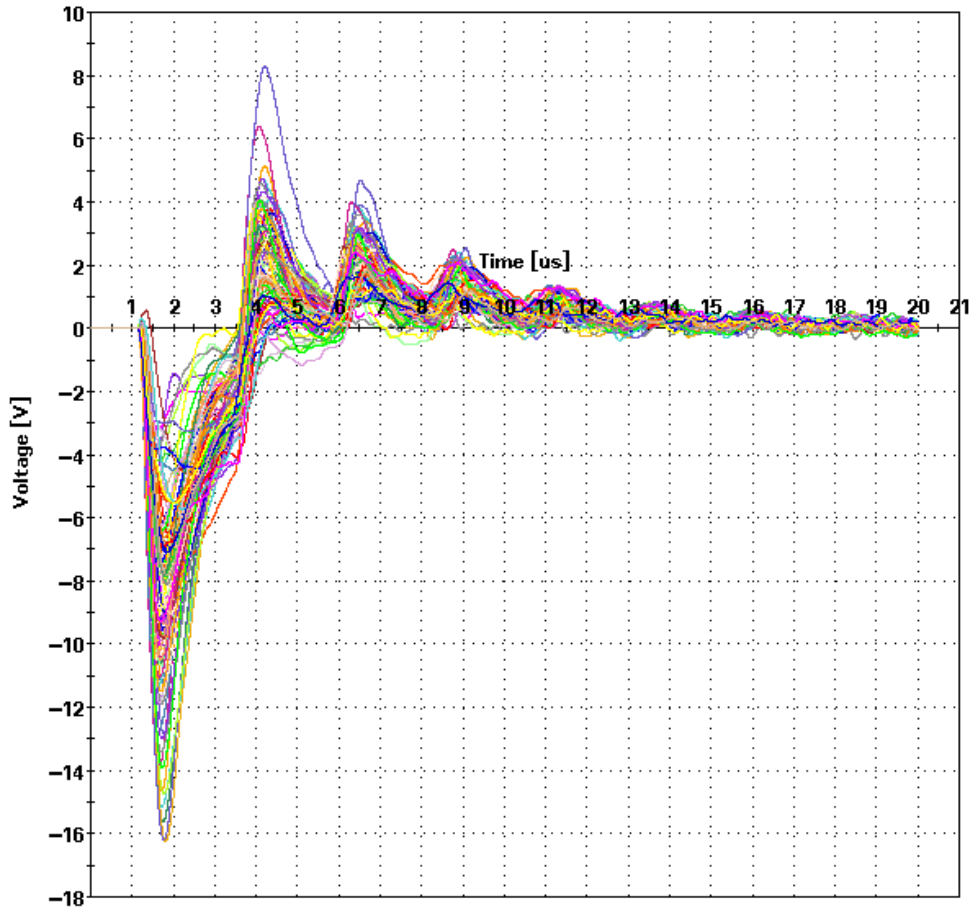
Maximum current-4.6 kA; Rise-time-0.22 us; Ground permittivity: 4-6



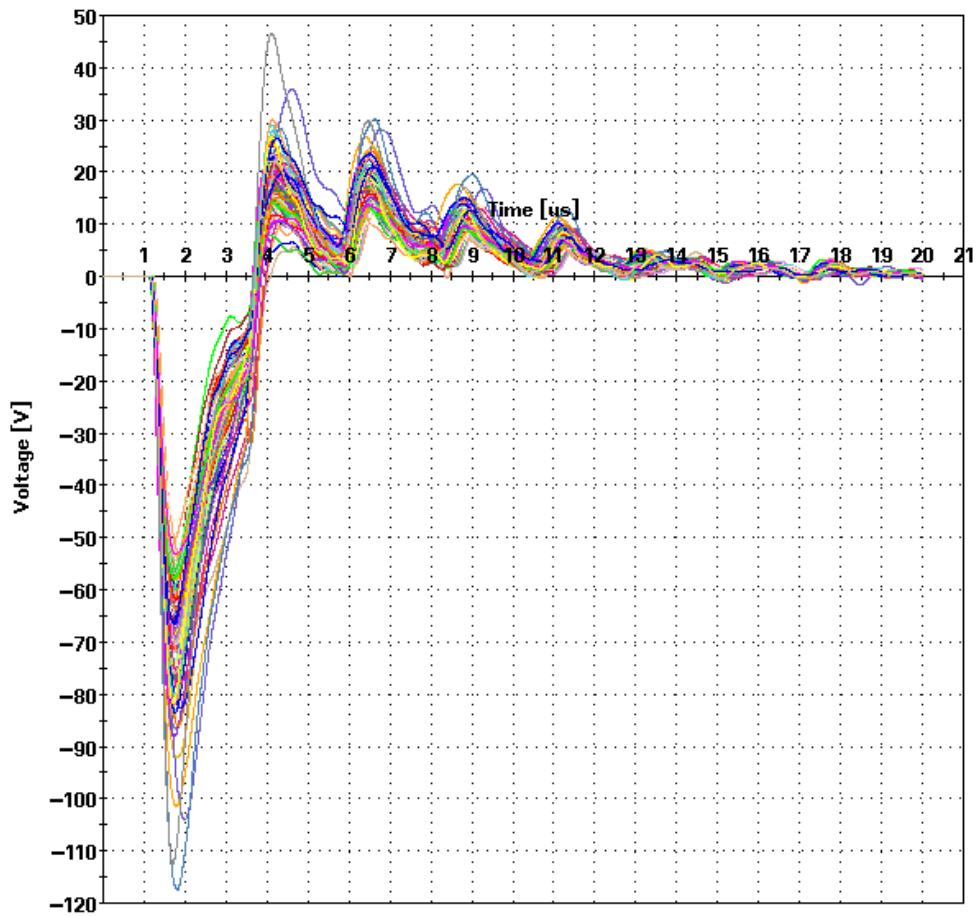
Maximum current-4.6 kA; Rise-time-0.22 us; Ground permittivity: 15-30



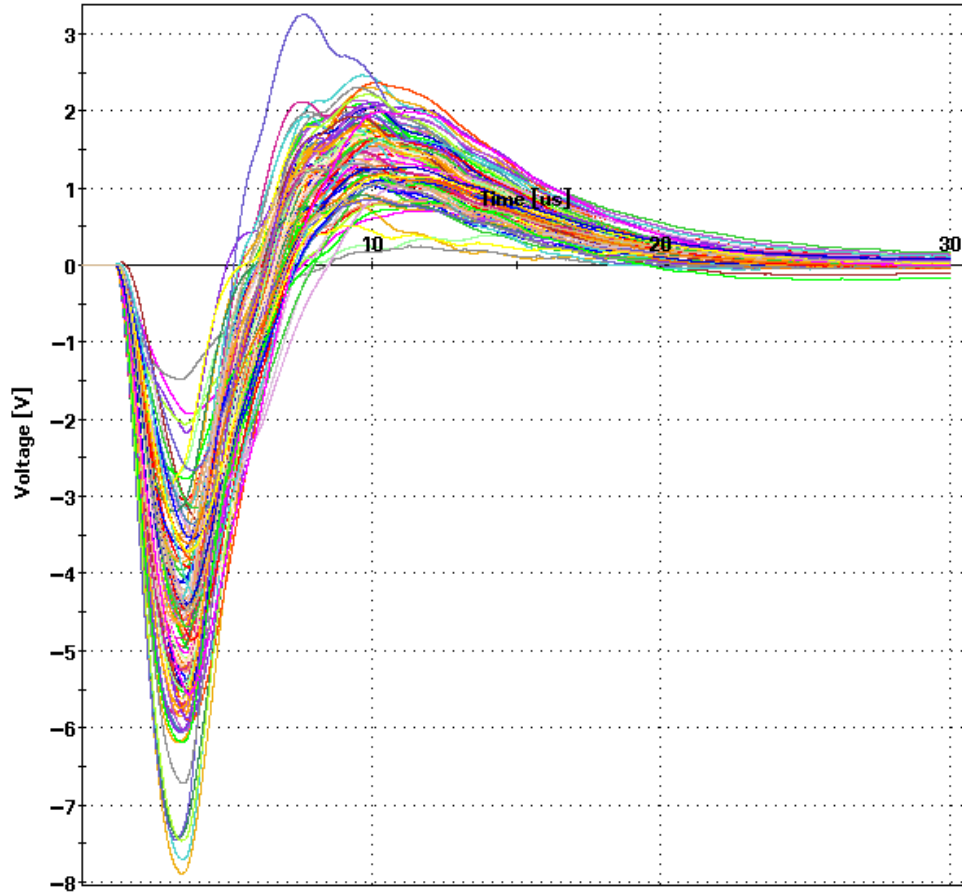
Maximum current–4.6 kA; Rise-time–1.1 us; Ground permittivity: 4–6



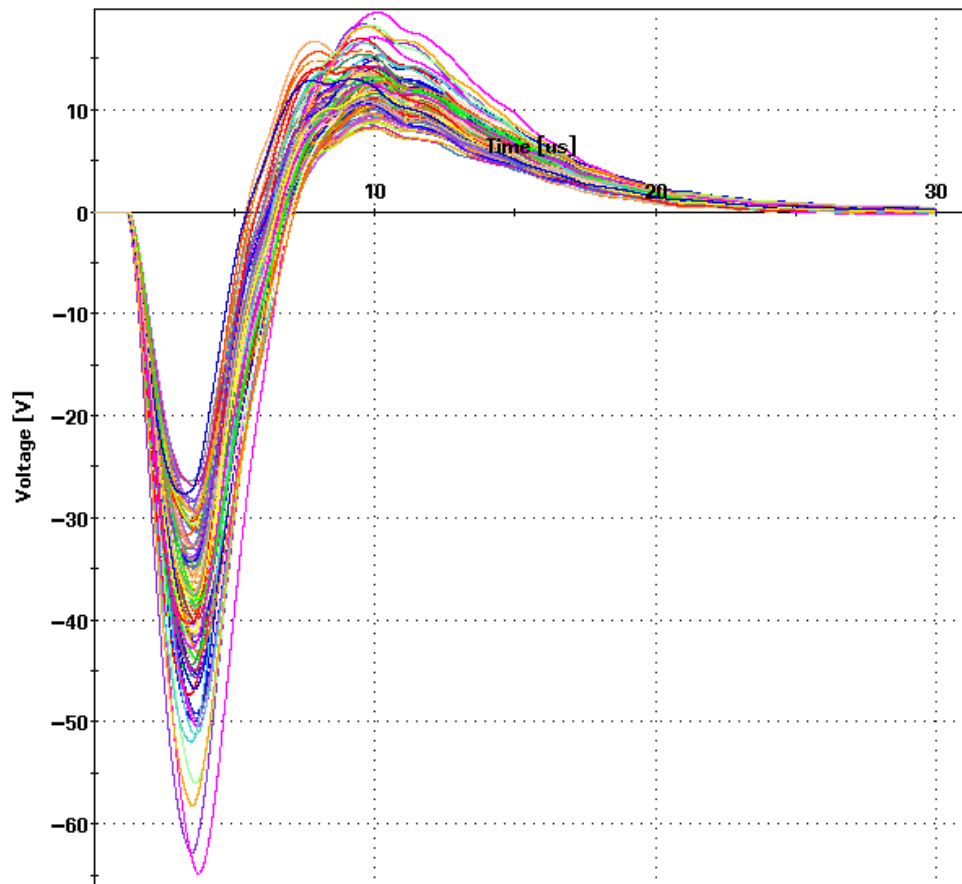
Maximum current–4.6 kA; Rise-time–1.1 us; Ground permittivity: 15–30



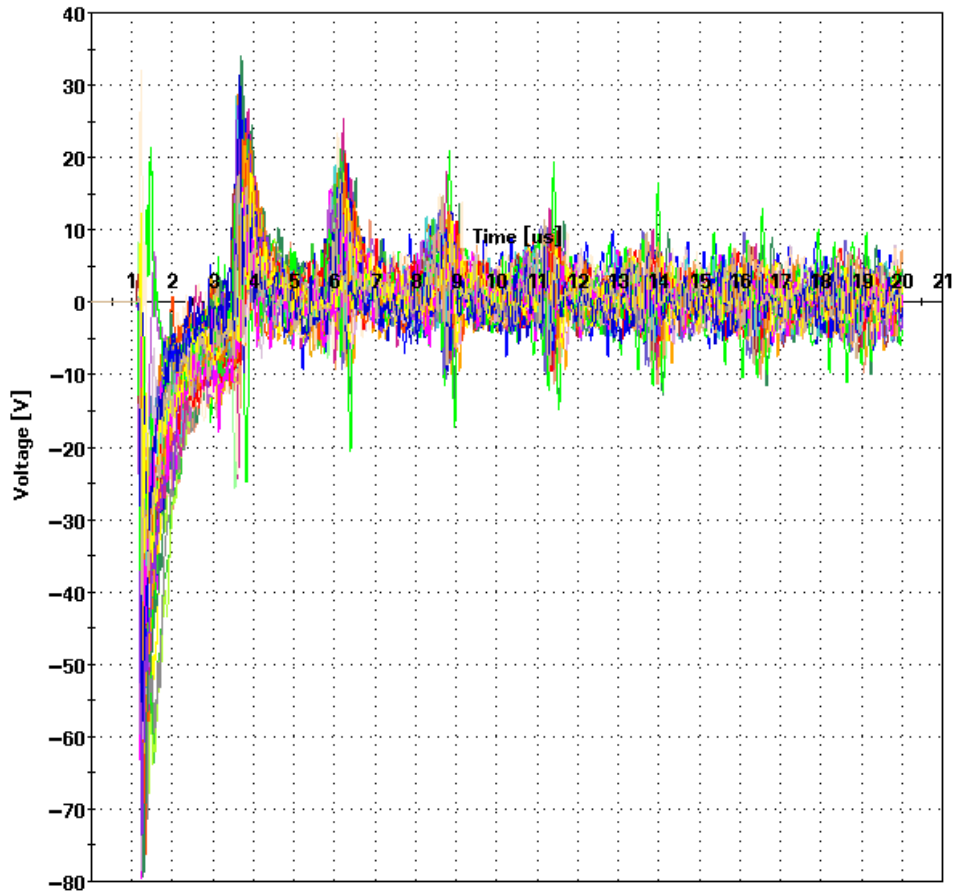
Maximum current 4.6 kA; Rise-time 4.5 us; Ground permittivity: 4-6



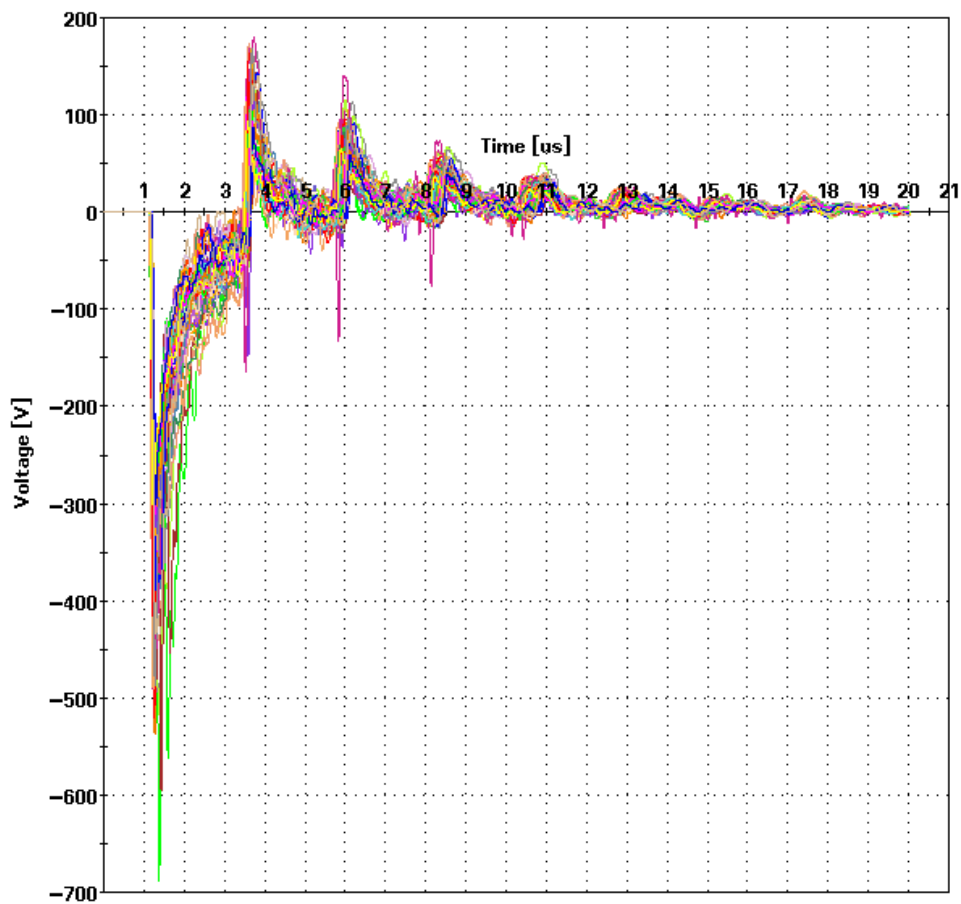
Maximum current 4.6 kA; Rise-time 4.5 us; Ground permittivity: 15-30



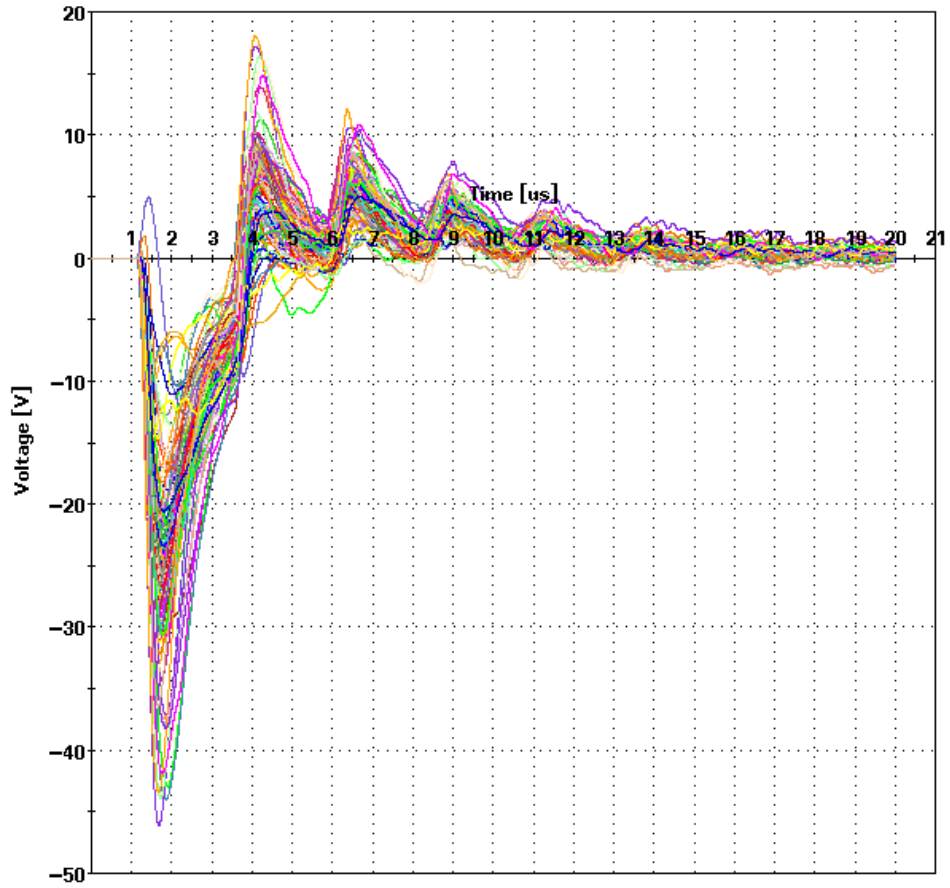
Maximum current–13 kA; Rise–time–0.22 μ s; Ground permittivity: 4–6



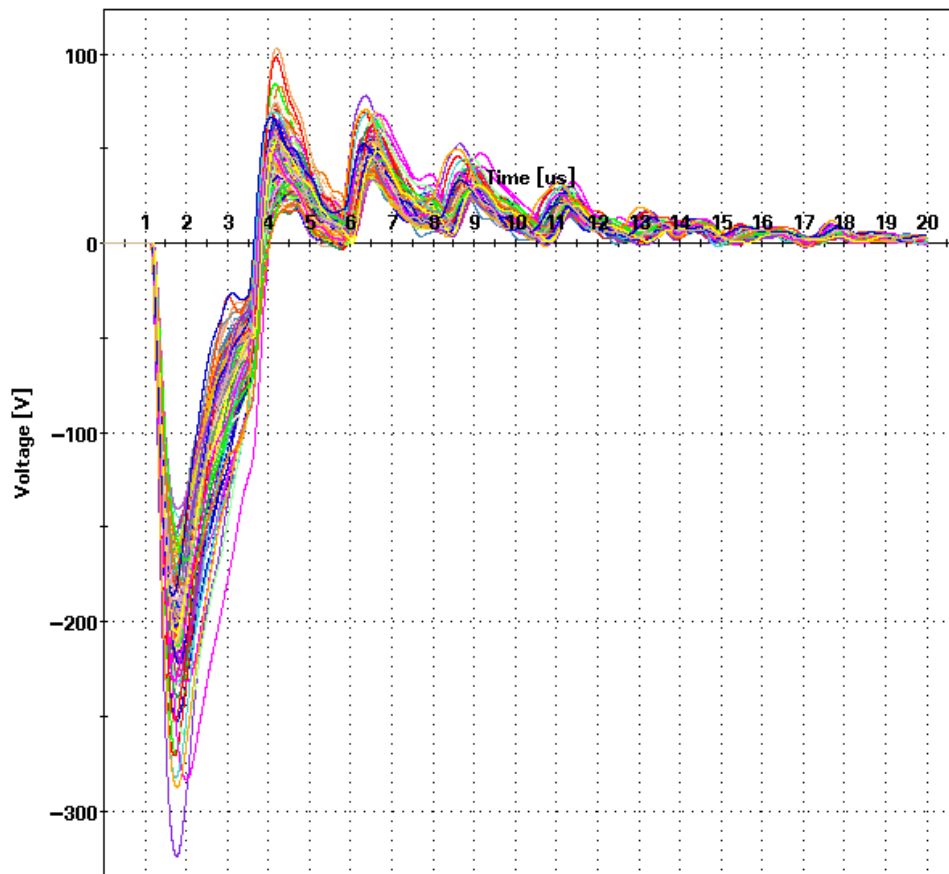
Maximum current–13 kA; Rise–time–0.22 μ s; Ground permittivity: 15–30



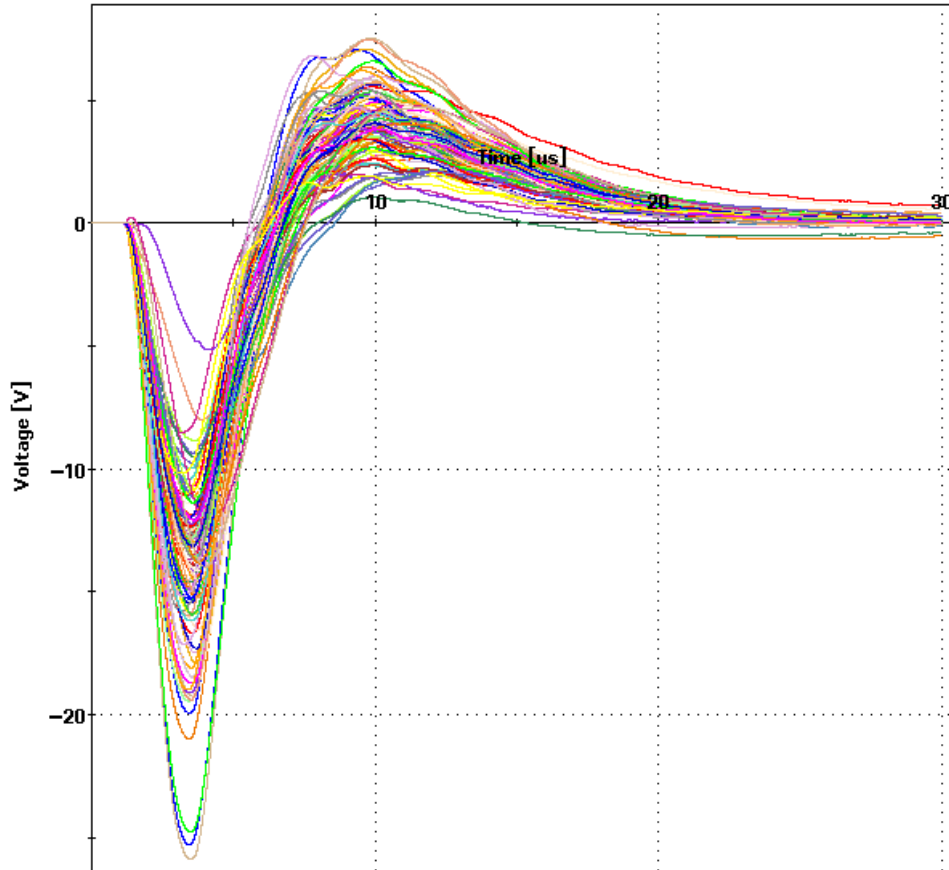
Maximum current–13 kA; Rise–time–1.1 us; Ground permittivity: 4–6



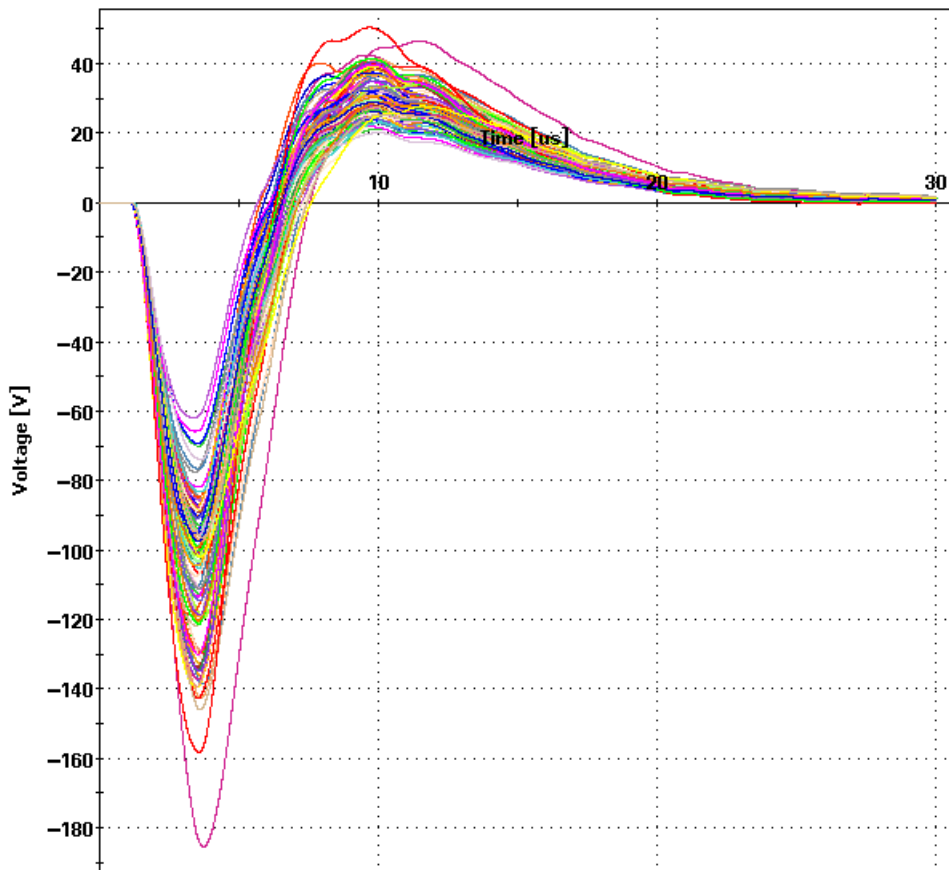
Maximum current–13 kA; Rise–time–1.1 us; Ground permittivity: 15–30



Maximum current-13 kA; Rise-time-4.5 us; Ground permittivity: 4-6



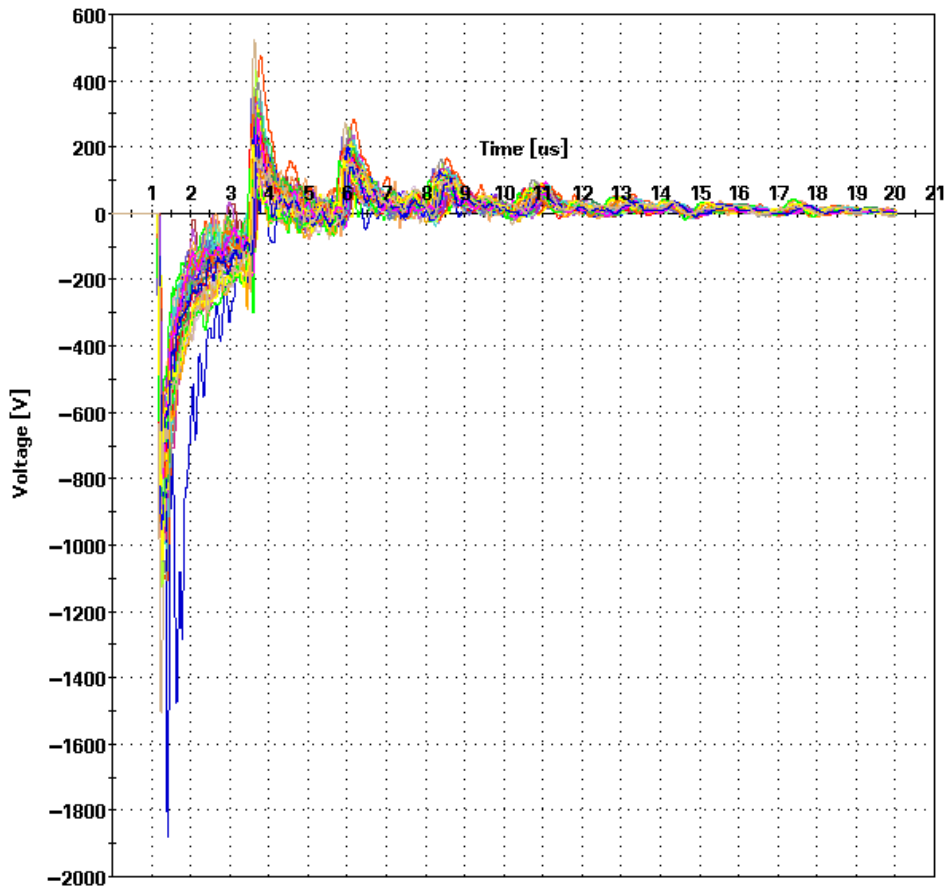
Maximum current-13 kA; Rise-time-4.5 us; Ground permittivity: 15-30



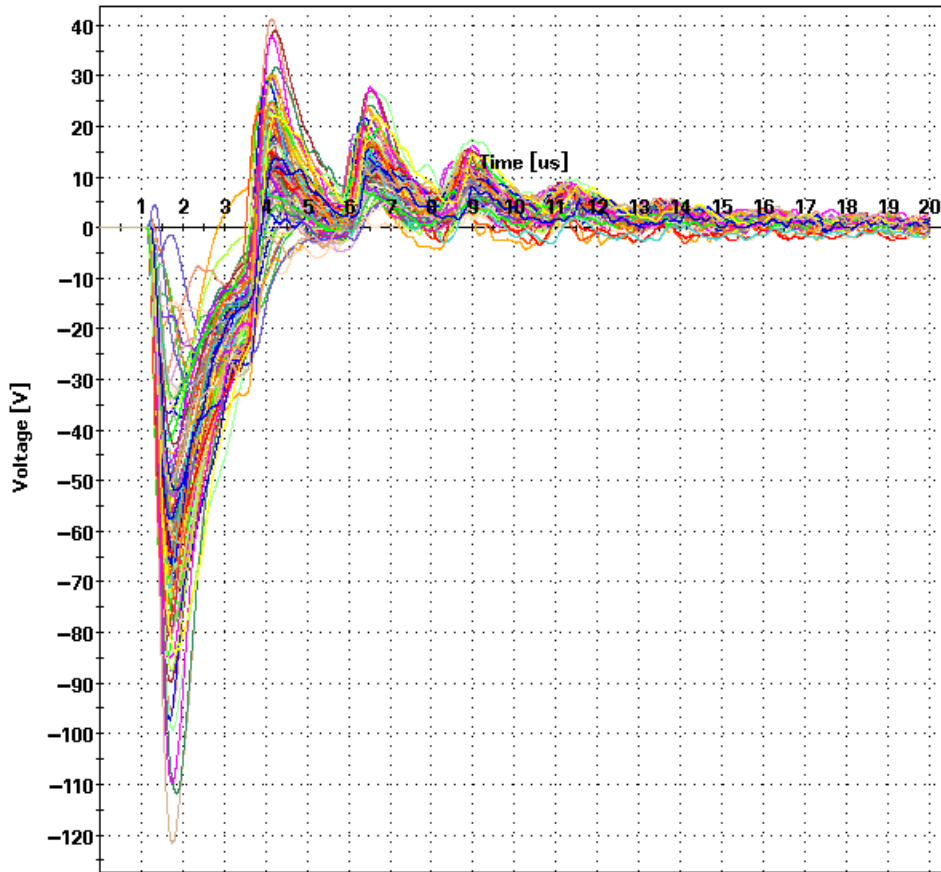
Maximum current–30 kA; Rise-time–0.22 us; Ground permittivity: 4–6



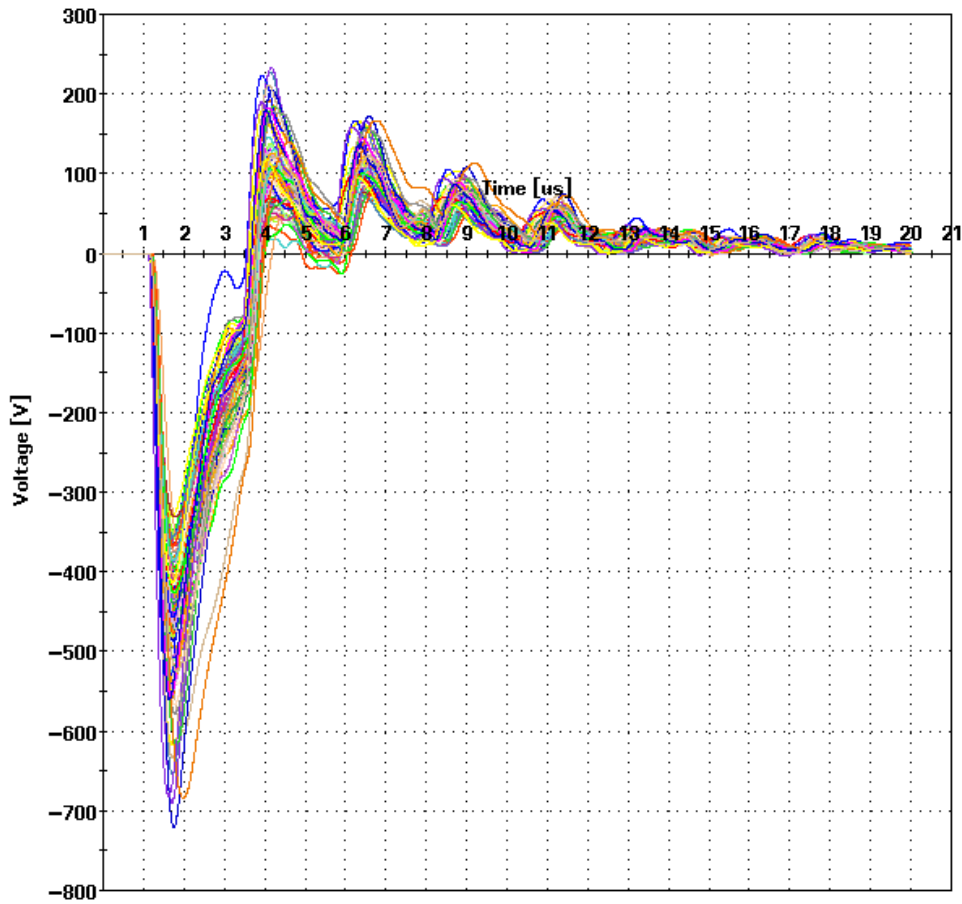
Maximum current–30 kA; Rise-time–0.22 us; Ground permittivity: 15–30



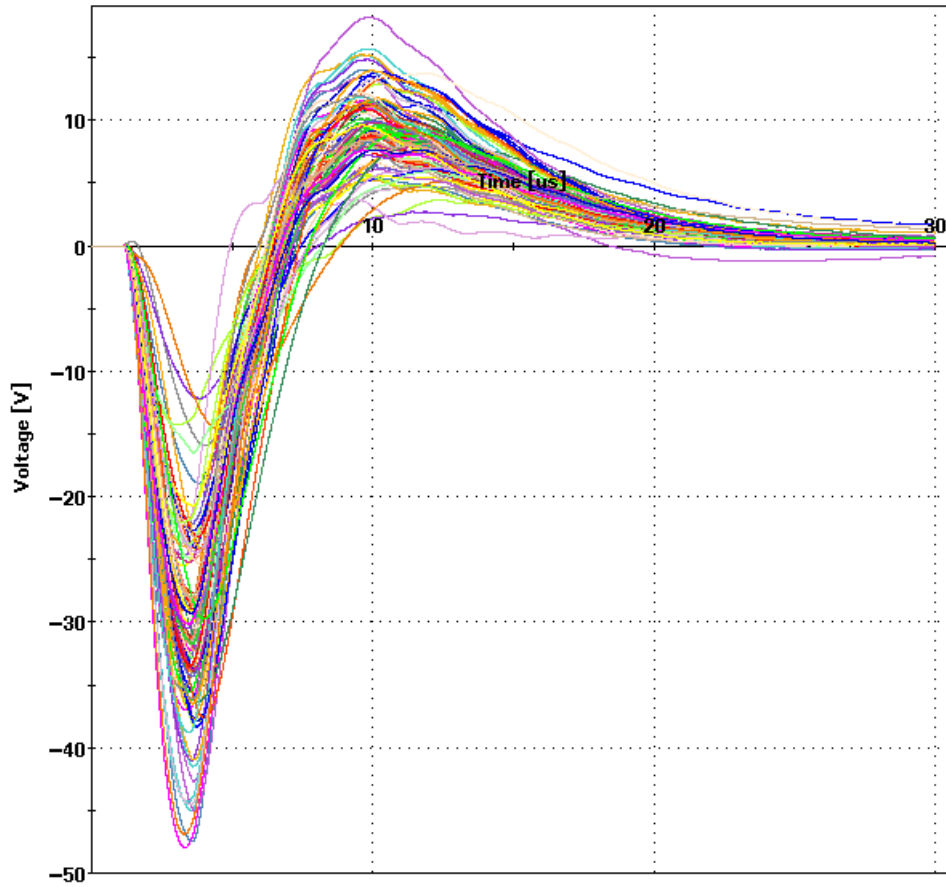
Maximum current–30 kA; Rise–time–1.1 us; Ground permittivity: 4–6



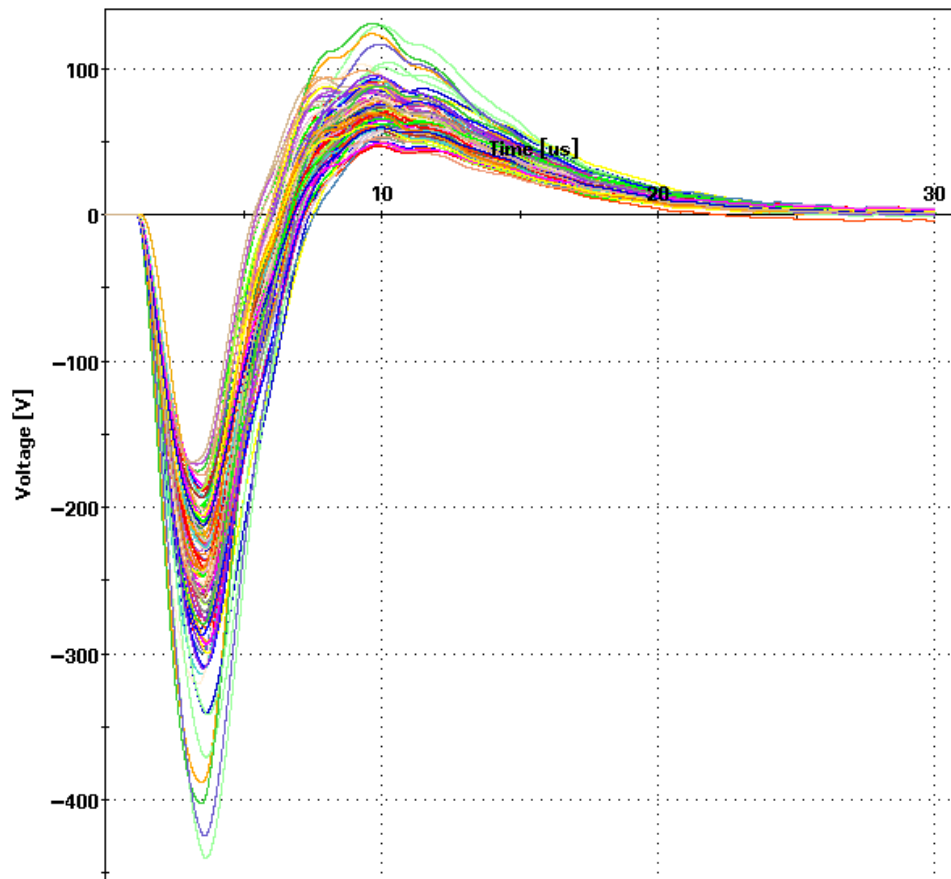
Maximum current–30 kA; Rise–time–1.1 us; Ground permittivity: 15–30



Maximum current-30 kA; Rise-time-4.5 us; Ground permittivity: 4-6



Maximum current-30 kA; Rise-time-4.5 us; Ground permittivity: 15-30



Appendix III

Short introduction to MTL theory

III.1 The transmission line equations in the time domain

For a two-conductor transmission line, the TL equations in time domain are given by

$$\frac{\partial V(z,t)}{\partial z} = -rI(z,t) - l \frac{\partial I(z,t)}{\partial t} \quad (\text{III.1})$$

$$\frac{\partial I(z,t)}{\partial z} = -gV(z,t) - c \frac{\partial V(z,t)}{\partial t} \quad (\text{III.2})$$

These equations represent a coupled set of first-order, partial differential equations in the line voltage $V(z,t)$ and line current $I(z,t)$. Their solution gives the voltages and currents at any point z along the line length for a given time t .

The form of the TL equations in the case of multiconductor transmission line is identical, but in this case matrix instead of scalar notion is used. The multiconductor transmission line equations take the form [106]

$$\frac{\partial}{\partial z} \mathbf{V}(z,t) = -\mathbf{R}\mathbf{I}(z,t) - \mathbf{L} \frac{\partial}{\partial t} \mathbf{I}(z,t) \quad (\text{III.3a})$$

$$\frac{\partial}{\partial z} \mathbf{I}(z,t) = -\mathbf{G}\mathbf{V}(z,t) - \mathbf{C} \frac{\partial}{\partial t} \mathbf{V}(z,t) \quad (\text{III.3b})$$

Where the voltage and current vectors are defined as

$$\mathbf{V}(z,t) = \begin{bmatrix} V_1(z,t) \\ \vdots \\ V_i(z,t) \\ \vdots \\ V_n(z,t) \end{bmatrix} \quad \mathbf{I}(z,t) = \begin{bmatrix} I_1(z,t) \\ \vdots \\ I_i(z,t) \\ \vdots \\ I_n(z,t) \end{bmatrix} \quad (\text{III.4})$$

And \mathbf{R} , \mathbf{L} , \mathbf{G} and \mathbf{C} are respectively per-unit-length resistance, inductance, conductance and capacitance matrices defined as follows [106]:

$$\mathbf{R} = \begin{bmatrix} (r_1 + r_0) & r_0 & \cdots & r_0 \\ r_0 & (r_2 + r_0) & \cdots & r_0 \\ \vdots & \vdots & \ddots & \vdots \\ r_0 & r_0 & \cdots & (r_n + r_0) \end{bmatrix} \quad \mathbf{L} = \begin{bmatrix} l_{11} & l_{12} & \cdots & l_{1n} \\ l_{21} & l_{22} & \cdots & l_{2n} \\ \vdots & \vdots & \ddots & \vdots \\ l_{n1} & l_{n2} & \cdots & l_{nn} \end{bmatrix} \quad (\text{III.5a})$$

$$\mathbf{G} = \begin{bmatrix} \sum_{k=1}^n g_{1k} & -g_{12} & \cdots & -g_{1n} \\ -g_{21} & \sum_{k=1}^n g_{2k} & \cdots & -g_{2n} \\ \vdots & \vdots & \ddots & \vdots \\ -g_{n1} & -g_{n2} & \cdots & \sum_{k=1}^n g_{nk} \end{bmatrix} \quad \mathbf{C} = \begin{bmatrix} \sum_{k=1}^n c_{1k} & -c_{12} & \cdots & -c_{1n} \\ -c_{21} & \sum_{k=1}^n c_{2k} & \cdots & -c_{2n} \\ \vdots & \vdots & \ddots & \vdots \\ -c_{n1} & -c_{n2} & \cdots & \sum_{k=1}^n c_{nk} \end{bmatrix} \quad (\text{III.5b})$$

The per-unit-length-resistance matrix represents the loss due to imperfections of conductors. The per-unit-length inductance matrix contains the individual per-unit-length self-inductances l_{ii} of the conductors and the per-unit length mutual inductances between the conductors l_{ij} . The per-unit-length conductance matrix \mathbf{G} represents the conduction current flowing between the conductors in the transverse plane. The per-unit-length capacitance matrix \mathbf{C} represents the displacement current flowing between the conductors in the x - y plane.

The fundamental parameters in the transmission line equations are the per-unit-length parameters r , l , g and c , respectively, the \mathbf{R} , \mathbf{L} , \mathbf{G} and \mathbf{C} matrices for the multiconductor line case. The form of the transmission line equations shown above is identical for all multiconductor transmission lines. The per-unit-length parameters are those which set the difference between the two different transmission lines with different cross-sections. Thus all cross-sectional dimensions characteristic of the particular line are contained in these per-unit-length parameters.

There are some basic line structures, as for example conductors with cylindrical form and circular cross section immersed in homogeneous medium, for which simple closed-form equations for the per-unit-length parameters can be obtained. Using the wide-wire separation assumption which implies that the separation must be much larger than either of the wire radii, the per-unit-length inductance in such two-conductor line is

$$l = \frac{\psi}{I} \cong \frac{\mu}{2\pi} \ln\left(\frac{s^2}{r_1 r_2}\right) \quad \text{H/m} \quad (\text{III.6})$$

where s is the distance between the centers of the conductors and r_1 and r_2 are the conductors radii.

The per-unit-length capacitance for this type of transmission line is given with

$$c = \frac{q}{V} \cong \frac{2\pi\epsilon}{\ln\left(\frac{s^2}{r_1 r_2}\right)} \text{ F/m} \quad (\text{III.7})$$

III.2 The transmission line equations for a multiconductor line in frequency domain

The following expressions describe the MTL equations in frequency domain [106].

$$\frac{d}{dz} \hat{\mathbf{V}}(z) = -\hat{\mathbf{Z}}\hat{\mathbf{I}}(z) \quad (\text{III.8a})$$

$$\frac{d}{dz} \hat{\mathbf{I}}(z) = -\hat{\mathbf{Y}}\hat{\mathbf{V}}(z) \quad (\text{III.8b})$$

where the per-unit-length impedance matrix $\hat{\mathbf{Z}}$ and admittance matrix $\hat{\mathbf{Y}}$ are given by

$$\hat{\mathbf{Z}} = \mathbf{R} + j\omega\mathbf{L} \quad (\text{III.9a})$$

$$\hat{\mathbf{Y}} = \mathbf{G} + j\omega\mathbf{C} \quad (\text{III.9b})$$

Because of the assumption that the per-unit-length parameter matrices \mathbf{R} , \mathbf{L} , \mathbf{G} and \mathbf{C} are independent of time, equations (III.8) are a set of coupled first-order ordinary differential equations with complex coefficients. They can be put in a more compact matrix form as [106]

$$\frac{d}{dz} \hat{\mathbf{X}}(z) = \hat{\mathbf{A}}\hat{\mathbf{X}}(z) \quad (\text{III.10a})$$

where

$$\hat{\mathbf{X}} = \begin{bmatrix} \hat{\mathbf{V}}(z) \\ \hat{\mathbf{I}}(z) \end{bmatrix} \quad (\text{III.10b})$$

$$\hat{\mathbf{A}} = \begin{bmatrix} \mathbf{0} & -\hat{\mathbf{Z}} \\ -\hat{\mathbf{Y}} & \mathbf{0} \end{bmatrix} \quad (\text{III.10c})$$

The coupled first-order phasor MTL equations in (III.8) can be placed in a form of uncoupled, second-order ordinary differential equations by differentiating both of them with respect to line position z and substituting the first order equations given in (III.8) which leads to

$$\frac{d^2}{dz^2} \hat{\mathbf{V}}(z) = \hat{\mathbf{Z}}\hat{\mathbf{Y}}\hat{\mathbf{V}}(z) \quad (\text{III.11a})$$

$$\frac{d^2}{dz^2} \hat{\mathbf{I}}(z) = \hat{\mathbf{Y}}\hat{\mathbf{Z}}\hat{\mathbf{I}}(z) \quad (\text{III.11b})$$

Usually, the per-unit-length parameter matrices $\hat{\mathbf{Z}}$ and $\hat{\mathbf{Y}}$ do not commute so that the proper order of multiplication must be observed. Also in differentiating (III.8) with respect to the line position z , it is assumed that the per-unit-length parameter matrices \mathbf{R} , \mathbf{L} , \mathbf{G} and \mathbf{C} are independent of z . In other words, the line is assumed to be a uniform line.

III.3 Crosstalk between the conductors – solving the MTL equations for the line voltages and currents

Crosstalk denotes a near-field coupling phenomenon. It is defined as an unintentional electromagnetic coupling between conductors which are in close proximity. The solution of the MTL equations gives the voltages at the end of the line and potential disturbing signals at some of the terminals which as mentioned above are described as crosstalk.

The MTL equations introduced in eq. (III.8) are solved using a similarity transformation method. The core of this method consists of defining a change of variables as [106]

$$\hat{\mathbf{V}}(z) = \hat{\mathbf{T}}_V \hat{\mathbf{V}}_m(z) \quad (\text{III.12a})$$

$$\hat{\mathbf{I}}(z) = \hat{\mathbf{T}}_I \hat{\mathbf{I}}_m(z) \quad (\text{III.12b})$$

The $n \times n$ complex matrices $\hat{\mathbf{T}}_V$ and $\hat{\mathbf{T}}_I$ are said to be similarity transformations between the actual phasor line voltages and currents $\hat{\mathbf{V}}$ and $\hat{\mathbf{I}}$ and the mode voltages and currents $\hat{\mathbf{V}}_m$ and $\hat{\mathbf{I}}_m$. Physically, these modes correspond to the cross-sectional distribution of voltages and currents on the conductors that propagate at the same velocity on the line. The transformation matrices $\hat{\mathbf{T}}_V$ and $\hat{\mathbf{T}}_I$ must be non-singular, i.e. their inverse matrices $\hat{\mathbf{T}}_V^{-1}$ and $\hat{\mathbf{T}}_I^{-1}$ must exist. As discussed in [106], these matrices are defined in such a way that $\hat{\mathbf{T}}_V$ diagonalizes the matrix $\hat{\mathbf{Z}}\hat{\mathbf{Y}}$ and $\hat{\mathbf{T}}_I$ diagonalizes the matrix $\hat{\mathbf{Y}}\hat{\mathbf{Z}}$ and the diagonalization of these two matrices gives the same matrix. Additionally $\hat{\mathbf{T}}_V$ and $\hat{\mathbf{T}}_I$ are related with [106]

$$\hat{\mathbf{T}}_I^t = \hat{\mathbf{T}}_V^{-1} \quad (\text{III.13})$$

where the transpose of the matrix $\hat{\mathbf{T}}_I$ is denoted by $\hat{\mathbf{T}}_I^t$.

Now, consider the uncoupled second-order MTL equations given in (III.11)

$$\frac{d^2}{dz^2} \hat{\mathbf{V}}(z) = \hat{\mathbf{Z}}\hat{\mathbf{Y}}\hat{\mathbf{V}}(z) \quad (\text{III.14a})$$

$$\frac{d^2}{dz^2} \hat{\mathbf{I}}(z) = \hat{\mathbf{Y}}\hat{\mathbf{Z}}\hat{\mathbf{I}}(z) \quad (\text{III.14b})$$

Let us choose to decouple (III.11b) as

$$\frac{d^2}{dz^2} \hat{\mathbf{I}}_m(z) = \hat{\mathbf{T}}^{-1} \hat{\mathbf{Y}}\hat{\mathbf{Z}}\hat{\mathbf{T}} \hat{\mathbf{I}}_m(z) = \hat{\boldsymbol{\gamma}}^2 \hat{\mathbf{I}}_m(z) \quad (\text{III.15})$$

where

$$\hat{\mathbf{T}} = \hat{\mathbf{T}}_l \quad (\text{III.16})$$

and $\hat{\boldsymbol{\gamma}}^2$ is diagonal matrix as

$$\hat{\boldsymbol{\gamma}}^2 = \begin{bmatrix} \hat{\gamma}_1^2 & 0 & \cdots & 0 \\ 0 & \hat{\gamma}_2^2 & \ddots & \vdots \\ \vdots & \ddots & \ddots & 0 \\ 0 & \cdots & 0 & \hat{\gamma}_n^2 \end{bmatrix} \quad (\text{III.17})$$

The problem of finding transformation matrix $\hat{\mathbf{T}}$ which diagonalizes the matrix (in our case the product of per-unit-length parameter matrices $\hat{\mathbf{Y}}\hat{\mathbf{Z}}$) as

$$\hat{\mathbf{T}}^{-1} \hat{\mathbf{Y}}\hat{\mathbf{Z}}\hat{\mathbf{T}} = \hat{\boldsymbol{\gamma}}^2 \quad (\text{III.18})$$

where $\hat{\boldsymbol{\gamma}}^2$ is diagonal, is a classic problem in matrix analysis. The n values of $\hat{\boldsymbol{\gamma}}^2$ are the eigenvalues of the matrix $\hat{\mathbf{Y}}\hat{\mathbf{Z}}$. The columns of $\hat{\mathbf{T}}$ are its eigenvectors. Digital computer subroutines exist that find the eigenvalues and eigenvectors of a general complex matrix. However, as discussed in [106], efficient and numerically stable solutions exist in some cases, as for example, perfect conductors in a homogeneous medium, lossy conductors in a homogeneous medium and perfect conductors in an inhomogeneous medium. In the general case of lossy conductors in an inhomogeneous medium there is no certainty that numerically stable diagonalization can be achieved.

Assuming that the transformation $\hat{\mathbf{T}}$ exists, then the general solution to the uncoupled equation in (III.15) is [106]

$$\hat{\mathbf{I}}_m(z) = \mathbf{e}^{-\hat{\boldsymbol{\gamma}}z} \hat{\mathbf{I}}_m^+ - \mathbf{e}^{\hat{\boldsymbol{\gamma}}z} \hat{\mathbf{I}}_m^- \quad (\text{III.19})$$

where the matrix exponentials are defined as

$$\mathbf{e}^{\pm \hat{\boldsymbol{\gamma}}z} = \begin{bmatrix} e^{\pm \hat{\gamma}_1 z} & 0 & \cdots & 0 \\ 0 & e^{\pm \hat{\gamma}_2 z} & \ddots & \vdots \\ \vdots & \ddots & \ddots & 0 \\ 0 & \cdots & 0 & e^{\pm \hat{\gamma}_n z} \end{bmatrix} \quad (\text{III.20})$$

and the vectors of undetermined constants are

$$\hat{\mathbf{I}}_m^\pm = \begin{bmatrix} \hat{I}_{m1}^\pm \\ \hat{I}_{m2}^\pm \\ \vdots \\ \hat{I}_{mn}^\pm \end{bmatrix} \quad (\text{III.21})$$

The actual currents are obtained by multiplying these mode currents by the transformation matrix $\hat{\mathbf{T}}_I = \hat{\mathbf{T}}$, to give [106]

$$\hat{\mathbf{I}}(z) = \hat{\mathbf{T}}\hat{\mathbf{I}}_m(z) = \hat{\mathbf{T}}(\mathbf{e}^{-\hat{\gamma}z}\hat{\mathbf{I}}_m^+ - \mathbf{e}^{\hat{\gamma}z}\hat{\mathbf{I}}_m^-) \quad (\text{III.22})$$

Similarly, the uncoupled second-order differential equation in terms of the mode voltages is [106]

$$\frac{d^2}{dz^2}\hat{\mathbf{V}}_m(z) = \hat{\mathbf{T}}_V^{-1}\hat{\mathbf{Z}}\hat{\mathbf{Y}}\hat{\mathbf{T}}_V\hat{\mathbf{V}}_m(z) = \hat{\mathbf{T}}'\hat{\mathbf{Z}}\hat{\mathbf{Y}}(\hat{\mathbf{T}}')^{-1}\hat{\mathbf{V}}_m(z) = \hat{\mathbf{Y}}^2\hat{\mathbf{V}}_m(z) \quad (\text{III.23})$$

with the general solution

$$\hat{\mathbf{V}}_m(z) = \mathbf{e}^{-\hat{\gamma}z}\hat{\mathbf{V}}_m^+ + \mathbf{e}^{\hat{\gamma}z}\hat{\mathbf{V}}_m^- \quad (\text{III.24})$$

The actual voltages can be obtained by multiplying this result by the transformation [106]

$\hat{\mathbf{T}}_V = (\hat{\mathbf{T}}_I^{-1})^t = (\hat{\mathbf{T}}^{-1})^t$ to give

$$\hat{\mathbf{V}}(z) = (\hat{\mathbf{T}}^{-1})^t(\mathbf{e}^{-\hat{\gamma}z}\hat{\mathbf{V}}_m^+ + \mathbf{e}^{\hat{\gamma}z}\hat{\mathbf{V}}_m^-) \quad (\text{III.25})$$

The undetermined constants in these results are related. To determine this relation, we substitute eq. (III.22) into the second MTL equation in eq. (III.8b) and obtain [106]

$$\begin{aligned} \hat{\mathbf{V}}(z) &= \hat{\mathbf{Y}}^{-1} \frac{d}{dz} \hat{\mathbf{I}}(z) = \hat{\mathbf{Y}}^{-1} \hat{\mathbf{T}} \hat{\gamma} (\mathbf{e}^{-\hat{\gamma}z} \hat{\mathbf{I}}_m^+ + \mathbf{e}^{\hat{\gamma}z} \hat{\mathbf{I}}_m^-) \\ &= (\hat{\mathbf{Y}}^{-1} \hat{\mathbf{T}} \hat{\gamma} \hat{\mathbf{T}}^{-1}) \hat{\mathbf{T}} (\mathbf{e}^{-\hat{\gamma}z} \hat{\mathbf{I}}_m^+ + \mathbf{e}^{\hat{\gamma}z} \hat{\mathbf{I}}_m^-) = \hat{\mathbf{Z}}_C \hat{\mathbf{T}} (\mathbf{e}^{-\hat{\gamma}z} \hat{\mathbf{I}}_m^+ + \mathbf{e}^{\hat{\gamma}z} \hat{\mathbf{I}}_m^-) \end{aligned} \quad (\text{III.26})$$

where the characteristic impedance matrix is defined as [106]

$$\hat{\mathbf{Z}}_C = \hat{\mathbf{Y}}^{-1} \hat{\mathbf{T}} \hat{\gamma} \hat{\mathbf{T}}^{-1} = \hat{\mathbf{Z}} \hat{\mathbf{T}} \hat{\gamma}^{-1} \hat{\mathbf{T}}^{-1} \quad (\text{III.27})$$

The $2n$ undetermined constants $\hat{\mathbf{I}}_m^+$ and $\hat{\mathbf{I}}_m^-$ in eq. (III.19) and (III.26) can be found when applying the terminal constraints for the line. The terminal constraints are given by the following equations, if a general Thevenin equivalent representation for the voltages and currents at the both ends of the line is used

$$\hat{\mathbf{V}}(0) = \hat{\mathbf{V}}_S - \hat{\mathbf{Z}}_S \hat{\mathbf{I}}(0) \quad (\text{III.28a})$$

$$\hat{\mathbf{V}}(\mathcal{L}) = \hat{\mathbf{V}}_L + \hat{\mathbf{Z}}_L \hat{\mathbf{I}}(\mathcal{L}) \quad (\text{III.28b})$$

The $n \times 1$ vectors $\hat{\mathbf{V}}_S$ and $\hat{\mathbf{V}}_L$ contain the effects of the independent voltage and current sources in the termination networks at $z=0$ and $z=\mathcal{L}$ respectively. The $n \times n$ matrices $\hat{\mathbf{Z}}_S$ and $\hat{\mathbf{Z}}_L$ contain the effects of the impedances at the terminals.

If we substitute the expressions for the line voltages and currents given with (III.19) and (III.26) at $z=0$ and $z=\mathcal{L}$ into the terminal constraints given in (III.28), the following equations are obtained [106]

$$\hat{\mathbf{Z}}_C \hat{\mathbf{T}}(\hat{\mathbf{I}}_m^+ + \hat{\mathbf{I}}_m^-) = \hat{\mathbf{V}}_S - \hat{\mathbf{Z}}_S \hat{\mathbf{T}}(\hat{\mathbf{I}}_m^+ - \hat{\mathbf{I}}_m^-) \quad (\text{III.29a})$$

$$\hat{\mathbf{Z}}_C \hat{\mathbf{T}}(\mathbf{e}^{-\hat{\gamma}\mathcal{L}} \hat{\mathbf{I}}_m^+ + \mathbf{e}^{\hat{\gamma}\mathcal{L}} \hat{\mathbf{I}}_m^-) = \hat{\mathbf{V}}_L - \hat{\mathbf{Z}}_L \hat{\mathbf{T}}(\mathbf{e}^{-\hat{\gamma}\mathcal{L}} \hat{\mathbf{I}}_m^+ - \mathbf{e}^{\hat{\gamma}\mathcal{L}} \hat{\mathbf{I}}_m^-) \quad (\text{III.29b})$$

Writing this in matrix form gives

$$\begin{bmatrix} (\hat{\mathbf{Z}}_C + \hat{\mathbf{Z}}_S) \hat{\mathbf{T}} & (\hat{\mathbf{Z}}_C - \hat{\mathbf{Z}}_S) \hat{\mathbf{T}} \\ (\hat{\mathbf{Z}}_C - \hat{\mathbf{Z}}_L) \hat{\mathbf{T}} \mathbf{e}^{-\hat{\gamma}\mathcal{L}} & (\hat{\mathbf{Z}}_C + \hat{\mathbf{Z}}_L) \hat{\mathbf{T}} \mathbf{e}^{\hat{\gamma}\mathcal{L}} \end{bmatrix} \begin{bmatrix} \hat{\mathbf{I}}_m^+ \\ \hat{\mathbf{I}}_m^- \end{bmatrix} = \begin{bmatrix} \hat{\mathbf{V}}_S \\ \hat{\mathbf{V}}_L \end{bmatrix} \quad (\text{III.30})$$

Once this set of $2n$ simultaneous equations is solved for $\hat{\mathbf{I}}_m^+$ and $\hat{\mathbf{I}}_m^-$, the line voltages and currents are obtained at any z along the line by substitution into (III.22) and (III.26).

III.4 The electromagnetic field coupling

In the previous section, the effect of crosstalk between the conductors in the cable bundles was examined. Here, the second major phenomenon causing unintended excitation in the conductors, namely the incident field excitation of a transmission line is introduced. The incident fields may be in the form of uniform plane waves, if the source is far away from the line or they may be non-uniform fields such as generated by nearby radiating structures. The transmission line (TL) equations for this case will be presented and the resulting from these equations per-unit-length equivalent circuits will be shown.

Before beginning the derivation of the TL equations, it is very important to divide the total EM field into incident and scattered EM field. The incident field is the one which is produced by the distant or nearby source in the absence of the line conductors. The scattered field is produced by the currents and charges which are induced on the line conductors. Thus, the field is the sum of a scattered and an incident component as

$$\vec{\mathcal{E}}_t = \vec{\mathcal{E}}_t^i + \vec{\mathcal{E}}_t^s \quad (\text{III.31a})$$

$$\vec{\mathcal{E}}_z = \vec{\mathcal{E}}_z^i + \vec{\mathcal{E}}_z^s \quad (\text{III.31b})$$

$$\vec{\mathcal{B}} = \vec{\mathcal{B}}^i + \vec{\mathcal{B}}^s \quad (\text{III.31c})$$

where the superscript "i" denotes incident and superscript "s" scattered fields. Subscript "t" denotes the field component which lies in a plane transverse to line direction (the z direction) and subscript z denotes the longitudinal field component.

There are two possibilities to define the TL equations. The first form is in terms of the total voltage formulation $V(z,t)$. This approach was developed by Taylor and is referred to as Taylor formulation or Taylor approach. An alternative form of the TL equations is the scattered voltage formulation. Here, the line current and the scattered voltage $V^s(z,t)$ are considered to be unknown quantities. This form of the solution is described by Agrawal [3]. It is known as Agrawal approach.

III.4.1 Total voltage formulation (Taylor approach)

Assuming a two-conductor transmission line illustrated in Fig. III.1 is illuminated by an incident electromagnetic (EM) field as depicted in the figure.

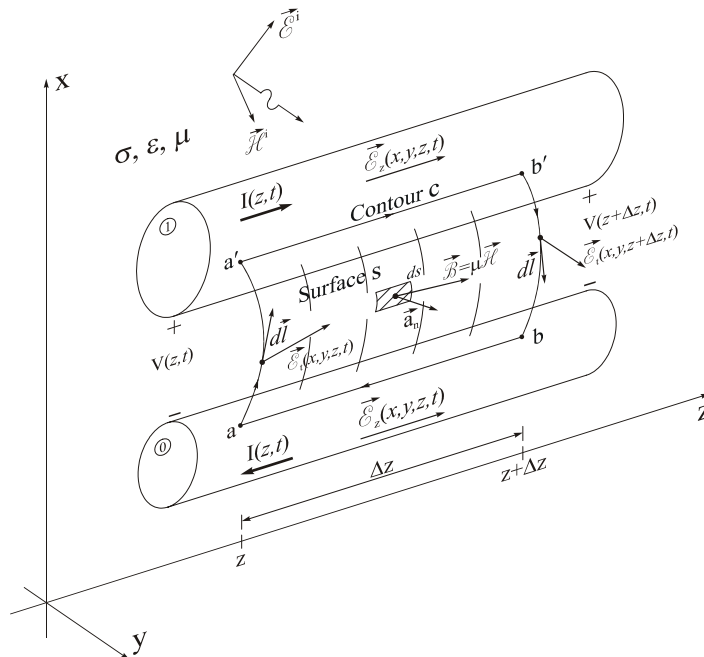


Fig. III.1 Differential section of a two-conductor transmission line excited by incident EM field

The transmission line equations in this case take the form

$$\frac{\partial}{\partial z} V(z,t) + rI(z,t) + l \frac{\partial}{\partial t} I(z,t) = V_{SI}(z,t) \quad (\text{III.32a})$$

$$\frac{\partial}{\partial z} I(z,t) + gV(z,t) + c \frac{\partial}{\partial t} V(z,t) = I_{SI}(z,t) \quad (\text{III.32b})$$

where per-unit-length voltage $V_{SI}(z,t)$ and current $I_{SI}(z,t)$ sources are defined as follows

$$V_{SI}(z,t) = \frac{\partial}{\partial t} \int_a^{a'} \vec{B}^i \cdot \vec{a}_n dl \quad (\text{III.33a})$$

$$I_{SI}(z,t) = -g \int_a^{a'} \vec{E}_t^i \cdot d\vec{l} - c \frac{\partial}{\partial t} \int_a^{a'} \vec{E}_t^i \cdot d\vec{l} \quad (\text{III.33b})$$

In the case of an incident field excitation of the line, the two TL equations in terms of the total voltages show that the incident EM field modifies the usual homogeneous TL equations by adding voltage $V_{SI}(z,t)$ and current $I_{SI}(z,t)$ sources.

These sources can be thought of as arising from a set of distributed voltage and current generators located along the length of the line, as depicted in Fig. III.2.

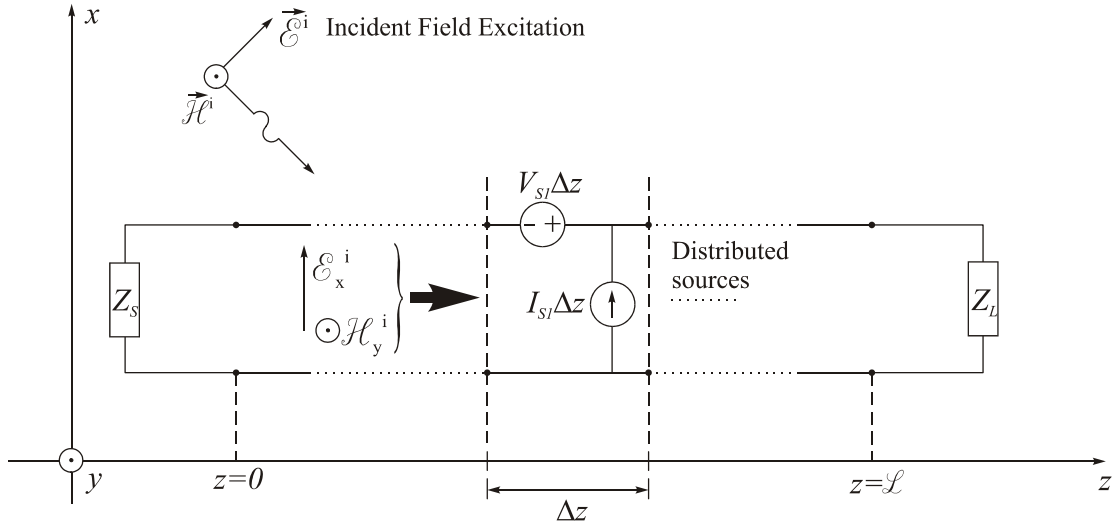


Fig. III.2 Field excitation of a transmission line using distributed voltage and current sources (i.e., the Taylor approach)

III.4.2 Scattered voltage formulation (Agrawal approach)

Alternatively, the TL equations can be derived in terms of the scattered voltages. This is done because scattered voltage formulation is considerably more convenient to apply than the total voltage formulation.

The form of the transmission line equations in terms of the scattered voltages is

$$\frac{\partial}{\partial z} V^s(z, t) + rI(z, t) + l \frac{\partial}{\partial t} I(z, t) = V_{S2}(z, t) \quad (\text{III.34a})$$

$$\frac{\partial}{\partial z} I(z, t) + gV^s(z, t) + c \frac{\partial}{\partial t} V^s(z, t) = 0 \quad (\text{III.34b})$$

where the per-unit-length voltage source $V_{S2}(z, t)$ is given as

$$V_{S2}(z, t) = \mathcal{E}_{z,l}^i(z, t) - \mathcal{E}_{z,0}^i(z, t) \quad (\text{III.35})$$

The Agrawal and Taylor formulations of the TL equations in case of an incident-field excitation are completely equivalent. This means that no matter which of them is used for simulating a specific case, the results must be the same. However, there is a significant difference between them when incorporating the terminal conditions. If we suppose, for example, that the terminal constraints are resistive with no lumped sources, as illustrated in Fig. III.2, and are in form of the generalized Thevenin equivalent, then we obtain

$$V(0, t) = -R_S I(0, t) \quad (\text{III.36a})$$

$$V(\mathcal{L}, t) = R_L I(\mathcal{L}, t) \quad (\text{III.36b})$$

In the case of the scattered voltage formulation, however, the boundary conditions must be in terms of the scattered voltages. They are given with the following set of equations

$$V^s(0, t) = \int_a^{a'} \vec{\mathcal{E}}_t^i \cdot d\vec{l} \Big|_{z=0} - R_S I(0, t) \quad (\text{III.37a})$$

$$V^s(\mathcal{L}, t) = \int_a^{a'} \vec{\mathcal{E}}_t^i \cdot d\vec{l} \Big|_{z=\mathcal{L}} + R_L I(\mathcal{L}, t) \quad (\text{III.37b})$$

Thus, in the Agrawal formulation the distributed voltage sources along the line are given by eq. (III.35), together with two lumped voltage sources at the ends given by

$$V_1(0, t) = \int_a^{a'} \vec{\mathcal{E}}_t^i \cdot d\vec{l} \Big|_{z=0} \quad (\text{III.38a})$$

$$V_2(\mathcal{L}, t) = \int_a^{a'} \vec{\mathcal{E}}_t^i \cdot d\vec{l} \Big|_{z=\mathcal{L}} \quad (\text{III.38b})$$

As a lumped circuit approximation the Agrawal approach is illustrated in Fig. III.3

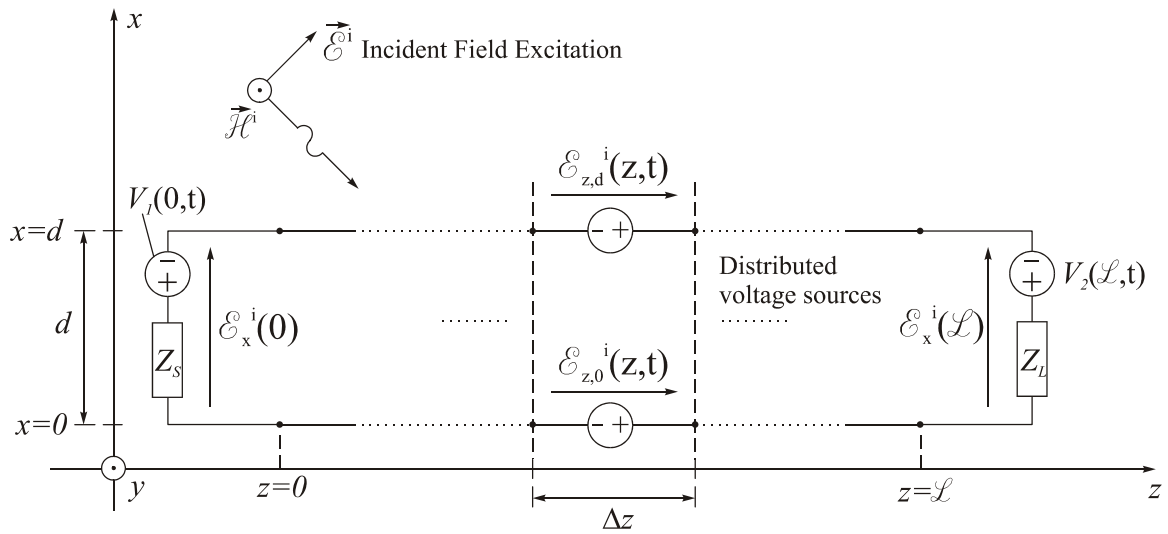


Fig. III.3 Lumped circuit approximation of the line excited by external EM field according to Agrawal formulation

Lebenslauf

Velislav Varbanov

Alter Markt 4
39104 Magdeburg
Deutschland
Tel.: +49 179 9005315
+49 391 5866070

e-mail: Velislav.Varbanov@student.uni-magdeburg.de



Persönliche Daten

Velislav Dimitrov Varbanov
geb. am 07.01.1972 in Burgas, Bulgarien
Familienstand: verheiratet, 1 Kind
Nationalität: bulgarisch

Schulbildung

09/1985 – 06/1990
Mathematisches Gymnasium in Burgas, Bulgarien
Abschluss: Allgemeine Hochschulreife

Hochschulbildung

09/1990 – 07/1995
Technische Universität – Sofia, Bulgarien
Vertiefungsrichtung: “Automatisierungstechnik im Maschinenbau”
Abschluss: Diplom

Diplomarbeit: 02/1995 – 07/1995
Diplomandentätigkeit an der Technische Universität – Sofia, Bulgarien
Thema: “Konzipierung und Projektierung einer Anlage für die automatische Verpackung von Nägeln”

Wehrdienst

09/1995 – 09/1996
Militärschule für Reserveoffiziere „Hristo Botev“ in Pleven, Bulgarien

Berufstätigkeit

03/1998 – 01/2001
Ingenieurprojekt Assistent in der “Spartak” AG, Burgas, Bulgarien
09/2004 – 12/2004
Tätigkeit mit befristetem Arbeitsvertrag im Kernkraftwerk Gundremmingen, Teilbereich TE

Doktorandentätigkeit

01/2001 – 07/2003
Tätigkeit als Graduiertenstipendiant an der Otto-von-Guericke-Universität Magdeburg
Fakultät für Verfahrens- und Systemtechnik
Thema: “Stochastic effects and uncertainties in assessing electromagnetic interaction with control systems”
07/2003 – 07/2004
Tätigkeit mit befristetem Arbeitsvertrag in der Abteilung Anlagentechnik und Anlagensicherheit der Otto-von-Guericke-Universität Magdeburg